PROCEEDINGS OF THE CONFERENCE ULTRASOUND IN BIOLOGY AND MEDICINE — UBIOMED VI

FOREWORD

This publication contains papers and communications which were delivered at the Conference on Ultrasound in Biology and Medicine – UBIOMED VI. This Conference was held in Warsaw–Jabłonna. It was the sixth successive international meeting under this name devoted to these problems. The previous conferences were held in Poland, GDR, Czechoslovakia, Hungary and in USSR. The present conference was held for the second time in Poland. It was organized by the Committee of Acoustics, Polish Academy of Sciences; Ultrasonic Medical and Biological Section, Polish Medical Society; and the Institute of Fundamental Technological Research, Polish Academy of Sciences.

The Conference covered the following fields:

I. Physics and biophysics,
II. New developments in instrumentation,
III. Vascular Doppler,
IV. Cardiac Doppler,
V. Echocardiography,
VI. Ultrasonography and oncology,
VII. Ophthalmology.

About 120 participants from Poland and from 10 European and other countries took part in the Conference. In all, 64 papers and communications were delivered and have been gathered in the present volume.

An additional volume, containing the papers of these authors who did not manage to submit complete papers in time, during the Conference, will be published later on.

The Conference showed the significant role that is now played by ultrasonic techniques in various fields of medicine, and also indicated new, interesting trends, particularly in Doppler problems, at the same time revealing a large number of problems in the physics and biophysics of ultrasound which are now far from solved.

L. Filipczyński

ARCHIVES OF ACOUSTICS
9, 1-2, 5-14 (1984)

THE ACTION OF THERAPEUTIC ULTRASOUND ON THE CATALYTIC ACTIVITY OF THE DISSOCIATING ENZYMES

N. A. ROZANOVA, E. P. CHETVERIKOWA

Institute of Biological Physics, Academy of Sciences of the USSR
(Pushchino, 142292, USSR)

The action of low intensity therapeutic ultrasound (0.88 MHz; 0.05—1.0 W/cm^2) on the activity and dissociation of the enzymes with labile quarternary structure was investigated (creatine kinase — CK, pyruvate kinase — PK, hexokinase — HK and urease). It was shown that ultrasound does not affect the activity of these enzymes in solution. Dissociation of CK was activated by ultrasound when equilibrium forms in solution were not reached. Activation of the rate of the catalytic reaction in the case of immobilized HK was also obtained. This effect may consist in enhancement of the reaction product transport from the bottom of the experimental cell up to where the aliquote volume was replaced for measuring.

1. Introduction

In the investigations of the mechanisms of the biological action of low intensity therapeutic ultrasound it is important to reveal the primary targets. In the publications of BELEVA-STAIKOWA [1] and POSPISHILOVA [7] changes of activity of different enzymes *in vivo* under the action of therapeutic ultrasound were reported. However, in these publications it is impossible to separate the primary and the secondary effects of sonication and consider the possibility of direct action of ultrasound on the enzyme itself.

The work of DUNN and MC LEOD published 15 years ago was the first investigation devoted to the problem whether enzymes in aqueous solutions and enzymic reactions can be affected by noncavitation ultrasound [3]. They showed that a wide range of ultrasonic frequencies and intensities had no effect upon the catalytic rate of five purified enzymes *in vitro* (α-chymotrypsin, trypsin, lactate dehydrogenase, aldolase and ribonuclease). These enzymes have stable quarternary structure. The conditions of the experiments were not va-

ried: concentrations of enzymes, its substrates and pH were constant. The latter is especially important, because the enzymic reaction, in some conditions, can be more sensitive than the enzyme molecule. Besides, there is a special group of dissociating enzymes having very labile quarternary structure which was not investigated. Without investigation of these sensitive and important enzymes in a wide enough range of conditions, it is impossible to make a final decision about the absence or existence of direct action of ultrasound on the enzymic reactions.

Dissociation of these labile enzymes is accompanied by significant changes in catalytic activity. The property of dissociating enzymes to change their catalytic activity according to the oligomeric state is the basis of one of their regulation mechanisms [6]. The change of activity occurs by allosteric mechanism. The allosteric effectors are known: pH, metabolites, changes of the protein concentration and ionic strength [6]; these are very weak factors. Fig. 1

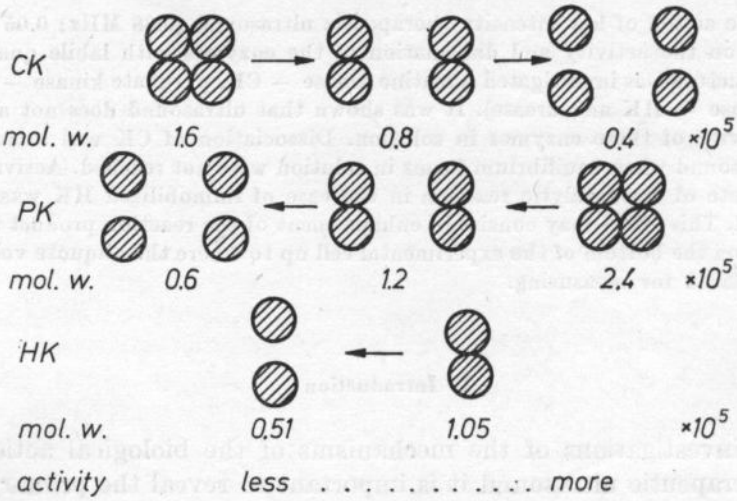

Fig. 1. Two ways of the enzyme dissociation. CK — creatine kinase dissociation accompanied by a high increase in catalytic activity; PK, HK — pyruvate kinase and hexokinase dissociation accompanied by loss of enzyme activity in monomeric form

shows two ways of dissociation of enzymes: creatine phosphokinase (CK), pyruvate kinase (PK) and hexokinase (HK). Dissociation of PK and HK is accompanied by a decrease in their activity; monomeric form has no activity at all [5, 4]. Dissociation of CK is accompanied by a high increase in catalytic activity: monomer is hundred times more active than tetramer [8].

The purpose of our work was to investigate the action of low intensity therapeutic ultrasound on dissociating enzymes: CK, PK, HK and urease.

2. Materials and methods

a. Enzymes and methods of measuring their activity

1. *Creatine kinase* (E.C.2.7.3.2) was purified from rabbit skeletal muscle by the method described by CHETVERIKOVA [2]. The rate of the enzymic reaction was registered by measuring pH changes in a typical reaction mixture consisting of 5 mM ATP, 6 mH magnesium acetate, 36 mM creatine and 2 mM Tris buffer maintaining the initial pH at 8.35.

2. *Pyruvate kinase* (E.C.2.7.1.40) was purified from rabbit muscle and supplied by "Reanal". The rate of reaction was estimated by pH changes. The reaction mixture consisted of 3 mM ADP, 5 mM magnesium acetate, 0.7 mM PEP, 100 mM KCl, 1.3 μg/ml of protein and 2 mM Tris buffer to maintain the initial pH of 7.8.

3. *Hexokinase* (E.C.2.7.1.1) from yeasts was purchased in purified form from "Fluka" and "Boeringer". The concentration of ATP in the reaction mixture was varied between 0.3 and 3.0 mM. Other components were 15 mM glucose, 5 mM magnesium Acetate and 2 mM Tris buffer. The rate of this reaction was measured by pH changes and spectrophotometrically with glucose-6-phosphate dehydrogenase of NADPH absorbance at 340 nm. This reaction mixture consisted of 66 mM glucose, 3 mM ATP, 6 mM magnesium acetate, 0.3 mM NADP, 2.5 μg/ml HK and 0.5 μg glucose-6-phosphate dehydrogenase. The aliquote of the solution was stopped by addition of 50 mM EDTA in 0.5 N NaOH and then changes in absorbance at 340 nm were measured. Hexokinase was also supplied by "Sigma" in an immobilized form lined to agarose.

4. *Urease* (E.C.3.5.1.5) was obtained from a water-melon as a tissue preparation in lyophilised form. This enzyme was kindly suppied to us by Prof. KURGANOV. The reaction mixture consisted of 0.8 per cent urea in 2 mM Tris buffer, pH 7.5. The rate of the reaction was measured by pH changes.

b. Characteristics of acoustic system

The experiments was performed in two chambers.

Chamber I. The measuring cell was placed in a thermostated box containing a reflector and absorber for ultrasound (Fig. 2*a*). It was made of lucite and had a very thin glass window transparent to ultrasound. Irradiation was performed by using a commercial therapeutic device with a piezoceramic transducer with a 1.5 cm diameter and a frequency of 0.88 MHz within the intensity range 0.05 —0.7 W/cm². The distance between transducer and measuring cell was 3 cm. The ratio of the spatial peak to the spatial averaged intensity over the irradiated surface of the cell was about 3. Samples were sonicated during catalytic reaction.

Chamber II. This chamber is shown in Fig. 2*b*. The sample for sonication was placed in a vertical cylindrical lucite tube with a thin glass bottom for ultrasound. This chamber was thermostated as well and samples were sonicated in it before contact with the reaction mixture.

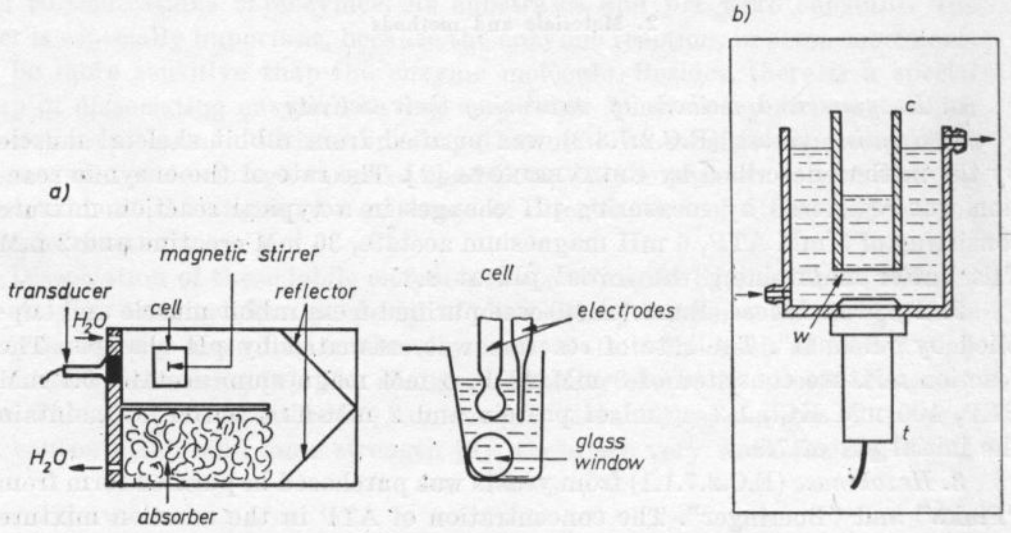

Fig. 2. Schematic diagrams of the chambers for sonication: *a* — chamber I for sonication during catalytic reactions; *b* — chamber II for the preliminary sonication, *c* — cell for the sample, *w* — window for ultrasound, *t* — transducer

3. Results and discussion

The dissociating enzymes are characterised by nonlinear dependence of enzymic activity on the protein concentration. Our results on the dissociation of cytoplasmic CK are shown in Fig. 3. This dissociation is caused by dilution of the enzyme solution. In the range of high protein concentration (about a few mg/ml) where the enzyme is mainly in tetrameric form, according to the data of sedimentation analysis, $S^0_{20,w} = 8.7$ (Fig. 3, the first line under the diagram), the activity was low. The decrease of CK concentration is accompanied by an increase in its activity. The plateau in this diagram (Fig. 3) characterises the stable dimer both by catalytic activity and sedimentation data $S^0_{20,w} = 5.25$. The further substantial increase in activity and the change in the Swedberg coefficient ($S^0_{20,w} = 3.5$) is evidence of dissociation of the dimer and formation of a highly active monomer. The dissociation of the polymeric forms of creatine kinase following dilution takes up to an hour to reach equilibrium.

These samples were sonicated in chamber I during the catalytic reaction. Irradiation of solution with different enzyme concentration and therefore of different quarternary structure of enzyme produced no changes in the catalytic activity (Fig. 4). The left bars in each pair show the activity of the CK in control, and the right bars show the activity in sonicated samples.

Similar negative results were obtained in the case of sonication of the reactions catalysed by PK and HK. The experiments on HK were carried out

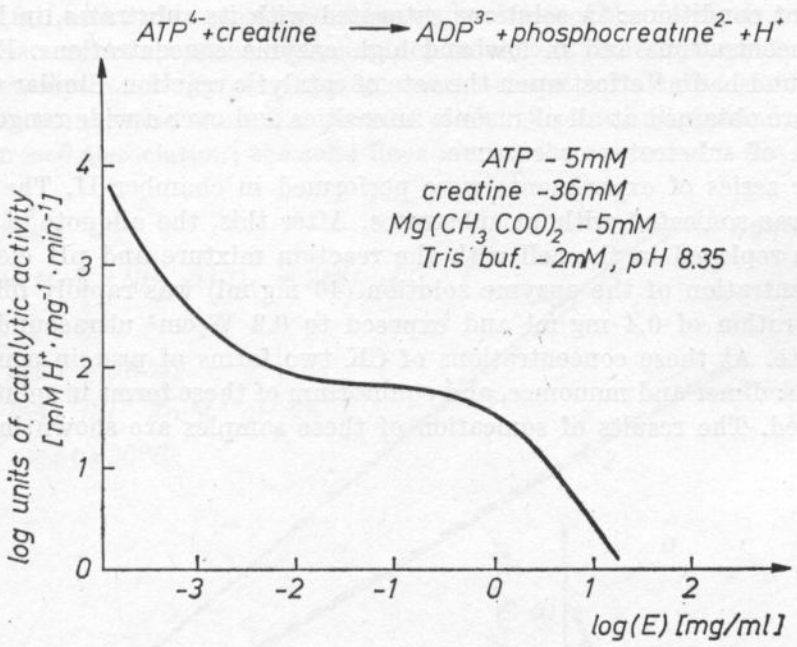

sedimentation constant	3.57 ±0.3	5.25 ±0.16	8.7 ±0.6
olygomeric structure	M	D	T
molecular weight $\cdot 10^5$	0.4	0.8	1.6

Fig. 3. Dissociation of creatine kinase; increase in catalytic activity of creatine kinase

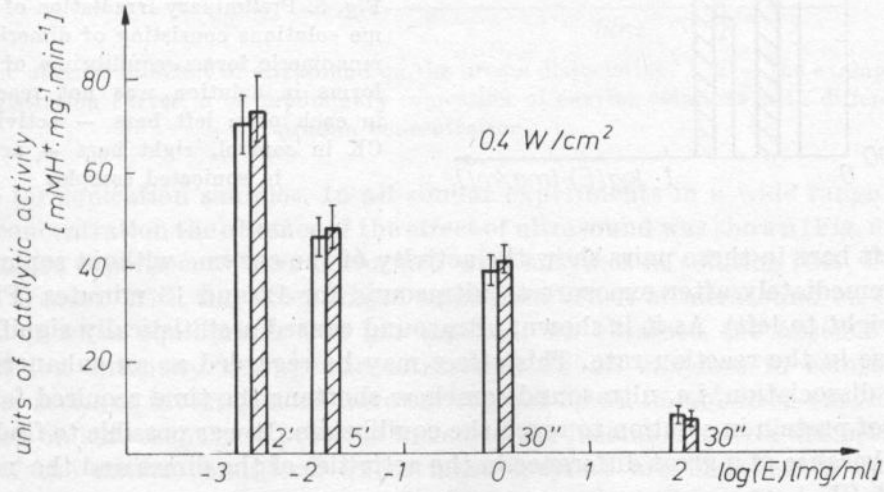

Fig. 4. Irradiation of the reaction mixture with an enzyme in different quarternary structure (equilibrium of forms was reached in every solution); in each pair: left bars — activity of CK in control, right bars — activity in sonicated samples

in different conditions: in solutions saturated with its substrates, in low substrate concentrations and in low and high enzyme concentrations. Exposure to ultrasound had no effect upon the rate of catalytic reaction. Similar negative results were obtained at all ultrasonic intensities and over a wide range of concentration of substrates or enzyme.

Other series of experiments were performed in chamber II. The protein solution was sonicated without substrates. After this, the aliquote of the enzyme was replaced in the cell with the reaction mixture and pH electrodes. The concentration of the enzyme solution (40 mg/ml) was rapidly diluted to a concentration of 0.4 mg/ml and exposed to 0.2 W/cm² ultrasound within one minute. At these concentrations of CK two forms of protein could exist in solution: dimer and monomer, and equilibrium of these forms in solution was not reached. The results of sonication of these samples are shown in Fig. 5.

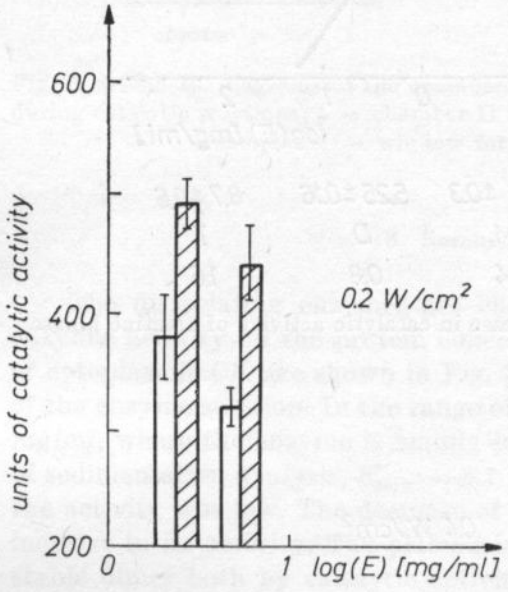

Fig. 5. Preliminary irradiation of enzyme solutions consisting of dimeric and monomeric forms (equilibrium of these forms in solution was not reached); in each pair: left bars – activity of CK in control, right bars – activity in sonicated samples

The left bars in these pairs show the activity of the enzyme without sonication and immediately after exposure to ultrasound for 12 and 15 minutes (Fig. 5, from right to left). As it is shown, ultrasound caused a statistically significant increase in the reaction rate. This effect may be regarded as an enhancement of the dissociation, i.e. ultrasound somehow shortens the time required for the forms of protein in solution to reach the equilibrium. It was possible to find this effect because of a great difference in the activities of the dimer and the monomer of CK.

The action of ultrasound on urease dissociation was investigated by preliminary sonication in chamber II. The results are shown in Fig. 6. These two

curves (Fig. 6, 1 and 2) are examples of the registration of the catalytic reaction kinetics. These curves show the nonlinear dependence of the enzyme concentration on its catalytic activity — a typical characteristic for all dissociating enzymes. These curves also show the absence of the action of ultrasound on the process of urease dissociation; the solid lines are for the control and the dotted

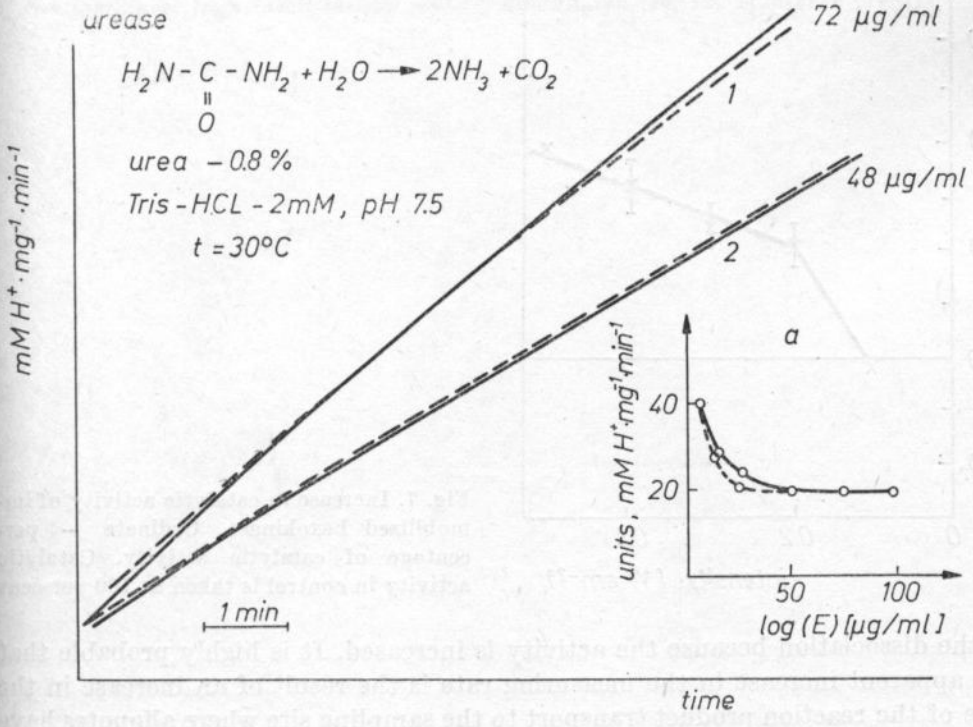

Fig. 6. The absence of effect of ultrasound on the urease dissociation. *1, 2* — the examples of the registration curves, *a* — preliminary sonication of enzyme solutions with different protein concentration

lines are for sonication samples. In all similar experiments in a wide range of protein concentration the absence of the effect of ultrasound was shown (Fig. 6*a*).

All these experiments were performed with enzymes in solution (CK, PK, HK and urease). With the exception of significant effect of ultrasound on CK dissociation when equilibrium was not reached, we obtained the absence of action of low intensity therapeutic ultrasound on all enzymes in solution.

Other series of investigations were carried out on an immobilized enzyme: KH linked on agarose. These proteins linked to the insoluble matrix are better models of the native conditions where most enzymes are included in large complexes in cytoplasm. HK has activity only in dimeric form. If sonication leads to dissociation of this enzyme it must lose the activity. The experiments which were performed in the stable stirring conditions show no effect of ultra-

sound. Ultrasound with the intensities greater than about 0.2 W/cm² caused a small but statistically significant increase in the measured activity of the immobilized hexokinase, but the magnitude of this effect apparently increased with increasing intensity of ultrasound (Fig. 7). These data cannot be a result

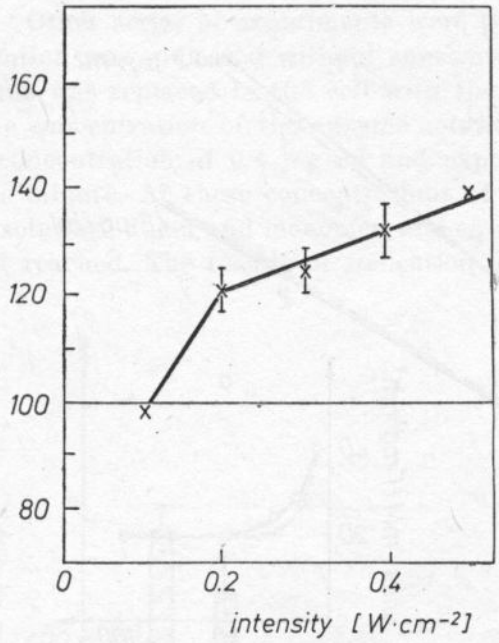

Fig. 7. Increase in catalytic activity of immobilized hexokinase. Ordinate — percentage of catalytic activity. Catalytic activity in control is taken as 100 per cent

of the dissociation because the activity is increased. It is highly probable that the apparent increase in the measuring rate is the result of an increase in the rate of the reaction product transport to the sampling site where aliquotes have been removed for the measuring.

References

[1] R. Beleva-Staikova, S. Chifchiiski, M. Dragev, *The influence of biophysical factors on the oxidation-reduction processes and biological oxidation. Changes in succinate dehydrogenase activity after the action of ultrasound,* Radiobiol. Radiotherapy, **11**, 6, 661-666 (1970).

[2] E. P. Chetverikova, A. V. Krinskaya, N. A. Rozanova, V. V. Rubina, L. L. Alevskaya, *The content and kinetic properties of creatine kinase from skeletal muscles,* Biokhimya, **35**, 5, 953-961 (1970).

[3] F. Dunn, R. M. Mc Leod, *Effects of intense noncavitating ultrasound on selective enzymes,* J. Acoust. Soc. Am., **44**, 4, 932-940 (1968).

[4] J. C. Hoggett, G. L. Kellett, *Yeasts hexokinase: substrate-induced association-dissociation reactions in the binding of glucose to hexokinase II,* Eur. J. Biochem., **66**, 1, 65-77 (1976).

[5] M. G. Irving, J. F. Williams, *Kinetic studies on the regulation of rabbit liver pyruvate kinase,* Biochem. J., **131**, 1, 287-301 (1973).

[6] B. I. Kurganov, *Allosteric enzymes,* Nauka, Moscow 1978.

[7] J. Pospishilova, *Biological changes in granulating tissues after the action of ultrasound,* Wiss. Zeitschr. der Humbold-Universität zu Berllin, **XXII**, 4, 382-384 (1973).

[8] N. A. Rozanova, E. P. Chetverikova, *The dynamics of the quarternary structure of creatine kinase from rabbit skeletal muscle,* Biokhimiya, **46**, 12, 2125-2135 (1981).

ARCHIVES OF ACOUSTICS
9, 1-2, 15-22 (1984)

THERMOGRAPHIC INVESTIGATION OF ULTRASONICALLY INDUCED TEMPERATURE DISTRIBUTION IN TISSUES AND TISSUE-EQUIVALENT PHANTOMS

T. PASHOVKIN, E. KHIZNYAK, A. SARVAZYAN

Institute of Biological Physics, Academy of Sciences of the USSR
(Pushchino, USSR)

The purpose of the paper was to develop a computerised thermographic method for the investigation of the temperature fields in tissue phantoms irradiated by ultrasound and to study heating patterns in sonicated heterogeneous and homogeneous phantoms. The developed thermographic system provided the possibility of obtaining threedimensional images of the temperature distributions in the irradiated samples. It is shown that the temperature pattern in the heterogeneous tissue phantoms irradiated by ultrasound can be dependent not only on the differences in bulk acoustical properties of the adjacent tissues but also on the differences in their shear properties.

1. Introduction

One of the most important problems involved in the effective therapeutic application of ultrasonic hyperthermy is that of obtaining required temperature distributions in the sonicated tissue. There are two methods for the investigation of ultrasonically induced temperature fields in tissues described in literature. One, the most widely used, method is the thermocouples method described in the works of LELE, HYNYNEN, WATHMOUGH, G. TER HAAR and others [4, 5, 7]. Another is the thermographic method which was first used by L. FILIPCZYŃSKI [1] and was recently described in the work of G. TER HAAR and CARNOCHAN [6]. In spite of the fact that the thermocouples method has given better quantitative results, it has a number of disadvantages, namely: a long and complicated procedure of preparation of the object, limited spatial resolution and the possibility of artifacts caused by destructions in the tissue as a result of introduction of thermocouples.

The purpose of the present study was to develop a computerized thermographic method and to investigate temperature fields in homogeneous and heterogeneous tissue phantoms irradiated by ultrasonic pulses.

2. Materials and methods

Tissue phantoms mimicking the properties of biological tissues with regard to velocity and attenuation of longitudinal ultrasonic waves, velocity of shear waves, density and heat capacity, were made of aqueous agar gels with addition of sodium chloride and chalk powder. Table 1 shows the composition of

Table 1. Tissue-equivalent phantom

Composition		Physical properties
water	—100%	U_l = 1570 m/s
agar	— 3%	α_l = 0.24 neper/cm
NaCl	— 7%	U_s = 6 m/s
chalk powder	— 3%	C_p = 1.17 cal/g.deg °C
		ϱ = 1.06 g/cm^3

the physical properties of one of the tissue phantoms used in most of the experiments described below. The values of the parameters given in Table 1 are similar to those of liver [2, 3]. Usually, the value of shear velocity in tissue is not considered as an important parameter in making tissue equivalent phantoms. We have tried to investigate the role of this factor in the production of heat by ultrasound, on the basis of the hypothesis according to which shear properties can be responsible for some thermal effects of ultrasound, in the case of heterogeneous soft tissues at the boundaries between adjacent tissues having similar bulk properties but different shear properties [9].

We measured this velocity and attenuation of longitudinal waves by a resonator device described previously [8]. The velocity of shear waves was calculated from measurements of the time-of-flight of a shear pulse between two piezoelectric transducers. Density was measured by a pycnometer and heat capacity was measured by the calorimetric method. Heterogeneous tissue phantoms were made by composing some pieces of gels with required parameters, pieces of fat, muscle, etc., into a bigger piece of gel having parameters shown in the table.

A schematic diagram of the experiments is presented in Fig. 1. Ultrasonic irradiation was performed by plane or focusing piezoceramic transducers at frequencies of 0.88 MHz and 0.5 MHz respectively and intensities 0-0.1 kW/m^2 (spatial average and time peak) for plane waves and 0.3-15 kW/m^2 (average over the section of the focal region) in the case of focusing transducers. The length of focal region was l = 0.03 m and the diameter r = 0.003 m. The intensity of ultrasound was measured by radiation pressure techniques and by a differential thermocouple which was precalibrated by a known ultrasonic source.

Temperature distributions were measured on the surface of a sample irradiated either by a plane transducer, in the near field, or by a focusing transducer

using distilled degassed water as the coupling medium. Measurements of the temperature fields inside the sample were made by cutting the sample along a chosen axis such that after heating it could be split in less than one second and exposed to an infrared probe.

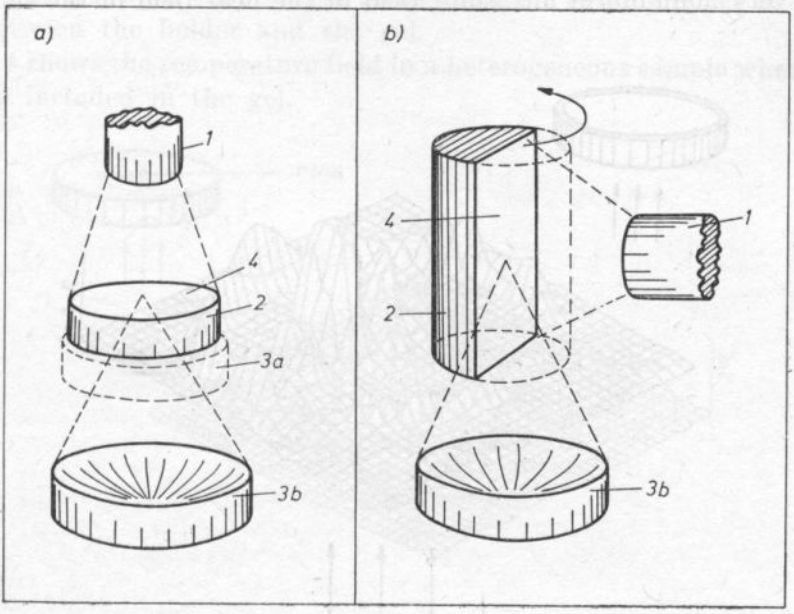

Fig. 1. A schematic diagram of the experiments. *a* — measurements of the heating patterns on the surface of the cylindrical sample 0.005 m thick and 0.035 m in diameter; 1 — infrared-probe, 2 — sample, 3a — plane transducer, 3b — focusing transducer, 4 — surface exposed to the probe. *b* — measurements of the heating patterns on the surface of the sample section. The diameter of the sample 0.024 m and the height —0.1 m

The exposed plane was imaged by a scanning thermographic system, AGA-Thermovision-780, having the spatial resolution of about 10^{-3} m and accuracy of measurements of temperature changes 0.2°C. The obtained image was than recorded digitally on magnetic tape and was displayed as a threedimensional picture after computer analysis. The computer analysis provided the possibility of obtaining differential images of the temperature fields before and after ultrasonic heating of the sample. Just before the measurements the distribution of the temperature fields was not uniform, because of the differences in the rate of evaporation, so that by making this differential picture we could analyse much more precisely the heating pattern produced by ultrasound. The system also provided the possibility of measurements of the kinetics of heating and cooling of the sample surface.

3. Results and discussion

Fig. 2 shows the temperature field on the surface of a sample surrounded by a circular plastic holder in the near field of a plane ultrasonic transducer. A complicated temperature distribution in the middle of the heating area is due to a very nonuniform ultrasonic field in the near field of the source. The

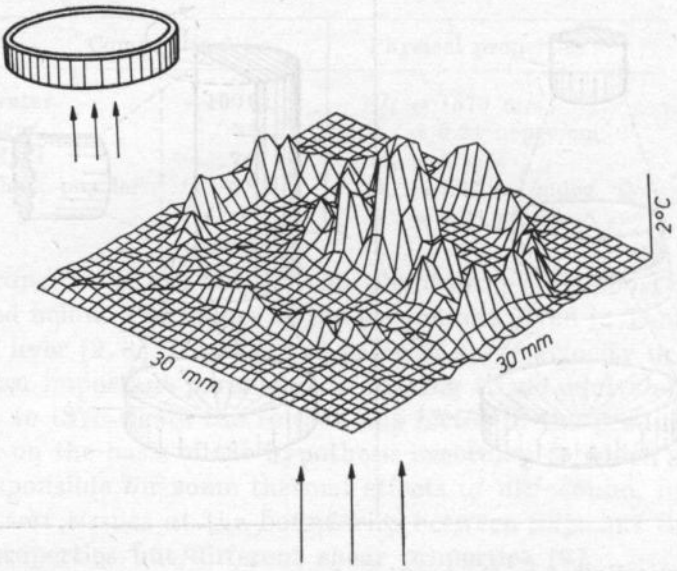

Fig. 2. The thermogram of the surface of a sample 0.005 m thick. The frequency of ultrasound, f, is 0.88 MHz, the intensity of ultrasound, J, is 0.1 kW/m^2, the time of irradiation, τ, is 2s, the temperature scale is 2°C, the transducer is plane, the direction of irradiation is shown by arrows

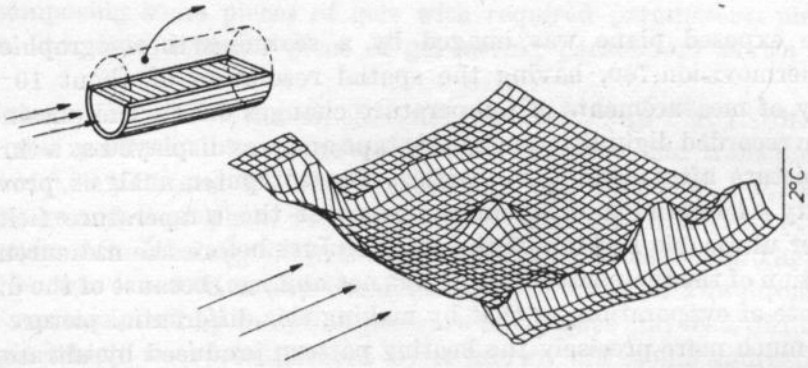

Fig. 3. The thermogram of the surface of the sample section (focusing transducer, $f = 0.5$ MHz, $J = 14.0$ kW/m^2 averaged over the section of the focal region; $\tau = 10$ s. The coupling medium is degassed distilled water)

heating on the boundary between the sample and the holder is due to the well known fact of the heat production at the interfaces between tissue and any solid (e.g. bone) and it is usually explained by the formation of highly attenuated shear waves in the solid.

Fig. 3 shows the heating inside a sample irradiated by focused ultrasound. One can clearly see the shape of the focus and some heating effect at the boundaries between the holder and the gel.

Fig. 4 shows the temperature field in a heterogeneous sample where a small bone was included in the gel.

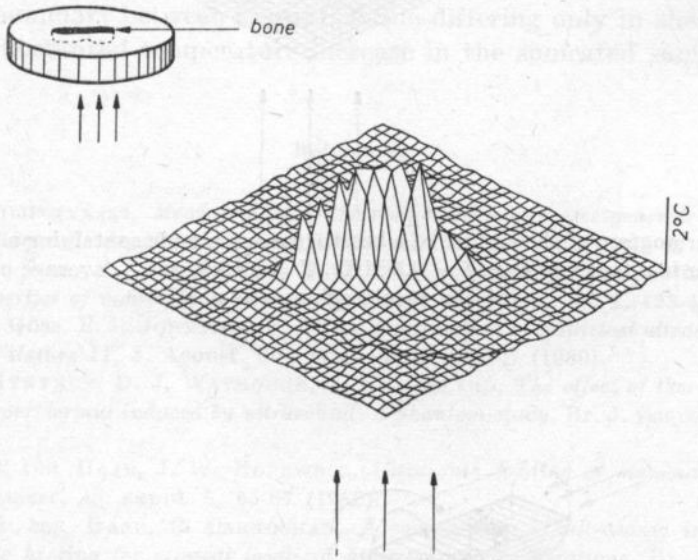

Fig. 4. The thermogram of the surface of a heterogeneous sample with a bone inclusion. The transducer is plane (f = 0.88 MHz, J = 0.1 kW/m^2, τ = 0.5 s)

It is interesting to note that even at such a short exposure (half a second at the intensity close to that used in theraphy: 0.1 kW/m^2) we have a substantial increase in temperature up to 3 degrees.

Fig. 5 shows the temperature field on the surface of the same sample but irradiated by focused ultrasound. The temperature increase on the bone is about 75°C and the rate of heating is about 20°C/c.

Fig. 6 shows a thermogram of a heterogeneous tissue phantom containing an inclusion of a piece of gel having the same value of ultrasound velocity and attenuation as the bulk gel but different values of the velocity of shear waves. The difference in shear properties is about 20 per cent. For longitudinal waves there is no physical boundary between the inclusion and the bulk gel. One can see here that at the first interface between the inclusion and the bulk gel the increase in temperature reaches about 2°C. This is just one example out of many such images which we obtained for inclusions different from the bulk sample in terms of shear properties.

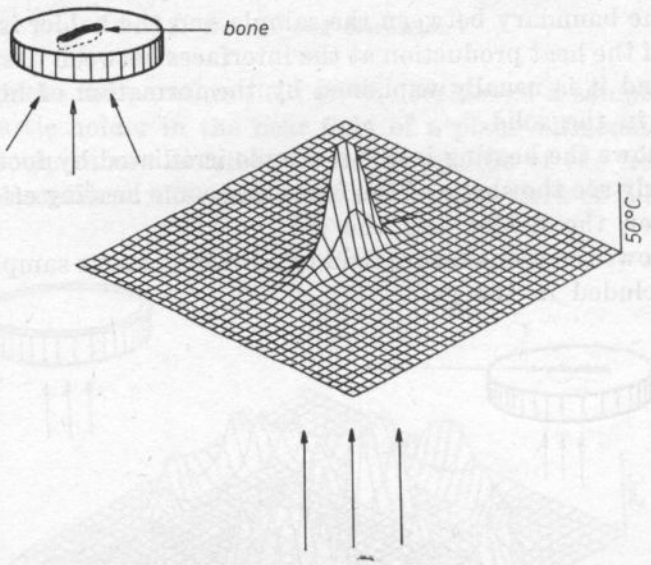

Fig. 5. The thermogram of the surface of a heterogeneous sample containing a bone inclusion. The transducer is a focusing one ($f = 0.5$ MHz, $J = 14$ kW/m^2 – average over the section of the focal region, $\tau = 4$ s)

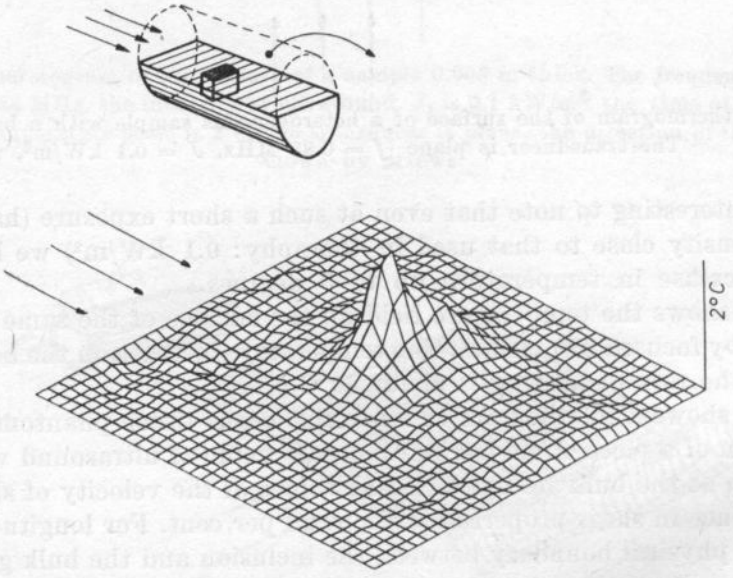

Fig. 6. The thermogram of the surface of a heterogeneous sample containing as an inclusion a piece of gel differing from the bulk gel only in terms of shear properties. The transducer is a plane one ($f = 0.88$ MHz, $J = 0.1$ kW/m^2, $\tau = 3$ s)

4. Conclusions

1. A computerized differential thermographic method is developed for visualisation of temperature distributions in sonicated homogeneous and heterogeneous tissue phantoms.

2. The temperature pattern in irradiated heterogeneous tissue phantoms depends on the differences among the acoustical characteristics of the inclusions.

The rate of temperature increase at the interface bone-soft tissue may reach 4-5°C per second at intensity of plane ultrasonic wave of about 0.1 KW/m².

3. The boundary between two soft tissue differing only in shear properties can give a substantial temperature increase in the sonicated sample.

References

[1] L. Filipczyński, *Measurement of the temperature increases generated in soft tissue by ultrasonic diagnostic doppler equipment,* Ultrasound in Med. and Biol., 4, 151-155 (1978).

[2] S. A. Goss, R. L. Johnston, F. Dunn, *Comprehensive compilation of empirical ultrasonic properties of mammalian tissues,* J. Acoust. Soc. Am., **64**, 2, 423-457 (1978).

[3] S. A. Goss, R. L. Johnston, F. Dunn, *Compilation of empirical ultrasonic properties of mammalian tissues II,* J. Acoust. Soc. Am., **68**, 1, 93-107 (1980).

[4] K. Hynynen, D. J. Watmough, J. R. Mallard, *The effect of thermal conduction during local hyperthermia induced by ultrasound: a phantom study,* Br. J. Cancer, 45, suppl. 5, 68-70 (1982).

[5] G. R. ter Haar, J. W. Hopewell, *Ultrasonic heating of mammalian tissues in vivo,* Br. J. Cancer, 45, suppl. 5, 65-67 (1982).

[6] G. R. ter Haar, P. Carnochan, *A comparison of ultrasonic irradiation and R. F. inductive heating for clinical localized hyperthermia applications,* Br. J. Cancer, 45, suppl. 5, 79-81 (1982).

[7] P. P. Lele, K. J. Parker, *Temperature distributions in tissues beams of unfocused or focused ultrasound,* Br. J. Cancer, 45, suppl. 5, 108-121 (1982).

[8] A. P. Sarvazyan, *Development of methods of precise ultrasonic measurements in small volumes of liquids,* Ultrasonics, **20**, 4, 151-154 (1982).

[9] A. P. Sarvazyan, *Acoustic properties of tissues relevant to therapeutic applications,* Br. J. Cancer, 45, suppl. 5, 52-54 (1982).

ARCHIVES OF ACOUSTICS
9, 1-2, 23-28 (1984)

THE INFLUENCE OF LOW-INTENSITY ULTRASOUND ON THE PROPERTIES OF CELL CULTURES

JIŘÍ ADLER, IVO HRAZDIRA, JITKA HANZLOVÁ, VERA ZAJÍCOVÁ

Department of Biophysics, Department of Anatomy and Department of Epidemiology, Faculty of Medicine, Purkyně University, Brno, Czechoslovakia

In the present paper bovine kidney cell cultures were used as an experimental model for the study of the biophysical mechanism of ultrasonic action.

In the first series of experiments functional and morphological changes in the cells immediately after sonication were evaluated. A decrease in viability and degenerative morphological changes in the cells were found.

In the second series the sonicated cells were seeded in Roux bottles and grown in the optimal conditions. The growth properties of the cells were evaluated at different time intervals after sonication. Significant stimulation of the cell growth was demonstrated after the action of ultrasound intensity of 1.0 kWm^{-2}. However, after the action of ultrasound intensities above 3.0 kWm^{-2} the inhibition of the cell growth was found.

1. Introduction

Increased use of ultrasound devices in medical diagnostics, especially in obstetrics, has accentuated the question of its possible risk for the patient. In the 1976 WHO report [5] the value of 1 kWm^{-2} of ultrasound SATA intensity was recommended as the threshold of biological effectiveness "in vivo". However, changes in some morphological and functional properties of sensitive biological systems, for example isolated cells and cell cultures at ultrasound intensities lower than the recommended threshold of biological effectiveness, were found.

The effects observed in mammalian cells after ultrasound exposure include modification of macromolecular synthetic pathways, alteration of cell membrane properties, intracellular ultrastructural changes and alteration of the growth properties.

Ultrasonically induced functional alterations in the plasma membrane showed increased permeability, decreased active and non-mediated transport and changes in the electrophoretic mobility of cells. A mechanical stress mechanism of ultrasound action was suggested as the cause of an increase in the permeability of human erythrocyte membranes to potassium ions which were described by LOTA and DARLING [10]. BUNDY *et al.* [2] demonstrated a decrease in the transport of leucine in avian erythrocytes. In our laboratory [1], [7] there were described alterations of the electrophoretic mobility of erythrocytes treated with diagnostic ultrasound and changes in the aggregation ability of erythrocytes in polyethylene glycol solutions. SIEGEL *et al.* [11] reported that dispersed cultured human cells seeded in plastic Petri dishes showed significantly reduced cellular attachment after diagnostic ultrasound exposure.

Numerous reports have appeared describing ultrastructural damage to cells exposed to ultrasound. Electron microscopic examination of rat liver cells and fibroblasts irradiated with pulsed ultrasound revealed more free ribosomes, increased damage to mitochondria, endoplasmatic reticulum and lysosomal membranes and more cytoplasmic vacuolation [4], [6]. It has been suggested that cells are particularly susceptible to damage by ultrasound during mitosis, because major changes in the cell membrane and internal structure occur during this phase of the cell cycle [3].

2. Materials and methods

In the present study the Madine-Darby bovine kidney and primary calf kidney cell cultures were used as an experimental model for a complex study of the biophysical mechanism of ultrasonic action. The cell cultures were grown in the Minimum Essential Medium supplemented with 5-10% calf serum in Roux bottles. Suspensions of approximately 10^6 cells in millilitre were prepared using trypsin.

The source of ultrasound was a laboratory CW generator operating at a frequency of 0.8 MHz. The sonication of cells over the ultrasound intensity range from 0.5 kWm^{-2} to 10.0 kWm^{-2} in the horizontal field in a 37°C water bath was carried out for 10 or 20 minutes. The incident intensity levels were controlled by means of callibrated hydrophone.

The morphological changes in sonicated and control cells were evaluated using both the optical and the electron microscope. The viability of cells was tested using trypan blue vital dye.

3. Results

Our preliminary experiments were directed to morphological changes in cells caused by sonication of cell monolayers at very low intensity levels of ultrasound (i.e. 0.5 kWm^{-2} and 1.0 kWm^{-2}). In micrographs of sonicated cells, disap-

pearing of protoplasmatic bridges, rounding off and desquamation of cells were proved.

In the first series of experiments the morphological and functional changes in Madine-Darby bovine kidney cell suspensions immediately after sonication were evaluated. One part of the sonicated cells was fixed using glutaraldehyde and prepared for electron microscopic examination. The other part of sonicated cells was incubated with trypan blue vital dye. After three minutes the viability of cells was tested. Electron microscopic examination of cells revealed ultrastructural damage to cells exposed to ultrasound of low intensity level. There were observed enlargement and damage to mitochondria, enlargement of endoplasmatic reticulum and vacuolation. Incubation of cells with trypan blue vital dye demonstrated changes in viability of cells after ultrasound exposure. In control conditions 13.9 per cent of cells were stained. Using ultrasound intensity of 1.0 kWm^{-2} 25.4 per cent of cells were stained and finally using ultrasound intensity of 5.0 kWm^{-2} 51.0 per cent of cells were stained.

In the second series of experiments the sonicated primary calf cells were seeded in Roux bottles and grown in the optimal conditions. The growth and morphology of the cells were evaluated microscopically at different time intervals after sonication, up to three weeks. The action of ultrasound of intensity above 3.0 kWm^{-2} caused the death of all sonicated cells. However, there was a difference in the behaviour of cells sonicated at different intensities of ultrasound. Cells exposed to ultrasound intensity of 3.0 kWm^{-2} or 5.0 kWm^{-2} were able to attach to the glass surface of Roux bottle, but could not divide themselves. Cells exposed to ultrasound intensity of 10.0 kWm^{-2} were not able to attach to the glass surface and died immediately. On the other hand, the action of ultrasound intensity of 1.0 kWm^{-2} stimulated significantly the growth of sonicated cells and formation of the monolayer. The control and sonicated cell cultures were observed over 8 passages after sonication and the difference in growth mentioned above was expressed over the whole period of observation.

4. Discussion

LIEBESKIND *et al.* [9] described morphological changes in the surface characteristics and post-sonication ultrastructural changes in cell cultures after pulsed diagnostic ultrasound exposure. The cells were examined up to 37 days after a single exposure and authors demonstrated abundant microvilli and cell pro-ections, indicating a hereditary change in the cell membrane after at least 50 generations (cell cycle time 16 hours). Shape changes in sonicated erythrocytes were described by HRAZDIRA [8]. The postsonication ultrastructural changes [9] included an increasing number and clustering of perichromatin granules, invagination of cytoplasm into the nuclear domain, separation of nuclear membrane leaflets and aggregation microtubules around the nucleus.

The authors showed that up to one week after sonication the cells continued to divide normally, but there were dramatic differences in mobility and surface behaviour. The authors concluded that low level pulsed ultrasound could alter both the cellular ultrastructure and metabolism. They suggested that persistance of disturbances in cell mobility many generations after sonication was especially important, and it can be speculated that if embryonic cells were to be subtly damaged by ultrasound, it might affect cell migration during ontogenesis.

In our laboratory, in accordance with the results mentioned above the alterations of growth properties of sonicated cells were observed. However, in contrast with results of LIEBESKIND *et al.* [9] significant stimulation of cell growth was demonstrated after the action of ultrasound intensity of 1.0 kWm^{-2} during 8 passages after sonication. Microstreaming and shear stress were suggested as the main components of ultrasonic action on cell culture growth stimulation.

5. Conclusions

In the first series of our experiments the Madine-Darby bovine kidney cell cultures were used. The decrease in viability and the degenerative morphological changes in cells immediately after the action of low intensity ultrasound were proved.

In the second series of experiments the primary calf cell cultures were sonicated using ultrasound intensity range from 1.0 kWm^{-2} to 10.0 kWm^{-2}. The growth properties of sonicated cells were evaluated at different time intervals after ultrasonic action. Significant stimulation of the cell growth was demonstrated after action of ultrasound intensity of 1.0 kWm^{-2} during 8 passages. However, after the action of ultrasound intensities above 3.0 kWm^{-2}, inhibition of the cell growth was found. In the future these findings would be completed by quantitative analysis of cell growth parameters with special respect to the behaviour of cells influenced by ultrasound over the intensity range from 1.0 kWm^{-2} to 3.0 kWm^{-2}. The results described have shown that further studies along this line are needed.

References

[1] J. ADLER, I. HRAZDIRA, *The evaluation of ultrasonic action by means of cell electrophoresis,* Scripta medica Fac. Med. Univ. Brun. Purk., **53**, 329-332 (1980).

[2] M. L. BUNDY, J. LERNER, D. L. MESSIER, J. A. ROONEY, *Effects of ultrasound on transport in avian erythrocytes,* Ultrasound Med. Biol., **4**, 259-262 (1978).

[3] P. R. CLARKE, C. R. HILL, *Physical and chemical aspects of ultrasonic disruption of cells,* J. Acoust. Soc. Am., **50**, 649-653 (1970).

[4] M. DVOŘÁK, I. HRAZDIRA, *Changes in the ultrastructure of bone narrow cells in rats following exposure to ultrasound,* Zschr. Mikroskop. Anat. Forsch., **75**, 451 (1967).

[5] C. R. HILL, *Manual of health aspects of exposure to non-ionizing radiation,* WHO Regional Office for Europe, Kopenhagen 1977.

[6] I. Hrazdira, *Changes in cell ultrastructure under direct and indirect action of ultrasound,* in: J. Böck, K. Ossoinig, Ultrasonographia medica, **1**, 457-463 (1971).

[7] I. Hrazdira, J. Adler, *Electrokinetic properties of isolated cells exposed to low levels of ultrasound,* in: *Ultrasound interactions in biology and medicine,* Plenum Publishing Corporation, 1983, 165-168.

[8] I. Hrazdira, V. Procházka, *Ultrazvuk jako echinocytární faktor,* Slov. lek. listy (in press).

[9] D. Liebeskind, R. Bases, M. Koenigsberg, L. Koss, C. Raventos, *Morphological changes in the surface characteristics of cultured cells after exposure to diagnostic ultrasound,* Radiology, **138**, 419-423 (1981).

[10] M. J. Lota R. C. Darling, *Changes in permeability of red blood cell membrane in a homogeneous ultrasonic field,* Arch. Phys. Med. Rehab., **36**, 282-287 (1955).

[11] E. Siegel, J. Goddard, A. E. James Jr., E. P. Siegel, *Cellular attachment as a sensitive indicator of the effects of diagnostic ultrasound exposure on cultured human cells,* Radiology, **133**, 175-179 (1979).

ARCHIVES OF ACOUSTICS
9, 1-2, 29-34 (1984)

THE ULTRASONIC NONLINEARITY PARAMETER FOR BIOLOGICAL MEDIA

F. DUNN, W. K. LAW, L. A. FRIZZELL

Department of Electrical Engineering, Bioacoustics Research Laboratory, University of Illinois
(1406 West Green Street, Urbana, Illinois 61801, USA)

The nonlinearity parameter B/A of several soft tissues was measured using two independent methods. The B/A values of most soft tissues were found to be between 7 and 8, with the exception of fat which has a B/A value close to 11. It is proposed that structural hierarchy contributes to the B/A values of tissues.

1. Introduction

Ultrasound has been used extensively in the diagnosis of diseases and in therapeutic applications and its employment continues to increase. However, evidence is accumulating to indicate that ultrasonic propagation associated with biomedical applications may not always be considered linear [3, 4, 10]. The effects of the nonlinear propagation, which include harmonic generation, additional attenuation over that expected from the fundamental frequency component alone, increased heat development, and change in beam profile, can have important consequences on both the diagnostic and therapeutic applications. It is believed that detailed understanding of these nonlinear phenomena should lead to improved accuracy and increased information from procedures using diagnostic instruments. With regard to the therapeutic application, additional understanding should lead to more sophisticated control of heat deposition in the selected tissue volumes.

In order to predict accurately the effect of nonlinear propagation of ultrasound in biological media, it is necessary first to determine the degree of nonlinearity that the medium itself exhibits. Two independent methods of measuring the nonlinearity parameter in biological materials have been developed for this purpose. The first method, the finite amplitude technique, determines

the nonlinearity parameter in a medium by measuring the magnitude of the second harmonic generated. This method has the potential for use in making *in vivo* measurements. The second method, the thermodynamic technique, involves determination of the change of sound speed with hydrostatic pressure and temperature. The accuracy of the thermodynamic technique is superior to that of the finite amplitude technique, though it is limited to *in vitro* measurements only. This paper is a report on the *in vitro* measurement of the nonlinearity parameter in soft tissues by both techniques. Based on the present tissue observation, and previously reported observations with tissue models, it is proposed that the B/A value (the nonlinearity parameter) for biological materials reflects structural hierarchy.

2. Methods of measurement

For a nonlinear fluid medium, the relation between p, the pressure of the liquid, and ϱ, the density, is nonlinear and can be expressed in a Taylor's series expansion of p about the point of equilibrium density and entropy (ϱ_0, s_0), [2]

$$p = p_{\varrho_0,s_0} + A\frac{(\varrho-\varrho_0)}{\varrho_0} + \frac{1}{2}B\frac{(\varrho-\varrho_0)^2}{\varrho_0^2} + \ldots; \tag{1}$$

$$A = \varrho_0\left(\frac{\partial p}{\partial \varrho}\right)_{\varrho_0,s_0};$$

$$B = \varrho_0\left(\frac{\partial^2 p}{\partial \varrho^2}\right)_{\varrho_0,s_0}.$$

From (1) and from the definition of sound speed,

$$c^2 = \left(\frac{\partial p}{\partial \varrho}\right)_{\varrho_0,s_0}, \tag{2}$$

it is possible to express the ratio of the coefficient of the quadratic term to that of the linear term, B/A, as

$$\frac{B}{A} = 2\varrho_0 c_0\left(\frac{\partial c}{\partial p}\right)_{\varrho_0,s_0}. \tag{3}$$

Equation (3) is the basis for the thermodynamic method for determining B/A, the nonlinear parameter, since ϱ_0, c_0, and $(\partial c/\partial p)_{\varrho_0,s_0}$ are quantities that can be determined experimentally. However, for experimental ease, it is desirable to transform equation (3) using thermodynamic relations and to deal with conditions of constant temperature and pressure, instead of constant

entropy. The new expression [1] is

$$\frac{B}{A} = 2\varrho_0 c_0 \left(\frac{\partial c}{\partial p}\right)_{T,s} + \frac{2c_0 T\beta}{C_p}\left(\frac{\partial c}{\partial T}\right)_{p,s}, \tag{4}$$

where T is temperature in degrees Kelvin, p is the pressure, C_p is the heat capacity per unit mass at constant pressure and β is the volume coefficient of thermal expansion. For the materials of interest in this study, the second term in equation (4) is less than 5 per cent as compared to the first term so that the precision required in determining β and C_p is not very stringent. By measuring the change of sound speed with pressure and temperature, together with a knowledge of the density and sound speed and an estimation of the values for β and C_p, the parameter B/A can be determined. Details of the instrumentation and procedures of the technique are described in Ref. [9].

The finite amplitude method involves measurement of the magnitude of the second harmonic component at several distances from the sound source and then extrapolation to the source to eliminate the effect of absorption in the medium. For a medium with near linear frequency dependence of absorption, specifically $(\alpha_2 - 2\alpha_1) < 1/2$, where α_1 and α_2 are, respectively, the absorption coefficients at the fundamental and second harmonic frequencies, the magnitude of the second harmonic component, averaged over a phase sensitive receiver the same size as the source, can be written as

$$p_2(z) = p_0^2(z)\left(\frac{B}{A} + 2\right)\frac{\pi f}{2\varrho_0 c_0^3}\exp\left[-\left(\alpha_1 + \frac{\alpha_2}{2}\right)z\right]F(z), \tag{5}$$

where z is the axial distance from the sound source, f is the frequency of the fundamental, p_0 is the average source pressure at the fundamental frequency, and $F(z)$ is a correction term for the diffraction effect of the finite aperture sound source [5, 6]. Over the range of distances between one and three centimeters from the source, $F(z)$ is an exponentially decreasing function. When $p_2(z)/p_0^2(z)$ is extrapolated exponentially to the source, one may write

$$\left.\frac{p_2(z)}{p_0^2(z)}\right|_{z\to 0} = \left(\frac{B}{A} + 2\right)\frac{\pi f}{2\varrho_0 c_0^3}\left.F(z)\right|_{z\to 0}. \tag{6}$$

For a 1/2″ diameter sound source resonating at 4 MHz, $F(z)|_{z\to 0}$ is 0.91. The value of B/A can then be calculated using equation (6) when $p_2(z)/p_0^2(z)|_{z\to 0}$ and c_0 are measured. Details of the instrumentation for the finite amplitude technique and for sample preparation are described in Ref. [6].

3. Results and discussion

Results of B/A measurements in soft tissues are shown in Table 1. The finite amplitude technique was emphasized in these measurements because of the possibility of extending it to *in vivo* measurements in the future. Tissue samples were obtained from different animals for each of the measurements.

Table 1. B/A value in soft tissues measured by the thermodynamic and the finite amplitude methods

Material	Thermodynamic method	Finite amplitude method
water	5.31	5.5 ±0.5*
beef liver	7.23, 7.0	7.7 ±0.9**
pig fat	10.9	11.0, 11.3
beef heart		6.75, 7.4
pig muscle		7.53, 8.1
beef brain		7.6

Entries represent single measurements, except those otherwise labelled.

* Average of seven samples, ** average of five samples

It is observed that B/A values of soft tissues range from about 7 to 8, with the exception of fatty tissues, which have a B/A value of approximately 11. The variations in B/A value for samples of the same tissue type can be as high as ±10 per cent. It is not clear whether such variation results from differences in B/A values of different specimens, or is caused by artifacts arising from tissue preparation, e.g., phase cancellation induced by inhomogeneities in the tissues, or air bubbles resulting from autolysis after excision.

The typical B/A value of a soft tissue is greater than that of a protein solution of the same dry weight content [8], and yet with the exception of fatty tissues, 70 per cent of the dry weight content of the tissues measured are proteins [7]. This observation suggests that besides the protein concentration, other factors exist to contribute to the B/A value of tissues. Based on observations reported previously [6, 8, 9], the structural hierarchy of the material being measured is believed to be one of these factors. The B/A value of blood, which has higher structural hierarchy than a simple protein solution because the hemoglobin solution is contained within a membranous enclosure, has a slightly greater B/A value than a protein solution of the same dry weight content. Whole liver, which is much more complex in structure than blood, has a correspondingly greater B/A value. Homogenization of the liver, which destroys an unspecified portion of the structure, decreases the B/A value.

4. Concluding remarks

It is felt that the knowledge of the nonlinearity of the medium provides information for better understanding of the propagation details of ultrasound in tissues. Further, this should lead to improvements of present diagnostic and therapeutic applications of ultrasound, and may actually provide information about the structure of these media not available through existing means of tissue characterization.

References

[1] R. T. Beyer, *Parameter of nonlinearity in fluids,* J. Acoust. Soc. Am., **32**, 719-721 (1960).

[2] R. T. Beyer, *Nonlinear acoustics,* Naval Ship System Command, Dept. of the Navy, 1974, 91-164.

[3] E. L. Carstensen, W. K. Law, N. D. McKay, T. G. Muir, *Demonstration of nonlinear acoustical effects at biomedical frequencies and intensities,* Ultrasound Med. Biol., **6**, 359-368 (1980).

[4] E. L. Carstensen, A. S. Becroft, W. K. Law, D. B. Barbee, *Finite amplitude effects on the thresholds for lesion production in tissue by unfocused ultrasound,* J. Acoust. Soc. Am., **70**, 302-309 (1981).

[5] W. N. Cobb, *Finite amplitude method for the determination of the acoustic nonlinearity parameter B/A,* J. Acoust. Soc. Am., **73**, 1525-1532 (1983).

[6] F. Dunn, W. K. Law, L. A. Frizzell, *Nonlinear ultrasonic wave propagation in biological materials,* IEEE Ultrasonics Symposium, 1981, 527-532.

[7] S. A. Goss, L. A. Frizzell, F. Dunn, *Dependence of the ultrasonic properties of biological tissue on constituent proteins,* J. Acoust. Soc. Am., **67**, 1041-1044 (1980).

[8] W. K. Law, L. A. Frizzell, F. Dunn, *Ultrasonic determination of the nonlinearity parameter B/A for biological media,* J. Acoust. Soc. Am., **69**, 1210-1212 (1981).

[9] W. K. Law, L. A. Frizzell, F. Dunn, *Comparison of thermodynamic and finite amplitude methods of B/A measurement in biological materials,* J. Acoust. Soc. Am., **74** (1983) (in press).

[10] T. G. Muir, E. L. Carstensen, *Prediction of nonlinear acoustical effects at biomedical frequencies and intensities,* Ultrasound Med. Biol., **6**, 345-357 (1980).

ARCHIVES OF ACOUSTICS
9, 1-2, 35-40 (1984)

THRESHOLDS OF BIOLOGICAL ACTION OF ULTRASOUND

VALENTIN AKOPYAN

Moscow Veterinary Academy (109472, Moscow, Scriabina, 23, USSR)

The character of the regulative mechanisms in a cell depends on the degree to which the intracellular medium has changed and, hence, on the degree of change in the cell membrane permeability which is dependent on the intensity of ultrasound action. Therefore, for biological action, the threshold intensity is the intensity below which there appear no changes in the cell membrane permeability. Judging by well-known data, this threshold is $\leqslant 0.1$ kWm^{-2} (1 MHz). In a certain interval of higher ultrasound intensitities no visible changes are observed in the structure and function of cells, which is due to the development of the regulative processes. The upper limit of this interval represents another "registered" threshold of biological action of ultrasound (~ 1 kWm^{-2}). In a definite interval of ultrasound intensities exceeding 1 kWm^{-2} the observed biological effects are reversible. The upper limit of this interval (10 kWm^{-2}) can be taken as still another threshold.

The values of thresholds of biological action of ultrasound are of practical interest for ultrasound diagnostics, therapy and surgery. However, experimental determination of thresholds involves certain difficulties in each particular case, and extrapolation of values, characterizing the biological effect on threshold intensity of ultrasound, does not give the same results. There are a lot of cases [20] when bioeffects are produced at ultrasound intensities much less than the generally accepted curve obtained by means of extrapolation [18].

It seems possible to use another approach to the determination of thresholds of ultrasound bioeffects which is based upon a probable model of the mechanism of biological action of ultrasound.

A chain of successive reactions of cells to ultrasound action can be considered as such a model. The first reactions of this chain are due to physicochemical factors — mechanical, heat and chemical — which form the biological action of ultrasound. The effectiveness of separate factors which constitute the ultrasound action depends on the ultrasonic parameters and experimental conditions in different ways. Yet, each of these factors is capable of influencing

the cell microenvironment and changing the substance transport through its membrane.

Thus, mechanical factors in the ultrasound field — variable displacements, gradients of vibrating velocity, radiation pressure, microstreamings — can change the cytoplasma viscosity [11], disturb the concentration gradients in the immediate vicinity of cell membrane [5], cause barodiffusion processes [15]. In all cases, the final result will be the change of conditions of transport of polar and non-polar molecules as well as ions through cell membrane.

Mechanical action upon cell membranes is greatly increased under the conditions of stable cavitation, which is observed at diagnostic ultrasound intensities [25] in certain cases.

The possibility of ultrasound action on the structure of the membrane itself was not taken into account in the above consideration. Nevertheless, already at rather small ultrasound intensities biomacromolecule desorption from the cell surface is observed [3, 17]. As a result, the conditions for monitoring membrane charges change, which also influences their permeability [2].

Intensive microstreamings are capable of breaking the integrity of cell membrane through the holes in which cell content flows out. This effect can be considered as a limit case of the change of conditions of substance transport through the cytoplasma membrane at ultrasound irradiation.

Also, an increase in temperature at the expense of absorption of ultrasound energy changes the conditions of substance transport in biological media. Each degree of temperature increase (in the field of 35-45°C) leads to a 2-3 per cent decrease in the viscosity of water and water solutions and a 3-5 per cent one in the viscosity of lipids. The coefficients of diffusion and self-diffusion increase correspondingly. The transfer conditions can be changed as well at the expense of thermodiffusion due to temperature gradients appearing when biological media [16] are irradiated by ultrasound.

According to calculations the Debye potential (otherwise called vibropotential) occurring in cell suspention and in tissues under the action of therapeutic ultrasound reaches a value comparable with the cell membrane potential [1]. The pulses of intensive ultrasound used in diagnostics can be responsible for tissue vibropotentials reaching hundreds of mV. Vibropotentials can cause depolarization of cell membranes and, therefore, an increase in permeability, at least with respect to ions.

The probability of the appearance of transient cavitation in biological tissues becomes possible if the intensity of ultrasound irradiation exceeds 3 kWm^{-2} (*SA*) [4]. In this case along with energetic microstreamings, thermal gradients and the Debye potentials, the permeability of cell membranes may be influenced by hydrogene peroxide [23] and, perhaps, by the ultraviolet component of ultrasound luminescence as well [19]. However, the effects due to hydrogene peroxide and ultrasound luminescence can most probably be neglected in comparison with those due to the influence of intensive microstreaming accompanying cavitation.

It follows from the above that the change in the cell membrane permeability is a universal reaction to ultrasound action no matter which of the ultrasound factors influencing the cells prevails in a particular case.

The change of transport of various substances through the cell membrane is, in turn, responsible for the disturbance of the composition of the intracellular medium and the cell microenvironment. The concentration of substances within the cell and near the membrane changes and along with it there are changes in the ratio of their concentrations. The disturbance of these compositions cannot but have an effect on the rates of biochemical reactions with the participation of enzymes being quite sensitive to the content of particular ions in the medium.

In some cases, the change of medium composition within the cell can lead to an acceleration in enzymatic reactions, since in physiological conditions most enzymes function without realizing their catalytic possibilities to the full extent. It is at the expense of this kind of reserve that the regulation of rates of enzymatic reactions in the cell is carried out [12]. This means that the regulation of enzymatic reactions is likely to take place in cells at low ultrasonic intensity when the disturbance of membrane permeability is slight and when changes in the cell do not exceed the possibilities of its regulating systems.

As the ultrasound intensity increases the effect of suppression of enzymatic reactions in the cell becomes more likely, since as a result of depolarization of the cytoplasmatic membrane the concentration of potassium ions in the intracellular medium decreases as the concentration of sodium ions increases [27]. A lot of intracellular enzymes are activated by potassium ions. Their activation by sodium ions is observed to be much less [14].

As a result of suppresion of catalytic processes in the cell, after a while there appears to be a deficiency of some metabolites and the reparative systems of the cell speed up the synthesis of new enzymes. A large number of investigations have confirmed the fact of acceleration of protein synthesis in cells and tissues as well as increase of RNA content in these tissues necessary for new synthesis, if biological objects are irradiated by low intensity ultrasound [7, 8, 26, 28].

Summing up the results of the above reasoning one can build up the following chain — a hypothetical mechanism of ultrasound action on the cell: Physico-chemical ultrasound effects → disturbance of microenvironment of cell membranes → change of cell membrane transport → disturbance of composition of intracellular medium → change of rates of enzymatic reactions in the cell → appearance and development of reparative reactions in the cell.... A lot of well known facts can be accounted for by the mechanism suggested: for example, ultrasound causes a spontaneous contraction of muscles [9] and activates lymphocytes increasing cell membrane permeability with respect to calcium ions; it speeds up wound healing; it is responsible for an increase in the rate of synthesis of some proteins and RNA [8, 10, 26, 28]. These, as well as many other experimental facts, indicate that the suggested model — the mechanism of the biological action of ultrasound — reflects the actual state

of affairs. The above model allows the thresholds of biological action of ultrasound to be determined.

The character of the regulative and reparative processes in the cell depends upon the extent to which the intercellular medium has changed and, hence, upon the extent of changes in the cell membrane permeability which is, in turn, dependent on the duration and intensity of the action influencing membrane permeability. The reparative processes will not come into being and develop provided the changes in membrane permeability are too small. And so one of the possible definitions of the threshold of biological action of ultrasound follows from this.

For the biological action of ultrasound the threshold ultrasonic intensity is that below which there appear to be no changes in the permeability of cell membranes and therefore no regulative and reparative processes aimed at the elimination of consequences caused by these changes start in the cells. According to many researchers [6, 22, 29, etc.), this threshold does not exceed 0.1 kWm^{-2}.

In an interval of higher ultrasonic intensities, disturbances arising in cytoplasmatic membranes do not, as a rule, result in visible changes in the structure and function of the cell, which is due to the development of regulative processes compensating for the consequences of the change of membrane permeability directly during ultrasound irradiation. The upper intensity boundary of this interval can be accepted as another "registering" threshold of the biological action of ultrasound.

By the registered threshold of biological action of ultrasound we shall denote the value of its intensity above which one can observe morphological, electrophysical, physiological and other changes in biological systems both in the process of irradiation and after it.

The registered threshold corresponds to that found by NYBORG [18] and is in the range of 1 kWm^{-2}.

The observed biological effects are reversible in the particular interval of ultrasound intensities exceeding 1 kWm^{-2}. The upper boundary of this interval ($\gtrsim 10$ kWm^{-2}) can be taken to be another threshold. Exceeding this threshold results in pronounced destructive changes and with this background reparative processes in cells are not revealed. The ultrasound intensity of 10 kWm^{-2} is considered to be maximum in modern physiotherapy. Exceeding this intensity value leads as a rule to the suppression of protein and RNA synthesis, then the suppression of exchange processes in a cell and certain biological functions of organism [13, 28].

If the changes in biological object under the action of ultrasound not exceeding the possibilities of the regulative systems of the cell are considered to be such a result, then the threshold of biological action of ultrasound must be quite small (< 0.1 kWm^{-2}). If the result of biological action of ultrasound is a registered change observed after ultrasound treatment as well (which coincides

with the concept of "biologically significant effect" introduced by NYBORG [18]), then the threshold is approximately equal to 1 kWm^{-2}, although its value depends on the duration of irradiation. If we suppose that the results of ultrasound action are destructive changes in biological systems and these changes are due to transient cavitation or temperature increase to a level catastrophic for biological objects, then the threshold is $\geqslant 10$ kWm^{-2}.

All these three thresholds are relative and vary depending upon biological peculiarities and object state, duration of the ultrasound action and irradiation conditions, upon registered parameter and the sensitivity of the method used for registering this parameter.

References

[1] V. B. AKOPYAN, *The ultrasonic vibropotential in the biological action of ultrasound,* in: *Ultrasound in biology and medicine,* Proc. Symp. UBIOMED III, Nove Mesto na Morave 1977, 14.

[2] V. B. AKOPYAN, *The determination of biological action of ultrasound according to electrophysical properties of cell membranes,* Proc. All-Union Symp. Interaction of ultrasound with biological media, Pushchino, 1979, 22-23 (in Russian).

[3] V. B. AKOPYAN, *Action of ultrasound on cellular level,* in: *Ultrasound in biology and medicine,* Proc. Symp. UBIOMED V, Pushchino, 1981, 65-66.

[4] V. B. AKOPYAN, *Cavitation thresholds in biological tissues,* in: *Ultrasound interaction in biology and medicine,* Plenum Publ. Corp., New York 1983, 137-142.

[5] V. B. AKOPYAN, A. P. SARVAZYAN, *The investigation of mechanisms of ultrasound action on biological media and objects,* Acoust. J. **25**, 3, 462-463 (1979) (in Russian).

[6] D. W. ANDERSON, J. I. BARRETT, *Depression of phagocytosis by ultrasound,* Ultrasound in Med. and Biol., **7**, 3, 267-272 (1981).

[7] A. A. CHIRKIN, *Biochemical objective laws of the development of the organism responses to ultrasound,* in: Ultrasound in Biology and Medicine, Proc. Symp. UBIOMED-V, Pushchino, 1981, 101-102.

[8] M. DYSON, J. SUCHLING, *Stimulation of tissue repair by ultrasound,* Physiotherapy, **64**, 4, 105-108 (1978).

[9] G. W. GERSTEN, *Muscle shortening produced by ultrasound,* Phys. Med. Rehabilitation, **8**, 13, 83-87 (1957).

[10] W. HARWEY, M. DYSON, J. B. POND, R. GRAHAM, *The "in vivo" stimulation of protein synthesis in human fibroblastes by therapeutic level of ultrasound,* Proc. 2nd Europ. Congr. Ultrasound in Medicine, 1975, 10-21.

[11] A. JOHNSON, A. LINDWALL, *Effects of low-intensity ultrasound on viscous properties of Helodea cells,* Naturwiss., **56**, 1, 40 (1969).

[12] K. A. KAFIANI, *Regulation of fermentative system of cell metabolism,* in: *Ferments,* Moscow, "Nauka", 1964, 269 (in Russian).

[13] Z. V. KOBAKHIDZE, V. M. OKUJOVA, *State and perspectives of research of the physical basis of therapeutical usage of ultrasound,* Accoust. J., **25**, 3, 471-472 (1979) (in Russian).

[14] A. KOTYK, K. JANACEK, *Membrane transport,* Plenum Press, New York – London 1977, 341.

[15] I. LENART., D. AUSLÄNDER, *The effect of ultrasound on diffusion through membranes,* Ultrasonics, **18**, 5, 216-218 (1980).

[16] L. A. Lowe, F. W. Kremkan, *Intracellular temperature distribution produced by ultrasound,* J. Acoust. Soc. America, **67**, 3, 1045-1050 (1980).

[17] B. N. Nanjappa, H. K. Chang, G. A. Glomski, *Trauma of the erythrocytes membrane associated with low shear stress,* Biophys. J., **15**, 1212-1222 (1973).

[18] W. L. Nyborg, *Physical mechanisms for biological effects of ultrasound,* DHEW Publ. Maryland 1978, 59.

[19] R. O. Prudhomme, Th. Guilmar, *Photogenese ultraviolette par irradiation ultrasonore de l'eau en présence des gas rares,* J. Chim. Phys. et Phys. -Chim. Biol., **54**, 4, 336-340 (1957).

[20] A. P. Sarvazyan, *Some general problems of biological action of ultrasound,* preprint of Academy of Sciences of the USSR, Pushchino 1981, 37.

[21] M. R. Sikov, B. P. Hildebrand, *Embriotoxity of ultrasound exposure at ten or twelve days of gestation in the rat,* Ultrasound in Medicine, Plenum Press, New York—London 1978, **4**, 599-600.

[22] I. E. Smolen, S. B. Shoket, *Permeability changes induced by peroxidation in liposomes prepared from human erythrocyte lipides,* J. Lipid Res., **15**, 3, 273-280 (1974).

[23] K. J. W. Taylor, J. B. Pond, *A study of the production of haemorragic injury and paraplegic in rat spinal cord by pulsed ultrasound in low megaherz frequencies in the context of the safety for clinical usage,* Br. J. Radiol., **45**, 533, 343-352 (1972).

[24] G. ter Haar, S. Daniels, K. C. Eastoogh, C. R. Hill, *Ultrasonically induced cavitation in vivo,* Brit. J. Cancer, **45**, Suppl., 5, 151-155 (1982).

[25] L. M. Tkemaladze, *Action of ultrasound on dynamics of nucleic acids and histomorphological changes in liver,* Proc. Research Institute of Kurortology and Physiotherapy, Tbilissi, **29**, 49-55 (1967) (in Russian).

[26] Yu. M. Vaslev, A. G. Malenkov, *Surface of cells and cell reactions,* "Meditsina" Leningrad, 1969, 291 (in Russian).

[27] D. F. Webster, M. Dyson, W. Harwey, *Ultrasonically induced stimulation of collagen synthesis "in vivo"*, in: Ultrasound in Biology and Medicine, Proc. Symp. UBIOMED-II, Visegrad, 1979, **1**, 135-140.

[28] G. Yaroniene, *Response of biological systems to low-intensity ultrasonic waves,* II Congress FASE, Warszawa, 1978, **2**, 13-16.

ARCHIVES OF ACOUSTICS
9, 1-2, 41-50 (1984)

ESTIMATION OF CALCIFICATION DETECTABILITY IN BREAST TISSUES BY MEANS OF THE ULTRASONIC ECHO AND SHADOW METHODS

L. FILIPCZYŃSKI, G. ŁYPACEWICZ

Department of Ultrasound, Institute of Fundamental Technological Research, Polish Academy of Sciences
(00-049 Warsaw, ul. Świętokrzyska 21 Poland,)

Microcalcifications originate at an early stage of the breast cancer. Assuming their mechanical properties to be similar to those of the bone tissue, analysis was performed to find the smallest calcification size to be determined with ultrasonic echo and shadow methods. Taking into account the tissue interference background which has been determined experimentally, the electrical properties of the ultrasonograph and attenuation loss, basing on the theory of reflection from rigid and elastic spheres, the theoretical detectivity of calcifications in breasts could be estimated. It has been shown that at a frequency of 3 MHz spherical calcifications with the radii $a > 0{,}15$ mm situated at the depth $R = 4$ cm may be theoretically detected when using the echo method and a linear receiver.

With the shadow method calcifications with radii greater than $a = 1.5$ mm are estimated to be detectable. This could be shown theoretically and experimentally using spheres made of plasticine.

1. Introduction

The ultrasonic method is one of the more recent ways of detecting breast tumors [7]. The reactions which proceed in breast tissue cells and which cause calcifications when the cancer occurs are present at a very early stage of its development. They usually occur prior to the infiltration phase, which is visible in a mammogram or an X-ray microgram preparation [8]. In view of this, the question arrises as to what are the possibilities of detecting small calcifications by the ultrasonic method. This paper presents an attempt to explain the problem and to estimate the minimum calcification size which can be detected by the ultrasonic echo and shadow methods.

2. Assumptions of the analysis

It is assumed that the acoustic parameters of calcifications are the same as those of the bone tissue [11]; the longitudinal wave velocity $c_L = 3.2$ km/s, the density $\varrho = 2.23$ g/cm^3. As we do not have any information regarding the transverse wave velocity c_T, the Poisson ratio ν will be assumed in computations as a parameter. It is assumed that the calcification has the shape and properties of elastic and rigid spheres placed in a fluid medium (soft tissue).

3. Reflexion from the sphere

If $\lambda \ll a$, then the power contained in an area πa^2 of the incident beam is equal to the power reflected equally in all directions from a rigid sphere [9]. With p_0 denoting the acoustic pressure amplitude of the plane incident wave, ϱc the acoustic impedance of the soft tissue, we obtain at the distance $r \gg a$:

$$\pi a^2 p_0^2/2\varrho c = 4\pi r^2 p_s^2/2\varrho c, \tag{1}$$

or

$$p_s = p_0 \frac{a}{2r} f_\infty(ka) \tag{2}$$

where p_s denotes the acoustic pressure amplitude of the scattered wave, $f_\infty(ka)$ the far field form function. For a rigid sphere when $\lambda \ll a$ the function $f_\infty(ka) \to 1$; for an elastic sphere it depends on the elastic properties of the sphere, that of the surrounding medium, on the wavelength and on the sphere radius.

To determine the far field form function $f_\infty(ka)$ for the parameters of calcifications given above, a computer program was elaborated with different values of the Poisson ratio ν on the basis of the theory given by several authors [1, 5, 6]. Fig. 1 shows the results obtained [2]. It follows from these curves that the function $f_\infty(ka)$ does not depend on ν until the value $ka < 1.5$. Considering the Poisson ratio for various solids [2], it seems to us that for calcifications the value $\nu \approx 0.2$ may be assumed for the interval $ka = 1.5 \div 3$. For $ka > 3$ the far field form function $f_\infty(ka)$ shows many peaks which correspond to many resonances occurring in the sphere. FLAX *et al.* [3] has shown that in this case the scattering is the superposition of wave scattering by a rigid sphere and a number of resonances arising in the sphere. These resonances differ in character, since they correspond to different wave types, including, for example, also surface waves, of the "whispering gallery" type and so on.

Therefore, in the case of calcifications with irregular shapes and corrugated surfaces, one should expect that a number of resonances will not occur at all and the function $f_\infty(ka)$ will come closer to the curve for a rigid sphere. Thus we assume $f_\infty(ka) \approx 1$ for $ka > 3$ [2].

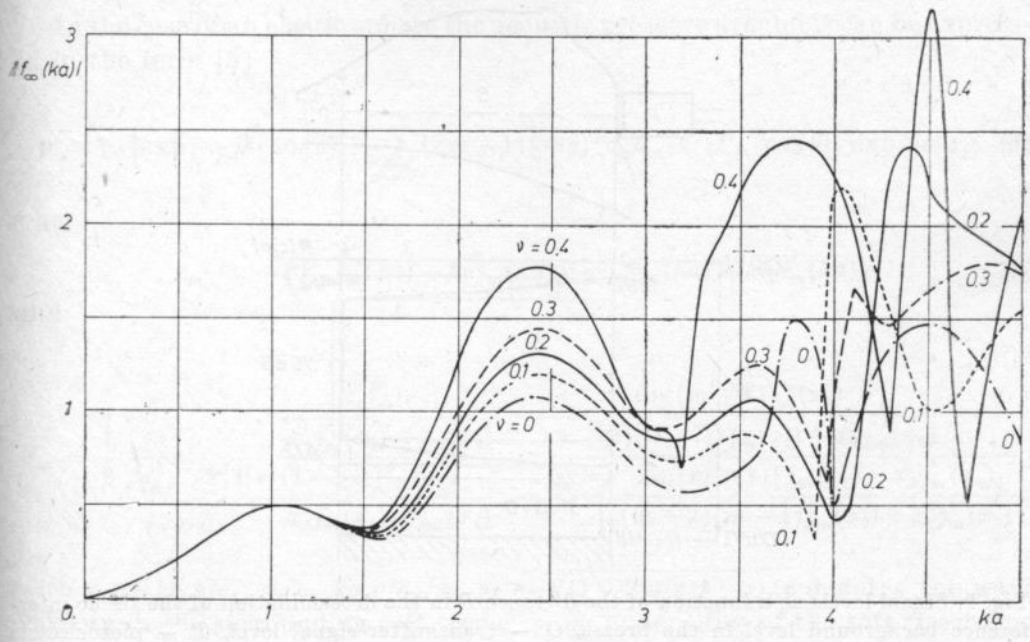

Fig. 1. The far field form function $f_\infty(ka)$ computed for an elastic spherical calcification model with various Poisson ratios ν

4. Detectability of calcifications with the echo method

For quantitative estimation of the detectability we assume the following typical parameters of the ultrasonograph [2]: sensitivity 10 μV, transmitter voltage (in pulse) 250 V, frequency 3 MHz, piezoelectric transducing losses — 15 dB, attenuation in breast tissue — 1.1 dB/MHz cm. Many echoes obtained at the boundaries of fat, fibre and gland tissues and on their inhomogeneities form a tissue interference background whose level is much higher than the electronic noise level of the ultrasonograph.

To determine this tissue interference background level, measurements were performed in the normal breasts of 30 women 25-45 years old by means of a USK 79/M ultrasonocardiograph [2] (frequency 3 MHz, transducer diameter 15 mm, weak focusing beam). The level of the tissue interference background was found to be $D = 31 \pm 4$ dB (in small breasts) and 49 dB (in large breasts) higher than the electronic noise level of the ultrasonocardiograph at a depth of 4 cm (Fig. 2). Taking into consideration the electronic noise level $N = -148$ dB (in respect to the transmitter voltage level), the value of D, piezoelectric transducing losses T, attenuation losses A, one obtains the remaining value of the electrical dynamics W for the ratio p_s/p_0. Hence from formula (2) one determines the product $ka = 1.9$ ($a = 0.15$ mm), of the sphere-shaped calcification which gives (in large breasts) an echo at the level of the tissue interference background $N + D$, at the depth $R = 4$ cm.

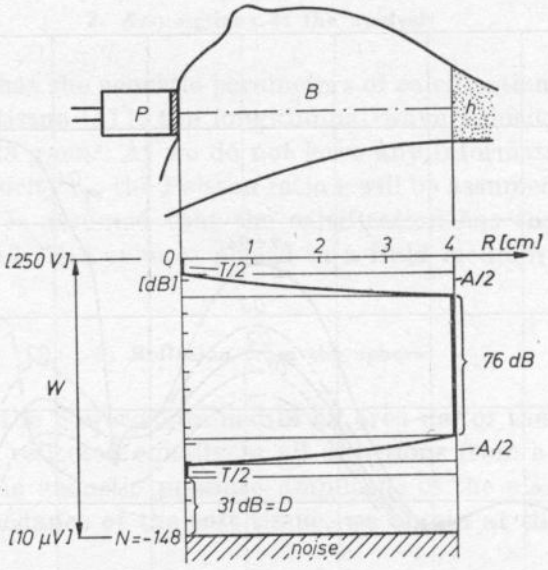

Fig. 2. Signal levels as a function of the distance R in the determination of the tissue interference background level in the breast, O — transmitter signal level, T — piezoelectric transducing losses, A — attenuation losses, N — electronic noise level, D — experimentally determined level increase due to the tissue interference background, W — electrical dynamics of the ultrasonograph, h — hypothetic tissue reflector, P — ultrasonic probe, B — breast

5. The shadow method

In this method one observes instead of the echo a shadow which occurs behind the calcification. It arises against the white background of many small echoes caused by the waves which are scattered by tissue inhomogeneities. Let us assume a rigid sphere as the model of the calcification. The acoustic field around the sphere can be expressed in the form [10],

$$p = p_0 \left\{ \exp(jkr\cos\vartheta) - \sum_{m=0}^{\infty} j^m (2m+1) \frac{j'_m(ka)}{h'_m(ka)} P_m(\cos\vartheta) h_m(kr) \right\} \exp(j\omega t), \quad (3)$$

where p denotes the acoustic pressure around the sphere, $k = 2\pi/\lambda$, $P_m(\cos\vartheta)$ — a Legendre polynomial, ϑ — the angle between the direction of the incident wave and the direction under consideration, h_m and h'_m — a spherical Hankel function of the second kind and its derivative, j' — a derivative of the spherical Bessel function, m — a natural number, $j = \sqrt{-1}$, ω — pulsation, t — time. To determine the shadow behind the rigid sphere from expression (3) a computer program was elaborated and the results are presented in Fig. 3. They show that the shadow starts forming when $ka = 10$; if $ka = 15$ the shadow becomes better visible; for $ka = 20$ and 25 it is very distinct.

In the case of an elastic sphere the acoustic pressure around it can be expressed in the form [5]

$$p = p_0\left\{\exp(-jkr\cos\theta) + \sum_{m=0}^{\infty}(2m+1)(-j)^m c_m h_m(kr) P_m(\cos\theta)\right\}\exp(j\omega t), \quad (4)$$

where

$$c_m = -[F_m j_m(ka) - ka j_m'(ka)]/[F_m h_m(ka) - ka h_m'(ka)] \quad (5)$$

and

$$F_m = \frac{1}{2}\frac{\varrho}{\varrho_s}x_2^2 \frac{\dfrac{x_1 j_m'(x_1)}{x_1 j_m'(x_1) - j_m(x_1)} - \dfrac{2m(m+1)j_m(x_2)}{(m+2)(m-1)j_m(x_2) + x_2^2 j_m''(x_2)}}{\dfrac{x_1^2\{[\nu/(1-2\nu)]j_m(x_1) - j_m''(x_1)\}}{x_1 j_m'(x_1) - j_m(x_1)} - \dfrac{2m(m+1)[j_m(x_2) - x_2 j_m'(x_2)]}{(m+2)(m-1)j_m(x_2) + x_2^2 j_m''(x_2)}}, \quad (6)$$

with $x_1 = ka\ c/c_L$, $x_2 = ka\ c/c_T$, $c_T = c_L\sqrt{(1-2\nu)/2(1-\nu)}$. c denotes the wave velocity in the surrounding soft tissue, ϱ, ϱ_s — densities of the soft tissue and the sphere, respectively, θ — the angle between the shadow axis and the direction under consideration. Fig. 4 shows angular distributions of the acoustic pressure amplitude computed from formulae ((4), (5), (6)) for various values of ka, when $\nu = 0.2$.

6. Experiments with sphere shadows

The experiments were performed with the same ultrasonocardiograph USK 79/M in water with suspended talcum powder. This enabled us to obtain an inhomogeneous medium and thus to make the shadow visible. The spheres used first were made of stainless steel and the next of plasticine. The last ones made it possible to eliminate internal multiple reflexions which distorted completely the shadows. The plasticine spheres with the radii $a = 2$, 1 and 0.5 mm were easily detected with the echo method as well as steel spheres and even steel wires with the radii 0.25 and 0.05 mm perpendicular to their axis and situated parallel to the ultrasonic beam.

The shadow behind the plasticine sphere was very distinct only when the radius was equal to $a = 4\lambda = 2$ mm ($ka = 25$), while for $a = 2.5\ \lambda = 1.25$ mm ($ka = 16$) it was difficult to observe, although readily seen in the photograph (Fig. 5). The visibility of the shadow also depends on the ratio of the shadow radius to the ultrasonic beam radius, which in our case was ~ 0.3. White points in the right picture, near to the left shadow zone, are caused by greater talcum particles suspended in water.

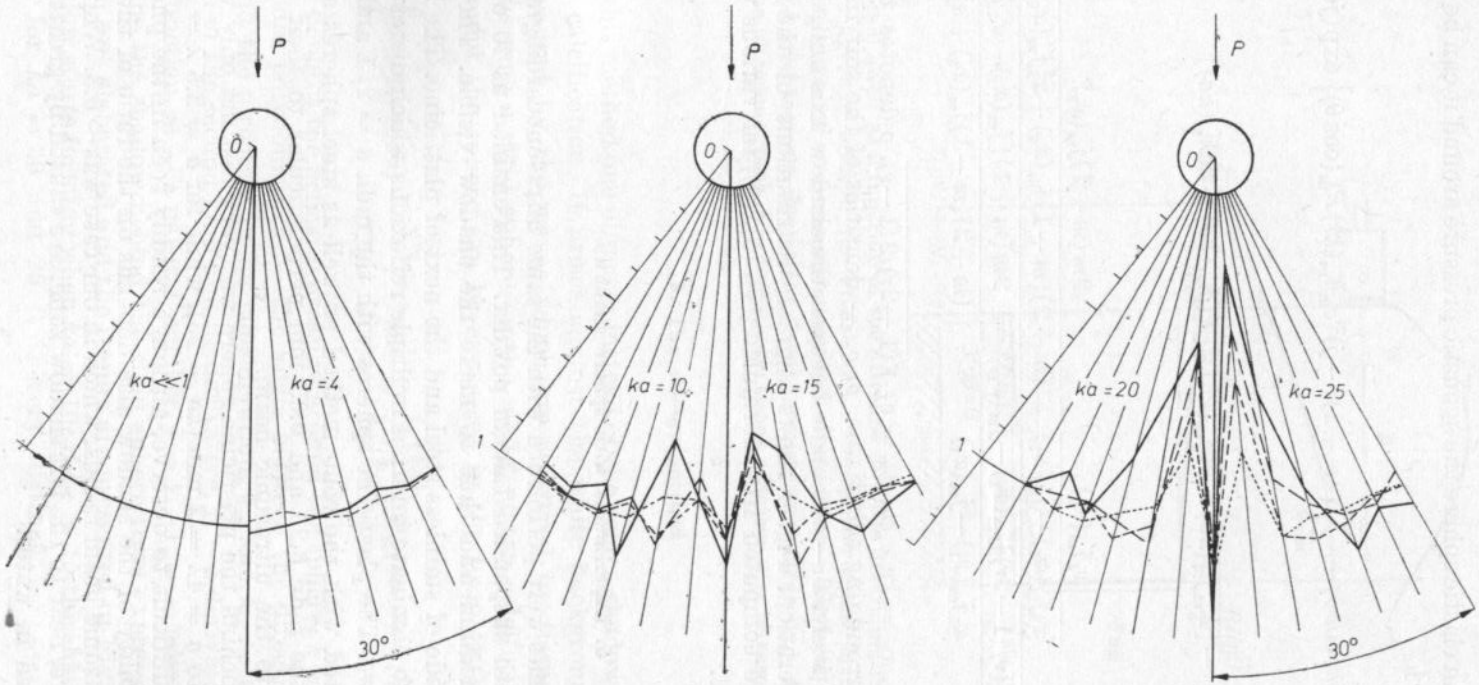

Fig. 3. The angular distribution of the acoustic pressure amplitude behind a rigid sphere. P — incident plane wave, a — radius of the sphere, r — distance from the sphere center, solid line — $r = 20\lambda$, long dashed line — $r = 40\lambda$, short dashed line — $r = 60\lambda$, dotted line — $r = 80\ \lambda$

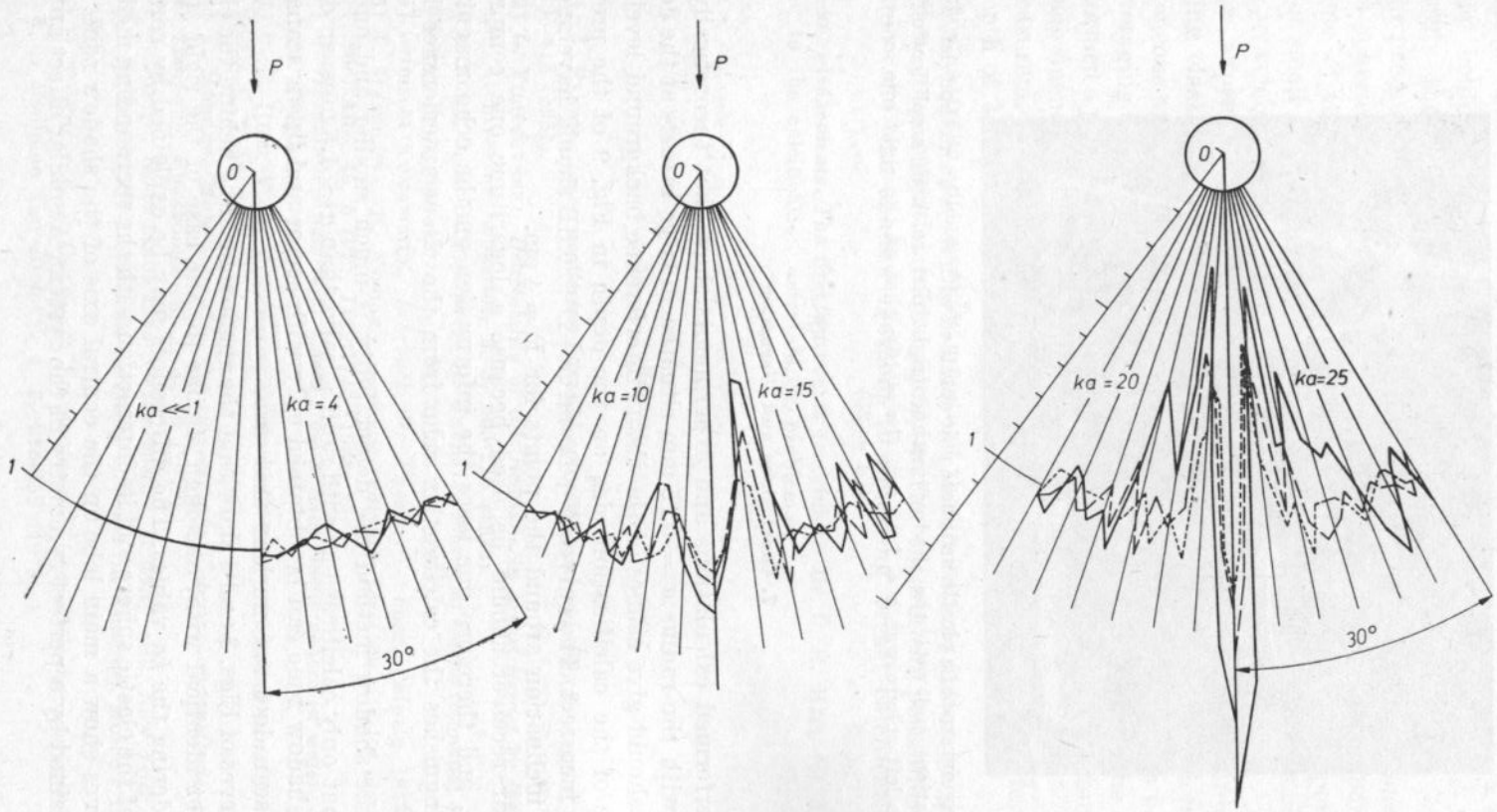

Fig. 4. The angular distribution of the acoustic pressure amplitude behind an elastic sphere (see Section 2) at the distance $r = 20\,\lambda$ (solid line), $r = 40\lambda$ (long dashed line) and $r = 60\lambda$ (short dashed line). Poisson ratio $\nu = 0.2$

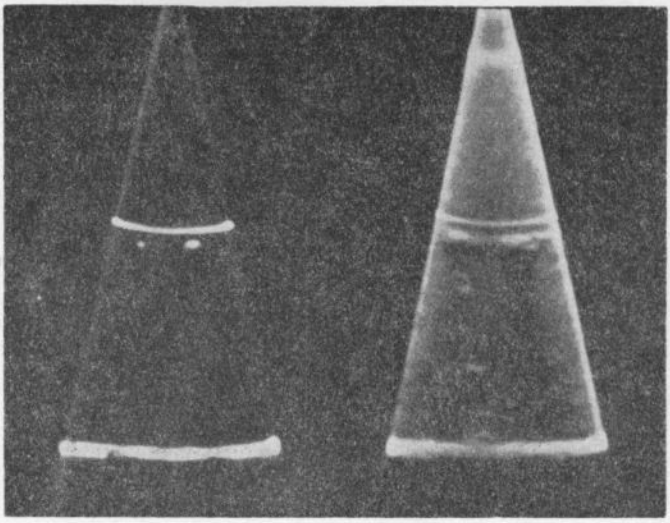

Fig. 5. Ultrasonograms of a plasticine sphere pair obtained with the echo method (left picture, low amplification) and with the shadow method (right picture, high amplification). The radius of the left sphere was $a = 1.25$ mm ($ka = 16$); that of the right one, $a = 2$ mm ($ka = 25$)

7. Conclusions and discussion

The performed calculations and experiments show that theoretically calcifications with the radius $a = 0.15$ mm situated in large breasts at the depths $R = 4$ cm, should give echoes of the tissue interference background level. The dependence of the calcification size on the depth in Fig. 9 of the previous paper [2] is incorrect. The curves $N+D$ and $N+D+20$ dB should have another shape and inclination around the points for $R = 4$ cm.

A linear receiver should be used because a logaritmic one compresses the signals, and therefore one loses the information on the echo magnitude, which distinguishes the calcification echo from the tissue interference background.

With the shadow method the detectability is much smaller and one can conclude that only calcifications with radii greater than $a \cong 1.5$ mm are detectable. The shadow zone can be obtained only with sector and linear scans, the compound scan does not work in this case.

The curves of Figs. 3 and 4 show that the shadow forming behind the elastic sphere is not identical with, although similar to, the case of the rigid sphere when considering the ka values. The differences may be explained by complex vibrations of the elastic sphere and its interaction with the surrounding medium. All the curves show a main lobe on the central axis of the shadow zone. This can be explained by a perfect symmetry of the system. A similar effect appears

in optics behind a circular screen where it is explained by means of Fresnel diffraction theory [4].

The present conclusions are based on a number of approximations which include a spherical shape of calcifications and their mechanical properties being the same as those of the skull bone. The steady-state analysis performed is valid for small calcifications; however, when the calcification size is comparable to the wavelength the obtained results are approximate.

Our experimental case did not correspond exactly to computed cases regarding elastic properties of the spheres. Also, the incident wave was not homogeneous and the ultrasonic beam scanned the spheres 25 times per second, thus averaging the shadow behind them. It was also assumed that the ultrasonic beam formed a parallel homogeneous wave, when a weak focusing beam was used in measurements of the tissue interference background.

Measurements of the tissue interference background were performed only at a depth of 4 cm.

It seems to the authors that in spite of the limitations discussed, the present estimation gives essential information on the theoretical possibilities of the ultrasonic echo and shadow methods in detecting breast calcifications.

Acknowledgements. The first author is grateful to Dr. C. R. HILL for drawing his attention to the calcification detectability problem.

References

[1] J. FARAN, *Sound scattering by solid cylinders and spheres,* J. Acoust. Soc. Am., **23**, 4, 405-418 (1951).

[2] L. FILIPCZYŃSKI, *Detectability of calcifications in breast tissues by the ultrasonic echo method,* Archives of Acoustics, **8**, 3, 203-220 (1983).

[3] L. FLAX, C. R. DRAGONETTE, H. UBERALL, *Theory of elastic resonance exitation by sound scattering,* J. Acoust. Soc. Am., **63**, 3, 723-731 (1978).

[4] Grimsehl TOMASCHEK, *Lehrbuch der Physik,* Teubner, Leipzig 1943, **II**, 589.

[5] T. HASEGAWA, K. YOSIOKA, *Acoustic radiation force on a solid elastic sphere,* J. Acoust. Soc. Am., **46**, 5 (P2), 1139-1143 (1969).

[6] R. HICKLING, *Analysis of echoes from a solid elastic sphere in water,* J. Acoust. Soc. Am., **34**, 1582-1592 (1962).

[7] C. R. HILL, V. R. MCCREADY, D. O. COSGROVE, *Ultrasound in tumor diagnosis,* Pitman Medical, Kent 1978.

[8] V. MENGES, *Mammographie, die zuvelässigste Untersuchungsmethode zur Brustkrebs-Früherkennung,* Electromedica, **2**, 42-49 (1979).

[9] O. MORSE, K. INGARD, *Theoretical acoustics,* McGraw Hill, New York 1968.

[10] S. N. RSHEVKIN, *Lectures on the theory of sound* (in Russian), Moscow University, Moscow 1980.

[11] D. N. WHITE, G. R. CURRY, R. J. STEVENSON, *The acoustic characteristic of the scull,* Ultrasound in Medicine and Biology, **4**, 3, 225-252 (1978).

ARCHIVES OF ACOUSTICS
9, 1-2, 51-56 (1984)

PHOTOACOUSTIC SPECTROSCOPY AS A METHOD IN BIOLOGICAL INVESTIGATIONS

JERZY MOTYLEWSKI, JERZY RANACHOWSKI

Institute of Fundamental Technological Research, Polish Academy of Sciences
(00-049 Warsaw, ul. Świętokrzyska 21, Poland)

The present paper describes a new method of photoacoustic spectroscopy for the investigation of the properties of materials. This method is applied in studies of both inorganic and organic materials, including biological structures.

The paper also gives the physical basis of the method, the construction principle of the measuring apparatus and examples of application of photoacoustic spectroscopy in biology and medicine.

Photoacoustic spectroscopy is based on the phenomenon observed for the first time by Graham BELL in 1880 [1]. He observed that when irradiating the solid body with light pulses, the acoustic signals, corresponding to the sequence of light pulses, occurred. A similar phenomenon consisting in generation of acoustic waves in a gas contained in a chamber and irradiated by a chopped light beam was reported in 1881 by John TYNDALL [2] and Wilhelm ROENTGEN [3].

Theoretical works concerning this effect were developed in recent years, mainly due to ROSENCWAIG and GERSHO [4, 5, 6]. Since that time (the seventies) we have noted a rapid development of methods of photoacoustic spectroscopy (PAS) applied to investigate the absorption processes in solid state, in liquids and in gases.

The PAS methods allow one to obtain the absorption spectra (similar to optical ones) for substances in any phase, and in any form, like powders, gels, coloids etc.

A particular advantage of PAS methods is the possibility of registering absorption spectra of substances characterized by a very large coefficient of light attenuation, which was obviously impossible to achieve by optical spectroscopy methods. In Poland PAS methods were studied in order to apply them to investigate the physico-chemical properties of various materials [7, 8].

Photoacoustic spectroscopy consists in placing the studied sample in a closed chamber and irradiating it by chopped light. The molecule excited by a

strong laser beam or by a xenon lamp returns to its ground state via the radiative or nonradiative disactivation processes. The nonradiative decay of excited states results in the production of heat, which causes local change in the temperature field T. This causes (e.g. during investigation of liquids) simultaneous local changes in the density field ϱ, in the pressure field p, and in the molecular velocity field $\boldsymbol{v}$. The state of the liquid before heating the particular region may be regarded as the equilibrium state, while the local heating causes the perturbation of this state.

Fluctuations of the density, pressure, molecular velocity and temperature fields are the parameters which characterize this perturbation. These fluctuations propagate from the region where the equilibrium is perturbed. When the fluctuations of density and pressure satisfy the conditions of small amplitude

$$\frac{|\delta\varrho|}{\varrho_0} \ll 1; \quad \frac{|\delta_p|}{p_0} \ll 1;$$

the equations of mass, momentum and energy conservation may be linearised. Thus one obtains a set of linear differential equations describing the propagation of the above mentioned perturbation as acoustical waves.

Assuming that there is no flow in the liquid being in the equilibrium state, i.e. that $\boldsymbol{v}_0 = 0$, we obtain equations of the following form:

— mass conservation equation

$$\frac{\partial(\delta\varrho)}{\partial t} + \varrho_0 \operatorname{div}(\delta\boldsymbol{v}) = 0; \tag{1}$$

— momentum conservation equation

$$\varrho_0 \frac{\partial(\delta\boldsymbol{v})}{\partial t} + \operatorname{grad}(\delta p) - \eta\Delta(\delta\boldsymbol{v}) - (\xi + \eta/3)\operatorname{grad}\operatorname{div}(\delta\boldsymbol{v}) = 0; \tag{2}$$

— energy conservation equation

$$\frac{\partial}{\partial t}(\varrho_0\delta E + E_0\delta\varrho) + \operatorname{div}[\varrho_0 w_0 \delta\boldsymbol{v} - \varkappa \operatorname{grad}(\delta T)] = 0; \tag{3}$$

where η — dynamical viscosity (internal friction), ξ — bulk viscosity, $\varkappa$ — coefficient of heat conduction, δE — perturbation of internal energy with respect to its equilibrium value, E_0 — equilibrium value of the specific internal energy, w_0 — equilibrium value of the specific enthalpy.

Perturbation of the medium may be described by means of the Fourier integral of harmonic perturbations with respect to time. In this sense, one may assume that the perturbation generates a beam of acoustic harmonic plane waves. In the case when the effects of viscosity and heat conduction can be neglected, and when one may assume that the propagation of perturbations

is an adiabatic process, then the wave equation for the perturbation δF of the physical quantity F is as follows:

$$\frac{\partial^2(\delta F)}{\partial t^2} = c^2 \nabla^2(\delta F), \tag{4}$$

where c — the velocity of propagation of the perturbation, F — one of physicall quantities, ϱ, p, v.

Considering the photoacoustic phenomenon one has to take into account the relations between three important factors: μ_a — the depth of light penetration into the investigated material; μ_s — depth of heat penetration, and l — thickness of the sample. Moreover, the power of the light source, the frequency of modulation of the light beam, the properties of the gas surrounding the sample in chamber, the state of the sample surface and the properties of the material which fastens the sample in the chamber, also influence the photoacoustic phenomenon.

In the PAS method one applies two basic types of measurement apparatus:
— spectrometers with a single light beam,
— spectrometers with a double light beam.

The prototype of the photoacoustic spectrometer was worked out at the Institute of Fundamental Technological Research. It is shown in Fig. 1. It is a single beam spectrometer with a xenon lamp being the source of exciting light.

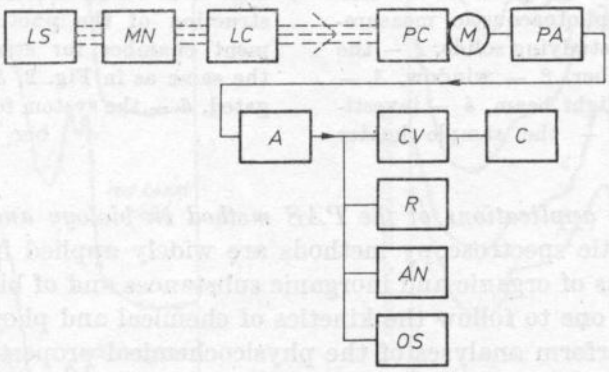

Fig. 1. A block diagram of the single beam photoacoustic spectrometer. *LS* — light source, *MN* — monochromator, *LC* — light beam chopper, *PC* — photoacoustic measurement chamber, *M* — microphone, *PA* — preamplifier, *A* — measuring amplifier, *CV* — analogue-to-digital converter, *C* — computer, *R* — registration apparatus, *AN* — spectrum analyzer, *OS* — oscilloscope

This spectrometer consists of three basic parts:
— light excitation system;
— measurement chamber with a microphone;
— electronic measuring and analyzing system.

The measurement chamber containing the sample of the material investigated is an essential part of the photoacoustic spectrometer. The acoustic receiving transducer is an integral part of this chamber. In the spectrometer prototype there is a possibility of applying exchangeable measurement chambers depending on the kind of investigated substance.

Figs. 2, 3 give examples of constructions of such chambers for investigating solids and liquids.

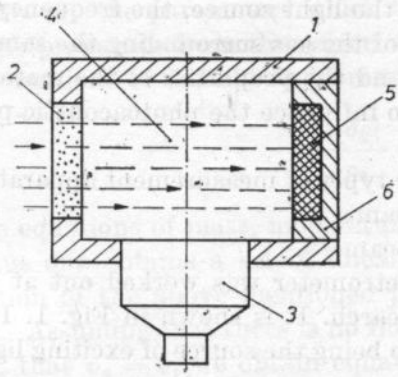

Fig. 2. A schematic diagram of the construction of the photoacoustic measurement chamber for studying solids. *1* — the body of the chamber, *2* — window, *3* — microphone, *4* — light beam, *5* — investigated sample, *6* — the sample holder

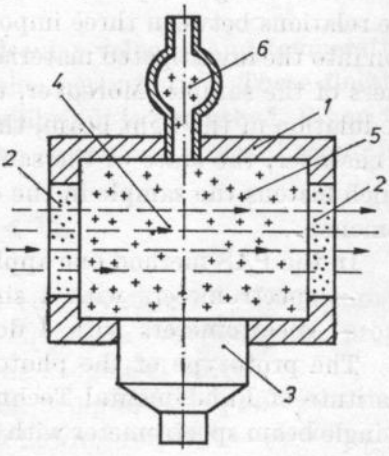

Fig. 3. A schematic diagram of the construction of the photoacoustic measurement chamber for studying liquids. *1-4* the same as in Fig. *2*, *5* — liquid investigated, *6* — the system for filling the chamber

Examples of the applications of the PAS method in biology and medicine

Photoacoustic spectroscopy methods are widely applied in physicochemical investigations of organic and inorganic substances and of biological structures. PAS allows one to follow the kinetics of chemical and photochemical reactions, and to perform analyses of the physicochemical properties of materials. PAS enables one to detect vestigial guantities of substances like and groups, enzymes, metalic inclusions etc. Apart from technical applications, the PAS method is particularly advantageous in biological and medical studies. In this case it is possible to investigate dead and living tissues and organisms. The PAS method was applied to study the structure of samples, to estimate the growth of colonies of bacteria, to follow the development of tumours, etc. Examples of the photoacoustic spectra for sick and healthy human eye lenses are given in Fig. 4 [6]. Fig. 5 shows the PAS spectrum of whole blood [6].

The presence of protein and lipid material in whole blood, which causes so much difficulty in conventional spectroscopy from light scattering, creates

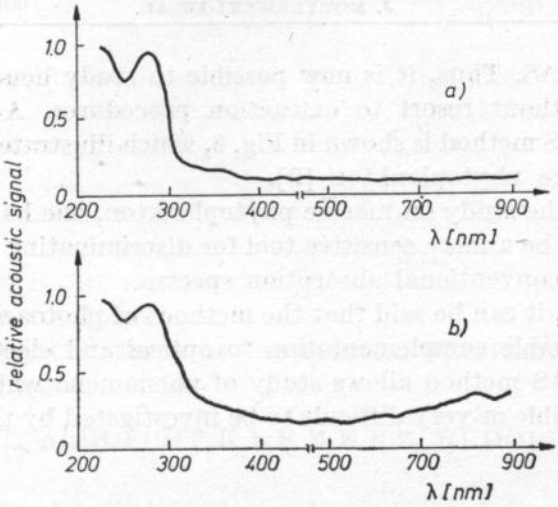

Fig. 4. The PAS spectrum of the lens of the human eye [6]. *a*) healthy lens, *b*) the lens with cataract

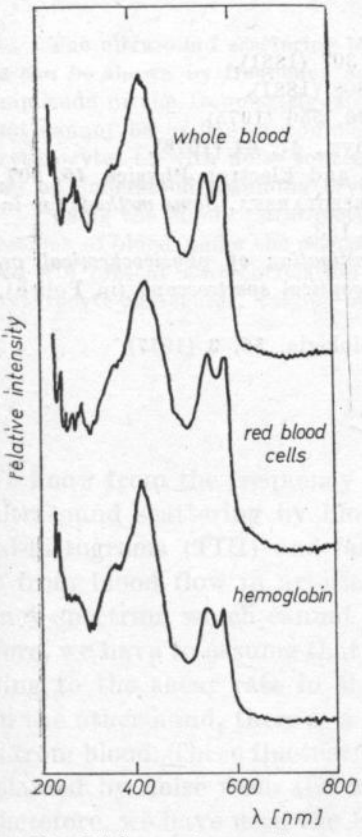

Fig. 5. The PAS spectrum of smears of whole blood, red blood cells and hemoglobin [6]

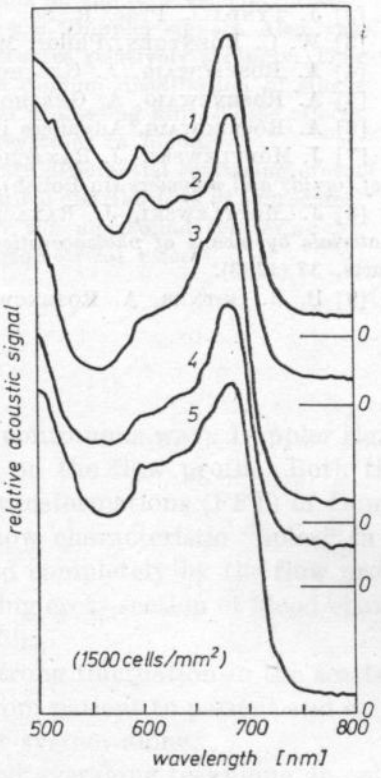

Fig. 6. Photoacoustic spectra of representative marine phytoplankton [9]; *1* — thalasiosira, *2* — coccolithus, *3* — pyramimonas, *4* — dunaliella, *5* — platymonas

no problem in PAS. Thus, it is now possible to study hemoglobin directly in whole blood, without resort to extraction procedures. Another example of the use of the PAS method is shown in Fig. 6, which illustrates the photoacoustic spectra of marine phytoplankton [9].

Concerning the study on marine phytoplankton, one has to admit that the PAS method can be a more sensitive tool for discriminating quite similar specimens than the conventional absorption spectra.

In summary, it can be said that the methods of photoacoustic spectroscopy constitute a valuable complementation to optical and electrical spectroscopic methods. The PAS method allows study of phenomena which, in many cases, are either impossible or very difficult to be investigated by the existing conventional methods.

References

[1] A. G. Bell, Am., J. Sci., **20**, 305 (1880).

[2] J. Tyndall, Proc. R. Soc. London, **31**, 307 (1881).

[3] W. C. Roentgen, Philos. Mag., **11** (5), 308 (1881).

[4] A. Rosencwaig, A. Gersho, Science, **190**, 556 (1975).

[5] A. Rosencwaig, A. Gersho, J. Appl. Phys., **47**, 64 (1976).

[6] A. Rosencwaig, Advances in Electronics and Electron Physics, **46**, 207 (1978).

[7] J. Motylewski, J. Ranachowski, J. Rzeszotarska, *Some methods for investigation of liquids and polymers* (in Polish), IPPT, 1979, 183.

[8] J. Motylewski, J. Ranachowski, *Investigation of physicochemical properties of materials by means of photoacoustical and acoustooptical spectroscopy* (in Polish), IFTR Reports, 37 (1983).

[9] P. B. Ortner, A. Rosencwaig, Hydrobiologia, **56**, 3 (1977).

ARCHIVES OF ACOUSTICS
9, 1-2, 57-66 (1984)

MONTE CARLO CALCULATIONS OF ULTRASOUND SCATTERING BY BLOOD

ULRICH COBET, ALBRECHT KLEMENZ, RUDOLF MILLNER

Institute of Applied Biophysics, Martin-Luther-Universität
(4014 Halle/Saale, Strasse d. DSF 81, GDR)

The ultrasound scattering by blood depends on the flow velocity profile, as can be shown by frequency analysis of the *c.w.* Doppler signals. Also, the amplitude of the Doppler signals received fluctuates relatively strongly. This fact cannot be explained completely with the random distribution of single erythrocytes or with noise sources in the signal processing unit. These effects can be understood assuming erythrocyte aggregations in blood.

Using the Monte Carlo method we calculate differential scattering cross-sections of blood under the assumption of empirical distributions of aggregates. We will present auto-correlation functions for the ultrasound scattering by erythrocyte-aggregates, taking into account geometrical effects.

1. Introduction

We know from the frequency analysis of continuous wave Doppler signals that ultrasound scattering by blood depends on the flow profile. Both time-interval-histograms (TIH) and fast-Fourier-transformations (FFT) of Doppler signals from blood flow in arterial vessels show characteristic "holes" in the frequency spectrum which cannot be explained completely by the flow profile. Therefore, we have to assume that the scattering cross-section of blood changes according to the shear rate in the flow profile.

On the other hand, there is a relatively strong fluctuation in the scattered signals from blood. These fluctuations differ from patient to patient and cannot be explained by noise from the measurement system alone.

Therefore, we have used the ECG-triggered averaging technique, in on-line with a computer, for more than 4 years [4]. By this method we have achieved an essential improvement, both in the Doppler pulsation curves and in their reproducibility [8].

The Monte Carlo calculations of ultrasound scattering were carried out to improve understanding of these influences. Theories on the ultrasound scattering of statistically distributed inhomogenities have been given in the works of RAYLEIGH [11], CHERNOW [3], FOLDY [5], TWERSKY [13], MORSE and INGARD [9], and applied to biological tissues by NICHOLAS [10] and WAAG [14]. The ultrasound scattering of blood has been calculated by BRODY and MEINEL [2], SHUNG *et al.* [12], ANGELSON [1] and HANSS and BOYNARD [6].

Nevertheless, a whole series of requirements must be met in order to obtain an analytical solution. The most essential requirements are:

1. The validity of the Born approximation, i.e. that the disturbance of the incident wave by the particles remains slight. The kinematic theory of wave diffraction is then valid.

2. The radius of the scatterers should be small compared to the wavelength.

3. The mean distance between the scatterers should be large compared to the wavelength. For other cases an empirical autocorrelation function of the spatial distribution of the scatterers is introduced. In many cases the autocorrelation function found by LIEBERMANN [7] when investigating inhomogenities in the ocean, is used. This autocorrelation function is transfered to the calculation of the ultrasound scattering of biological tissues.

On the one hand, the mean distance of scatterers in human blood at a level of 45 per cent in a normal hematocrite is small compared to the wavelength. On the other hand, small changes in the autocorrelation function have important influence on the results.

4. The dimensions of the scattering region should be large in comparison to both the wavelength and the correlation length of the ultrasound wave.

If we compare these results quantitatively we find that

— the results differ to varying degrees;
— they also differ from the experimental values given by SHUNG *et al.* [12];
— the influences of geometric interferences are not taken into account;
— there is either no or incorrect information on the signal fluctuation.

2. Monte Carlo model 1

The spatial co-ordinates x_i, y_i and z_i are calculated by the means of three random numbers, and thus the position of the scatterer in the scattering region is ascertained. In order to compare our results with those in the aforementioned literature, a spherical scattering region is adopted too. Therefore, a conversion to polar co-ordinates follows (Fig. 1):

$$r_i = R\sqrt[3]{x_i};\ \varphi_i = 2\pi y_i; \quad \vartheta_i = \pi z_i, \tag{1}$$

when R is the spherical radius of the scattering region.

We assume the incident wave in the direction of the unit vector $\mathbf{s}_0$, and the scattered wave in the direction $\mathbf{s}$ beneath the scattering angle θ, to be even.

Furthermore it is assumed that the receiver is situated in the farfield of the scattering region (Frauenhofer's diffraction). The scattered wave now under-

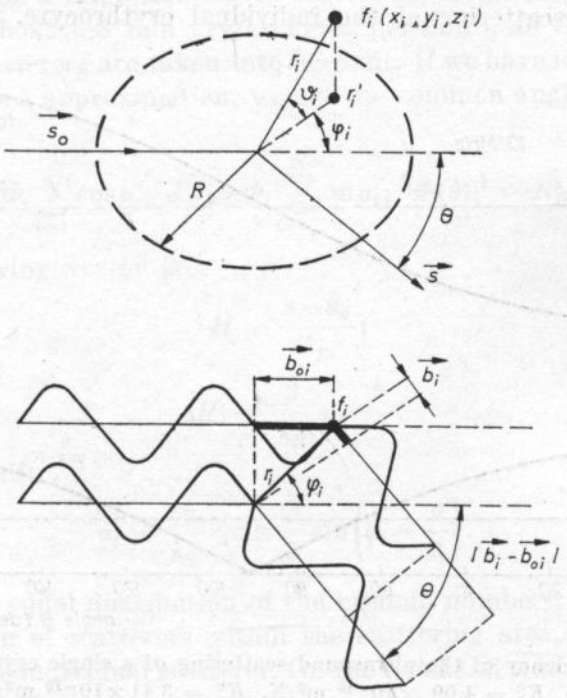

Fig. 1. Scattering geometry

goes a phase shift that depends on the spatial co-ordinates of the particle and on the scattering angle a_i

$$a_i = \frac{2\pi}{\lambda}(\boldsymbol{b}_i - \boldsymbol{b}_{0_i}), \tag{2}$$

where λ is the wavelength, $\boldsymbol{b}_{0_i}$ the projection of r_i on the unit vector $\mathbf{s}_0$ and $\boldsymbol{b}_i$ the projection on $\mathbf{s}$.

We must add that the scattered wave goes through an additional phase shift on each particle.

The angle-dependent scattering factor of a single erythrocyte $\varphi(\theta)$; with

$$p_s(r, \theta) = A \frac{\exp(jkr)}{r} \Phi(\theta), \tag{3}$$

where A is equal to the amplitude of the incident wave, $k = 2\pi/\lambda$ the number of waves and p_s the scattered ultrasound pressure; was calculated for a non-

rigid sphere with a constant volume: $V_0 = 4\pi a_0^3/3$. The angle-dependent scattering factor consists of 3 components: an inhomogenity of compressibility, density and, to a lesser extent, of viscosity (Fig. 2).

Inhomogenities of compressibility and viscosity act as monopole sources. The sum of the three components yields — with regard to the phase shifts — a preferred backscattering of the individual erythrocyte.

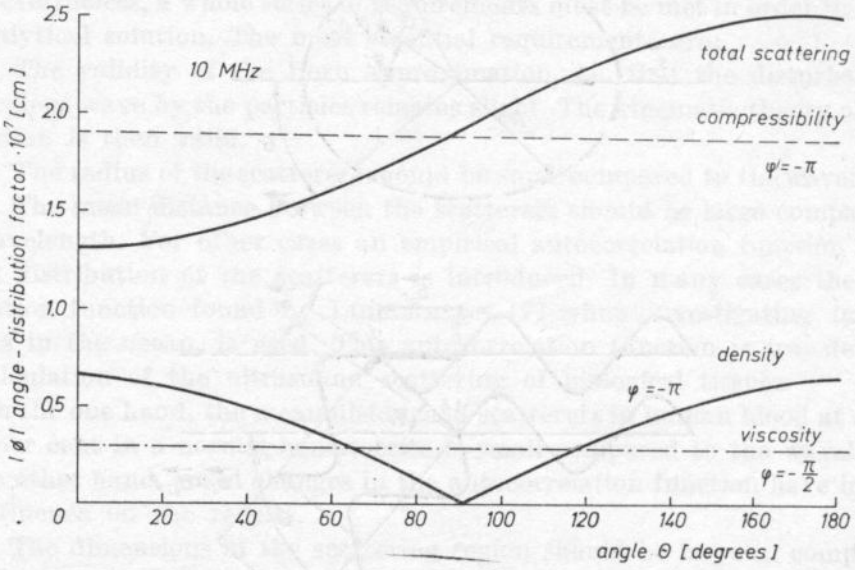

Fig. 2. Angle-dependency of the ultrasound scattering of a single erythrocyte at 10 MHz, where $a_0 = 2.75$ µm, $K_0^c = 4.09 \times 10^{-10}$ m²/N, $K_n^c = 3.41 \times 10^{-10}$ m²/N, $\varrho_0 = 1.03$ g/cm³, $\varrho_n = 1.09$ g/cm³, $\alpha_0 = 0.056$ cm^{-1}, $\alpha_n = 0.56$ cm^{-1}, φ the phase shift of the erythrocyte

Although too high a viscosity for the erythrocytes was assumed, the viscosity contributed relatively little to the total scattering as a result of the phase shift of $-\pi/2$. The Born approximation produces a simplified solution which gives a good approximation of erythrocytes up to $ka < .5$ regardless of their shape — whether spherical or rouloux aggregates:

$$\Phi_i = \frac{1}{4\pi} k_R^2 V_0 \left(\frac{K_n^c - K_R^c}{K_R^c} + \frac{\varrho_n - \varrho_R}{\varrho_n} \cos\theta \right), \tag{4}$$

where the mean number of waves in the coherent solution is

$$k_R = \varrho_R \cdot k_R \cdot \omega^2 \tag{5}$$

and the mean compressibility (K_R^c) and the mean density (ϱ_R):

$$K_R^c = K_0^c + h' \cdot (K_n^c - K_0^c); \quad \frac{1}{\varrho_R} = \frac{1}{\varrho_0} + h' \left(\frac{1}{\varrho_n} - \frac{1}{\varrho_0} \right), \tag{6}$$

with the number of hematocrites being $h' = V_0 N'$ and $N' = \bar{N}/V$ the mean number of particles $\bar{N}$ per volume V (where V_0 is the volume of the individual scatterer, K_n^c and ϱ_n the compressibility and density of the scatterer, K_0^c and ϱ_0 those the surrounding medium, and ω the radian frequency).

In the case of a large number of scatterers, for example a hematocrite of 45 per cent (about 6-8 mln erythrocytes per mm³), all the phase shifts of the individual scatterers are taken into account. If we have identical scatterers and adapt the Born approximation, we get the common angle-dependent scattering factor:

$$R_H = \Phi_i \sum_{i=1}^{N} \cos a_i; \; J_H = \Phi_i \sum_{i=1}^{N} \sin a_i; \; |\Phi(\theta)|^2 = R_H^2 + J_H^2, \tag{7}$$

where the scattering vector is

$$\boldsymbol{H} = \frac{\boldsymbol{s} - \boldsymbol{s}_0}{\lambda_R}; \qquad |H| = \frac{2}{\lambda_R} \sin \frac{\theta}{2}, \tag{8}$$

and the phase shift

$$a_i = \frac{2\pi}{\lambda_R} r_i' \sin \frac{\theta}{2} \sin\left(\varphi_i - \frac{\theta}{2}\right). \tag{9}$$

If we use an equal distribution of the random numbers, we obtain an isotropic distribution of scatterers within the scattering area. Fig. 3 shows the interference of the individual scatterer. On the left-hand side we see the projec-

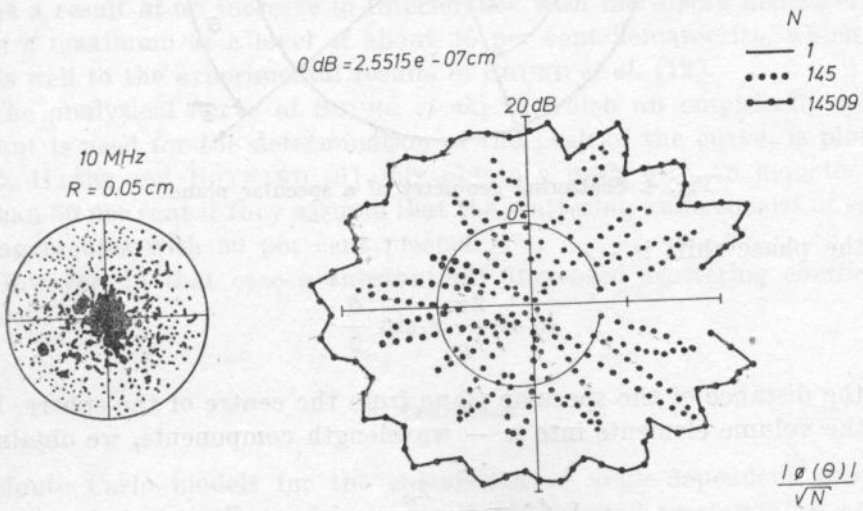

Fig. 3. Angle-dependent ultrasound scattering at 10 MHz of a blood-filled sphere with a radius; $R = 0.05$ cm

tion of the spatial distribution of the scatterers in the sphere. This is calculated using random numbers. In this example of a relatively small sphere with a radius $R = 1$ cm, we find that, in addition to a geometric effect, all contributions from the individual scatterers add up by analogy with the coherent solution (9).

However, calculations for a large number of particles would have required a relatively long period of time. For this reason we developed a second, simplified Monte Carlo model for higher hematocrite values.

3. Monte Carlo model 2

We collected all volume elements ΔV_i of the same phase shift a_i (Fig. 4). The respective volume elements were calculated to

$$\Delta V_i = 2\pi R^2 \cdot \Delta x - \frac{2}{3}\pi \Delta x^3 - 2\pi x_i^2 \Delta x, \tag{10}$$

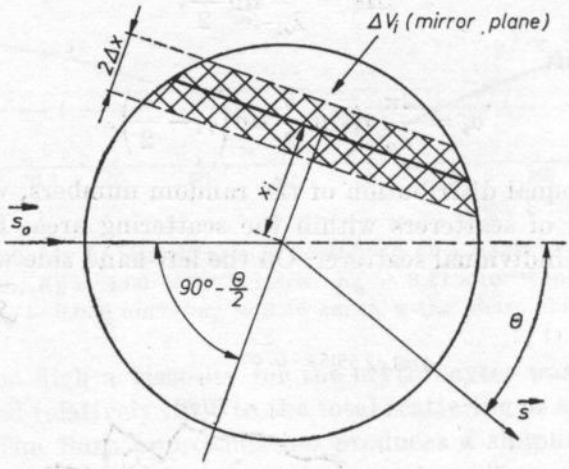

Fig. 4. Scattering geometry of a specular plane

where the phase shift is

$$a_i = \frac{2\pi}{\lambda_R} x_i \sin\frac{\theta}{2} \tag{11}$$

and x_i the distance of the specular plane from the centre of the sphere. If we divide the volume elements into n — wavelength components, we obtain

$$\Delta x = \frac{\lambda_R}{4n \sin\dfrac{\theta}{2}}. \tag{12}$$

The number of scattering particles that are contained in the volume element, must be calculated using a random number W_i. We assume that the number of scatterers in the volume element is Poisson distributed.

Thus:

$$W_i = \exp(-N' \Delta V_i) \frac{(N' \Delta V_i)^N}{N!}. \tag{13}$$

The number of scatterers N in the volume element ΔV_i with the phase shift a_i is calculated using a random number W_i.

Since the sum of Poisson distributed processes is also Poisson distributed, all specular planes of equal phase shift at the spacing

$$\Delta x_m = \frac{\lambda_R}{2 \sin \frac{\theta}{2}} \tag{14}$$

can be collected.

Fig. 5 gives the calculated scattering coefficient

$$\frac{\sigma_s}{V} = \frac{|\Phi(\theta)|^2}{V} \tag{15}$$

for the back-scattering as the function of the hematocrite of the Monte Carlo calculations (model 2), in comparison to the quantities given by RAYLEIGH [11], SHUNG *et al.* [12], HANSS and BOYNARD [6], MORSE and INGARD [9].

As a result of an increase in interference with increasing hematocrite, we obtain a maximum at a level of about 20 per cent hematocrite, which corresponds well to the experimental results of SHUNG *et al.* [12].

The analytical curve of SHUNG *et al.*, in which an empirically adjusted constant is used for the determination of the peak of the curve, is plotted in Fig. 5. HANSS and BOYNARD [6] only obtain a peak with an hematocrite of less than 50 per cent if they assume that the scattering units consist of erythrocyte aggregates with 50 per cent plasma.

However, in that case a substantially increased scattering coefficient is obtained.

4. Conclusion

Monte Carlo models for the calculation of angle-dependent ultrasound scattering of statistically and isotropically distributed scatterers by adopting the Born approximation for continuous waves, have been given. The calculated results correspond well to the experimental values of the aforementioned lite-

rature. It is possible to study independently the influences of geometrical interferences, signal fluctuations, the correlation length of ultrasound impulses and the influence of the density of aggregates with this method.

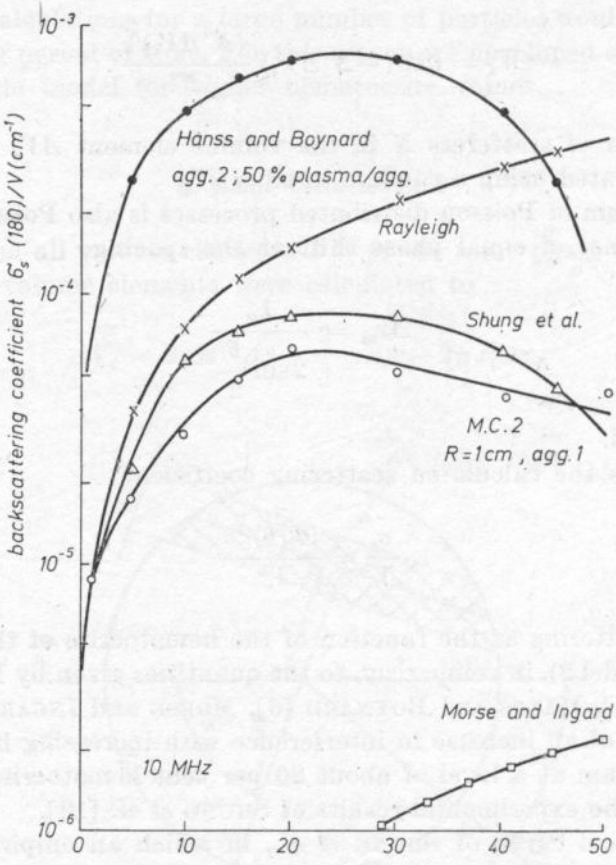

Fig. 5. The ultrasound back-scattering dependent upon the hematocrite mean values over 10 Monte Carlo calculations ○, in contrast to SHUNG *et al.* [12] △, RAYLEIGH [11] ×, and HANSS and BOYNARD [6] ●

References

[1] B. A. J. ANGELSEN, *A theoretical study of scattering of ultrasound from blood,* IEEE Trans. on Biomed. Eng., **BME — 27**, 61-67 (1980).

[2] W. R. BRODY, D. J. MEINDL, *Theoretical analysis of the cw-Doppler ultrasonic flowmeter,* IEEE Trans. on Biomed. Eng., **BME — 21**, 183-192 (1974).

[3] L. A. CHERNOW, *Wave propagation in a random medium,* Dover, New York 1960.

[4] U. COBET, R. SCHARF, A. KLEMENZ, R. MILLNER, *Das UBD-2 ein Ultraschall--Blutflußdoppler für Forschung und Routine,* Wiss. Beiträge d. Martin-Luther-Univ. Halle--Wittenberg, **63 R 59**, 33-36 (1979).

[5] L. L. FOLDY, *The multiple scattering of wave: general theory of isotropic scattering by randomly distributed scatterers,* Phys. Rev., **67**, 107-119 (1945).

[6] M. HANSS, M. BOYNARD, *Ultrasound back scattering from blood: hematocrite and erythrocyte aggregation dependence,* in: *Ultrasonic tissue characterization II,* Ed. M. LINZER, National Bureau of Standards, Spec. Publ. 525, Washington, D. D., 165-169 (1979).

[7] L. J. LIEBERMANN, *The effect of temperature inhomogeneities in the ocean on the propagation of sound,* J. Acoust. Soc. Am., **23**, 563 (1951).

[8] R. MILLNER, U. COBET, A. KLEMENZ, G. BLUMENSTEIN, *Möglichkeiten der Ultraschall-Doppler-Untersuchungen bei höheren Frequenzen,* Therapiewoche, **32**, 5082-5088 (1982).

[9] P. M. MORSE, K. U. INGARD, *Theoretical acoustics,* McGraw Hill, New York 1968.

[10] D. B. NICHOLAS, *An introduction to the theory of acoustic scattering by biological tissues,* in: *Recent advances in ultrasound in biomedicine,* **1**, D. N. WHITE (ed.), Research Studies Press, Forest Grove 1-28 (1978).

[11] Lord RAYLEIGH, *Theory of sound,* Dover, New York-London 1945.

[12] K. P. SHUNG, R. A. SIGELMANN, J. M. REID, *The scattering of ultrasound by blood,* I.E.E.E. Trans. on Biomed. Eng., **BME — 23**, 6, 460-467 (1976).

[13] V. TWERSKY, *On scattering of waves by random distribution, I. Free space scatterer formalism,* J. Math. Phys., **3**, 700-723 (1962); *II. Two space scatterer formalism,* J. Math. Phys., **3**, 724-734 (1962).

[14] R. C. WAAG, P. P. K. LEE, Q. M. LERNER, L. P. HUNTER, R. GRAMIAK, E. A. SCHENK, *Angle scan and frequency-swept ultrasonic scattering characterization of tissue,* in: *Ultrasonic tissue characterization, II,* M. LINZER (ed.), National Bureau of Standards, Spec. Publ. 525, Washington D. C., 143-152 (1979).

ARCHIVES OF ACOUSTICS
9, 1-2, 67-74 (1984)

FOCUSED ULTRASOUND AS A STIMULATOR OF THE NERVE STRUCTURES

L. R. GAVRILOV

Acoustical Institute, USSR Academy of Sciences
(USSR, 117036 Moscow V-36, USSR)

Pulsed focused ultrasound can stimulate the receptor and conductive nerve structures of man and animals, as well as neurons of the central nervous system of the invertebrates. The possibility of a wide practical use of this method in medicine and physiology is considered. For example, the stimulating ability of focused ultrasound is applied for neurological disease diagnosis, to study skin and tissue sensitivity of man, to diagnose hearing disorders and to introduce auditory information to the deaf with certain forms of hearing pathology. The effecting factors of focused ultrasound as a stimulus for nerve structures irritation are discussed.

1. Introduction

It was shown in our previous investigation [1-4] that pulses of focused ultrasound with the duration of the order of parts and units of milliseconds could stimulate various human peripheral receptor structures. The main advantages of the ultrasonic method for stimulation of nerve structures are as follows. The use of this method makes it possible not only to avoid operative intervention for effect on deep structures, but also ensures precise control of stimulus characteristics: intensity, duration of action, as well as change of area to be stimulated, if necessary. All this holds much promise for application of focused ultrasound as a stimulus of nerve structures.

2. Stimulation of skin and tissue receptors and neurons

Using pulses of focused ultrasound directed towards sensitive points of man's arm, it is possible to evoke sensations, the character of which depends on the parameters of ultrasonic action and localisation of the focal region [1–4]. By applying different ultrasonic intensities and action durations it is possible to evoke all the sensations that a man can perceive through his skin: tactile,

tickling, temperature (warmth and cold), pain, etc. Pain sensations can be evoked by focused ultrasound stimulation not only of surface nerve structures, but also of deep ones.

Experiments on the invertebrates (edible snail) showed the possibility of using focused ultrasound for stimulation not only of receptor structures but also of central nerve structures. The thresholds for stimulation of the latter proved to be much higher than those for stimulation of receptors. For instance, the thresholds of the oscillation displacement amplitude that corresponded to the stimulation of receptor and central nerve structures of the snail were 0.1 and 0.25 μm, respectively. The results of these studies form the basis for promotion of similar investigations on the vertebrates including mammals.

3. Diagnosis of neurological diseases

The ultrasonic method was employed to diagnose a number of neurological diseases relating to changes of skin sensitivity [4]. The frequency of ultrasound was 1.95 MHz. A comparison was made between tactile sensations on the skin of the fingers in a control group of healthy people (21 subjects) and 30 patients with 8 forms of neurological diseases. All the patients showed deviation of tactile sensitivity from normal: ranging from considerable increase of tactile thresholds up to the entire absence of tactile sensitivity.

For example, Fig. 1 presents the results of examination of the tactile

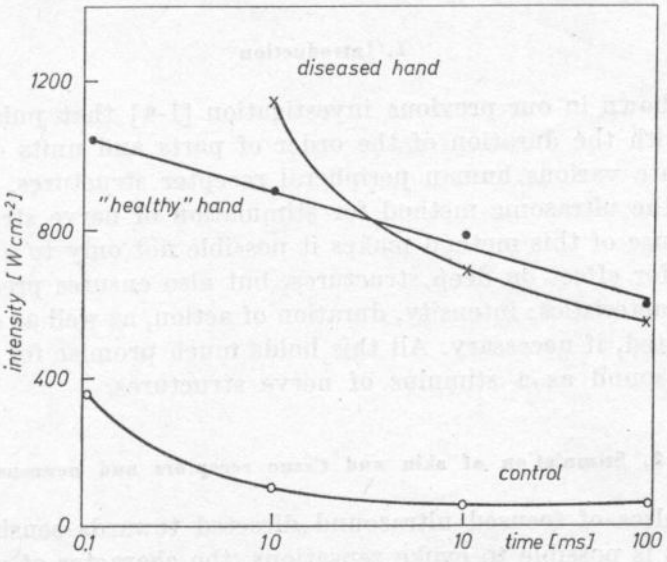

Fig. 1. Tactile sensitivity thresholds in the patient with syringomyelia: ○ — thresholds in normal people (control group); × — thresholds in the right (affected) hand; ● — thresholds in the left hand, where clinico-neurological examination showed no sensitivity disorders

sensitivity in one of the patients with syringomyelia. The y-axis is the intensity of ultrasound in the focal region, the x-axis is the stimulus duration. One can see that with the stimulus duration 0.1 ms the tactile sensitivity on the right (affected) hand was absent even at maximum intensities. On the left hand, where standard clinical examination showed no sensitivity disorders, there was a considerable deviation from normal.

The application of this method made it possible not only to characterize quantitatively the extent of sensitivity disorders for every form of pathology, but also to identify "subclinical" disorders, which the traditional methods failed to record.

4. Introduction of auditory information to the deaf

It is know that 3-5 per cent of the population in developed countries suffer from deafness and hearing disorders. In combatting this affliction much success has been achieved. New methods of operative and medicamental treatment appear, more and more improved models of hearing aids are designed. However, there is a large group of practically deaf people for whom the existing means are ineffective or of little effectiveness. It has just been with this aim at assisting such people that an attempt has been undertaken to use the ultrasonic method for hearing prosthesis.

In the initial experiments on frogs it was shown [2, 4] that under the action of focused ultrasound stimuli on the internal ear the auricular centers of the brain responded with electrical reactions similar to the responses to auditory stimuli.

In the course of further investigations a new method for introduction of auditory information to man was suggested [4]. The essence of the method resides in the fact that amplitude-modulated ultrasonic oscillations are directed to the labyrinth; the carrier frequency in this case is far above the upper limit of frequency perceived by man (for instance, from 0.5 to 3 MHz) and modulation frequency corresponds to the transmitted auditory information. In essence, this method has no limitations in the frequency of modulating (audio) signals. Under the action of focused ultrasound modulated in amplitude by oscillations of a complex form (for example, signals from a microphone, tape recorder, etc.) on the internal ear, normal people hear the transmitted undistorted acoustic information (speech, music).

The most substantial result is that by means of focused ultrasound it is possible to stimulate not only the receptors (hair cells) of the internal ear, as in the event of ordinary sound stimulation, but also auditory nerve fibers, which could be stimulated until recently only by implanted electrodes. This significant result was supported by experiments on animals with preliminary destroyed receptor system of the labyrinth. In the midbrain auditory centers in ani-

mals, responses to ultrasonic stimulation were recorded, which were comparable with responses from the opposite, normally functioning receptor system, but with higher thresholds.

Finally, the possibility of direct stimulation of auditory nerve fibers by ultrasound is supported by the fact that the deaf whose receptor system is diagnosed to have been destroyed, may perceive auditory informtion delivered by means of amplitude-modulated ultrasound, whereas the standard hearing aids cannot help them.

5. Diagnosis of aural diseases

The possibility of using ultrasound not only for stimulation of receptors, but also the nerve fibers of the auditory system is very important for clinical diagnosis in order to determine hearing disorders at different levels.

A comparison was made between frequency-threshold curves obtained by means of amplitude-modulated ultrasound and the curves of audibility thresholds obtained by sound stimulation of the labyrinth [4]. For normally hearing subjects these curves are quite comparable, despite some differences. It should be noted that for subjects with various forms of hardness of hearing these curves differ greatly.

For instance, Fig. 2 shows the audiogram and ultrasonic frequency-threshold curve of a patient with otosclerose. The y-axis presents loss of hearing relative to the level of normal hearing, the x-axis gives the frequency of tone

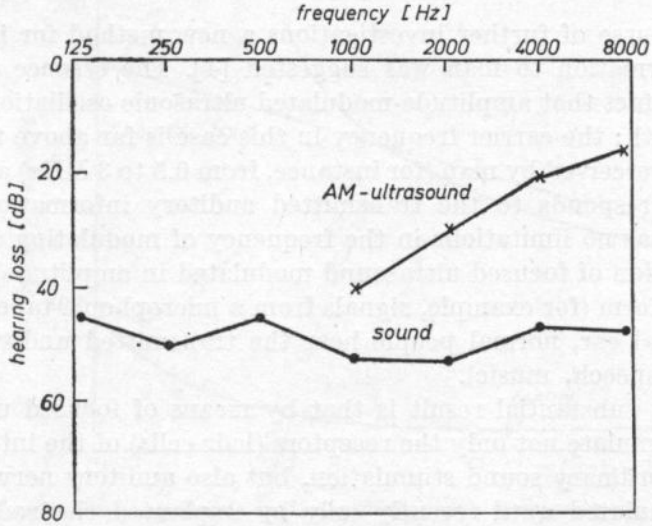

Fig. 2. Audiogram and ultrasonic frequency-threshold curve for the patient with otosclerose:
● — audiogram; × — ultrasound frequency-threshold curve

or amplitude modulation of ultrasound. Otosclerose is characterized by absence of auditory sensation at one or several ultrasound modulation frequencies (Fig. 2 – 125, 250 and 500 Hz), while the sounds of the same frequencies are distinctly heard by subjects with otosclerose. In the cases of other diseases the form of ultrasonic frequency-threshold curves is rather individual. This is already being employed in clinical practice to diagnose not only otosclerose, but also neurosensory hearing disorders, auditory nerve neurinoma, etc.

6. Possible mechanisms of focused ultrasound stimulation

A study was made on the factors of focused ultrasound responsible for stimulation of skin receptors and emergence of tactile, temperature, pain and other sensations.

Fig. 3 [4] displays relative changes in some characteristics of focused ultrasound with frequency changing from 0.5 up to 3 MHz for tactile and thermal sensations on human hand. The characteristics for a frequency of 0.5 MHz are assumed to be unitary. From the graph, it is obvious that only one characteristic – displacement amplitude – remains unchanged for every form of sensations with frequency changing over a wide range. The rest of the characteristics (intensity, ultrasonic pressure, increment of tissue temperature, particle velocity, acceleration, radiation pressure, etc.) greatly change, sometimes over a range of several orders of magnitude.

There are some of the experimental data below concerning the threshold values of the displacement amplitude necessary to realize stimulation of peripheral nerve structures by means of focused ultrasound [4]:

Receptors of labyrinth (frog)	0.004 –0.01 μm
Pacinian corpuscles (cat)	0.03 –0.05 μm
Tactile sensations on the skin of human fingers	0.08 –0.11 μm
The same on palm	0.13 –0.18 μm
The same on forearm	0.2 –0.58 μm
Warmth and cold sensations on the skin of palm	0.43 –0.6 μm
Pain sensation on the skin of palm	0.38 –0.64 μm

However, the actual mechanism of stimulation of the nerve structures is most probably related to a certain unidirectional, "rectified" action rather than sign-alternating oscillation displacement of the medium per se. Indeed, the subjects could not differentiate tactile sensations in response to a long stimulus or two short stimuli. A change of the carrier frequency at the same displacement amplitude exerted no effect on the character of sensations. However, the mechanism that transforms sign-alternating displacement into a unidirectionally acting factor is still unknown.

Under the action of amplitude-modulated ultrasound on the internal ear, other acting factors are added. First of all, one should bear in mind that the organ of hearing is an extremely sensitive instrument reacting to the action of adequate sound information. Therefore, it is necessary to take into account the possible effect of the sound component on it, resulting from the radiation pressure of amplitude-modulated ultrasound. In this case, adequate, that

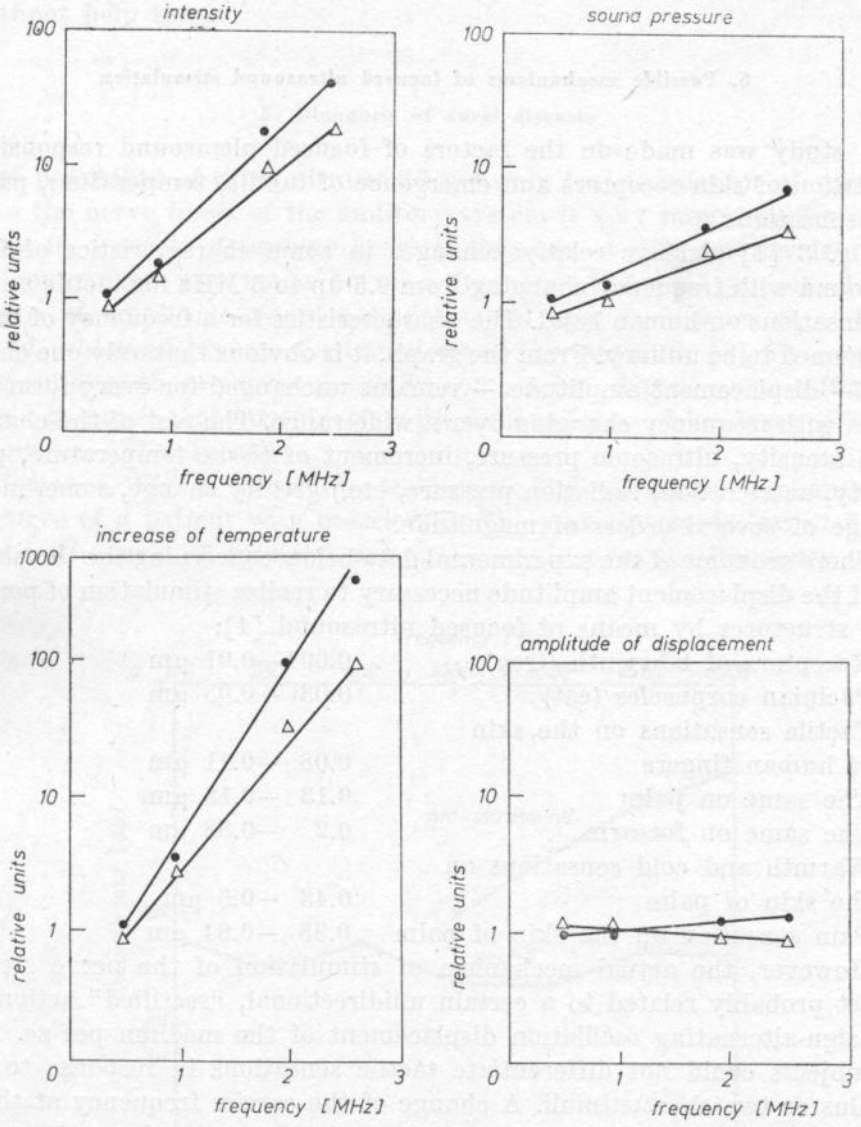

Fig. 3. Relative changes in the characteristics of focused ultrasound, which correspond to the emergence of tactile and thermal sensations in the hand at an ultrasonic frequency of 0.5-3 MHz: △ — tactile sensations; ● — thermal sensations

is sonic, information is channelled into the labyrinth, whereas ultrasound serves as a means of its delivery.

As has been mentioned above, amplitude-modulated ultrasound exerts a direct stimulating effect on the fibers of the auditory nerve. The basic acting factor of focused ultrasound in this event still remains to be discovered. This may be the mechanical action of ultrasound which has been discussed above. However, a certain role of transformation of ultrasonic oscilations into the electrical stimulus in this process cannot be ruled out. The physical character of this effect may be related to well known piezoelectric, and to be more precise, electromechanical properties of bone tissues.

7. Conclusion

The investigations carried out have shown that focused ultrasound is a useful and promising mean enabling the stimulation of both surface and deep nerve structures. It is not improbable that in the nearest future one can see the emergence of a new broad field of ultrasonic medical diagnosis, based on comparison of thresholds for various sensations in a normal man and in one or another pathological case. Great social importance is attached to the possibility of using ultrasonic methods for diagnosis of aural diseases and hearing prosthesis in patients with disorders of the receptor system.

This method holds much promise for physiological studies. It is of interest to elucidate the possibilities for stimulation of visual, olfactory, taste receptors, nerve fibers and central nerve structures, as well as to investigate the mechanisms of thermal reception, thermal production and thermal regulation in man and animals. Certain practical advantages may be gained from the use of focused ultrasound for acting on acupunctural points, for controlling the efficiency of anesthetics by measuring the threshold of pain sensations prior to administration of drugs and after it. At present it is difficult to circumscribe even approximately the medical and physiological problems, in tackling of which stimulating focused ultrasound may prove to be beneficial.

References

[1] L. R. Gavrilov, G. V. Gersuni, O. B. Ilyinski, E. M. Tsirulnikov, *A study of reception with the use of focused ultrasound. I. Effects on the skin and deep receptor structures in man,* Brain Res., **135**, 265-277 (1977).

[2] L. R. Gavrilov, G. V. Gersuni, O. B. Ilyinski, E. M. Tsirulnikov, E. E. Shchekanov, *A study of reception with the use of focused ultrasound. II. Effects on the animal receptor structures,* Brain Res., **135**, 279-285 (1977).

[3] L. R. Gavrilov, G. V. Gersuni, O. B. Ilyinski, M. G. Sirotyuk, E. M. Tsirulnikov, E. E. Shchekanov, *The effect of focused ultrasound on the skin and deep nerve structures of man and animal,* Progress in Brain Research, **43**, 272-292 (1976).

[4] L. R. Gavrilov, E. M. Tsirulnikov, *Focused ultrasound in physiology and medicine,* Nauka, Leningrad 1980 (in Russian).

ARCHIVES OF ACOUSTICS
9, 1-2, 75-82 (1984)

ULTRASONIC INVESTIGATION OF FIBRE TEXTURE IN PLANTS

H. GAWDA

Agricultural University, Department of Technical Physics, Lublin, Poland

J. LEWANDOWSKI

Institute of Fundamental Technological Research, Polish Academy of Sciences, Department of Physical Acoustics
(00-049 Warsaw, ul. Świętokrzyska 21)

The propagation velocities of an ultrasonic dilatational wave in different segments of a cereal stalk were measured and the averaged orientations of crystallites in the same segments were determined applying X-ray diffraction method. Using the principle of maximum entropy the analytical form of the probability density function of the crystallite orientation in a segment was found for the different values of the propagation velocity observed. Subsequently the fractions of crystallites with orientation angles lying in a given finite angle interval were calculated for the arbitrarily chosen propagation velocities.

1. Introduction

This work is a continuation of a series of papers [1-5] devoted to the microstructure and mechanical properties of the cereal stalk materials. Such information is very important for developments in breeding of plants, technology of harvest, textile and paper industries, and so on. The purpose of this paper is to present some experimental and theoretical investigations concerning the possibility of predicting the mechanical properties of the wheat stalk from ultrasonic measurements.

2. Formulation of the problems

It is obvious that the characteristic properties of the microstructure are the only reliable basis for the theoretical prediction of the mechanical properties of plant materials. For this reason the investigations presented here were car-

ried out in two steps. The first step was to establish experimentally the relation between some characteristics of the local microstructure of the stalk and the local velocity of ultrasonic waves propagating in it as well as other mechanical properties of the stalk. The second step was an attempt to solve an inverse problem to the first one, that is to determine to some extent the local microstructure from measurements of the local propagation velocity of ultrasonic waves in the stalk. The inverse problem was solved on the basis of information theory. In this paper we are interested only in the material of the internodal parts of the stalk.

Seeking solutions for the effective mechanical properties of the plant material of a stalk segment lying between two neighbouring nodes, let us regard this material as a two-phase and fibre-reinforced one. In this approximation one phase is taken to be composed of circular cellulose fibres embedded in a continuous and amorphous phase, called the matrix phase. Generally speaking, the effective mechanical properties of such a medium depend on the fibre phase properties, the matrix phase properties and the volume concentration of each phase. On the basis of an analysis of such a model it can be expected that the effective mechanical behaviour of the plant material between two neighbouring nodes of the stalk is dominated by viscoelastic phenomena in the fibre phase with the volume concentration of about 70 per cent. For this reason we are interested only in the microstructure of the fibres.

In the cellulose fibres there form crystalline areas called micelles or crystallites separated from one another, along the fibre, by amorphous areas of lesser degree of particle ordering. Let θ denote the orientation of a crystallite in relation to the axis of the fibre, that is θ denotes the angle between the axis of the crystallite and the axis of the whole fibre. Let $p(\theta)d\theta$ denote the probability that the orientation angle of an arbitrarily chosen crystallite has a value between θ and $\theta+d\theta$. The probability density function $p(\theta)$ introduced here describes the so-called texture of the plant material. It should be stressed here that the mechanical, acoustical, sorbtion and some other properties of the stalk material are determined mainly by the texture. For this reason the texture was the only parameter of the stalk microstructure of interest for us.

3. Experiments and analysis

In order to determine the orientation angle $\bar{\theta}$ averaged over all the crystallites in different internodal parts of the stalk, segments were taken from different internodal parts lying along the whole length of the dried stalk. A macroscopic sample in the form of a rod with the longitudinal axis parallel to that of the stalk was cut off from each segment.

These samples were first investigated using X-ray diffraction. A Debye-Scharer camera using radiation from a copper lamp with a nickel filter was employed. These observations permitted quantitative measurements of the mean orientation angle $\bar{\theta}$.

Subsequently the values of the propagation velocity of ultrasonic dilatational waves, c_L, were determined for 1 MHz waves propagating in the samples along their longitudinal axes. The propagation velocity was determined for each sample from the measurement of the time of the passage of an ultrasonic impulse between two points of some distance between them. The thickness, d, of each sample was several times smaller than the wave length, λ, and the conditions

$$d/\lambda < 0.3, \quad \lambda/l \ll 1 \tag{3.1}$$

were fulfilled, where l denotes the sample length. Under these conditions the effective dynamic Young's modulus, $E(\omega)_{\text{eff}}$ and the propagation velocity, $c(\omega)_L$, are related to each other by the following relationship

$$E(\omega)_{\text{eff}} = \langle \varrho \rangle [c(\omega)_L]^2, \tag{3.2}$$

where ω denotes the angular frequency of the ultrasonic wave and the angular brackets $\langle \ldots \rangle$ denote averaging over the sample volume. This formula enables us to determine the values of the dynamic effective Young's modulus of plant material from measurements of the propagation velocity of the dilatational ultrasonic wave. The respective curve in Fig. 1 shows how the mean orienta-

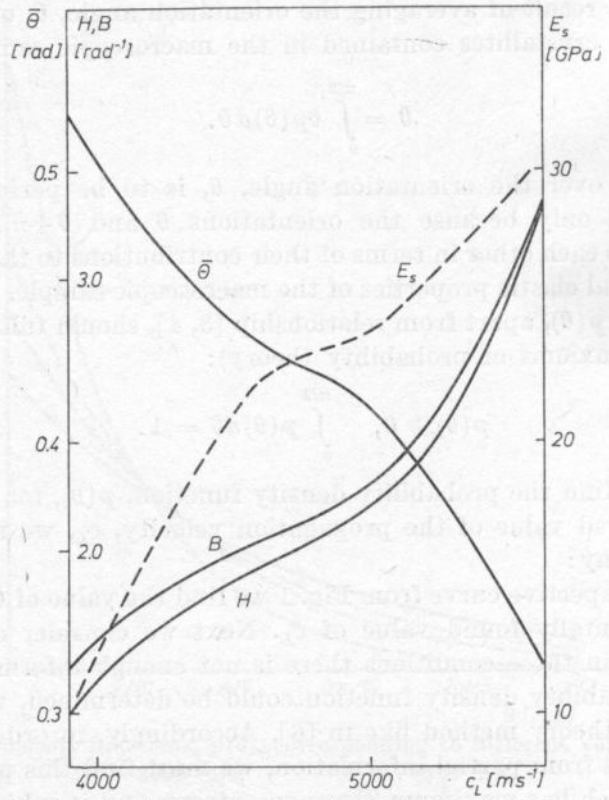

Fig. 1. Changes in the mechanical properties of the stalk material produced by changes in the texture of the stalk fibres

tion angle, $\bar{\theta}$, and the propagation velocity, c_L, are related to each other. The relationship between $\bar{\theta}$ and c_L can be expressed, for example, in the following form

$$\bar{\theta} = \sum_{k=0}^{6} A_k^{(\theta)} (c_L)^k, \qquad [A_k^{(\theta)}] = [m^{-k} s^k]. \tag{3.3}$$

The numerical values of the coefficients $A_k^{(\theta)} (k = 0, 1, \ldots, 6)$ are listed in the first column of Table 1. On the other hand, the mean orientation, $\bar{\theta}$, can

Table 1

k	$A_k^{(\theta)}$	$A_k^{(H)}$	$A_k^{(B)}$
0	-13367.5	-67850.06	131496.8
1	17.806	83.428	-166.21048
2	$-9.84866 \cdot 10^{-3}$	-0.04246	0.08725
3	$2.899574 \cdot 10^{-6}$	$1.114506 \cdot 10^{-5}$	$-2.4347 \cdot 10^{-5}$
4	$-4.79275 \cdot 10^{-10}$	$-1.72504 \cdot 10^{-9}$	$3.80983 \cdot 10^{-9}$
5	$4.21707 \cdot 10^{-14}$	$1.37638 \cdot 10^{-13}$	$-3.169755 \cdot 10^{-13}$
6	$-1.543134 \cdot 10^{-18}$	$-4.54343 \cdot 10^{-18}$	$1.0956 \cdot 10^{-17}$

be regarded as a result of averaging the orientation angle, θ, over a statistical ensemble of the crystallites contained in the macroscopic sample, i.e.,

$$\bar{\theta} = \int_0^{\pi/2} \theta p(\theta) d\theta. \tag{3.4}$$

Integration over the orientation angle, θ, is to be performed over the interval $[\theta, \pi/2]$ only because the orientations θ and $\theta + \pi/2$ $(0 \leqslant \theta \leqslant \pi/2)$ are equivalent to each other in terms of their contributions to the determination of the longitudinal elastic properties of the macroscopic sample. The probability density function $p(\theta)$, apart from relationship [3, 4], should fulfill the following two conditions (axioms of probability theory):

$$p(\theta) \geqslant 0, \qquad \int_0^{\pi/2} p(\theta) d\theta = 1. \tag{3.5}$$

In order to find the probability density function, $p(\theta)$, for a given sample from the measured value of the propagation velocity, c_L, we may proceed in the following way:

Using the respective curve from Fig. 1 we find the value of $\bar{\theta}$ corresponding to the experimentally found value of c_L. Next we consider conditions (3.4) and (3.5). Since in these conditions there is not enough information available so that the probability density function could be determined, we make use of the information theory method like in [6]. Accordingly, in order to make statistical inferences from partial information, we must find this probability density function which has maximum Shannon entropy and is subject to whatever

is known [7], i.e., subject to constraints (3.4), (3.5). From this, it follows that the probability density function, $p(\theta)$, should be taken in the following form:

$$p(\theta) = B(c_L)\exp[-H(c_L)\theta], \qquad B = H/[1-\exp(-\pi H/2)]. \tag{3.6}$$

The functional relationships $H = H(c_L)$ and $B = B(c_L)$ can be expressed, for example, in the following form:

$$H = \sum_{k=0}^{6} A_k^{(H)}(c_L)^k, \quad B = \sum_{k=0}^{6} A_k^{(B)}(c_L)^k, \qquad [A_k^{(H)}] = [A_k^{(B)}] = [\mathrm{rad}^{-1} m^{-k} s^k]. \tag{3.7}$$

The numerical values of the coefficients $A_k^{(H)}$ and and $A_k^{(B)}$, corresponding to the experimental relationship (3.3), are listed in the second and third column of Table 1, respectively. The respective curves in Fig. 1 show how H and B depend on the propagation velocity.

Making use of these results we can plot the probability density function, $p(\theta)$, corresponding to all reasonable values of the propagation velocity c_L. Fig. 2 presents four curves of four probability density functions corresponding

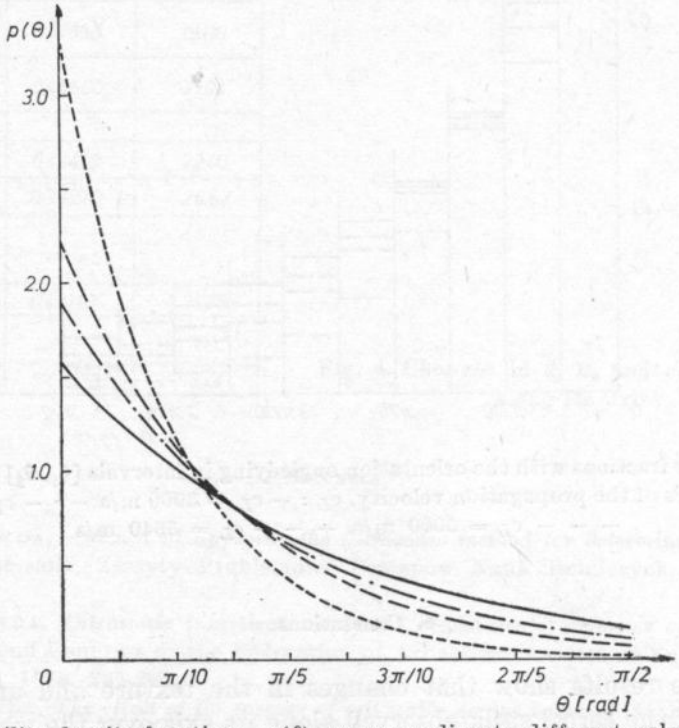

Fig. 2. Probability density functions, $p(\theta)$, corresponding to different values of the propagation velocity, c_L : — c_L = 3900 m/s, — · — c_L = 4340 m/s, — — — c_L = 5000 m/s, — — — c_L = 5640 m/s

to the four different values of the propagation velocity. The angle between the vertical axis and the tangent of the curve $p(\theta)$ can be regarded as a measure of isotropy. The anisotropy of the material considered increases as this angle decreases. From changes in this slope, it can easily be seen that the propagation velocity, c_L, observed along the stalk axis diminishes with decreasing the longitudinal anisotropy of the stalk material.

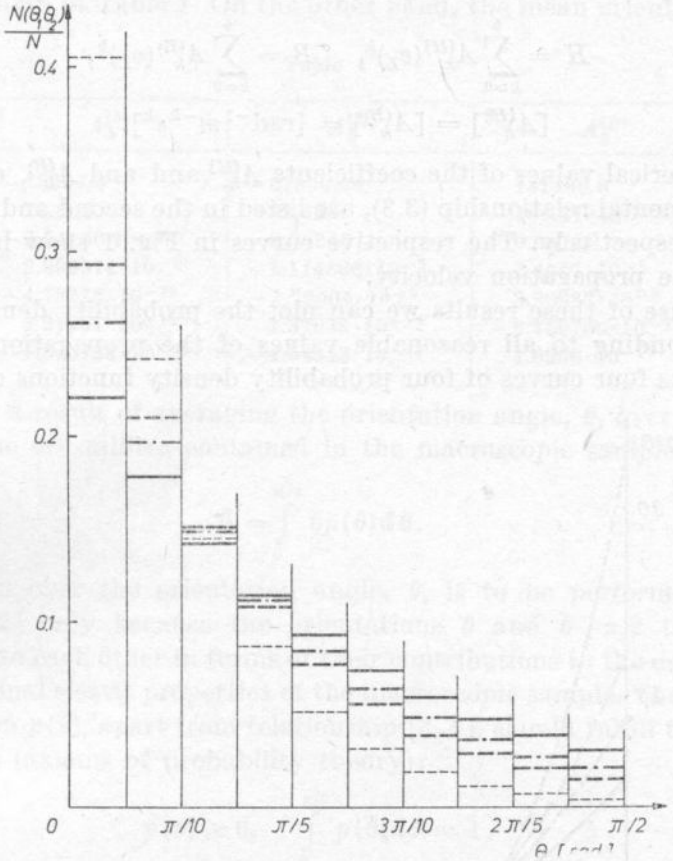

Fig. 3. Crystallite fractions with the orientation angle lying in intervals $[\theta_1, \theta_2]$ corresponding to different values of the propagation velocity, c_L : — c_L = 3900 m/s — · — c_L = 4340 m/s, — — — c_L = 5000 m/s, — — — c_L = 5640 m/s

4. Conclusions

The above results show that changes in the texture and anisotropy of the material of the cereal stalk observed along its axis over the whole distance between the root and ear cause changes in the propagation velocity, c_L, and are expected to produce essential changes in all the mechanical properties of the

material. Of course, these changes can be measured or observed by suitable techniques. For example, results obtained by sample stretching on the Instron testing machine indicate such a great differentiation in the properties of material of the stalk along its axis. For internodal segments in which ultrasonic waves propagate with a high velocity, 4000-5600 m/s, linear stress-strain characteristics occur for axial stresses until the sample rupture which is dominated in this case by the phenomenon of brittle fracture. Conversely, for those internodal segments below the ear in which the wave velocity is about 3000 m/s, stress-strain characteristics for axial stresses are similar to the characteristics of plastics materials. Fig. 4 presents the changes in $\bar{\theta}$, c_L and the effective Young's modulus, E_s, obtained by sample stretching on the Instron testing machine. The values of this modulus are also plotted in Fig. 1.

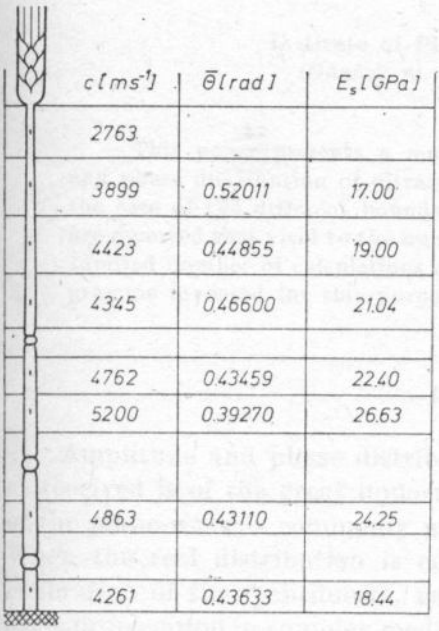

$c\,[ms^{-1}]$	$\bar{\theta}$ [rad]	E_s [GPa]
2763		
3899	0.52011	17.00
4423	0.44855	19.00
4345	0.46600	21.04
4762	0.43459	22.40
5200	0.39270	26.63
4863	0.43110	24.25
4261	0.43633	18.44

Fig. 4. Changes in $\bar{\theta}$, E_s and c_L in the stalk along its axis

References

[1] H. Gawda, *Attempt at applying the ultrasonic method for determining the Young modulus of cereal stalk,* Zeszyty Problemowe Postępów Nauk Rolniczych, 203, 145-152 (1978).

[2] H. Gawda, *Ultrasonic investigations of the mechanical properties of the stalks of a wheat,* The Second Congress of the Federation of Acoustical Societes of Europe, Warsaw 18-22 September, 1978, 287-290.

[3] H. Gawda, *The effect of the texture of cell walls on the value of the Young modulus of plant material,* II International Conference on Physical Properties of Agricultural Materials, Gödöllö, Hungary, 26-28 August 1980, 1-21.

[4] H. Gawda, J. S. Haman, *An ultrasonic methods of determining Young's modulus in cereal plants,* Transactions of ASAE **26**, 1, 250-254 (1983).

[5] H. Gawda, J. Lewandowski, *Ultrasonic method of determination of the probability density function of the crystallites orientation in plant fibres* (in Polish), Proc. XXX Open Seminar on Acoustics 83, Gdańsk, September 1983, **1**, 185-188.

[6] J. Lewandowski, *Correlation function determination for a solid random medium from an averaged acoustic field,* ULTRASOUND' 81, Praha CSSR 1981, Proceedings Sections I and II, 6-10; VII, 10-12.

[7] E. T. Jaynes, *Information theory and statistical mechanics,* Physical Review, **106**, 4, 620-630 (1957).

ARCHIVES OF ACOUSTICS
9, 1-2, 83-94 (1984)

CALCULATION OF ULTRASONIC FIELD DISTRIBUTION RADIATED BY PLANAR TRANSDUCERS*

ANNA MARKIEWICZ

Institute of Physics, University of Gdańsk
(Gdańsk ul. Wita Stwosza 57, Poland)

This paper presents a method for numerical calculation of amplitude and phase distribution of ultrasonic fields radiated by a planar transducer in the case of the different boundary conditions. Some theoretical consideration are reported that yield to the numerical approach for the investigated problems. Limited number of calculations are presented to illustrate facilities of the programme invented for this purpose.

1. Introduction

Amplitude and phase distribution of ultrasonic fields transmitted as well as received is of the great importance to many investigators. The assumption of the plane-wave is commonly used, however, it is not fulfiled in most cases. When the real distribution is considered, especially in such applications as calibration of the transducers, velocity and attenuation measurements, ultrasonic propagation in complex media, it helps to obtain the correct results [2-4].

2. Theory

An ultrasonic field radiated by a planar transducer can be regarded as a diffraction problem of an arbitrary incident wave $u(x, y, z)$ through an aperture A in an infinite plane screen S of vanishing thickness and can be solved by means of integral equations. Any solution u of the wave equation that is regular inside a close surface Σ is expressible in terms of the boundary values on Σ of either u or $\partial u/\partial n$, at least if the corresponding Green's functions of

* This work was supported by British Council and performed at University of Surrey, Physics Department, Guildford, Surrey, U.K.

the first and second kinds are known [1]. (Σ consists of an infinite plane $S+A$ and a half-sphere at infinity). Accordingly, if u is any wave function that is regular for $z \geqslant 0$ and satisfies appropriate conditions at infinity [1] the Rayleigh formulae express u:

$$u = -\frac{1}{2\pi}\int \frac{\partial u}{\partial n}\frac{\exp(ikr)}{r}\,d\Sigma, \tag{1}$$

or

$$u = \frac{1}{2\pi}\int u\frac{\partial}{\partial n}\left(\frac{\exp(ikr)}{r}\right)d\Sigma, \tag{2}$$

where the integration is over the plane $z' = 0$ (a planar diffraction problem) and r denotes the distance between the field point (x, y, z) and the source point (x', y', z').

If two different boundary condition are considered

$$u|_S = 0 \quad \text{soft screen}, \tag{3}$$

$$\left.\frac{\partial u}{\partial n}\right|_S = 0 \quad \text{— rigid screen (or baffled transducer)}, \tag{4}$$

and applied to (1) and (2) the solutions of the problems are obtained

$$u = \frac{1}{2\pi}\int_A u\frac{\partial}{\partial n}\left(\frac{\exp(ikr)}{r}\right)d\Sigma \quad \text{soft screen}, \tag{5}$$

$$u = -\frac{1}{2\pi}\iint_A \left(\frac{\exp(ikr)}{r}\right)\frac{\partial u}{\partial n}\,d\Sigma \quad \text{rigid screen}. \tag{6}$$

The other well known approximation to this problems is Kirchhoff's approximation

$$u = \frac{1}{4\pi}\int_A \left\{\frac{\exp(ikr)}{r}\frac{\partial u}{\partial n} - u\frac{\partial}{\partial n}\left(\frac{\exp(ikr)}{r}\right)\right\}dA. \tag{7}$$

There is an inconsistency of Kirchhoff's theory because u and $\partial u/\partial n$ cannot be simultaneously prescribed on A, and that is why there exist various modification of Kirchhoff's theory. Kirchhoff's solution can be interpreted as the average of two Rayleigh's solutions. These three formulae give different results only within the near field of the aperture, and at a distance from it integrals (5), (6) and (7) tend to the same value.

3. Numerical approach

The programme was invented to calculate pressure distribution of the ultrasonic field in the plane parallel to the transducer face. The source was assumed to be planar and in that case Rayleigh's formulae can be treated as

the transform relation

$$p(x, y, z_{\text{const}}) = f_1(x, y, 0) ** f_2(x, y, z), \tag{8}$$

where ** denotes twodimensional convolution with respect to x and y and

$$f_1(x, y, 0) = \begin{cases} \dfrac{\partial p}{\partial n} & \text{rigid boundary condition} \\ p & \text{soft boundary condition} \end{cases} \tag{9}$$

$$f_2(x, y, z) = \begin{cases} \dfrac{1}{2\pi} \dfrac{\exp(-ikr)}{r} & \text{rigid boundary condition} \\ -\dfrac{1}{2\pi} \dfrac{\partial}{\partial n} \left(\dfrac{\exp(-ikr)}{r} \right) & \text{soft boundary condition} \end{cases} \tag{10}$$

The computations were performed by a convolution approach utilizing a Fast Fourier Transform routine. The programme was run on a PRIME computer, however, in order to optimize it, some parts were implemented by the Array Proccessor (*AP*).

4. Results

All calculations presented were performed for a circular transducer of a 5.7 mm radius and with a frequency of 0.948 MHz radiating into water. The uniform distribution on the transducer surface was assumed.

In Fig. 1 the amplitude and phase distributions are shown at a distance of 10 mm away from the transducer for three boundary conditions: rigid, soft boundary condition, and Kirchhoff's approximation. For quantitative comparison several cross-sections for previous results are shown in Fig. 2.

Computer simulated formation of ultrasonic field in the case of the rigid boundary condition (baffled transducer) is shown in Fig. 3.

5. Conclusions

Using the approach presented in this paper one can calculate the real field distribution, both amplitude and phase, radiated by a planar transducer for different boundary conditions, different shape of the transducers and different distribution across the transducer surface. The latter can be assumed theoretically [6] or obtained experimentally [7].

Acknowledgements. The author wish to acknowledge Dr Kurshid AHMAD from Computing Center of University of Surrey for help with using *AP*.

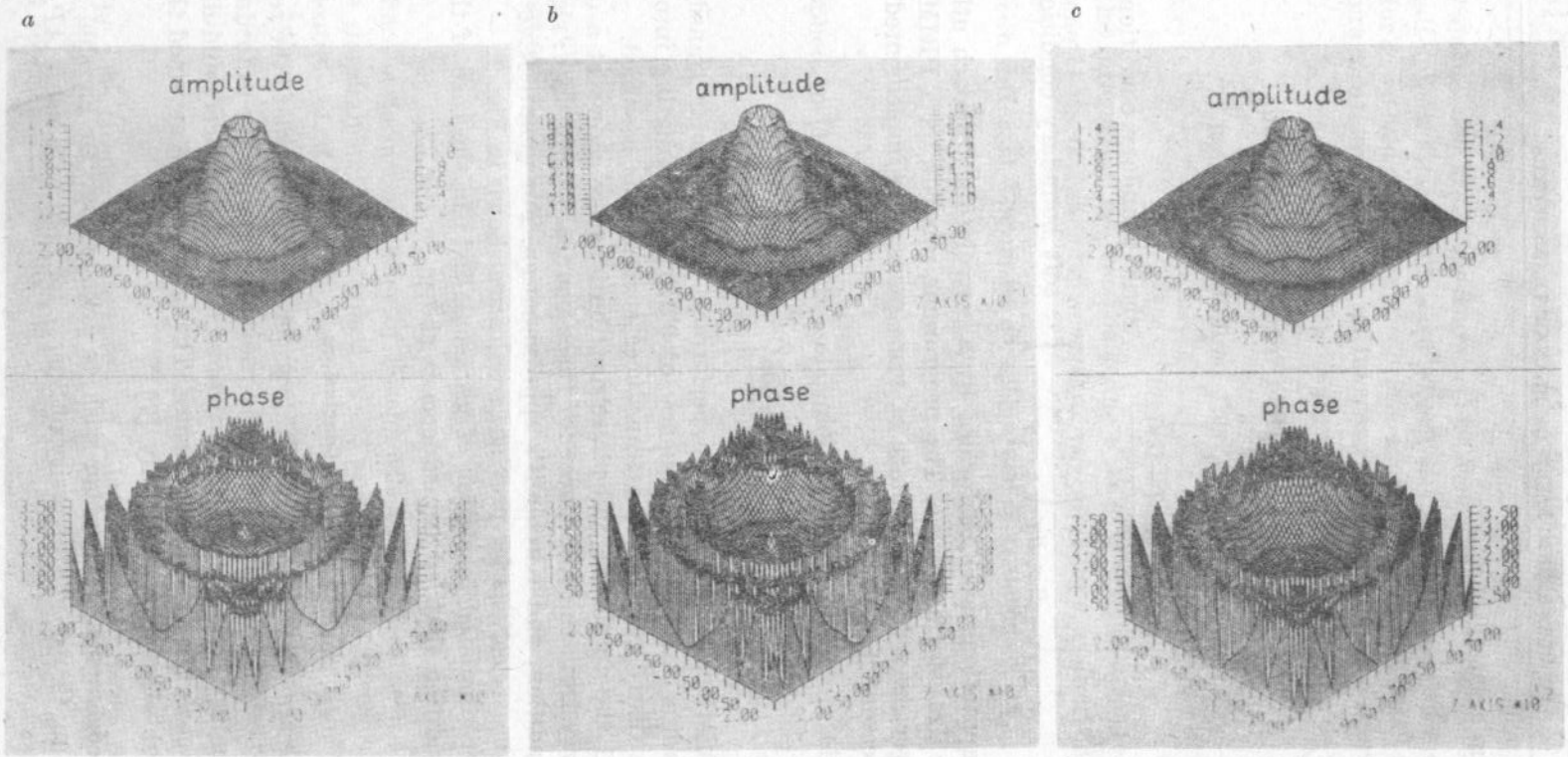

Fig. 1. Calculation of ultrasonic field distribution for the transmitter of 0.948 MHz frequency and 5.7 mm radius in the plane parallel to the transducer face at a distance of 10 mm away from it for different boundary conditions: *a*) rigid boundary, *b*) soft boundary condition, *c*) Kirchhoff's approximation. x and y axes are normalized to the radius of the transducer

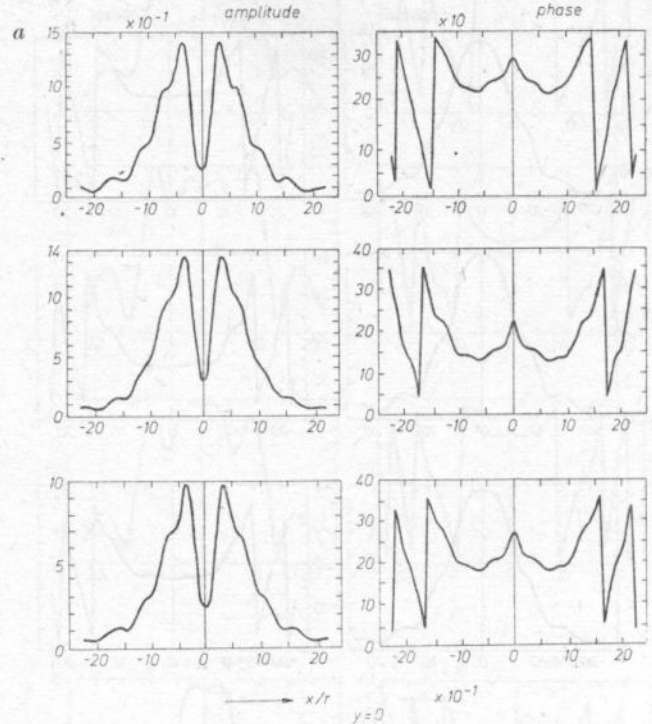
a
amplitude
phase
x 10⁻¹
x 10
x/r
y = 0
x 10⁻¹

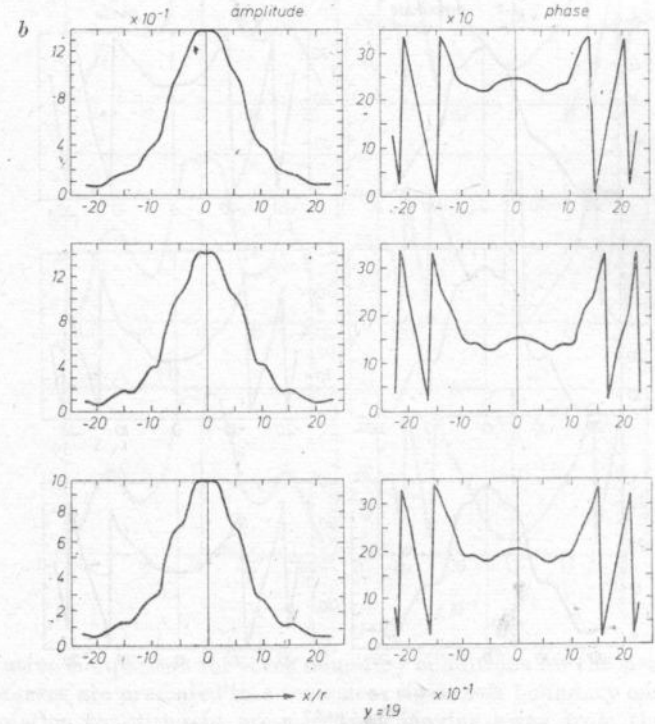
b
amplitude
phase
x 10⁻¹
x 10
x/r
y = 1.9
x 10⁻¹

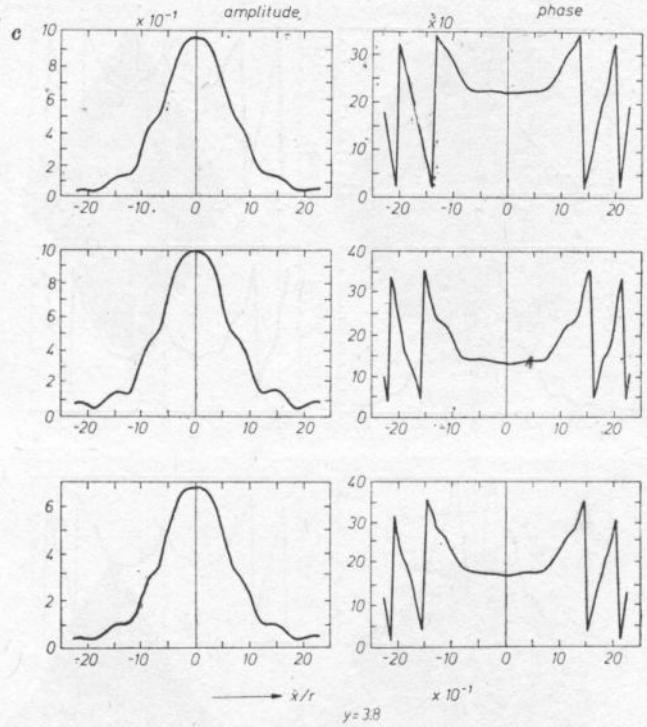
c
amplitude
x 10⁻¹
phase
x 10
x/r
x 10⁻¹
y = 3.8

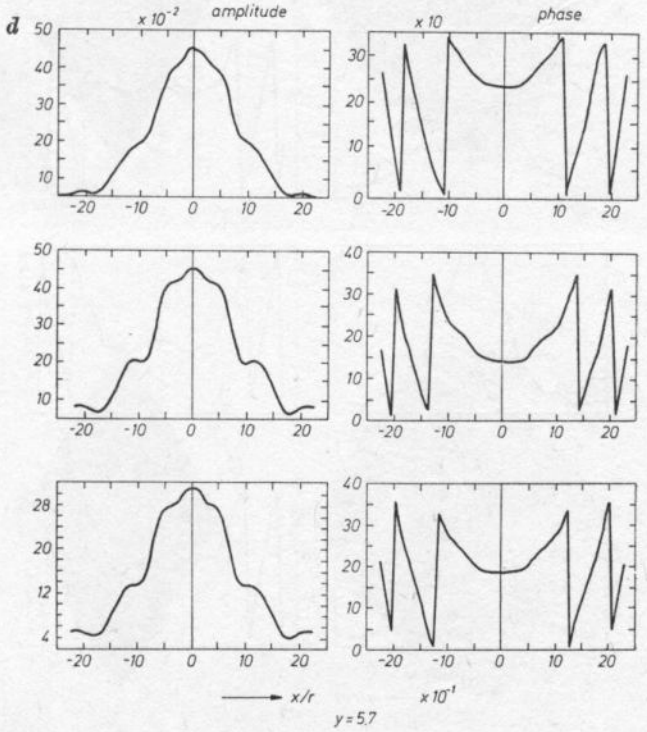
d
amplitude
x 10⁻²
phase
x 10
x/r
x 10⁻¹
y = 5.7

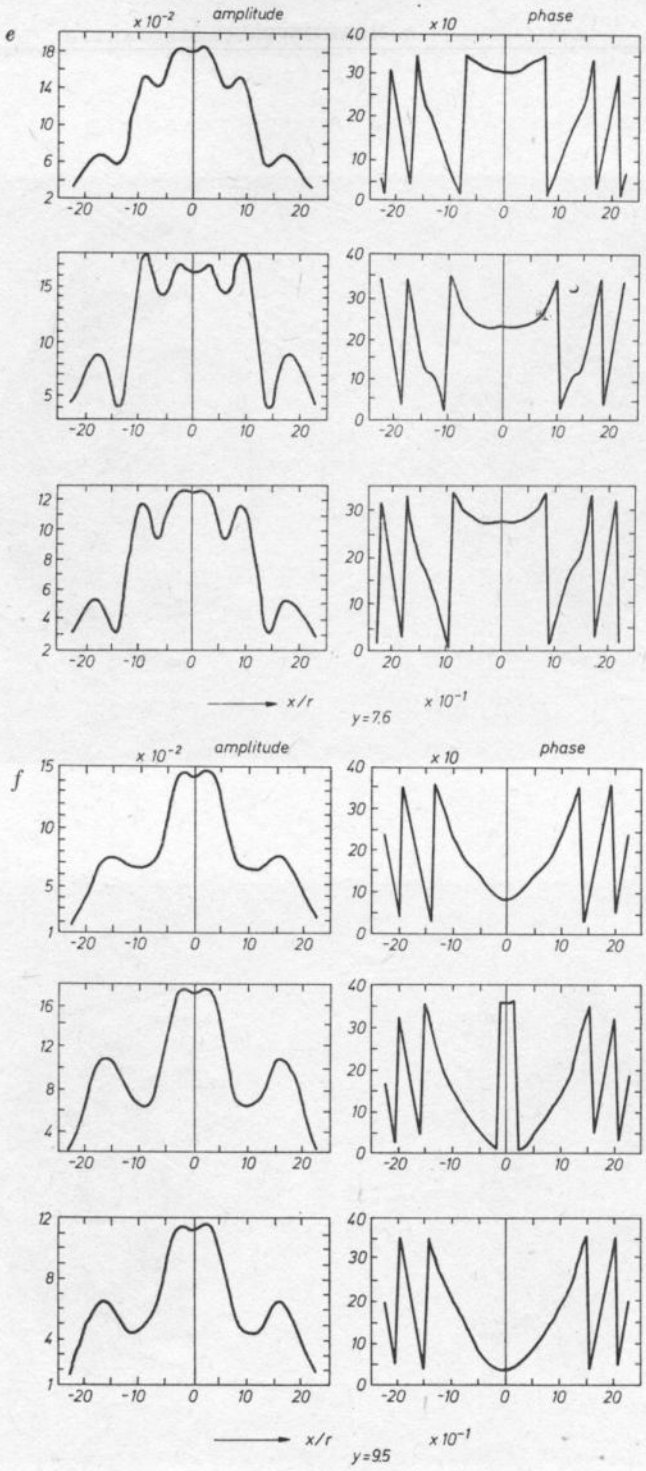

Fig. 2. Quantitative comparison for three boundary conditions for the situation as presented in Fig. 1. The curves are presented in a sequence: rigid, soft boundary condition and Kirchhoff's approximation for different cross-sections moving away from the transducer axis: *a*) $y = 0$ (on axis), *b*) $y = 1.9$ mm, *c*) $y = 3.8$ mm, *d*) $y = 5.7$ mm, *e*) $y = 7.6$ mm, *f*) $y = 9.5$ mm

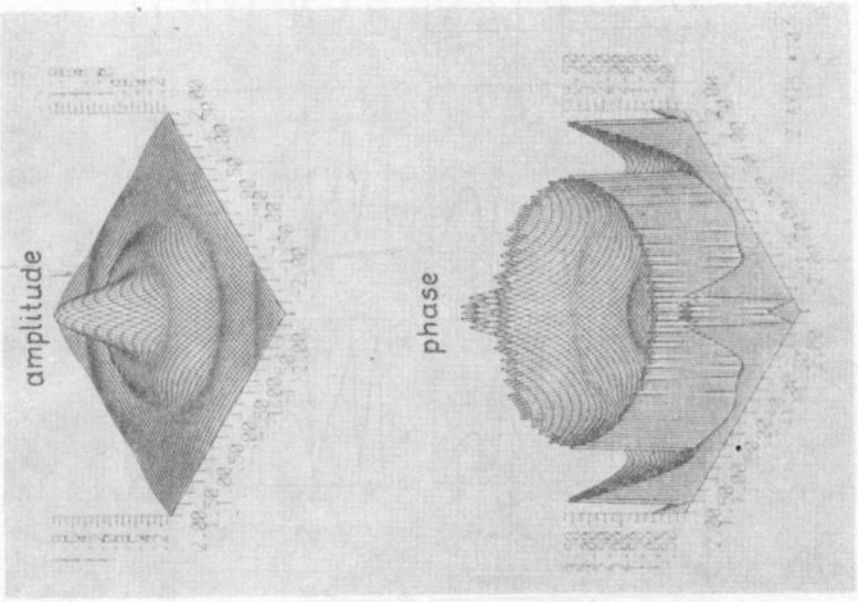

b

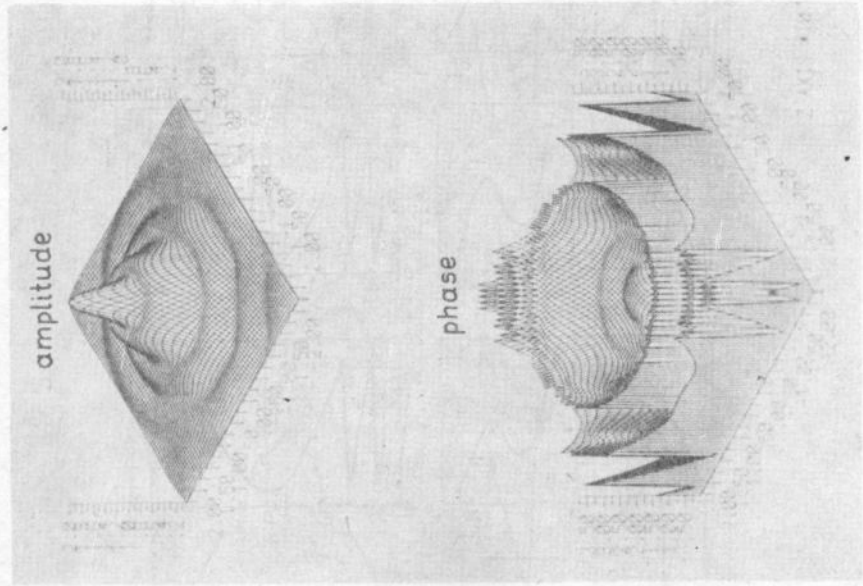

a

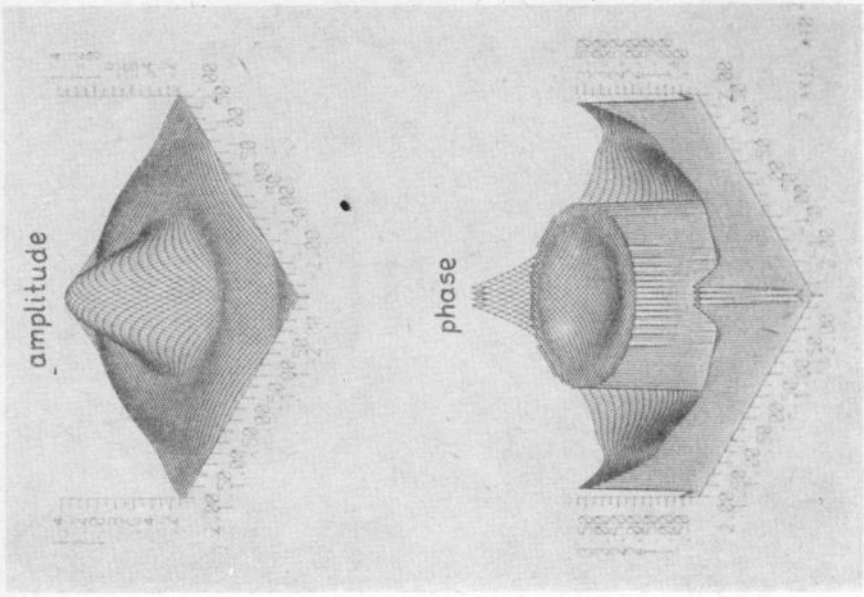

d

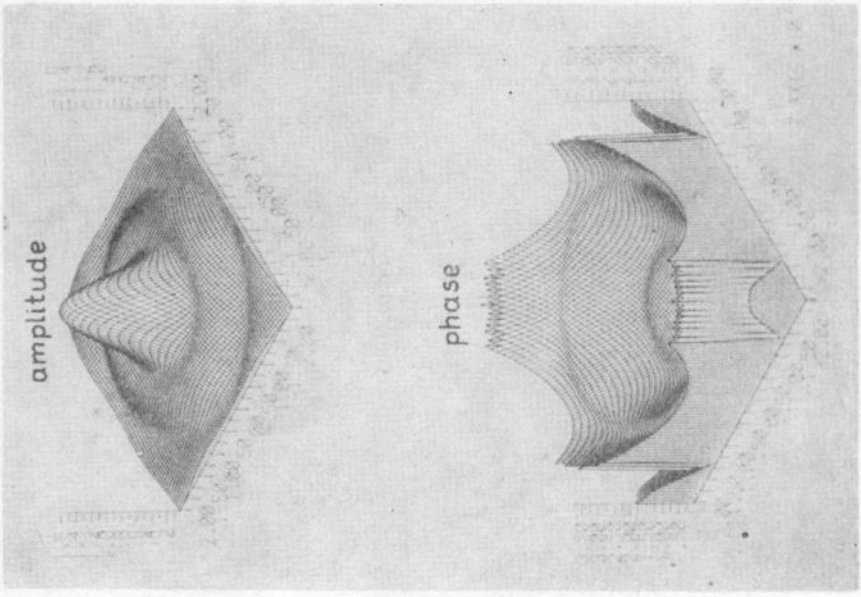

e

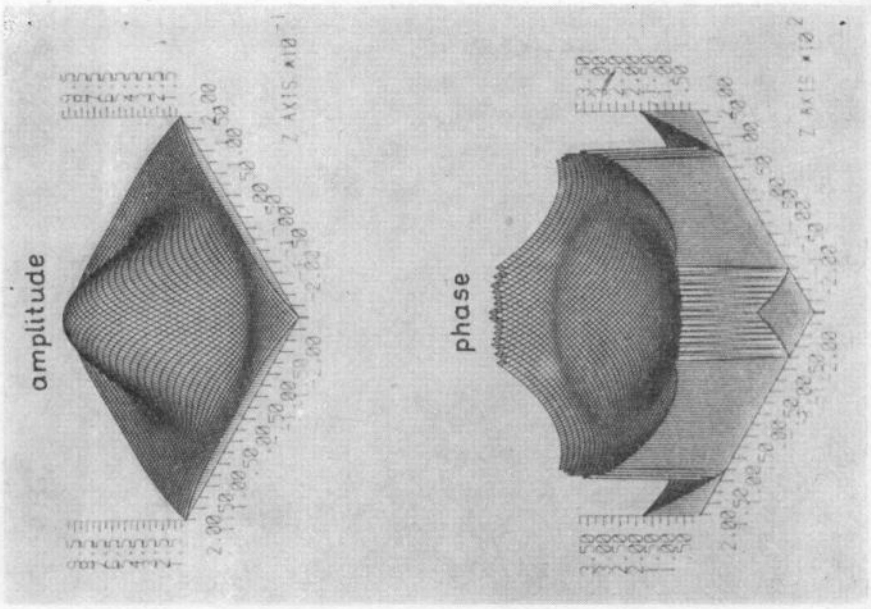

f

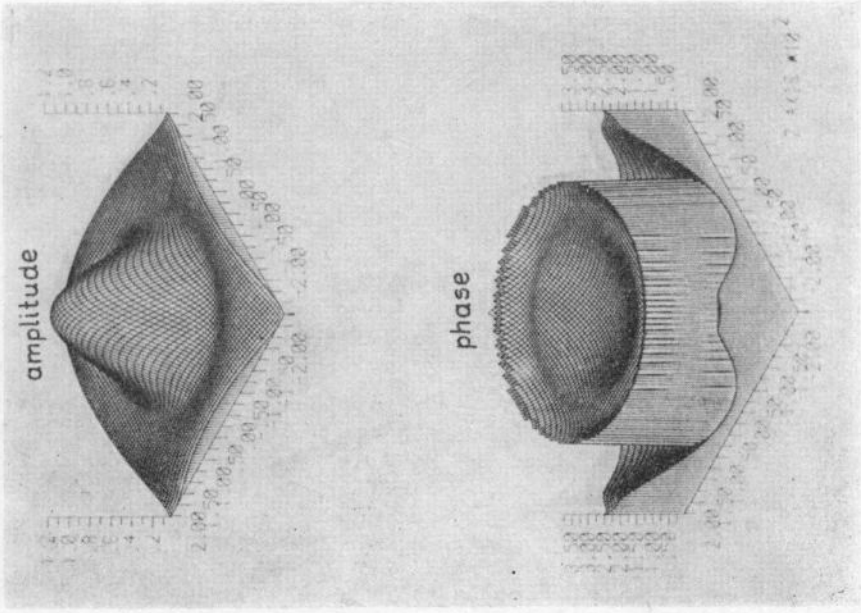

e

g

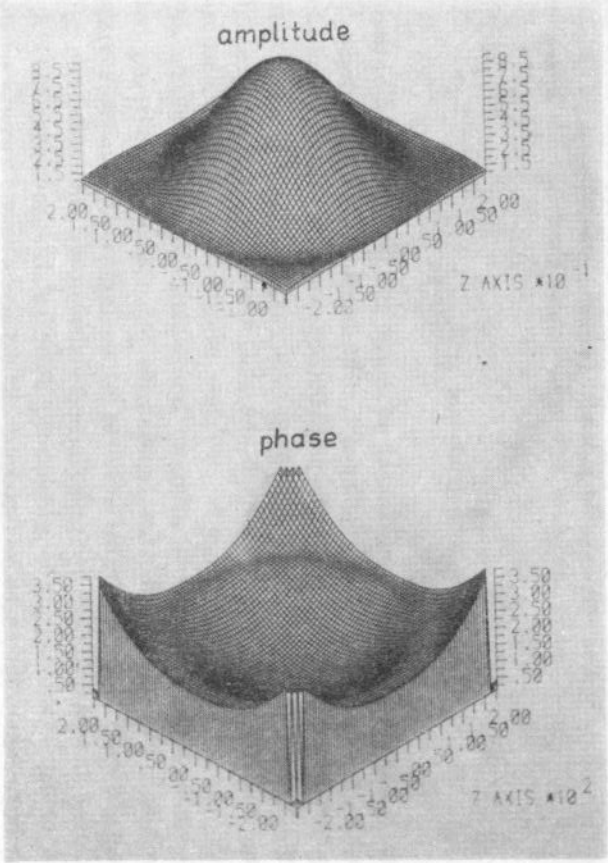

Fig. 3. Computer simulated formation of ultrasonic field radiated by a baffled transducer (of 0.948 MHz frequency and 5.7 mm radius) in the plane parallel to the transducer face at distances: *a*) $z = 18$ mm, *b*) $z = 27$ mm, *c*) $z = 36$ mm, *d*) $z = 45$ mm, *e*) $z = 54$ mm, *f*) $z = 63$ mm, *g*) $z = 72$ mm; x and y axes are normalized to the radius of the transducer

References

[1] C. J. Bouwkamp, *Diffraction theory,* Reports on Progress in Physics, **17**, 35, 35-91 (1954).

[2] H. Seki, A. Granato, R. Truel, *Diffraction effects in the ultrasonic field of a piston source and their importance in the accurate measurment of attenuation,* J. Acoust. Soc. Am., **28**, 2, 230-238 (1956).

[3] E. Papadakis, *Correction for diffraction losses in the ultrasonic field of a piston source,* J. Acoust. Soc. Am., **31**, 2, 150-152 (1959).

[4] M. B. Gitis, A. S. Khimunin, *Diffraction effects in ultrasonic measurements,* Soviet Physics-Acoustics, **14**, 4, 413-431 (1969).

[5] G. R. Harris, *Review of transient field theory for a baffled planar piston,* J. Acoust. Soc. Am., **70**, 10-20 (1981).

[6] A. Markiewicz, R. C. Chivers, *Typical errors in using finite miniature ultrasonic probes for far field measurements,* Acoustics Letters, **6**, 10, 142-146 (1983).

[7] I. Wojciechowska, A. Markiewicz, *Calculation of ultrasonic field used data obtained in holographic investigation of amplitude distribution throughout an ultrasonic transducer,* Proc. Second Spring School on Acousto-optics and Applications, 1983, 288-297.

ARCHIVES OF ACOUSTICS
9, 1-2, 95-100 (1984)

BIOPHYSICAL APPROACH TO THE PROBLEM OF SAFETY OF DIAGNOSTIC ULTRASOUND

IVO HRAZDIRA

Department of Biophysics, Faculty of Medicine, J. E. Purkyně University
(Brno, Czechoslovakia)

Every application of the ultrasonic technique in medical diagnostics involves the deposition of energy in tissues which can lead to some biological effects. The dependence of biological effects on physical characteristics of the ultrasonic field is often nonlinear. On the one hand, most of the mechanical factors of ultrasound are nonlinearly related to both the intensity and the frequency. On the other hand, the metabolic and regulatory processes of a given biological subject cause its nonlinear response to ultrasonic action. The nonlinearity increases with increasingly higher level of biological organisation. The biophysical approach to the problem of safety of diagnostic ultrasound consists in detailed assessment of relations between the acting ultrasonic impulse and the registered alteration of the biological system.

1. Introduction

Possible biological effects must be taken into account in each examining method when diagnostic information is conditioned by the emission of a certain amount of energy into a tissue studied. The situation is the same in all ultrasound diagnostic methods, extensive development of which needs the elaboration of obligatory recommendations that could either eliminate or reduce their risk to examined persons to a minimum.

The whole sphere of ultrasound examining methods belongs among the so-called passive interactions of ultrasound with living objects. They are called passive, because their aim is to provide information on the properties of a living environment by means of analysing ultrasound signal which came through this environment without provoking changes of the given medium by acoustic energy transferred by the signal. The essential constant characterizing the energy of ultrasound wave is its intensity (acoustic specific output).

To accomplish the condition of passive interaction, the intensity of ultrasound signal must be of sub-threshold value for the considered living system from the view of biological effectiveness. This condition mentioned above, however, makes the accurate establishment of biologically effective intensity very difficult. The causes are partly physical, partly biological.

2. Methods of expressing ultrasound intensity

Physical problems are connected with the expression of intensity and with methods of its accurate establishment. The expression of intensity depends on the character of ultrasound transducer and on the method of its exciting. Piezo-electrical transducers in the form of plates are used nearly exclusively in medical application. These transducers oscillate similarly to a piston, that is in an ideal case all points of their surface oscillate both with the same amplitude and the same phase. In fact, that is not the case and the emanating diagram of a piston-like oscillating transducer always shows, besides the central maximum, a few smaller side lobes and is not, in most cases, quite symmetrical rotarily. The consequence of this oscillation is then the disproportion between the central maximum intensity and the average spatial intensity of the whole transducer, which can vary from 1.5 to 3.6 in non-focused transducers. As the central maximum intensity of a transducer is decisive for the consideration of biological effectiveness, the average intensity, measured for example radiometrically, must be multiplied by this number.

To obtain diagnostic information, ultrasound is irradiated into tissues in the form of continuous harmonic waves (continuous Doppler systems) or in the form of short impulses (10^{-6}-10^{-5}s) with repetition frequency of 1.5-2.5 kHz. Intensity in continuous operations is given either as spatial average — SA or spatial peak — SP. Not only spatial but also time distribution of irradiated energy must be taken into account in pulsed reflection image-forming methods or in pulsed Doppler systems. Therefore, intensity can be expressed as spatial peak-temporal peak, SPTP, spatial peak-temporal average, SPTA, spatial average-temporal peak, SATP, and spatial average-temporal average, SATA. As the ultrasound pulses are not always of the exact rectangular form, another two terms have been used recently for the expression of intensity in pulsed mode: spatial average-pulse average, SAPA, which is the average intensity of pulse applied to the total cross-section of ultrasound beam. Spatial peak pulse average, SPPA, is the average intensity of pulse in the place of its maximum value.

Spatial average-temporal average, SATA, is most easily measurable and the most frequently given value. However, it is of limited importance for the appreciation of biological effectiveness. Here are of greater use the SPTA value determining the heat production by absorption in time dependence and

the SPTP value which is the expression of the maximum mechanical energy in a given place of the field at a given time moment.

Frequency is another important constant for appreciating biological effects. The dependence of absorption phenomena on the basic frequency of ultrasound source is well known. In pulsed operations biological effectiveness is also influenced by the repetition frequency of ultrasound impulses.

3. Problems with determining the threshold of biological effectiveness

Biological problems connected with determining a biologically effective threshold must therefore be judged from a few aspects. First, we must take into account the fact that most living organisms, including man, have neither specific receptors for ultrasound energy nor specific regulatory mechanisms. Thus, from this point of view, the reaction of a living organism is non-specific and the threshold of biological effectiveness is conditioned by dissimilar sensitivity of tissue cells to ultrasound. Therefore, the relation between the biological effect and the physical properties of ultrasound field is often non-linear. The microstructure and macrostructure of the tissue through which ultrasound passes is another important factor. This causes various ultrasound suppression and qualifies the development of interference phenomena, thus deepening the process non-linearity.

Ultrasound interactions with biological objects were studied on various levels of biological arrangement under various experimental conditions. Fundamental mechanisms of the biological effect can be analysed more easily on isolated cells and cultures. On higher levels (in tissues and organs, in the whole organism) there gets into action a complex system of feedbacks and compensation mechanisms that superimpose and modify the primary effect.

4. Are the recommended safety criteria respected by manufacturers of ultrasound diagnostic devices?

In 1976 efforts to establish the safety criteria in ultrasound investigation methods led the American Institute for Ultrasound in Medicine (AIUM) to state its stance. It was, after small modifications, accepted by the working group of the World Health Organization in the same year. The value of 1 kWm^{-2} expressed as SPTA was recommended as the limit of biologically effective intensity in vivo and the value of $5 \cdot 10^5$ Jm^{-2} as the limit of biologically effective exposition within 1-500 s. Both of these limit values were formulated on the basis of appreciating all accessible data on biological effects of ultrasound within 0.5-10 MHz frequencies.

Comparison of average and peak intensity values emitted by various ultrasound diagnostic devices was performed from the angle of the recommen-

ded limits. This comparison is given in Table 1. The large intensity range found results, on the one hand, from a wide choice of diagnostic devices manufactured recently, on the other hand, it is conditioned by various measuring techniques used and their unequal accuracy.

Table 1. Ultrasound intensities emitted by diagnostic systems

Type of device	Emitted intensity [Wm^{-2}]	
	SATA	SPTA
Static $A-$ and $B-$mode scanners, $M-$mode instruments	4 – 200	100 – 2000
Dynamic $B-$mode scanners, sector	27 – 600	450 – 2000
Dynamic $B-$mode scanners, linear	0.6 – 100	1 – 120
Pulsed Doppler systems	30 – 320	300 – 2900
Continuous wave Doppler systems for obstetrics	30 – 250	90 – 750
Continuous wave Doppler systems for angiology	380 – 8400	1100 – 25000

The underlined values are higher than the recommended limit.

It follows from Table 1 that with the exception of fetal detectors and devices using linear probes for dynamic scanning, there exist in all the other groups devices whose SPTA intensity is higher than the recommended level of SPTA (1000 Wm^{-2}).

5. Relation of biological effectiveness and risk of ultrasound application

Intensive research of the biological effectiveness of very low ultrasound intensities performed recently has, however, shown the possibility of influencing sensitive biological objects at intensities lower than the recommended level of biological safety. This was the matter of changes in some morphological and functional properties proved in isolated cells and tissue cultures. Direct interpretation of these experimental findings is indisputably very difficult for clinical diagnostic application, first of all because the term of biological effectiveness is not a synonym for risk. On the other hand, up to now we have not had sufficient knowledge on the possible cummulative effect of small doses of ultrasound energy in biological systems generally and in man particularly.

Difficulties connected with the formulation of obligatory technical and physical standards for the operation of ultrasound diagnostic devices from the

view of their biological effectiveness follow from the statement mentioned above. Ultrasound diagnosis is a complex of methods with dynamic development, where the optimum level of emitted intensity is a compromise between the effort for maximum differentiating abilities on the one hand and the maximum sensitivity of the device on the other hand.

Respecting the value of 1 kWm^{-2} as the recommended peak limit of emitted intensity for diagnostic systems, the manufacturers of these systems must aim at achieving the best quality picture of tissue examined at acoustic performance as low as possible. The examination itself must not exceed the time necessary for obtaining required diagnostic information.

References

[1] V. Akopyan, *Le mécanisme de l'action biologique de l'ultrason sur les cellules,* Proc. 11th International Congress on Acoustics, Paris 1983, **2**, 329-332.

[2] K. Brendel, G. Ludwig, *Diagnostic intensities and their measurement,* in: *Recent advances in ultrasound diagnosis,* A. Kurjak, A. Kratochwil (eds.), Excerpta Medica, Amsterdam-Oxford-Princeton 1981, 76-80.

[3] J. Cachon, M. Cachon, J-N. Bruneton, *An ultrastructural study of the effects of very high frequency ultrasound on a microtubular system,* Cell. Biol., **40**, 69-72 (1981).

[4] P. L. Carson, P. R. Fischella, T. V. Oughton, *Ultrasonic power and intensity produced by diagnostic ultrasound equipment,* Ultrasound Med. Biol., **3**, 341-350 (1977).

[5] E. L. Carstensen, *Biological effects of low-temporal, averageintensity, pulsed ultrasound,* Bioelectromagnetics, **3**, 147-156 (1982).

[6] J. Etienne, L. Filipczyński, A. Firek *et al., Intensity determination of ultrasonic focused beam used in ultrasonography in the case of gravid uterus,* Ultrasound Med. Biol., **2**, 119-122 (1976).

[7] L. Filipczyński, *Measurement of the temperature increases, generated in soft tissues by ultrasonic Doppler equipment,* Ultrasound Med. Biol., **3**, 341-345 (1978).

[8] G. M. Hahn, J. B. Marmor, D. Pounds, *Induction of hyperthermia by ultrasound,* Bull. Cancer (Paris), **68**, 3, 249-254 (1981).

[9] I. Hrazdira, *Ultrasonically induced cell surface alterations,* Proc. World Congress on Medical Physics and Biomedical Engineering, 1982, Hamburg, 23-11.

[10] D. Liebeskind, R. Bases, M. Koenigsberg *et al., Morphological changes in the surface characteristic of cultured cells after exposure to diagnostic ultrasound,* Radiology, **138**, 419-423 (1981).

[11] W. D. O'Brien, Jr., *Ultrasonic dosimetry. Ultrasound: its applications im medicine and biology,* F. Fry (ed.), Elsevier Scientific Publishing Co., New York 1978.

[12] D. J. Pizarello, A. Vivino, J. Newall, B. Madden, *Effect of pulsed low-power ultrasound on growing tissues. II. Malignant tissues,* Exp. Cell. Biol., **46**, 240-245 (1978).

[13] A. P. Sarvazyan, *Some general problems of biological action of ultrasound,* Academy of Sciences of the USSR, Pushchino, 1981.

[14] G. ter Haar, *Safety of medical ultrasound,* Progress in Medical Ultrasound, A. Kurjak (ed.), **1**, 313-320, Excerpta Medica, Amsterdam-Oxford Princeton, 1980.

[15] A. R. Williams, D. L. Miller, *Photoelectric detection of ATP release from human erythrocytes exposed to ultrasonically activated gas-filled pores,* Ultrasound Med. Biol., **6**, 251-256 (1980).

ARCHIVES OF ACOUSTICS
9, 1-2, 101-104 (1984)

FREQUENCY DEPENDENT ULTRASONIC ATTENUATION COEFFICIENT ASSESSMENT IN FRESH TISSUE

W. D. O'BRIEN, JR, L. A. SEGAL

Bioacoustics Research Laboratory, Department of Electrical Engineering, University of Illinois
(1406 W Green Street, Urbana, IL 61801, USA)
Department of Metallurgy (for W. D. O'Brien. Jr. only), University of Oxford
(Parks Road, Oxford, OX1 3PH United Kingdom)

The authors discuss the frequency dependent ultrasonic attenuation coefficient for fresh liver and fresh spleen from bovine, porcine and lamb, and fresh pancreas from bovine and futher discuss the role of these attenuation coefficients in terms of their collagen, actually hydroxyproline, concentration. The technical procedures of specimen handling and data gathering are reproducible. A higher order fit appears to be necessary for describing the frequency dependency of the attenuation coefficient. There does not appear to be any correlation between the attenuation coefficient and collagen concentration for these tissues.

1. Introduction

It is yet difficult to evaluate properly the mechanisms responsible for the propagation of ultrasound through tissue. This is due, in part, to the available data base. There does not yet exist a well documented and reproducible data basis which can be used to intercompare the ultrasonic propagation properties among various tissues.

If one considers the role collagen plays in terms of the ultrasonic attenuation coefficient, it is possible to group biological tissues, save bone and lung, into three general categories. The low attenuating materials consist of virtually no collagen, the high attenuating materials consist of high amounts of collagen and the balance of materials fall between these two categories. This latter group generally involves the parenchymal tissues of brain, liver, spleen, kidney, muscle, heart, etc. *This observation has been presented elsewhere [2]* and showed that while a general trend existed between ultrasonic attenuation

and collagen concentration, it was not evident whether any such trends were evident within this middle group.

This preliminary report discusses the frequency dependent ultrasonic attenuation coefficient for fresh liver from bovine, porcine and lamb, fresh spleen from bovine, porcine and lamb and fresh pancreas from bovine and further discusses the role of these attenuation coefficients in terms of their collagen, actually hydroxyproline, concentration. The unique features of this report are that the same tissue handling procedure, the same ultrasonic attenuation coefficient technique and the same hydroxproline analysis procedure were employed for all seven tissues, therefore providing a basis for comparison. The work reported herein is drawn from the thesis of Segal [4].

2. Methods

The tissue specimens were obtained from the University of Illinois slaughter house and transported to the Bioacoustics Research Laboratory in normal saline at room temperature. The specific specimen under investigation was then prepared for the radiation force balance technique, a phase insensitive procedure which determines the ultrasonic insertion loss of the specimen (of a known thickness) at the ultrasonic frequencies of 1.39, 4.21, 7.02 and 9.82 MHz. The specimen handling procedure and the radiation force balance technique are the same as described previously [3], in which fresh bovine liver tissue was studied. All measurements were made in saline at a temperature of 22°C within three and one half hours of slaughter.

The ultrasonic attenuation coefficient was determined via a linear regression technique from the slope of the insertion loss versus specimen thickness data at each frequency. At least six tissue measurements were made for each thickness and there were at least six thicknesses which ranged from 5 to 18 mm for each attenuation coefficient analysis.

A linear regression analysis procedure was then applied to the attenuation coefficient versus ultrasonic frequency data to yield a, the amplitude value at 1 MHz, and b, the frequency exponent in the expression

$$A = af^b. \tag{1}$$

Hydroxyproline concentration, a measure of the collagen concentration in tissue, was determined by hydrolyzing the specimen and measuring the amount of hydroxyproline in an automated amino acid analyzer by a technique similar to that described by EDWARDS and O'BRIEN [1].

3. Results and discussion

The ultrasonic attenuation coefficient data obtained in this study for fresh bovine liver compares favorably with that obtained from a previous study [3] under identical experimental conditions but with different indivi-

duals conducting the actual experimental work. Previously, a least squares fit of the attenuation coefficient (Np/cm) versus frequency (MHz) to the 1-100 MHz data base yielded

$$A = 0.043\ f^{1.270}, \tag{2}$$

whereas this study yielded (to the 1—10 MHz data base)

$$A = 0.038\ f^{1.36}. \tag{3}$$

This supports the view that the experimental procedure is reproducible. In both of these studies, a straight line fit to the log-log data base was quite sufficient to describe the results over the measured frequency range.

In addition to the bovine liver, a straight line adequately described the log-log relationship of the frequency dependent attenuation coefficient for lamb spleen in which

$$A = 0.037\ f^{1.29}. \tag{4}$$

So, for both bovine liver and lamb spleen, the amplitude value a and the frequency exponent b are sufficient to describe these tissues' attenuation coefficient as a function of frequency.

However, for the other five tissues examined, the simple power relationship of equation (1) does not appear to be adequate for describing the frequency dependency of the attenuation coefficient. While it has not been done for this preliminary report, an examination of the data suggests that a quadratic fit to the log-log data base would be more adequate. For these five tissues (bovine spleen and pancreas, porcine liver and spleen and lamb liver), the frequency dependent nature of the attenuation coefficient suggests that as the frequency increases, the actual attenuation coefficient values increase at a much greater rate than that of a linear fit. Thus, without this more complete analysis, it could be misleading to provide only a linear power fit equation to describe these data.

A brief examination of the attenuation coefficient data at 1.39 MHz and 9.82 MHz does not suggest any obvious trends between type of tissue or between source of tissue. In increasing order of the attenuation coefficient (in Np/cm) at 1.39 MHz is lamb spleen (0.055), bovine liver (0.060), porcine spleen (0.084), bovine spleen (0.11), porcine liver (0.12), lamb liver (0.12) and bovine pancreas (0.17). The 9.82 MHz attenuation coefficient data in increasing values yields porcine spleen (0.64), lamb spleen (0.69), lamb liver (0.76), bovine pancreas (0.81), porcine liver (0.87), bovine liver (0.87) and bovine spleen (0.89). In both cases the order is quite different.

An examination of the ultrasonic attenuation coefficient as a function of the hydroxyproline concentration at each ultrasonic frequency did not reveal any statistically significant trends. Only at 9.82 MHz was there even the slightest hint that the attenuation coefficient decreased as the hydroxy-

proline concentration increased, just opposite in trend to that of previous observations [2]. It must be kept in mind, however, that all of these tissues had approximately the same collagen concentration and thus this tissue property may not (and indeed appears not to) be the best or even the proper one to correlate with the ultrasonic attenuation coefficient. It must be obvious that the comparison of the attenuation coefficient data to a single tissue property is somewhat simplified. A more complete comparison to a combination of tissue properties would appear to be more reasonable and is being done.

In conclusion, the following observations can be made from this preliminary data analysis. The technical procedures of specimen handling and data gathering are reproducible and thus provide the basis for intercomparison. The attenuation data for these seven tissues are each distinct in their own way. Describing the frequency dependency of the attenuation coefficient by a single number, usually the frequency exponent, may not be proper for many tissues. A higher order power fit appears to be necessary. And finally, there does not appear to be any correlation between the attenuation coefficient and collagen concentration for these tissues.

Acknowledgements. This work was partially supported by a grant from the National Institutes of Health, National Cancer Institute (CA 36029). Part of the analysis was performed while one of the authors (W. D. O'Brien, Jr.) was on sabbatical leave at the University of Oxford, England and support from there is acknowledged.

References

[1] C. A. Edwards, W. D. O'Brien, Jr., Clin. Chim. Acta. **104**, 161-167 (1980).

[2] W. D. O'Brien, Jr., Proc. Ultrasonics International 1977, 194-205, IPC Science and Technology Press Ltd., Guildford, England 1977.

[3] J. D. Pohlhammer, C. A. Edwards, W. D. O'Brien, Jr., Medical Physics, **8**, 692-694 (1981).

[4] L. A. Segal, M. S. Thesis in Electrical Engineering, University of Illinois, 1983.

ARCHIVES OF ACOUSTICS
9, 1-2, 105-112 (1984)

THE INFLUENCE OF ULTRASOUND ON THE REACTION OF IMMOBILIZED ENZYMES

EIKE ROSENFELD, PETER SCHMIDT

Intitute of Applied Biophysics, Dept. of Medicine, Martin-Luther-University Halle
(DDR-4014 Halle, Strasse d. DSF 81, GDR)

The effect of ultrasonic waves in the MHz range on the activity of immobilized α-amylase and glucoamylase was investigated. Measurements of the catalytic efficiency were carried out in a flow cell, in dependence on the concentration, the flow rate, and the molecular weight of the substrate, as well as on the size of the carrier particles (porous polystyrene). The results show that the ultrasonic effect might be explained by the promotion of the diffusion processes predominately within the Nernst diffusion layer of the carrier beads.

1. Introduction

Ultrasonic effects on enzymes, hormones and other biological macromolecules are well described in the literature [1, 5]. An enhancement of the catalytic activity of enzymes in solution, however, has not yet been established in any case.

On the other hand, such ultrasonic effects could be demonstrated at immobilized enzymes [2], i.e. enzymes which have been confined to insoluble carriers either by chemical or physical attachment or entrapment [3].

Frequently the immobilization is accompanied by a loss of catalytic efficiency. An additional diffusion limitation in the vicinity of the active molecules, due to the presence of the carrier network, and an unstirred liquid layer on the surface of the support are the reasons for this phenomenon [4,8].

The present paper reports on experimental investigations to improve the catalytic efficiency of enzymes immobilized on a porous polystyrene carrier by means of ultrasonic waves.

2. Diffusion controlled enzyme-carrier systems

The mass transport during the heterogeneous catalysis may be classified into external and internal transportation. The former is limited to the substrate as well as to the product molecules by an unstirred layer, the so-called Nernst diffusion layer (Fig. 1). The mass transport rate per unit area of the substrate may be denoted by the equation [8]

$$\varphi = \frac{D(s - s')}{\delta}, \tag{1}$$

where D is the diffusion coefficient of the substrate in the unstirred layer; δ is the thickness of this layer; s and s' are the substrate concentrations in the

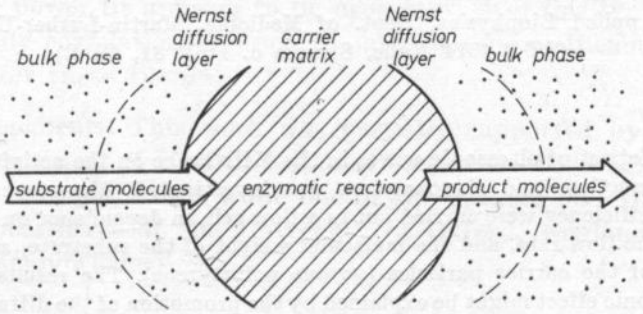

Fig. 1. Schematic representation of the mass transport during the heterogeneous catalysis

well mixed bulk phase and at the surface of the polymer matrix, respectively. The concentration profile across the carrier is illustrated in Fig. 2. The mass transport rate φ, which decisively influences the total rate of the catalytic reaction, may be accelerated by an increase in the concentration gradient $(s - s')/\delta$ within the Nernst diffusion layer. The thickness δ is dependent on the hydro-

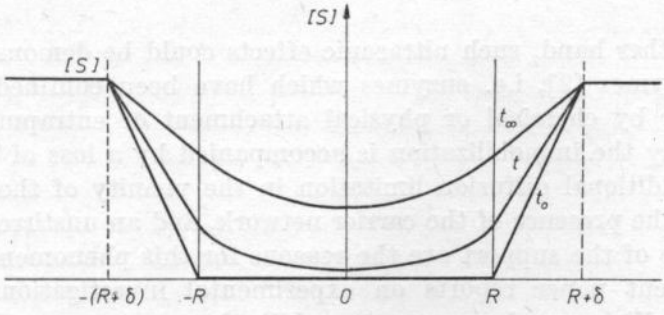

Fig. 2. Substrate concentration profile across the carrier matrix and the adjacent liquid range (after [4])

dynamic streaming around the carrier beads and cannot be reduced indefinitely in this way. In a well stirred reactor δ is of the order of magnitude of 100 μm. By means of ultrasonic waves, however, δ can be reduced to the thickness of the acoustic boundary layer

$$\delta_{\text{acoust.}} = \sqrt{\frac{2\nu}{\omega}}; \qquad \omega = 2\pi f, \tag{2}$$

where ν is the kinematic viscosity and f is the sound frequency. E.g., $\delta_{\text{acoust.}}$ amounts to 0.1 μm in aqueous solutions at 5 MHz.

The substrate concentration s' on the surface of the porous support is dependent on the rate of the internal mass transport (pore diffusion). Generally, a sound effect on this part of the diffusion may be neglected, since the diameter of the pores is small compared with the thickness of the acoustic boundary layer.

3. Material and method

The enzymes used were α-amylase (Novo A/S, Denmark) and glucoamylase (Merck, Darmstadt) with Zulkowsky starch (Merck, Darmstadt) and maltose (VEB Laborchemie, Apolda) as substrates. The enzymes were bound to porous polystyrene (type Y58, VEB Chemiekombinat Bitterfeld), used in two fractions (0.15-0.20 mm — charge 1; 0.63-0.80 mm — charge 2). The biochemical preparation and analysis procedures are described elsewhere [6].

The measuring cell (Fig. 3) has a cylindrical shape with a volume of 1 ml and is faced by two 30 μm thick plastic foils. The cell is placed in a thermo-

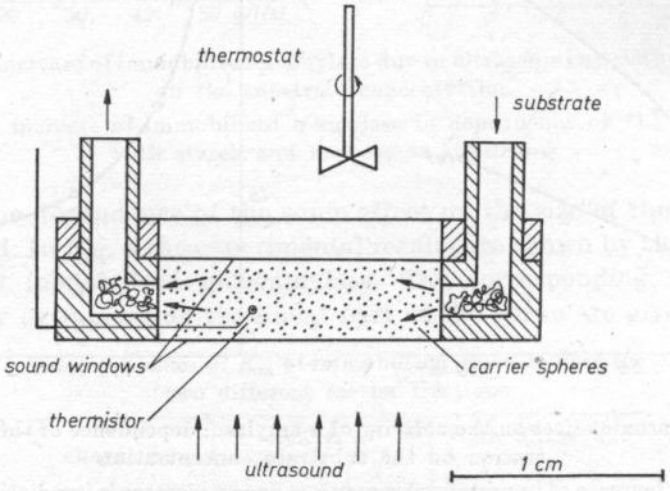

Fig. 3. Schematic representation of the reaction cell

stat-equipped vessel at a distance of about 2 cm from the transducer. The experiments were carried out in a continuous, non-focused soundfield at a frequency of 7 MHz. The maximum sound intensity, measured by a radiation force float, was 10^3 W/m^2.

4. Results and discussion

Immobilized α-amylase and starch as substrate were examined to demonstrate the effect of the ultrasound irradiation on the enzymatic reaction. The reaction is clearly accelerated in the presence of the soundfield, as represented in Fig. 4. The same result can be shown by the Lineweaver-Burk plot. The change of the Michaelis-Menton constant can be interpreted by the promotion of the substrate diffusion into the carrier matrix. The maximum reaction rate is changed, too.

A further indication of the sonic influence on the diffusion processes is the dependence of the activity increase in the sound field on the flow rate in the cell and on the substrate concentration, respectively (Figs. 5 and 6). An acceleration of the flow reduces the thickness of the unstirred layer around the carrier beads due to the hydrodynamic mechanisms, and consequently the sonic effect decreases. If the substrate concentration s is raised the concentration s' changes in the same measure. This procedure can be continued until

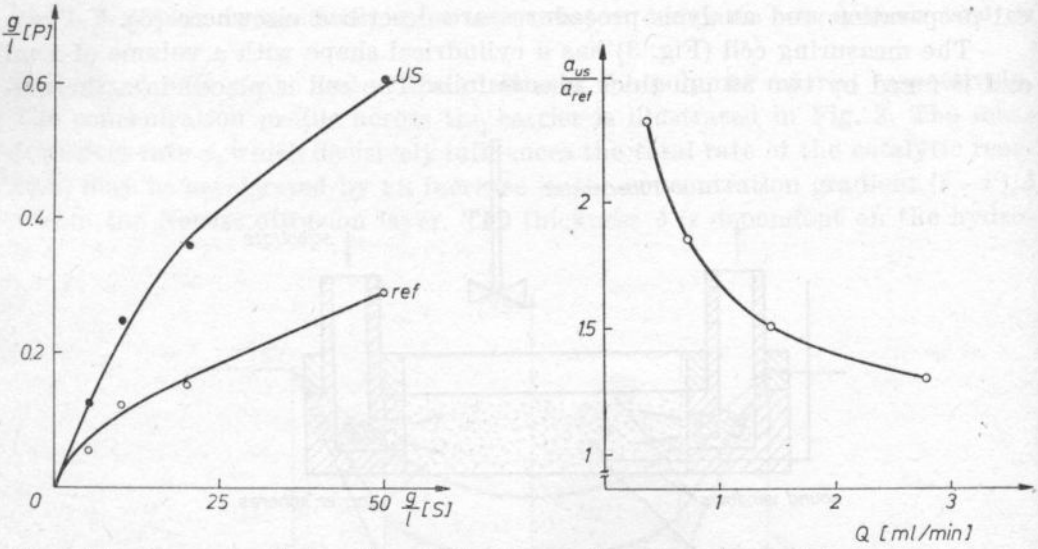

Fig. 4. The ultrasonic effect on the activity of α-amylase; dependence of the product concentration on the substrate concentration

Fig. 5. Activity increase of immobilized α-amylase due to ultrasonic irradiation in dependence on the substrate flow rate

the reaction is no longer controlled by the film diffusion. Obviously, the sonic effect diminishes correspondingly.

If α-amylase is replaced by glucoamylase two substrates can be used and the sound influence can be studied dependending on the molecular size. In Fig. 7 the activity increase is plotted versus the sound intensity for starch (MW $\approx$ $\approx$ 15.000) and maltose (MW 348), respectively as substrates. The effect is proportional to the sound intensity and, as expected from the results obtained hitherto, the effect is much smaller for the substrate with the lower molecular weight.

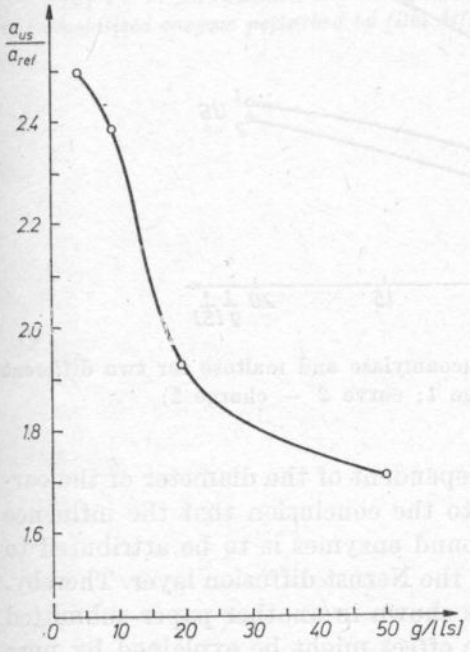

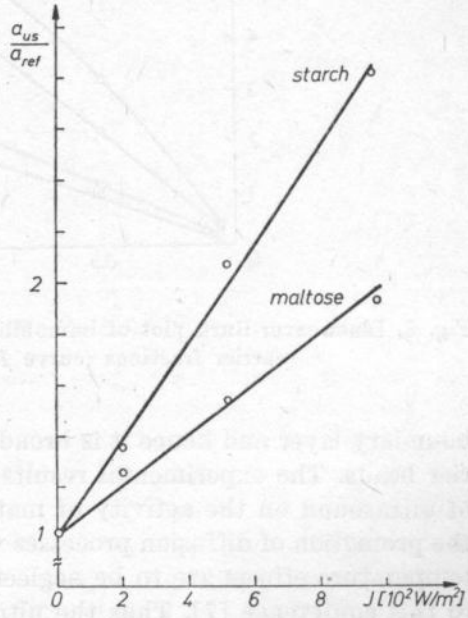

Fig. 6. Activity increase of immobilized α-amylase due to ultrasonic irradiation in dependence on the substrate concentration

Fig. 7. Activity increase of immobilized α-amylase in dependence on the sound intensity with starch and maltose as substrates

Finally the dependence of the sonic effect on the size of the carrier beads were examined. In Fig. 8 the experimental results are shown by the Lineweaver-Burk plot of immobilized glucoamylase. The corresponding values of K_m determined by extrapolating the linear part of the curve are given in Table 1.

Table 1. Values of K_m of immobilized glucoamylase for two different carrier fractions

charge no	Reference		With ultrasound	
	1	2	1	2
K_m [g/l]	40.6	49.1	11.3	9.2

The reference value for the charge with the smaller beads is lower than that for the bigger ones. Under ultrasound the two values agree within the limits of the experimental conditions. This is an indication that in the presence of an ultrasonic field the mass transport is determined by the thickness of the acoustical

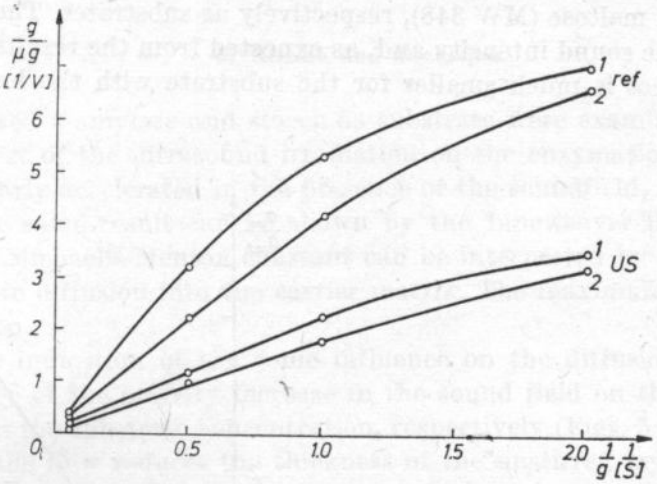

Fig. 8. Lineweaver-Burk plot of immobilized glucoamylase and maltose for two different carrier fractions (curve *1*: charge 1; curve *2* — charge 2)

boundary layer and hence it is broadly independent of the diameter of the carrier beads. The experimental results lead to the conclusion that the influence of ultrasound on the activity of matrix bound enzymes is to be attributed to the promotion of diffusion processes within the Nernst diffusion layer. Thereby, temperature effects are to be neglected, as shown in another paper submitted to this conference [7]. Thus the ultrasonic effect might be explained by pure mechanical, non-cavitational interactions like acoustic streaming or microstreaming.

Acknowledgements. The biochemical investigations of this work were done at the Dept. of Biochemistry, Div. of Biological Sciences, Martin-Luther-University Halle. We wish to thank Prof. Dr. Sc. Nat. A. SCHELLENBERGER, director of this institution, for his stimulating cooperation.

References

[1] I. E. EL'PINER, *Ultrasound, physical chemical and biological effects,* Consultants Bureau, New York 1964, 149-230.

[2] Y. ISHIMORI, I. KARUBE, S. SUZUKI, *Acceleration of immobilized α-chymotrypsin activity with ultrasonic irradiation,* J. Mol. Catal., **12**, 253-59 (1981).

[3] J. KONECNY, *Theoretical and practical aspects of immobilized enzymes,* Survey of Progress in Chemistry, New York, **8**, 195-251 (1977).

[4] J. LASCH, *Theoretical and experimental analysis of continuous flow enzyme reactor kinetics,* Mol. and Cell. Biochem., **2**, 1, 79-86 (1973).

[5] R. M. MACLEOD, F. DUNN, *Effects of intense noncavitating ultrasound on selected enzymes,* J. Acoust. Soc. Am., **44**, 4, 932-40 (1968).

[6] P. SCHMIDT, J. FISCHER, E. ROSENFELD, R. MILLNER, K. HAUPKE, A. SCHELLENBERGER, *On the influence of ultrasound on the porosity of the surface of polystyrene-enzyme-carriers* (in German), Die Angew. Makromol. Chemie, **97**, 179-87 (1981).

[7] P. SCHMIDT, E. ROSENFELD, *Temperature rise in artificial and biological cells due to ultrasonic absorption,* UBIOMED VI, Warsaw-Jabłonna 1983.

[8] P. V. SUNDARAM, *An analysis and interpretation of the Michaelis-Menton kinetics of immobilized enzyme perturbed by film diffusion,* J. Solid-Phase Biochem., **3**, 241-46 (1978).

ARCHIVES OF ACOUSTICS
9, 1-2, 113-116 (1984)

CAVITATION EFFECT IN SOME ERYTHROCYTE SUSPENSIONS

EVA VERESS

Ultrasonic Laboratory, Babeş-Bovai University
3.400 Cluj-Napoca, 1 Kogalniceanu Street, Romania

The destructive effects of ultrasound on cell suspensions depend on the parameters of the ultrasonic field and the experimental conditions. Erythrocytes of three origins were investigated: frog, chicken and rat. The frequency of the ultrasound was 1 MHz, with the intensity ranging from 0.4 to 1.2 Wcm^{-2}. The volume concentrations of the samples were in the range 0.5-2 per cent. The investigation determined the volume concentration limit at which, at a sufficiently high field intensity, the destructive effect may be produced.

In well defined conditions (at sufficiently low concentration) cavitation occurs, which has destructive effects (haemolysis). Haemolysis is produced at a well defined concentration in each case, depending on the physical, chemical and biological properties of the erythrocytes. The threshold concentration varies for different erythrocytes; thus the following values were obtained at 0.4 Wcm^{-2}: chicken 0.5 per cent, frog 1 per cent, rat 2 per cent. At low intensities ($J = 0.4$ Wcm^{-2}), high frequency, short duration and diluted suspensions, cavitation plays a mayor role in the haemolysing action.

1. Introduction

Under well determined conditions, ultrasound produces destructive effects in biological cells. The destructive effects in diluted suspensions of erythrocytes are caused by cavitation [4]. The erythrocyte suspensions may be used as a model system in the study of the cavitation effect of ultrasound, because the destructive effect (haemolysis) may readily be evaluated by measuring the haemoglobin concentration in the supernatant obtained after exposure and centrifugation.

This paper presents a study of the parameters which determine the biological, and expecially the destructive, effects of ultrasound, aimed at elucidating the aspects of the ultrasound action mechanism on diluted erythrocyte suspensions, in vitro.

2. Material and method

Diluted erythrocyte suspensions from frog, chicken and rat were used. In the preparation of the suspension we needed a relatively considerable quantity of blood. The blood was collected in different ways, adopting the method to the species. The collected blood had to be very pure.

In order to prevent coagulation heparine was used. The fresh blood was centrifugated 10 min. to 3000 rotations. Then the erythrocytes were separated and washed three times in the centrifuge [7]. The ultrasonic source was a piezoelectric generator made by Tesla, operating in a continuous mode. Sonication to traveling wave of the 1 ml erythrocyte suspensions was performed at ambient pressure and at 18°C, the temperature being controlled by a thermocouple [2].

The parameters of the ultrasonic field were: frequency 1 MHz, intensity varying between 0.4 and 1.2 Wcm^{-2}. The volume concentration of the samples was varied between 0.5-2 %. The occurrence of cavitation was detected using chemical and luminiscence methods [1, 5, 6]. The intensity of the cavitation process was assayed as the time necessary for haemolysis to occur. The haemolysis degree was determined photocolorimetrically using the standard Drabkin reagent as the concentration of haemoglobin released in the supernatants.

3. Results and discussion

Threshold intensities and concentrations were determined, at which haemolysis is induced (Table 1, for chicken). At constant concentration, the time

Table 1. The sonication time (in s) necessary to produce haemolysis in erythrocyte suspensions (chicken, frog, rat) of different concentrations at three intensities of the ultrasonic field

Suspension	Intensity [Wcm^{-2}]	Volume concentration [%]				
		0.5	0.7	1.0	1.5	2.0
		Sonication time [s]				
Chicken	0.4	60	×	×	×	×
	0.6	20	180	×	×	×
	1.0	5	30	120	×	×
Frog	0.4	50	60	100	×	×
	0.6	20	30	60	×	×
	1.0	5	10	30	×	×
Rat	0.4	40	50	70	80	×
	0.6	5	10	20	30	100
	1.0			5	10	60

× = no haemolysis occurs.

required for haemolysis to occur is shorter for higher intensities. The threshold concentration for chicken erythrocytes is 1 per cent at 1.0 Wcm^{-2}. The corresponding concentrations for other suspensions vary as shown in Table 2, indicating the dependence on the biological properties of the cells membrane resistance, structure and dimensions [8-9]. The chicken cells are the most resistant.

Table 2. The sonication time (in s) necessary to produce haemolysis in chicken erythrocyte suspension of different concentrations at six intensities of the ultrasonic field

Intensity [Wcm^{-2}]	Volume concentration [%]					
	0.5	0.6	0.7	0.8	0.9	1.0
	Sonication time [s]					
0.4	60	×	×	×	×	×
0.5	40	180	×	×	×	×
0.6	20	70	180	×	×	×
0.8	10	30	90	×	×	×
1.0	5	10	30	70	100	×
2.2		5	10	30	70	120

× = no haemolysis occurs.

The correlation coefficients ($r_{c,t}$) were calculated between the concentration (c) and the time necessary to obtain haemolysis (t), at different constant values of intensity (J).

Similarly, the correlation coefficients ($r_{J,t}$) were calculated between the intensity (J) and the exposure time (t) at different constant values of the concentration (c).

The values of correlation coefficient ($r_{c,t}$) at various intensities show a positive and very close correlation between the intensity and the time necessary to obtain haemolysis.

The values of the correlation coefficient ($r_{J,t}$) show a negative correlation between the intensity and the time necessary to obtain haemolysis. The values are very significant.

Below the intensity threshold, the time becomes asymptotically longer, provided the concentration is above the threshold by a certain amount.

The cavitation threshold is the limiting intensity under which cavitation does not occur, while above which the formation of cavitation bubbles is possible. It varies as a function of the experimental conditions and the properties of a biological system. The intensity threshold increases with frequency [3].

The occurrence of cavitation is favoured in cell suspensions over that in pure liquids. This is because one must overcome only the adhesion forces in suspensions which are smaller than the cohesion one forces so that cavitation may

occur at intensities as low as 0.5 Wcm^{-2} (for given concentrations). The lethal effect in cells caused by cavitation is produced according to the "all or nothing" law, i.e. after the critical dose is exceeded haemolysis involves simultaneously all the cells [10]. The process involves the transient cavitation type.

4. Conclusions

1. At high frequency (1 MHz) erythrocytes diluted in saline solutions are haemolysed by cavitation, provided the concentration is below a critical value.

2. The cavitation threshold varies with the concentration and the type of cells.

3. The resistance of erythrocytes to ultrasound decreases from chicken to frog to rat.

References

[1] R. P. Clarke, C. R. Hill, *Physical and chemical aspects of ultrasonic disruption of cells,* J. Acoust. Soc. Am., **47**, 2, 649-653 (1970).

[2] A. Cseko, E. Veress, *Comparison of ultrasonic intensity measurements in different experimental conditions,* Proc. 7 Int. Congr. on Acoust. Budapest, 18-26 August 1974, 561-564.

[3] R. Esche, *Unterzuchungen zur Ultraschallabsorbtion in tiereschen Geweben and Kuntstoffen,* Akust. Beih, **2**, 71-74 (1952).

[4] D. E. Hugher, W. L. Nyborg, *Cell disruption by ultrasound,* Science, **12**, 138, 35-37, 108-114 (1962).

[5] R. O. Prudhomme, *Etude des actions physico-chimiques et mechaniques des ultrasons,* Acta Chim. Sci. Hung., **23**, 1-4, 469-481 (1960).

[6] E. Veress, E. A. Pora, *Rezistence aux ultrasons de quelques erythrocytes des vertebres,* Proc. Int. Congr. on Acoust., Budapest, 1971, 653-656.

[7] E. Veress, J. Vincze, *The haemolysing action of ultrasound on erythrocytes,* Acustica, **36**, 2, 100-103 (1976/77).

[8] E. Veress, D. Auslander, I. Lenart, *Destruction par ultrasons et proprietes acoustiques des erythrocytes,* Proc. 9th Int. Congr. on Acoust., Madrid, 1977, 543-544.

[9] E. Veress, *Biological and biophysical action of ultrasound,* UBIOMED IV, 1979, 100-102.

ARCHIVES OF ACOUSTICS
9, 1-2, 117-120 (1984)

THE PASSIVE HAEMAGGLUTINATION REACTION WITH SONICATED *T. PALLIDUM* (NICHOLS STRAIN) IN THE SERODIAGNOSIS OF SYPHILIS (TPHA)

VOICHITZA LAZAR, FLORICA KEVORKIAN,
IULIU CĂPUŞAN, DEZIDERIU AUSLANDER, EVA VERESS

Clinic of Dermatology, Institute of Medicine and Pharmacy

Babes-Bolyai University, Ultrasonic Laboratory, Cluj-Napoca, Romania

The preparation of the antigen for TPHA sonicated suspension of *T. pallidum* (Nichols strain) being so far a "secret" of the procedures, we have attempted to reproduce it by our own means of ultrasonic irradiation. The best results in agreement with the standard reactions for syphilis were obtained by sonicating *T. pallidum* suspensions for a duration of 20 min. by the following parameters of the ultrasonic field: frequency 1 MHz, intensity 0.9 W/cm^2. Using this method we obtained microfragments of 1-1.3 microns. The most reliable dilution for the antigen was 1/1000. The haemagglutination was performed in 30 patients with different forms of late syphilis after treatment.

The results were in agreement with the clinical diagnosis, being more sensitive and consistent compared with the classical and standard reactions.

TPHA is highly useful in mass screenings, as an indicator of the therapeutical efficiency and in the evaluation of the persistent positive perological reactions or in discordant serology.

TPHA was introduced in 1965 by RATHLEV [6, 7] for syphilis serodiagnosis, and it was completed in a standardized reaction by TOMIZAWA and KASAMATSU in 1966 [8], a laboratory standardized technique being realized by COX *et al.* in 1968 [2].

The first attempt to introduce this technique in Romania, using treponemic antigens or standardized Japanese antigen (Fujikoki Pharm. Ltd.) was made by BĂDĂNOIU *et al.* in 1976 [1] and GEORGESCU and IONESCU in 1979 [3].

The advantages of TPHA include: simplicity, specificity by use of pathogen Treponema strains, high sensitivity, fidelity in excess of 95 per cent over the standard reaction, including the most specific reaction as FTA and TPI, precocity and persistence, permitting also a retrospective serological diagnosis [1]

The field in which TPHA is recommended is: mass syphilis screening together with a lipoidic reaction, serological diagnosis in the late syphilis replacing other treponemic reactions as FTA-Abs and TPI. TPHA can be used with a higher specificity than FTA-Abs and TPI as a control serological test after the treatment.

There are some geographical variations of TPHA, the test being used with antigens from Japan (Fujikoki — 5), England and BRD (Cellagnost — 4).

The preparation of the antigen (sonicated suspension of *T. pallidum* (Nichols strain)) being a "secret" of the above procedures, we have attempted to reproduce it by our own means of ultrasonic irradiation.

Using 1 ml of *T. pallidum* (Nichols strain) liofilized antigen diluted in distilled water, exposed to ultrasonic irradiation in an ultrasonic TESLA type apparatus with a 40 mm diameter quartz, we checked the fragmentation by an ultramicroscopic procedure in dark field.

The best results agreeing with the standard reactions for syphilis were obtained by sonicating *T. pallidum* suspensions for a period of 20 min., in several intervals (30 s, 5, 4 and 10 min.), by the following parameters of the ultrasonic field; frequency 1 MHz, intensity 0.9 W/cm². Using this method we obtained microfragments of 1-1.3 microns (Fig. 1).

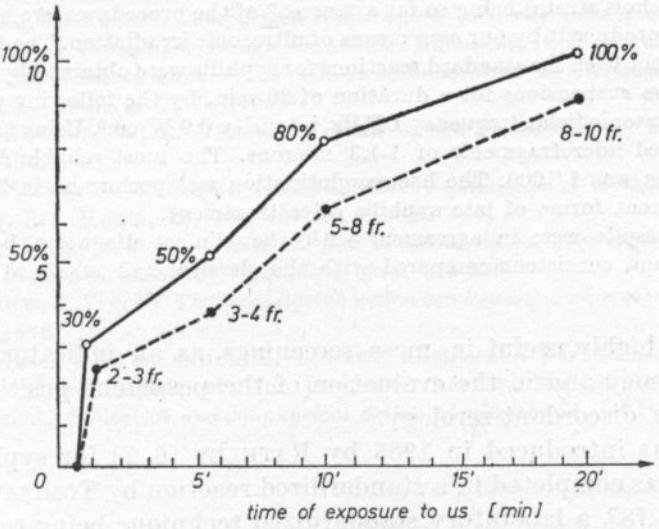

Fig. 1. T. pallidum fregmentation by ultrasound related to the time parameter. — fragmentation at % elements, — — number of fragments

A graduate disintegration of *T. pallidum* after ultrasonic exposure, using the same frequency and intensity of US and changing the time parameter, is due to the quality of treponemic suspension. This is a mixture of different susceptibilities of the microorganism varying with the length, age and biological stage.

The haemagglutination was performed with progressive dilutions of the sonicated *T. pallidum* antigen, the most reliable dilution being 1/100. The dilutions of patient serum ranged from 1/2 to 1/256.

We used the serum of 30 patients with different forms of late (secondary, latent) and congenital syphilis, the cases being after the treatment. The reference case was a patient with psoriasis and no clinical nor serological signs of syphilis (Table 1).

Table 1. The results of serological reactions for syphilis using TPHA with sonicated *T. pallidum*

Clinical diagnosis of syphilis	Number of cases	Type of serological reaction									
		RFC		Floculation		Reaction		Treponemic			
		RBW		Citochol		Kahn		VDRL		TPHA	
		+	−	+	−	+	−	+	−	+	−
Secondary syph.	12	7	5	7	5	7	5	7	5	10	2
Latent pyph.	11	2	9	10	1	10	1	10	1	6	5
Seroresistent syph.	2	2	—	2	—	2	—	2	—	2	—
Congenital syph.	1	1	—	1	—	1	—	1	—	1	—
Discordant serology	4	—	4	2	2	2	2	2	2	2	2
Total cases	30	12	18	22	8	22	8	22	8	21	9
[%]	100	40	60	73.3	26.6	73.3	26.6	73.3	26.6	70	30

The results show the following aspects:

1. The TPHA test was in agreement with clinical diagnosis, being more sensitive and consistent compared with the classical and standard reactions.

2. TPHA is more sensitive than RBW and with almost the same sensitivity than floculation reactions.

3. Cases with positive floculation reactions and negative RBW and TPHA were considered recovered, the floculation reactions being false because of liver dysfunctions (4 cases).

4. After the treatment TPHA is the only test that indicates a real recovery. The treatment will be continued when the TPHA test remains positive, even in cases with negative lipoidic reactions (7 cases).

5. TPHA can be erroneously positive in patients with severe disglobulinemia (1 case).

6. In condition of discordant serological reactions TPHA will coroborate with the floculation reactions, even when RBW gives different results (2 cases).

7. TPHA is highly useful when it is used together with VDRL in mass screenings, as an indicator of the therapeutical efficiency, and in the evaluation

of the persistent positive serological reactions or in discordant serology. Being much simpler than other treponemic reactions (FTA – Abs, TPI), this test must be introduced in all laboratories as a routine test for the diagnosis in syphilis.

8. Our method for antigen preparation by sonicating *T. pallidum* (Nichols strain), changing the time parameter, is the first attempt in Romania to obtained sonicated suspensions for TPHA.

References

[1] Al. Bădănoiu, G. Nicolau, Florica Brăilescu, *Observaţii privind comportarea testului de hemaglutinare pasivă cu antigene treponemice in cursul sifilisului,* Derm. Ven. (Buc.), **21**, 161-165 (1976).

[2] P. U. Cox, L. C. Logan, L. C. Norins, *Automated quantitative microchemagglutination assay for Tr. pallidum antibodies,* J. Appl. Microbiol., **18**, 485-489 (1968).

[3] M. Georgescu, D. Ionescu, Silvia Dumitru, *Reacţia de hemaglutinare pasivă in serodiagnosticul sifilisului,* Microbiologia (Buc.), **24**, 109-114 (1979).

[4] Jaj Barbare, Salker Rajas, Lalji Fatima, T. D. Davies, J. D. Harris, *An economical, simplified haemagglutination test for mass syphilis screening,* J. of Clinical Pathol., **33**, 1216-1221 (1980).

[5] J. Lesinski, J. B. Dudzisz, E. Kadziewicz, WHO/VDT/Res., 317-319 (1974).

[6] T. Rathlev, WHO/VDT/Res, 77-79 (1965).

[7] T. Rathlev, *Haemagglutination test utilizing pathogenic Tr. pallidum for the serodiagnosis of syphilis,* Brit. J. Vener. Dis., **43**, 142-148 (1967).

[8] T. Tomizawa, S. Kasamatsu, *Haemagglutination test for diagnosis of syphilis,* Japan, J. Med. Sci. Biol., **19**, 305-311 (1966).

ARCHIVES OF ACOUSTICS
9, 1-2, 121-130 (1984)

ECHOGRAPHIC SIGNAL PROCESSING

A. HERMENT, P. PERONNEAU

Hopital Broussais, (96, rue Didot, 75674 Paris, France)

G. DEMOMENT

L.S.S. C.N.R.S. E.S.E. (Plateau du Mouton, Gif-sur-Yvette, France)

The information received from the insonified tissues is strongly filtered by the echograph. The acoustic probe technology and the simplified processing of the echoes are mainly responsible for this loss of information.

Two deconvolution methods have been designed to correct partly the echograph characteristics. The first one, which is a sub-optimal Kalman filter, is easy to implement and offers short calculation time. It is consequently well dedicated to quasi real time imaging. The second one is slower but extracts from the processed signal some geometric information on the medium interfaces. This information may be used to obtain a more precise estimation of the coefficients of reflexion in the medium and thus to characterize the tissues by their acoustic impedance.

The ability of the methods to process real echographic signals is demonstrated on the rabbit eye and the human humeral artery.

1. Introduction

The performance of echographs has significantly been improved during the last years. The storage of the image and the numerical processing of the echoes have simplified the medicist's work. However, the treatment of the $R-F$ signals in the echograph is still very crude and a large amount of the received information is lost. Deconvolution technics, however, are able to restore partly this information by correction of the appliance's characteristics. These technics lead to the obtention of better defined images [2, 6]. In addition, if the medium geometry may be taken into account during signal processing, they allow the characterization of the tissues by their acoustic impedance [1, 5].

Two deconvolution processes are presented, both of which use the principle of "process-identification" and have been designed to combine a good improvement in the echograph discrimination with a convenient noise immunity in order to fit echographic signal characteristics.

2. "On line" deconvolution by sub-optimal Kalman filtering

The principle of the algorithm is explained in Fig. 1. The successive samples of the received signal S_n are introduced into the algorithm. After a delay of treatment, the different values E_n of the deconvoluted signal are obtained one by one at the input frequency.

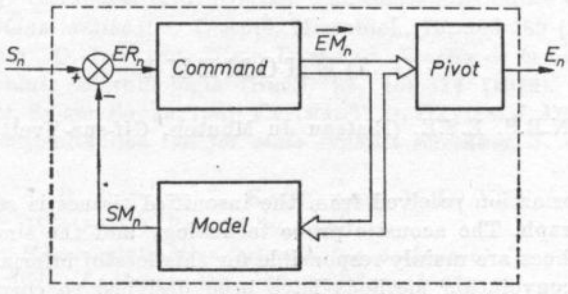

Fig. 1. "On-line" deconvolution : principle

2.1. *Error estimation*

At instant n the signal $\boldsymbol{EM}_n$ is a rough estimation of the deconvoluted signal. The algorithm will try to forecast from its knowledge, that is to say the echograph impulse response $\boldsymbol{h}$ and $\boldsymbol{EM}_n$, the value of the most probable incoming sample S_n. For this purpose the convolution at the instant n between the echograph impulse response and the estimated deconvoluted signal is computed.

$$SM_n = \boldsymbol{h}^t \cdot \boldsymbol{EM}_n. \tag{1}$$

The received sample S_n is then compared with this value and an error ER_n is obtained.

$$ER_n = S_n - SM_n. \tag{2}$$

2.2. *Initialisation of next* $\boldsymbol{EM}_n$

From this error, a new estimation of the deconvoluted signal is calculated as follows:

$$\boldsymbol{EM}_{n+1} = \Phi \cdot \boldsymbol{EM}_n - \lambda \cdot ER_n. \tag{3}$$

2.2.1. State transition matrix

The Φ operator which corresponds to the state transition matrix of the Kalman theory is used to initialise the first coordinate of the new vector $\boldsymbol{EM}_n$, because this value has not been affected by the previous operations. Φ has been chosen to simple shift $\boldsymbol{EM}_n$ and to duplicate its first coordinate:

$$(\boldsymbol{EM}_n)^t = (a, b, c, \ldots, n, 0); \quad (\Phi\boldsymbol{EM}_n)^t = (a, a, b, c, \ldots, n);$$

this means that without new information, the algorithm will suppose that the most probable value of the sample S_{n+1} will be equal to S_n. In other words, it is implicitly considered that the received signal cannot change extremely rapidly. This is effectively the case of the echographic signals which are collected through the acoustic probe acting as a low-pass filter.

2.2.2. Correction vector

The vector $\boldsymbol{\lambda}$ is chosen as the limit value of the Kalman gain vector [3]. This choice has been made in order to shorten the calculation time and to simplify the implementation of the method. The constant vector $\boldsymbol{\lambda}$ is independant of the received signal and can be calculated separately from the echograph impulse response and an estimation of the noise variance.

2.3. Extraction of the values E_n of the deconvoluted signal

The different values E_n of the deconvoluted signal are obtained by the extraction of one coordinate of $\boldsymbol{EM}_n$. This operation is done after a certain number of iterations of the loop in the algorithm so that the estimated $\boldsymbol{EM}_n$ has become precise enough.

$$E_n = \boldsymbol{P} \cdot \boldsymbol{EM}_n, \quad \text{with } P^t = (P0, P1, \ldots, P_p, \ldots, P_m), \quad \text{where } \begin{cases} P_p = 1 \\ P_i = 0 \forall i \neq p \end{cases} \tag{5}$$

a large value p will improve the sharpness of the processed signal but will lead to a more important delay between the input and the output of the system.

The algorithm is very fast because it needs no matrix inversion and because the vector $\boldsymbol{\lambda}$ may be calculated beforehand. The process is sub-optimal since this gain vector is taken as constant: consequently edge-effects are neglected in the deconvolution.

3. "Batch" deconvolution

The second method [4] is schematised in Fig. 2. It is based on overall comparison of the received signal, S, with a synthetized waveform, SM, generated by the computer. The construction of SM in the algorithm takes into account the known characteristics of the echograph: the acoustic device impulse response, h, and some unknown properties of the examined structures: position,

angulation and curvature of the interfaces, together with the value of their coefficient of reflexion.

The test of comparison has been designed to work with noisy input signals, and uses the properties of the correlation function.

Finally, the deconvoluted signal is reconstructed from the results of the test and from the different parameters used to built SM.

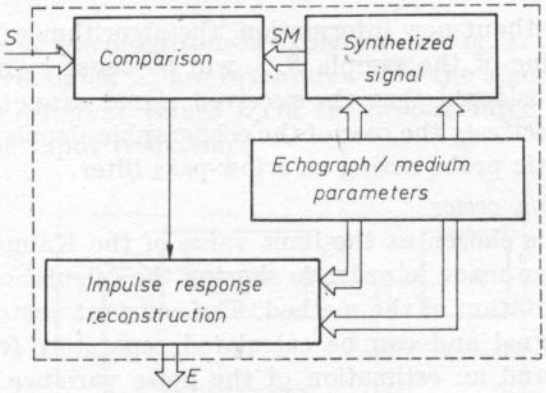

Fig. 2. "Batch" deconvolution : principle

3.1. Synthesis of SM

Two points have to be considered in the synthesis of the signal SM:

1. An increased number of parameters lead to a more sophisticated modelisation of the tissue but lengthens computation time.

2. These parameters have to be defined such as two different sets of them generate two different signals SM, in order to get a single solution to the identification of the insonified medium. Taking into account these two points, it has been chosen to construct SM under the following form

$$SM(p \cdot \Delta T) = \sum_{p=1}^{P} r_p^i \cdot h^{j,k}(p\Delta T - \theta_p^l), \tag{6}$$

where p corresponds to the order of the digital sample, P represents the number of samples in the signal and ΔT the sampling period.

$h^{j,k}$ characterizes the echo shape and depends in quite a complex way on the orientation and on the curvature of the interfaces. The analytical expression of $h^{j,k}$ from the parameter j and k is extremely difficult to establish. This is the reason why we used, in the implementation of the algorithm, a matrix of signals $h^{j,k}$ recorded on calibrated targets of known angulation and curvature which has been stored in the computer memory.

3.2. Test of comparison

The correlation function $C_{S,SM}$ between S and SM is computed and its symmetry with respect to a vertical axis is tested. Effectively, it can be demon-

strated from the properties of the correlation function that if $C_{S,SM}$ posseses a vertical symmetry, then SM is related to S by a multiplying constant. To test the symmetry, the ratio R is used:

$$R = \frac{\left[\int C_{S,SM}(\eta) \cdot C_{S,SM}(\tau - \eta)\, d\eta\right]_{\tau=0}}{\left[\int C_{S,SM}(\tau) \cdot C_{S,SM}(\tau - \mu)\, d\tau\right]_{\mu=0}}.$$

R which represents the ratio of the value of the autoconvolution function of $C_{S,SM}$ at the origin to the energy of this function will approach the value of one when the symmetry increases.

3.3. Reconstruction of the deconvoluted signal

When the maximum value of R has been determined, the corresponding parameters used to buit SM indicate the angulation and the curvature of each interface localised. This information allows correction of the apparent value of the coefficient of reflexion distorted by the medium geometry.

4. Experimentation on the eye

The method is now applied to the treatment of a series of signals collected on a rabbit eye. The eye was placed in a water tank, immediately after removing and insonified by a 5 MHz probe. The signals, collected within an angle of 90°, have been converted into eight-bit words at a frequency of 50 MHz.

4.1. High definition imagery of the eye

Both algorithms have been used to deconvolute the recorded data. The results have been presented in a crude four level greyscale on a variable persistance display. Fig. 3 presents for comparison an image obtained with a conventional echographic treatment of the signals for a 1 MHz bandwith detection and

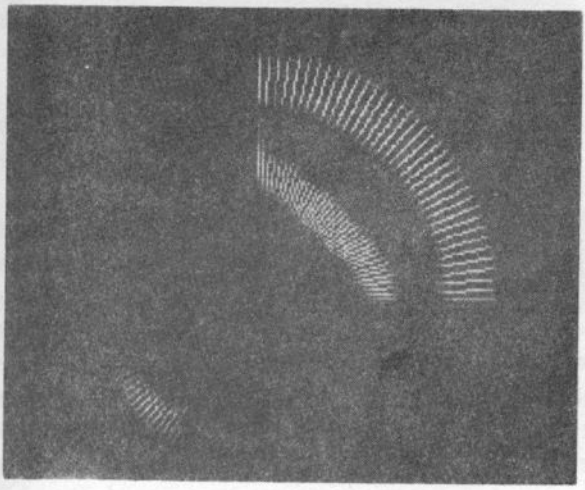

Fig. 3. Echographic image of the rabbit eye

without depth compensation. The image processed by the first algorithm is shown in Fig. 4 and the one obtained by the second method in Fig. 5. The four dotted lines correspond to the front and rear faces of the cornea (not visible in Fig. 3) and of the crystalline lens.

The higher definition of the deconvoluted image allows one 1) to distinguish interfaces masked in the echographic picture such as the two faces of the cornea, and 2) to obtain a better estimation of the shape of the interfaces.

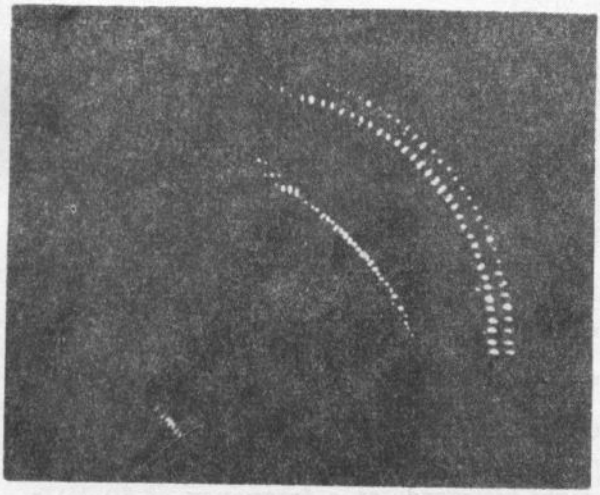

Fig. 4. "On line" deconvolution of the image

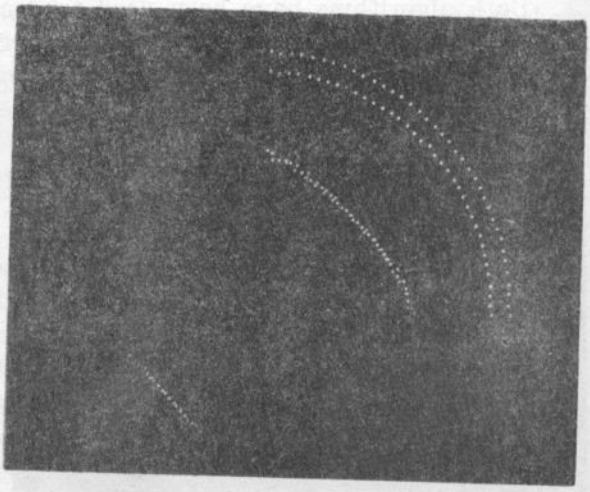

Fig. 5. "Batch" deconvolution of the image

4.2. Acoustic impedance of the eye

The signal recorded when the acoustic beam was centered on the eye axis has been used to calculate the impedance profile of the eye after deconvolution by the second method. It is shown in Fig. 6.

From left to right, one can observe a first zone of unitary normalized impedance which corresponds to the water in which the eye is submerged, then the cornea characterized by a relative impedance of 1.29. The zone with a low normalized impedance of 1.04 corresponds to the aqueous humour. The maximum

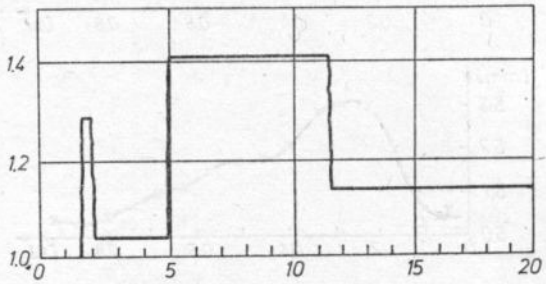

Fig. 6. Impedance profile of the rabbit eye

impedance zone, $Z/Zo = 1.41$ indicates the crossing of the crystalline lens and the last level corresponds to the vitreous humour whose relative impedance was estimated equal to 1.14.

Comparison with the density and propagation speed data given in the literature or measured in our laboratory indicates a good fitting between these calculations and the actual impedance profile.

5. Experimentation on the humeral artery

5.1. Signal recording

The probe was laid on the arm and oriented towards the vessel. Sixteen signals separated by 55 ms were recorded during a cardiac cycle. As for the eye, a 5 MHz probe was used and the signals sampled on eight bits at a rate of 50 MHz.

5.2. Signal processing

The signals were then deconvoluted and the position of the two sides of the second vessel wall was used to follow the wall displacement together with its thickness variations.

The vessel wall thickness is plotted in Fig. 7*a* and the wall position with respect to the probe in Fig. 7*b*. The variations in Fig. 7*b*, which are related in a ratio of 1/2 to the vessel diameter, look very similar to a classical intra-arterial pressure curve, in addition the amplitudes of the observed variations are in full agreement with the ones indicated in the literature. The wall thickness variations in Fig. 7*a* are very well correlated with the one of the previous curve: during systole the enlargment of the diameter corresponds to a thinner vessel wall. The amplitudes of these variations are again very close to the ones announced by the vessel mechanics.

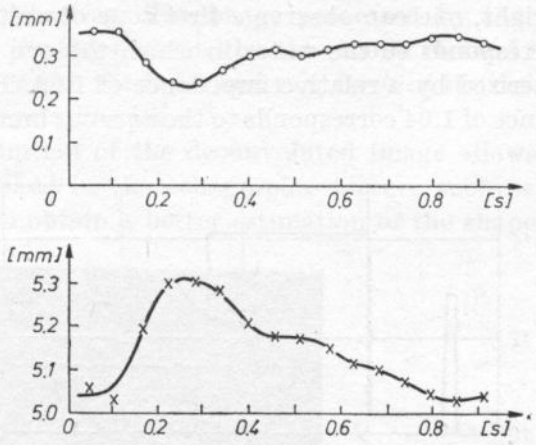

Fig. 7. Study of the humeral artery during one cardiac cycle: *a*) wall thickness variations, *b*) second arterial wall position

6. Conclusion

Two methods for the treatment of echographic signals have been proposed. The first process, derived from Kalman filtering, works "on line" and supplies rapid results with few calculations, it appears consistently well dedicated to the image processing. The second one which is able to take into account some characteristics of the interfaces leads to a finer characterisation of the medium and may be used for tissue characterisation. It is, however, longer and will only be applied when a limited number of structures is to be studied. In vitro experiments on the eye illustrate the performance of the methods and in vivo applications on the vessel show the ability of the methods to process signals recorded in vivo.

References

[1] I. Beretski, *Detection and characterization of atherosclerosis in a human arteria wall by raylographic technique, and in vitro study,* in: Ultrasound in Medicine, D. N. White, R. E. Brown (eds.), Plenum Press Publ., New York, 1977, **3B**, 1597-1612 (1977).

[2] B. Burgogne, J. Pavkovich, *Digital filtering of acoustic images,* in: Acoustical Imaging, J. P. Powers (ed.), Plenum Publ. Co., New York, **11**, 181-207 (1982).

[3] G. Demoment, R. Reynaud, A. Segalen, *Estimation sous-optimale rapide pour la déconvolution en temps réel,* Neuvième Colloque sur le traitement du signal et ses applications "GRETSI", 16-20 mai 1983, Nice.

[4] A. Herment, P. Peronneau, J. P. Moutet, *Echographic signal processing: a method*

taking into account the medium geometry, I.E.E.E. Catalog, I.E.E.E. Computer Society, **82 CH** 1804-4, 331-336, 1982.

[5] J. P. JONES, *Ultrasonic impediography and its applications to tissue characterization,* in: *Recent advances in ultrasound in biomedicine,* D. N. WHITE (ed.), Research Studies Press, Forest Grove, **1**, 131-156 (1977).

[6] A. PAPOULIS, C. CHAMZAS, *Improvement of range resolution by spectral extrapolation,* Ultrasonic Imaging, **1**, 121-135 (1979).

ARCHIVES OF ACOUSTICS
9, 1-2, 131-136 (1984)

ULTRASONIC GRAY SCALE DOPPLER IMAGING ANGIOGRAPHY

TADEUSZ POWAŁOWSKI, JERZY ETIENNE,
LESZEK FILIPCZYŃSKI, ANDRZEJ NOWICKI,
MACIEJ PIECHOCKI, WOJCIECH SECOMSKI

Department of Ultrasound, Institute of Fundamental Technological Research, Polish Academy of Sciences
(00-049 Warsaw, ul. Świętokrzyska 21, Poland)

ANDRZEJ WLECIAŁ

"Techpan" — Experimental Department, Institute of Fundamental Technological Research
(00-049 Warsaw, ul. Świętokrzyska 21)

MARIA BARAŃSKA

Institute of Psychoneurology (02-957 Warsaw)

Examination of the carotid artery stenosis is very important in the diagnosis of cerebrovascular diseases. New possibilities in the diagnosis of stenotic lesions are provided by ultrasonic Doppler angiography. The aim of this paper is to present a Doppler imaging system developed by the authors for the examination of blood flowing in carotid arteries. The system is based upon a 5 MHz bi-directional *c.w.* Doppler flowmeter with a separate output for anterograde and retrograde flows. A special bank of filters converts signals into various levels of the gray-scale display which correspond to the value of the blood flow velocity. The ultrasonic probe is held by the scanning arm. The position of the probe on the skin of the patient is electronically sensed by the position-sensing circuity which causes the bright spot on the image display to move according to the position of the probe. The Doppler image from the artery is stored in a digital memory system. The clinical results obtained by means of this system showed good agreement with X-ray arteriography for obstructions occluding more than 50 per cent of the arterial diameter.

1. Introduction

The brain stroke is one of the most dangerous diseases which causes a large number of deaths.

The diagnosis of brain diseases which result from ischaemia consists above all in the examination of the carotid artery patency.

X-ray angiography used previously involves the considerable risk of causing complications in patients and is totally excluded in a large number of cases.

New diagnostic possibilities in this field have been provided by ulrasonic Doppler angiography, permitting images of blood flow in vessels to be obtained. In 1972, REID and SPENCER [8] were the first to describe an ultrasonic *c.w.* system for imaging carotid arteries. In view of its similarity to vessel representation in X-ray angiography, this technique was called by its authors Doppler angiography. CURRY and WHITE [2] used colour to code the blood flow velocity, and NOWICKI [7] introduced to this technique a pulse method permitting two-plane imaging of vessels. In Poland the first model of an ultrasonic arterioscope was developed in 1980 [3].

The ultrasonic Doppler method for blood flow imaging maps the blood flow in a vessel, based on the scattering of ultrasonic waves by morphotic elements of blood flowing in the vessel. This permits estimation of the degree of occlusion of vessels from the flow image obtained, localization of stenotic spots and measurement of flow velocity in a given section.

Since 1979, the ultrasonic *c.w.* Doppler method has been used to investigate flows in carotid vessels, at the Institute of Psychoneurology.

The investigations carried out to date on 400 patients, using a UDP ultrasonic flow detector (manufactured by "Techpan") have made possible the study of

1) the usefulness of ultrasonic investigations in the diagnosis of vascular diseases, indicating a high percentage of agreement with the results of clinical studies and X-ray angiography (76 per cent in the material studied); emphasizing the fact that there are possibilities of multiple repetition of the investigation, which permits the evaluation of sclerotic changes [4, 5];

2) the correlation of the results of ultrasonic investigations and X-ray arteriography. Good agreement was found, particularly for occlusion or high vascular stenosis. In the material studied the results agreed in 79 per cent of cases [6]. It was found that it was particularly useful to use the ultrasonic method in the evaluation of the results of operations to improve the patency of extracranial brain-supplying arteries, on the basis of the examination of 25 patients. In those cases the use of X-ray arteriography is absolutely excluded [1].

The present ultrasonic Doppler method gives evidence of reliability, fully justifying the need for the development of this technique, of which the angiosonograph presented here is a consistent example.

2. Instrumentation

Fig. 1 shows a general view of the ultrasonic arterioscope developed by the authors. The system consists of the following units:

1. A mechanical unit, pantograph *1* fixed on a stand which permits the

operation of the device at the bed of the patient in hospital. The pantograph ensures translation of the motion of the probe over the surface of the patients skin at a constant angle of 60° with respect to the skin surface in the motion of a bright spot (cursor) on the display screen.

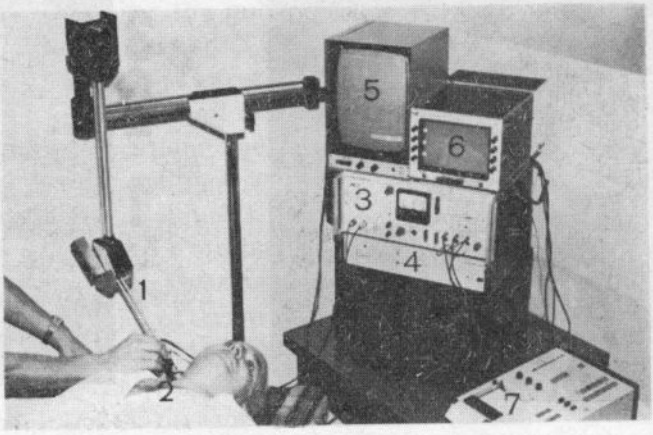

Fig. 1. A general view of the ultrasonic arterioscope: *1* — pantograph, *2* — ultrasonic probe, *3* — two-directional ultrasonic Doppler flowmeter with a system of filters, comparators, coding unit, amplifiers of the coordinate systems of the position of the probe, *4* — image memory system, *5* — TV monitor, *6* — cardiac monitor, *7* — recorder

2. Ultrasonic probe *2* at a frequency of 5 MHz, focusing the ultrasonic beam in the plane of the carotid vessels.

3. Two-directional ultrasonic Doppler flow detector *3*, ensuring the separation of Doppler signals in two channels corresponding to flow velocities in opposite directions. It is possible to register on the external recorder *7* the instantaneous value in the direction + (channel A) or − (channel B) and the resultant flow (channel $A+B$). The Doppler detector is complemented with an imaging signal processing unit. The unit includes filters, comparators and a logical system processing an analog signal of different frequency levels (flow velocities) into a 2-bit binary signal corresponding to a 4-degree grey scale on the display screen.

4. Image memory unit *4*, permitting the storing of arteriograms and their display on the screen. The capacity of the memory is 32k bits ($128 \times 128 \times 2$). The system generates a signal which ensures the achievement on the screen of a two-part image field, with a possibility of an independent recording and storing of the image in both. It also generates a grey-scale band and a flickering bright spot that shows the position of the probe.

5. Black and white or colour TV monitor *5*.

This system can be connected to TIH (Time Interval Histograph) analyser which permits histograms to be shown on the monitor screen.

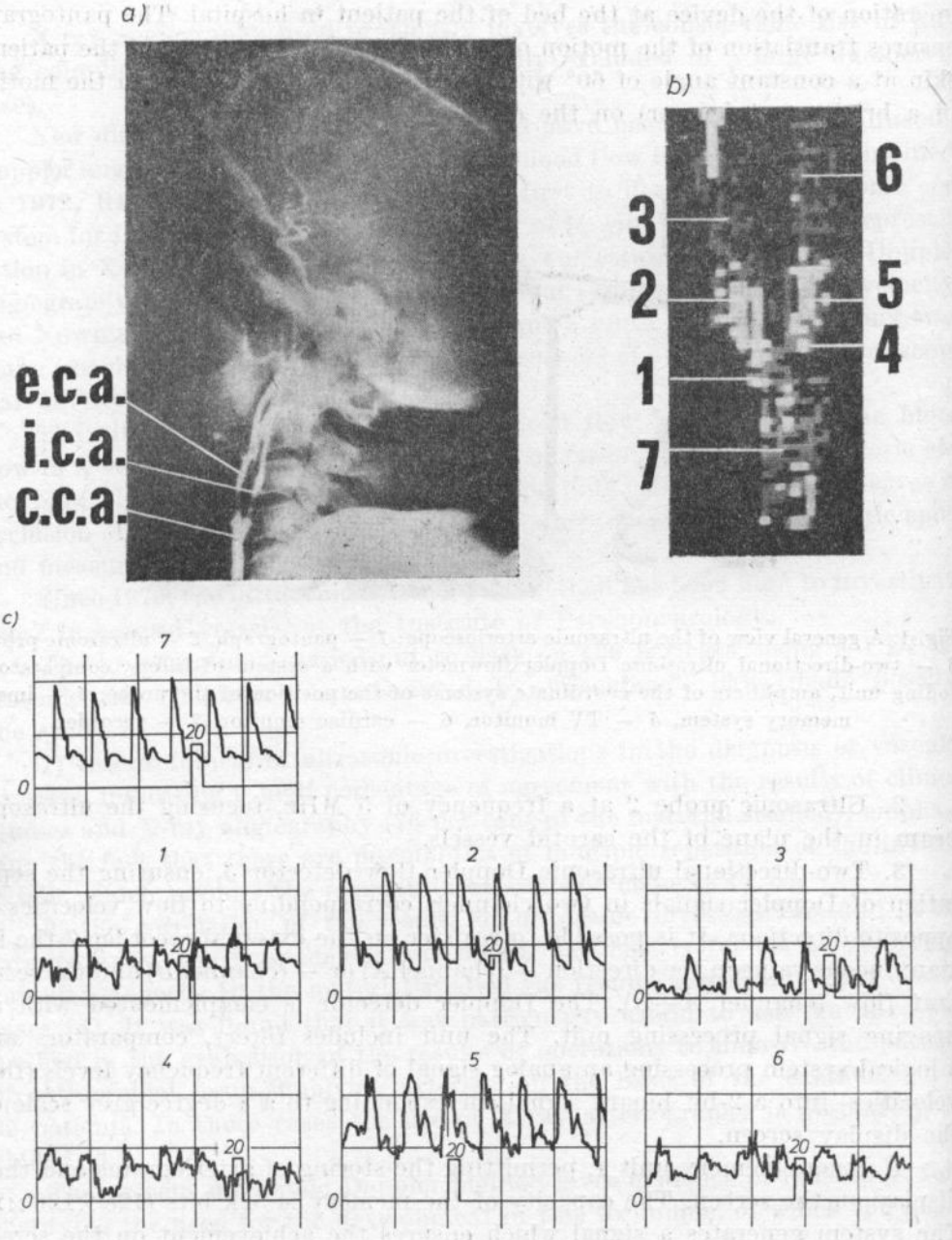

Fig. 2. X-ray (*a*) and ultrasonic (*b*) arteriogram of the carotid arteries and recordings of blood flow velocities in the area of the bifurcation (*c*). *1* — in the external carotid artery, before the stenosis, *2* — in the external carotid artery, in the stenosis, *3* — in the external carotid artery, after the stenosis, *4* — in the internal carotid artery, before the stenosis, *5* — in the internal carotid artery, in the stenosis, *6* — in the internal carotid artery, after the stenosis, *7* — in the common carotid artery. *c.c. a* — common carotid artery, *e.c.a* — external carotid artery, *i.c.a* — internal carotid artery

3. Clinical experimental investigations

The present ultrasonic angiosonograph was used in clinical investigations aimed at the evaluation of the carotid artery patency. A group of 11 patients were examined. The results of ultrasonic investigations were compared with the results obtained using the method of X-ray angiography. As an example, Fig. 2 shows an ultrasonic and X-ray arteriogram of a patient with a stenosis of the external and internal carotid arteries just after the bifurcation. It also shows recordings in a system of zero-crossings of blood flow velocities recorded in the area of the bifurcation. The recordings show a distinct increase in blood flow velocity in the stenotic spot compared with the blood flow velocities measured before and after the stenosis.

In the patient group examined using X-ray angiography the stenosis of the common carotid arteries was found in one case, of the internal carotid arteries in eight cases and of the external carotid arteries in two cases. The degree of all the stenosis cases exceeded 50 per cent. Moreover, in four patients complete occlusion of the internal (three cases) and external (one case) carotid arteries was found using the X-ray method.

The results of the investigations by ultrasonic Doppler angiography were in agreement with those of X-ray examinations in all the cases under study.

4. Conclusions

Preliminary clinical investigations have confirmed the usefulness of ultrasonic angiography in the evaluation of the patency of carotid arteries. The device developed by the authors ensures the possibility of mapping blood flows in blood vessels. The grey scale used by the authors permits the distinguishing of stenotic sections of the vessel through which blood is flowing at increased velocity bright and very bright fields on the monitor screen and the localization of occluded spots in the vessel, which is signalled by the absence of flow (dark field = background on the monitor screen).

Investigations performed on 11 patients have shown agreement between the results obtained by the ultrasonic method and those of the X-ray method in the localization of stenotic spots and occlusion in the carotid arteries.

Further investigations will attempt to determine to what extent the method of ultrasonic angiography permits the degree of the stenosis of a blood vessel to be found.

References

[1] M. Barańska-Gieruszczak, D. Ryglewicz, S. Tarnowska, J. Nielubowicz, *Ultrasonographic examination of patients after operations restoring the patency of extracranial brain-supplying arteries* (in Polish), Neur. Neurochir. Pol., **16**, 4, 211 (1982).

[2] G. R. Curry, D. N. White, *Colour coded ultrasonic differential velocity scanner (Echoflow)*, Ultr. in Med. and Biol., **4**, 27-35 (1978).

[3] J. Etienne, A. Nowicki, M. Piechocki, W. Secomski, *An attempt to visualize blood flow in a carotid artery using a laboratory system of an ultrasonic arterioscope* (in Polish), Proc. V National Conference on Biocybernetics and Biomedical Engineering, Warsaw 1981, 121-125.

[4] Z. Gralewski, *The use of Doppler ultrasonography of the common carotid artery in the evaluation of the state of the cerebral circulation in brain stroke pattients* (in Polish), Neur. Neurochir. Pol., **16**, 4, 205-209 (1982).

[5] H. Nielubowiczowa, M. Barańska-Gieruszczak, D. Ryglewicz, S. Tarnowska, *Usefulness of ultrasonographic Doppler investigations in the diagnosis of the diseases of brain vessels* (in Polish), Neur. Neurochir. Pol., **16**, 4, 191-196 (1982).

[6] H. Nielubowiczowa, M. Barańska-Gieruszczak, S. Tarnowska, *Results of ultrasonographic Doppler investigations of extracranial brain-supplying arteries compared with angiographic results* (in Polish), Neur. Neurochir. Pol., **16**, 4, 197-203 (1982).

[7] A. Nowicki, *Ultrasonic methods for imaging blood vessels and flows* (habilitational dissertation-in Polish), Prace IPPT, 1980.

[8] J. M. Reid, M. P. Spencer, *Ultrasonic Doppler technique for imaging blood vessels*, Science, **176**, 1235-1236 (1972).

ARCHIVES OF ACOUSTICS
9, 1-2, 137-142 (1984)

MEASUREMENT SYSTEM FOR MEDICAL ULTRASONIC PULSE SPECTROSCOPY

K. P. RICHTER, P. LANGE, R. MILLNER,
H. HEYNEMANN, M. I. RICHTER, H. PRESSLER,
Th. DRESCHER, H. LETTERER

Institute of Applied Biophysics, Urological Clinic, Pathological Institut, 1st Medical Clinic
Martin-Luther-University Halle-Wittenberg, Halle, GDR

A measurement system was developed to measure the ultrasonic attenuation of biological tissues in vitro. The apparatus works in transmission and pulse echo technique. The use of broad band transducers and PVDF hydrophones ensures a high sensitivity connected with a wide bandwidth. The ultrasonic attenuation of different fixed and unfixed tissues was measured. A comparison of ultrasonic data and histopathology was made.

1. Introduction

Ultrasonic spectroscopy is a useful tool to provide insight into the interaction of tissue with ultrasound. To apply this ultrasonic spectroscopy first for in vitro measurements and them to find a correlation between the clinical statement and the frequency dependent ultrasonic attenuation we developed a measuring system.

2. Measuring system

We used a modified *A*-scope device, followed by a linear gate and an electronic spectrum analyzer (Fig. 1). The data of the spectrum were stored or directly digitized. The computation of attenuation characteristics from the digitized spectra is performed by a calculator. The system allowed measurements within the frequency range from 2 to 20 MHz. In vitro measurements were carried out in transmission techniques with a transmitter and a receiver. A scan technique was used and the frequency dependent attenuation was measured

across a given scan line. The ultrasonic attenuation of each measuring point was computed as a function of frequency and compared with the histological statement.

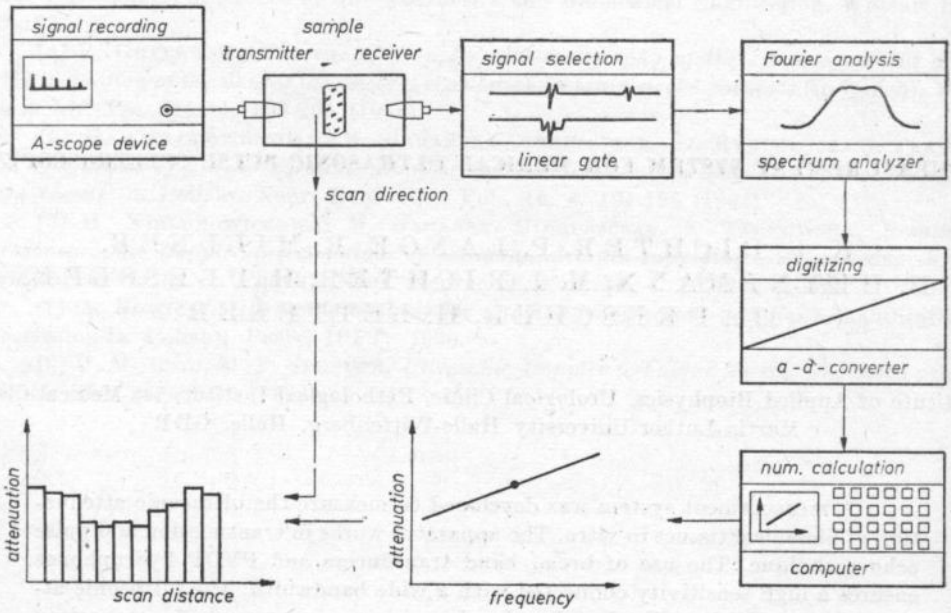

Fig. 1. Measuring system

3. Transducer

A broad band ceramic transducer acts as transmitter with a doublelayer matching section made from glass and epoxy resin. The bandwidth of the transducer is about 80 per cent of the center frequency. Transmitters with center frequencies of 6 MHz and 8 MHz were used. The receiver is a PVDF foil hydrophone of 12 μm thickness and an ordinary backing with a high acoustic impedance. Fig. 2 demonstrates the system in detail. The advantage of the PVDF hydrophone is the flat frequency response over a wide frequency range, restricted by the frequency response of the amplifier.

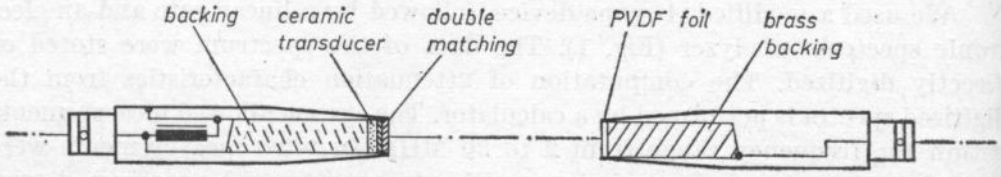

Fig. 2. Transmitter and receiver system

4. Application

Measurements of formalin fixed and unfixed tissues were performed in degassed water. Fig. 3 represents the attenuation of fixed human testes. The normal testis showed a low value and high values were measured for different carcinoma of testis. The chronical inflammation has an intermediate behaviour. Figs. 4 and 5 represent unfixed specimens of rat liver and human brain respectively.

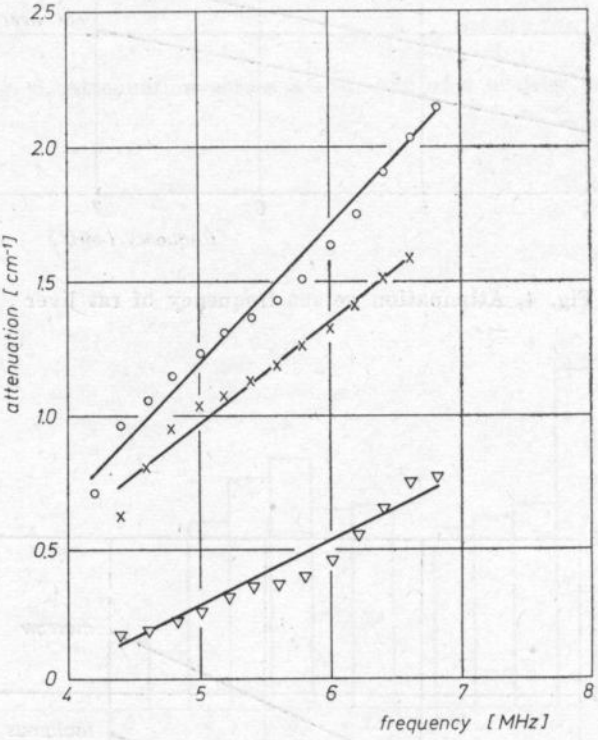

Fig. 3. Attenuation versus frequency: ▽ helthy testis, × inflammation of testis, ○ carcinoma of testis

To provide more exact insight into the resulting attenuation of pathological tissue changes the above mentioned scan technique was used. The computed attenuation of 6 MHz is shown in a block diagram across a scan distance. Figs. 6 and 7 give the attenuation of healthy testis and a melanom metastasis of testis. All pathological changes of testes showed a higher attenuation compared with healthy specimens. The method allowed to distinguish between different tissues and their pathological changes.

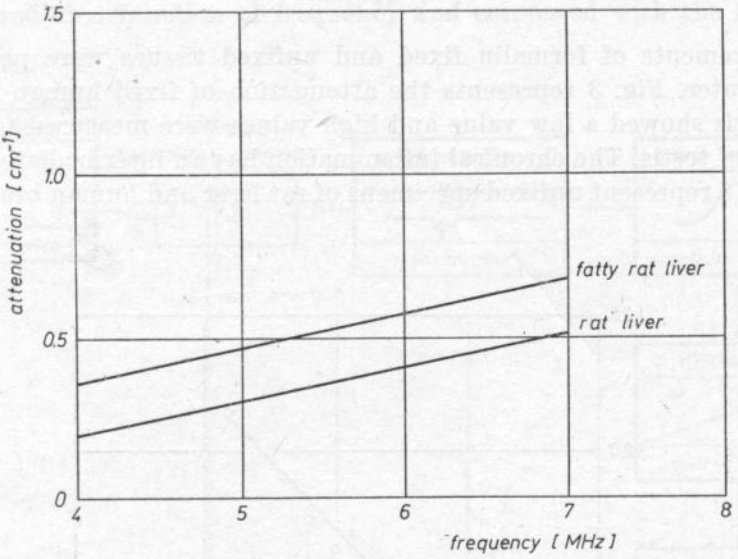

Fig. 4. Attenuation versus frequency of rat liver

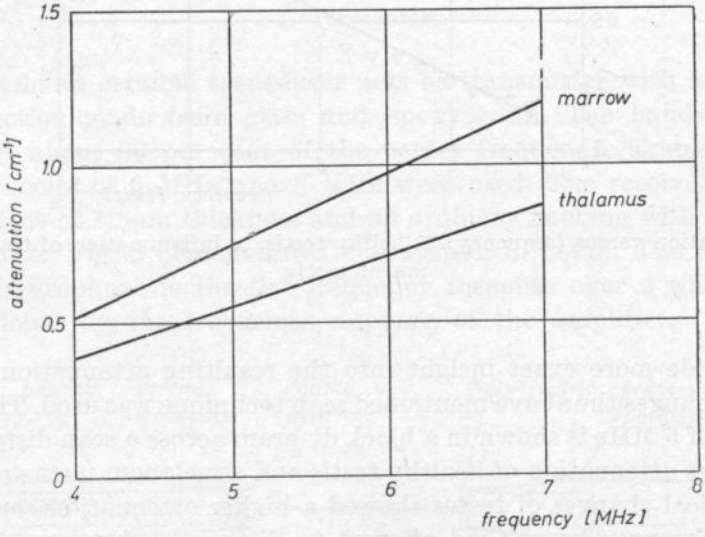

Fig. 5. Attenuation versus frequency of human brain

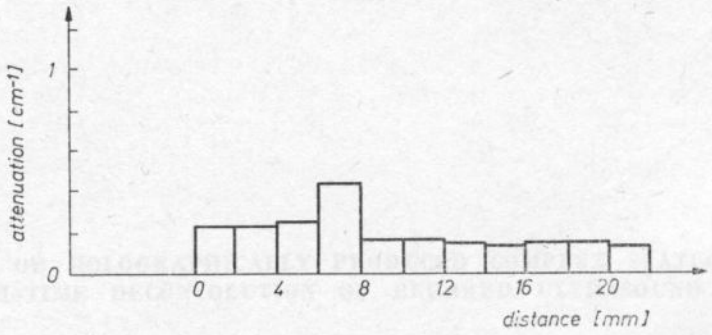

Fig. 6. Attenuation across a scan line of a healthy testis

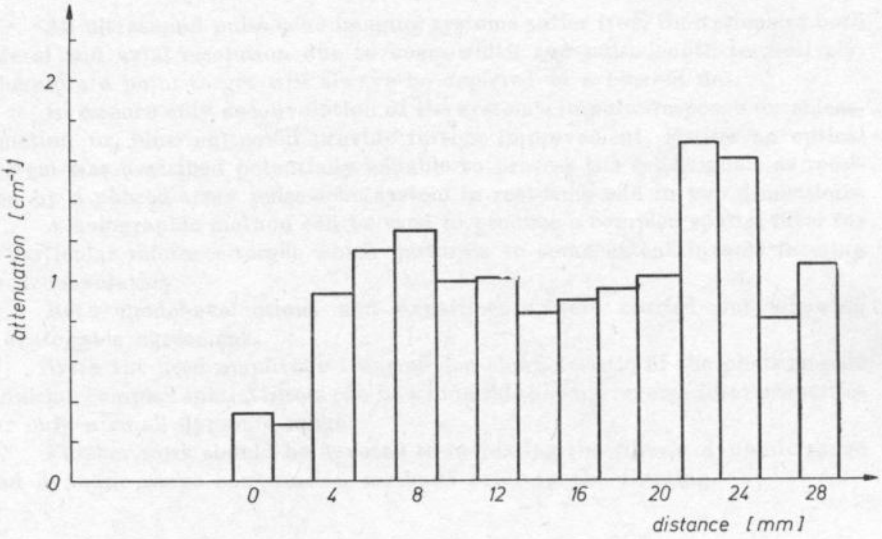

Fig. 7. Attenuation across a scan line of a melanoma

ARCHIVES OF ACOUSTICS
9, 1-2, 143-154 (1984)

PROPERTIES OF HOLOGRAPHICALLY PRODUCED COMPLEX SPATIAL FILTERS FOR REAL-TIME DECONVOLUTION OF BLURRED ULTRASOUND IMAGES

JAN SOMER, FRANS JONGSMA

Medical Faculty, University of Limburg, Maastricht, The Netherlands

All ultrasound pulse-echo imaging systems suffer from limitations of both lateral and axial resolution due to beam-width and pulse-length respectively. Therefore a point-target will always be depicted as a blurred dot.

In essence only deconvolution of the system's impulse-response (or smear-function or blurring) could provide further improvement. Earlier an optical system was described potentially capable to process the echo-signals as received by a phased-array pulse-echo system in real-time and in two dimensions.

A holographic method can be used to produce a complex spatial filter for a particular reference-target which performs to some extent inverse filtering or deconvolution.

Both model-evaluations and experiments were carried out, showing a reasonable agreement.

With the used amplitude transmission-characteristic of the photographic emulsion complex spatial filters can be produced showing inverse-filter properties for only a small dynamic range.

Further work should be devoted to increasing the filter's dynamic range and dynamic range compression methods prior to the filtering.

1. Introduction

Previous publications [2-6] have already described how an optical computer can perform direct and quasi-inverse Fourier-transformation, and how filtering in the spatial frequency plane can be achieved.

Also, the conversion of the electrical signals, as received by the ultrasound phased-array system, into optically modulatable signals, employing an Ultrasound Light Modulator (ULM) was described.

Therefore, here we confine ourselves only to a description of the holographic procedure to produce a complex spatial "inverse" — filter and its performance.

2. The complex spatial filter

2.1. Holographic process

Already in 1964 VANDER LUGT published a method for producing a complex filter by means of a holographic process [1]. A holographic plate is illuminated by an object beam and a reference beam simultaneously, see Fig. 1. It is assumed that both beams originate from the same laser source in order to ensure the light

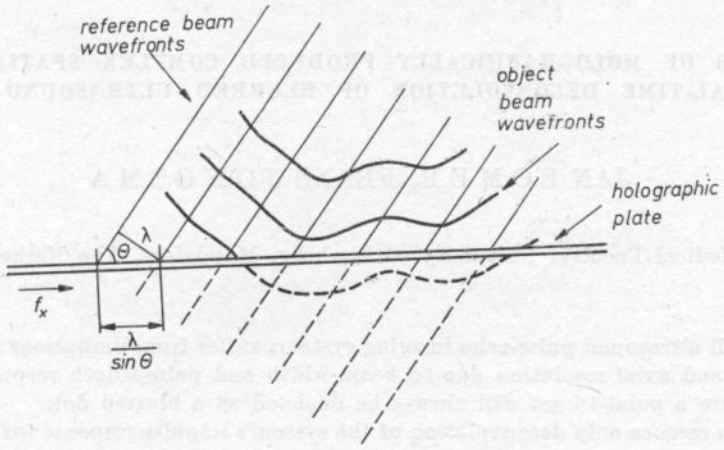

Fig. 1. Realization of a hologram

to be monochromatic and spatially and temporally coherent. Here, the object, beam is the spectrum $S_r(f_x, f_y)$ of the reference-target, of which both amplitude and phase are functions of f_x and f_y. The reference-target is a "point"-target, serving as a spatial δ-function input to the ultrasound system. At the surface of the holographic plate the complex function can be expressed as

$$\bar{S}_r = S_r(f_x, f_y) \exp\,[j\varphi(f_x, f_y)] = S_r \exp(j\varphi). \tag{1}$$

We require the reference beam to have a constant amplitude and an angle θ with the f_x — coordinate only.

It can be found from Fig. 1 that on the plate its complex amplitude can be described as

$$\bar{A}_r = A_r \exp(-j\alpha f_x) = A_r \exp(-j\psi), \tag{2}$$

where $\alpha = (2\pi \sin\theta)/\lambda$.

The total amplitude at the plate is now

$$\bar{A}_T = \bar{A}_r + \bar{S}_r = A_r \exp(-j\psi) + S_r \exp(j\varphi). \tag{3}$$

Since photographic emulsions respond to intensity, rather than to amplitude, we calculate the intensity, which is

$$I_T = \bar{A}_T \cdot \bar{A}_T^* = A_r^2 + S_r^2 + A_r S_r \exp[j(\psi+\varphi)] + A_r S_r \exp[-j(\psi+\varphi)] \tag{4}$$

$$= A_r^2 + S_r^2 + 2A_r S_r \cos(\psi+\varphi). \tag{5}$$

Equation (5) shows that the interference intensity-pattern consists of a "*DC*"-component (although S_r^2 is a variable) on which a modulation is superimposed, being proportional in amplitude with the object-beam and having a phase being the reference-beam phase which in its turn is modulated by the object-beam phase, since always $\varphi \ll \psi$. This illustrates that here in an intensity-function still both amplitude and phase are preserved, due to the use of a reference beam.

If the photographic emulsion would respond to the impinging light-energy such that the amplitude transmission of the developed plate would be a linear function of this energy, the amplitude transmission would also be expressed by equations ((4), (5)). An impinging reference-beam at zero angle would then fall apart into three beams as follows: $(A_r^2+S_r^2)$ at zero angle, and two beams proportional to S_r at angles $+\theta$ and $-\theta$, according to equation (2).

On the other hand, if in this special case the object-beam would impinge on the developed plate, the transmitted beams would be proportional to:

a. $(A_r^2+S_r^2)S_r\exp(j\varphi)$, being a distorted object beam at "zero" angle

b. $S_r^2\exp[j(\psi+2\varphi)]$, being the squared amplitude object-beam with distorted phase at an angle $+\theta$.

c. $S_r^2\exp(-j\psi)$, being again the squared amplitude object-beam with cancelled phase under an angle $-\theta$.

2.2. Holographic "inverse" filter

In [4, 5, 6] it was pointed out that the filter should have a transfer-function,

$$\bar{G} = 1/\bar{S}_r = 1/(S_r\exp(j\varphi) = (1/S_r)\exp(-j\varphi). \qquad (6)$$

In paragraph 2.1 it was found that in the $(-\theta)$-diffraction component of the hologram this negative phase is present (leading to the phase-cancellation as in case *c*), so this aspect is correct. However, instead of $1/S_r$, the amplitude transfer-function of the hologram in 2.1 is S_r so that to obtain an inverse filter the amplitude transmission-function of the holographic plate as a function of the exposure energy should definitely not be linear as was assumed in 2.1.

Fig. 2 shows a realistic amplitude transmission curve T_a as a function of $E = It$, the exposure-energy, with t = exposure-time. It also shows the intensity-function according to equation (5). Here, S_r runs linearly from 0 to 1 and the ratio $A_r/S_{r\max}$ is less than 1. Due to the very non-linear T_a-curve a high modulation-amplitude causes a low transmission-modulation and reversed.

Qualitatively this is just what we wish to achieve. However, to which extent the obtained transmission-modulation function approximates the actually wanted $1/S_r$ (according to equation (6)), will be investigated further.

2.3. Evaluation of a model

The result as shown in Fig. 2 suggests that, given a particular T_a-E function, the two possible parameters which can be varied are the beam-amplitude

ratio

$$R_a = A_r/S_{r\max} \tag{7}$$

and the T_{aDC}-value, being the transmission corresponding to the maximum *DC*-component value, see Fig. 2.

Alteration of R_a causes considerable variation of the *DC*-component as a function of S_r. The T_{aDC}-value can be adjusted by proper estimation of the exposure-time t.

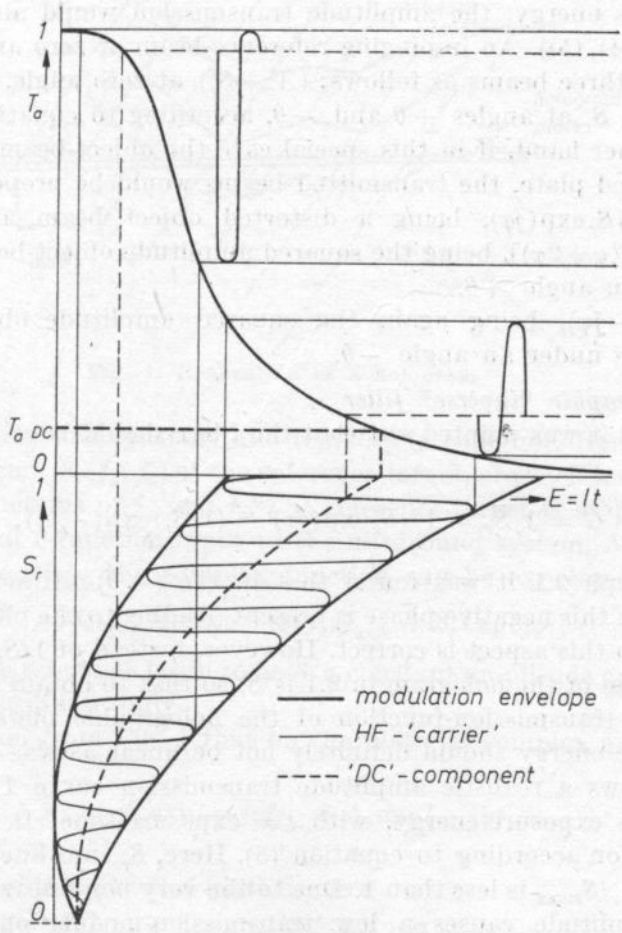

Fig. 2. Realization of a complex spatial "inverse" filter

The process as shown in Fig. 2 can be investigated further by fitting the measured T_a-curve of a particular type of photographic material under particular development-conditions by a mathematical function $T_a(E)$.

The exposure-energy E can be found from equations (5) and (7), together

with stating that $S_{r\max} = 1$ (for convenience), as follows

$$E = It = \{R_a^2 + S_r^2 + 2R_a S_r \cos(\psi + \varphi)\}t, \tag{8}$$

where t = exposure-time.

In practice θ, the angle of the reference beam, is always taken large enough to let $\psi = af_x = (2\pi \sin\theta \cdot f_x)/\lambda$ (see equation (2)) be much greater then φ (equation (1)). The modulation frequency, therefore, is mainly determined by ψ and is very close to $(\sin\theta)/\lambda\varphi$ and in our case approximately 100 cycles per millimeter.

Since for this model the phase of the spectral function S_r is assumed to be zero (again for convenience), we can write

$$E = \{R_a^2 + S_r^2 + 2R_a S_r \cos\psi\}t, \tag{9}$$

with

$$\psi = 2\pi\ 100\ f_x, \tag{10}$$

where f_x is measured in mm on the holographic plate.

Substitution of equation (9) into $T_a(E)$ yields

$$T_a = T_a(\psi), \tag{11}$$

with the parameters R_a as the beam-amplitude ratio, S_r as the spectral amplitude of the input-function to the system and t as the exposure-time to obtain the required T_{aDC}-value.

From Fig. 2 we will appreciate that the original cosine-function of equation (9) is highly distorted by the non-linear $T_a - E$ characteristic, resulting in an oscillating function with many harmonics ψ, 2ψ, 3ψ etc.

Illuminated by a beam this grating pattern will accordingly split it up in diffractions at $+\theta$ and $-\theta$, $+2\theta$ and -2θ, $+3\theta$ and -3θ, etc. In using such a grating as a complex spatial filter only the first order diffraction at $-\theta$ is selected out.

In our mathematical model we assume that S_r varies very slowly with the co-ordinate f_x, which means that at every position f_x the spectral amplitude S_r can be considered to be constant over several grating-oscillations. This makes $T_a(\psi)$, as represented by equation (11), a periodic function with ψ as the only variable and thus $T_a(\psi)$ can be expressed as a Fourier-series

$$\begin{aligned} T_a(\psi) &= A_0 + A_1 \cos\psi + A_2 \cos 2\psi + \ldots \\ &= A_0 + \frac{A_1}{2}\left(\exp(j\psi) + \exp(-j\psi)\right) + \frac{A_2}{2}\left(\exp(j2\psi) + \exp(-j2\psi)\right) + \ldots \end{aligned} \tag{12}$$

As mentioned above, we are interested in the first order $(-\theta)$-diffraction only so that we merely have to evaluate A_1.

From Fourier-series theory we calculate

$$A_1 = \frac{1}{\pi} \int_{-\pi}^{+\pi} T(\psi) \cos \psi d\psi \tag{13}$$

for several values of S_r. Herewith we in fact obtain A_1 and thus G as a function of the spectral amplitude S_r, still with R_a and T_{aDC} as parameters.

One should realize that we did not find the transfer-function $G(f_x)$ in the spatial-frequency plane of the holographic complex spatial filter for a spectrum S_r, unless $S_r(f_x)$ is defined.

If for all frequencies $G(f_x) = 1/S_r(f_x)$, which is required for an inverse filter equation (6), then $G(f_x)S_r(f_x) = 1$.

Accordingly, A_1S_r should be constant for all S_r. We can now determine the product of spectral amplitude and filter-function as a function of the spectral amplitude, in other words

$$A_1S_r = f(S_r). \tag{14}$$

The range of S_r over which A_1S_r is "constant" (within certain limits) then determines the maximum dynamic range of S_r for which the used T_a-E curve can produce a suitable inverse filter.

In Fig. 3*a*, *b*, *c* the model calculations are presented for $R_a = 2/3$, $1/2$ and $1/3$ respectively. Four curves are given representing four different T_{aDC}-values, according to Table 1. In Table 1 the dynamic ranges of S_r are also given for all cases (as far as applicable) within 3 dB and 6 dB limits respectively. The first conclusion is that the dynamic ranges are very small and more dependent on T_{aDC} than on R_a.

Further comments will be given in the next chapter.

2.4. Experiments

For confirmation of the model found, a number of experiments were carried out. A grey-wedge with a continuously and logarithmically varying density over a range of approximately 30 dB, was used for creating the function $S_r(f_x)$.

Holograms were made under conditions defined as well as possible with respect to R_a, T_{aDC} and a high enough oscillating frequency of the grating-pattern.

Each hologram was illuminated with the same spectral distribution $S_r(f_x)$ as used for creating the hologram with accurately co-inciding f-scales. Then the $(-\theta)$-diffraction was recorded (corresponding with A_1 in the previous chapter), together with the spectral distribution $S_r(f_x)$ itself. The data were processed by a computer and f_x was eliminated in order to obtain A_1S_r as a function of S_r, similarly to the model-evaluation in the previous chapter (equation (14)).

The results are given in Fig. 4 *a*, *b*, *c* in combination with Table 2.

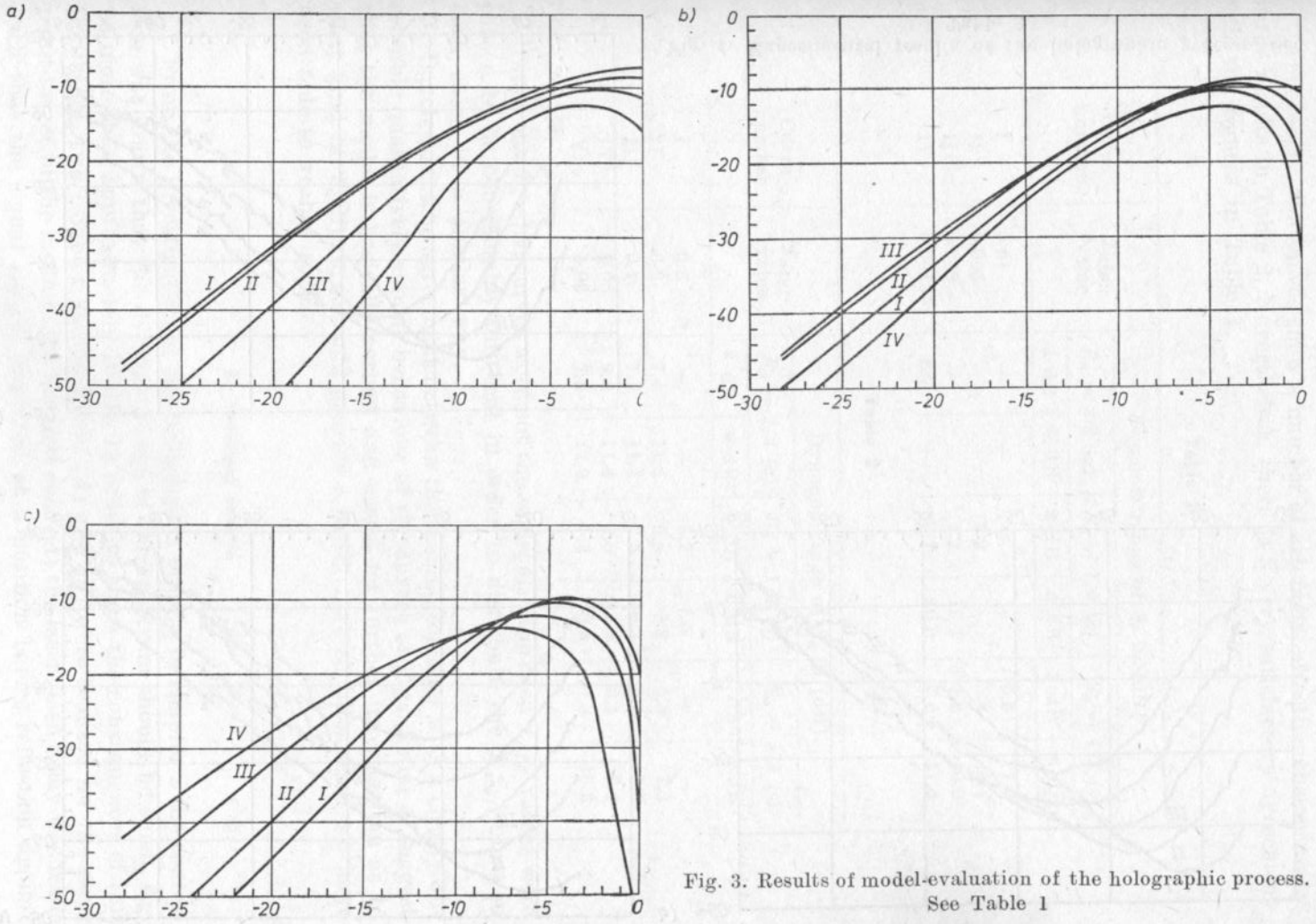

Fig. 3. Results of model-evaluation of the holographic process. See Table 1

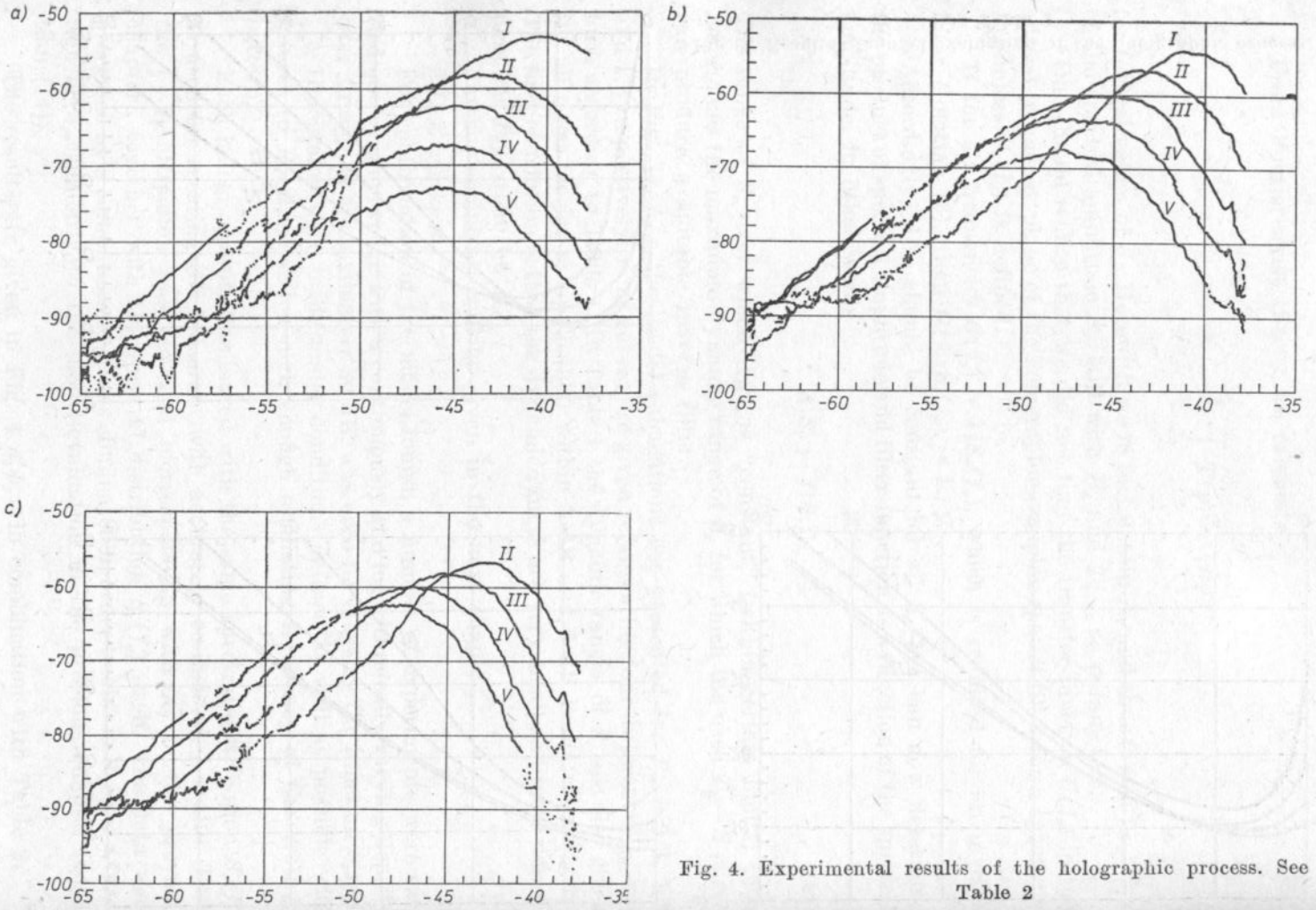

Fig. 4. Experimental results of the holographic process. See Table 2

Apparently, the curves show a number of artefacts, affecting the accuracy of the results in Table 2. Nevertheless, there is a very satisfactory agreement with the figures in Table 1.

Table 1

Curve number	T_{aDC}-value	Dynamic range of S_r in [dB]					
		$R_a = 2/3$ (*a*)		$R_a = 1/2$ (*b*)		$R_a = 1/3$ (*c*)	
		3 dB	6 dB	3 dB	6 dB	3 dB	6 dB
I	0.01	–	–	–	–	5.5	7.9
II	0.005	–	–	7.2	–	5.8	8.4
III	0.002	–	–	7.2	10.7	7.2	10.0
IV	0.00135	6.7	–	7.1	10.0	7.6	11.2

Table 2

Curve number	T_{aDC}-value	Dynamic range of S_r in [dB]					
		$R_a = 2/3$ (*a*)		$R_a = 1/2$ (*b*)		$R_a = 1/3$ (*c*)	
		3 dB	6 dB	3 dB	6 dB	3 dB	6 dB
I	0.5	–	–	5.2	7.5	–	–
II	0.2	7.4	11.2	5.8	9.2	5.3	7.3
III	0.1	7.5	11.4	7.5	10.3	5.4	8.0
IV	0.05	8.0	11.4	8.0	11.4	6.1	9.2
V	0.02	7.5	11.0	7.3	10.8	7.3	10.3

Since the $T_a-(E)$ curves were not the same, also the used T_{aDC}-values were chosen to be considerably different in order to distribute the T_{aDC}-values in both cases in a similar way.

Conclusion: The agreement between the results, together with a clearly observable qualitatively similar behaviour of the curves of Figs. 3 and 4, suggest that the model is basically correct and useful for further investigation as to what kind of $T_a(E)$-curve could provide a better inverse filter than we have been able to realize so far.

3. Practical results

From the investigation of the holographic process in chapter 2 the conclusion was drawn that the dynamic range of the spectrum should be small, e.g. no more than approximately 10 dB. In order to show the consequences of this limitation, two complex spatial filters (*A*) and (*B*) were realized for the same point-target in the medium. In the first case (*A*) the laser-flash delay was made such that the signal $s_r(x, y)$ appeared at a position before reflection against

the paraboloid reflector, whereas the second case (B) was the normal situation with the signal $s_r(x, y)$ shown after reflection.

Obviously the flattening of the wave-fronts at reflection against the paraboloid reflector causes a considerable increase of power-concentration through the Fourier-transformation.

Fig. 5 shows case (A) with respectively the obtained spectrum (a), the unfiltered signal supposed to be identical to $s_r(x, y)$ in the input plane (b) and zero and first diffraction orders in the output plane (c).

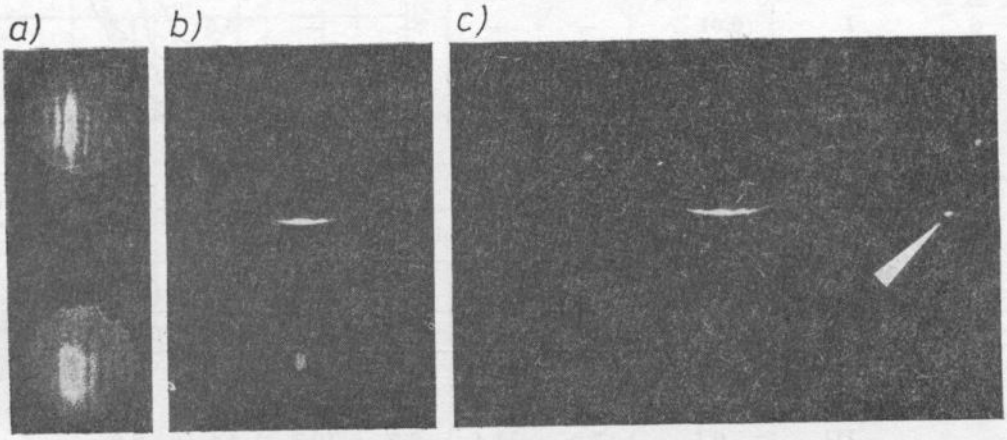

Fig. 5. Practical results for non-reflected signals

As explained in 2.3, the filter-result appears as the $(-\theta)$-diffraction and is indicated by an arrow in Fig. 5c.

Apparently, a very effective deconvolution has been obtained since this very small spot is depicted at the same scale as $s_r(x, y)$ in (b).

Fig. 6 represents results obtained in case (B). In (a) five signals are shown as they appeared unfiltered in the output plane, again supposed to be identical to the input-signals. The scanned object consisted of five "point"-targets in a rhombus-shaped configuration and the image shows clearly the position-deformation caused by the paraboloid reflector. A filter was realized with only the center-target present in the medium and after installing the filter the corner-targets were mounted at their positions. In Fig. 6b we see the filter-results, being much less spectacular than in case (A). In Fig. 6c and d the signals are shown as measured quantitatively.

It is clear that the gain in spatial invariance by using a paraboloid reflector (as a proof showing the five filtered signals in Fig. 6b as being quite similar) has been obtained at the expense of filter-performance because of the increased dynamic range of the spectra. Everything is in good agreement with the results of the model-investigation in chapter 2.

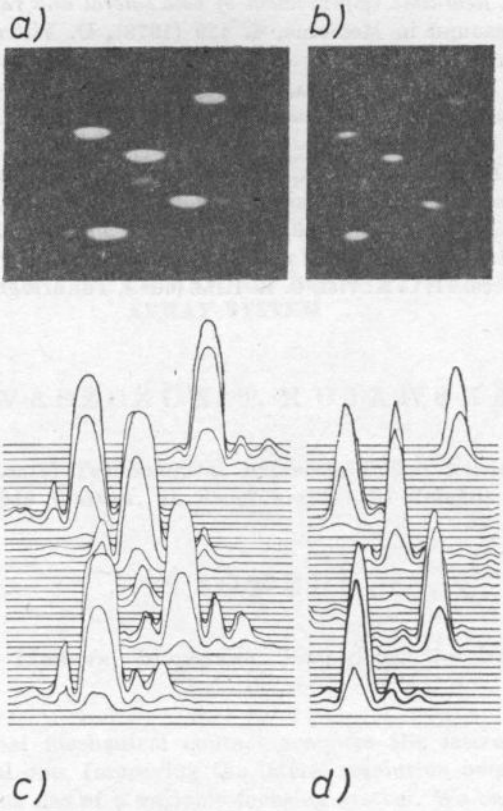

Fig. 6. Practical results for signals after reflection

8. Conclusions

With a complex spatial filter in the spatial frequency plane of an optical computer filtering can be performed. A holographic method has been described to realize such a filter which acts as an inverse filter provided that the spectrum to be processed has a small dynamic range.

Both increasing dynamic range of the filter and compression of the spectrum's dynamic range are the goals of further investigations.

References

[1] A. Vander Lugt, *Signal detection by complex spatial filtering,* IEEE Trans. on Information Theory, IT-10, 139 (1964).

[2] J. C. Somer, *Real-time improvement of both lateral and range resolution by optical signal processing,* 1977 Ultrasonics Symposium Proceedings, **77CH**-1264-1 SU, New York, IEEE 1002.

[3] J. C. SOMER, *Real-time improvement of both lateral and range resolution by optical signal processing,* Ultrasound in Medicine, **4**, 439 (1978), D. WHITE, E. A. LYONS (eds.), New York, Plenum Press.

[4] J. C. SOMER, E. H. M. JONGSMA, W. L. J. MARTENS, *Real-time two-dimensional resolution improvement by optical signal processing,* Proc. UBIOMED IV 1979, **1**, 14, P. GREGUSS, (ed.), Visegrad, Hungary.

[5] J. C. SOMER, E. H. M. JONGSMA, W. L. J. MARTENS, *Application of an acousto-optic device in an optical deconvolver for blurred ultrasound-diagnostic images,* Proc. 1st Spring School on Acoustooptics and Applications, 1980, 202, Gdańsk University, Physics Institute.

[6] J. C. SOMER, 1980. *Optical signal processing in ultrasound,* Investigative Ultrasonology, **1**, Technical Advances, 71, C. ALVISI, C. R. HILL (eds.), Tunbridge Wells, Pitman Medical, 1980.

ARCHIVES OF ACOUSTICS
9, 1-2, 155-162 (1984)

ELECTRONIC FOCUSING OF THE ULTRASONIC BEAM BY MEANS OF AN ANNULAR ARRAY SYSTEM

T. WASZCZUK, T. KUJAWSKA

Institute of Fundamental Technological Research, Polish Academy of Sciences
(00-049 Warsaw, ul. Świętokrzyska 21 Poland)

J. C. SOMER

University of Limburg, Biophysics, Maastricht, the Netherlands

In conventional mechanical contact scanners the lateral resolution is inferior to the axial one. Improving the lateral resolution over a wide range of depth requires the use of a variable focusing system. We choose the phase annular array system which may be used in obstetrics and gynaecology.

Calculations of the acoustical pressure were performed assuming pulse excited transducers. For the transmission the range of examination was divided into five focal zones. During reception the system permits dynamic focusing. Measurements of the ultrasonic beam were carried out. These results are in good agreement with calculations and indicate a considerable increase in the lateral resolution.

1. Introduction

In order to obtain the maximum amount of information about the tissues under examination by the *B*-mode ultrasonograph, it is necessary to have as good resolution of the ultrasonograph as possible.

In the present state of ultrasonic technology the most negative effect on the resolution is exerted by the lateral resolution of the ultrasonic system. The lateral resolution is determined by the transmitted beam and receiver directivity pattern.

The aim of this work is to indicate the possibilities of decreasing the width of the ultrasonic beam, i.e. improvement in the lateral resolution.

2. Method

The well known method to narrow the ultrasonic beam uses a transducer with a superimposed lens or a transducer which has a special concave aperture [1]. This kind of focusing is efficient only in a short range.

It is possible to focus over the whole observation range when a multi-element ultrasonic probe, controlled by an appropriate electronic system is used [2, 3, 6]. A multi-element annular array consists of coaxial elements: a disc and surrounding rings. The disc and the rings are excited to vibration. The moment of excitation of a successive element in the probe is related to the wave front as required for focusing at a proper distance on the axis of the transducer. At transmission the beams can be focused successively at discrete distances. This corresponds to several foci over the investigated range.

During reception it is possible to achieve continuous focusing, by continuous change of the delay of the signals received, with the velocity equal to the ultrasonic wave propagation velocity. This is so-called dynamic focusing (Fig. 1).

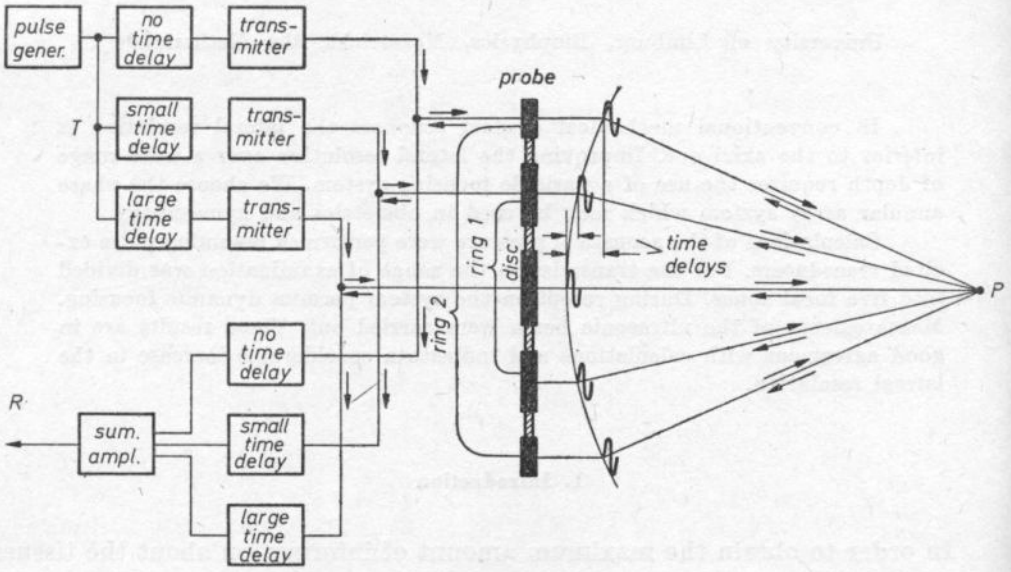

Fig. 1. Focusing during transmission and reception. T — transmission part, R — reception part

In our case we expect such an ultrasonic beam focusing system to be used in obstetrics and gynaecology, that is why 2.5 MHz frequency was chosen for the transducer with depth of range 0-24 cm; the surface of the transducer is in touch with the surface of the body. On the basis of theoretical analysis of the lateral resolution for an annular array excited by continuous wave and

short pulses, depending on the size, configuration and the excitation method, the ultrasonic probe was built. This probe consists of seven coaxial elements of piezoelectric ceramic: a disc and six rings [5]. The diameter of the disc is about 10 mm and the external diameter of the outside ring is about 40 mm. All the elements have the same surface area. This permitted the achievement of:

a) the same electric impedance of all elements, i.e. the same electric loading of all transmitters,

b) practically the same distance of the transition point between the near and far fields, for the disc and all the rings [6, 8].

The annular array works with an electronic system which was built with a large application of the TTL integrated circuits and the PROM memories [8]. A block diagram of such electronic system is shown in Fig. 2. The seven trans-

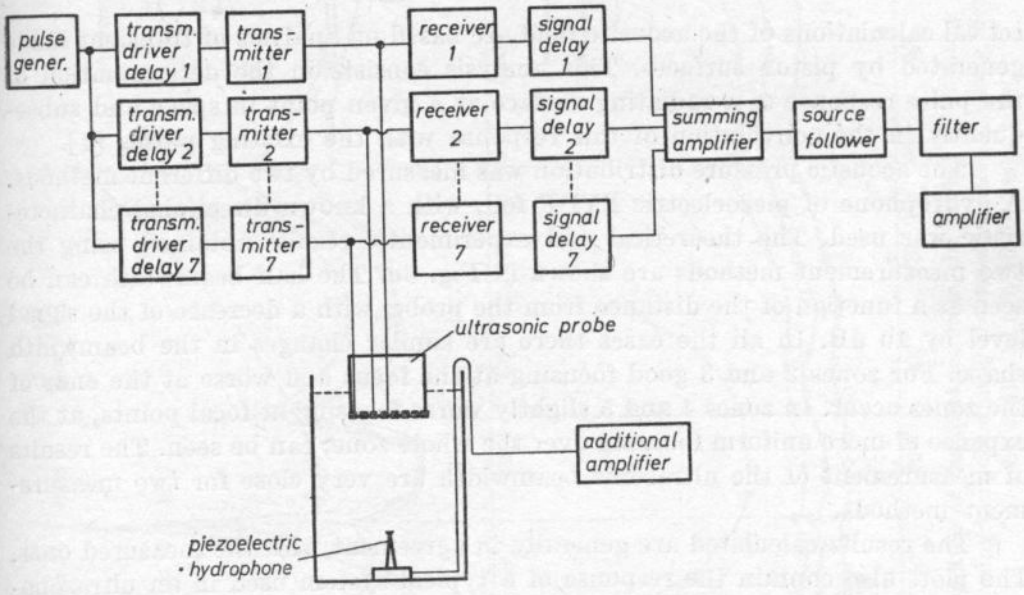

Fig. 2. Block diagram of the system for electronic focusing of the ultrasonic beam

mitter drivers in which the proper delays are programmed, steer the seven transmitters. Each transmitter excites the proper element of the annular array. A hydrophone measures the ultrasonic pressure distribution. The hydrophone can be replaced by a reflector and then the signals reflected after amplification are delayed continuously in the signal delay circuits, and added in the summing amplifier. On the basis of the earlier analysis and measurements [7], the whole range $0 \div 24$ cm was divided into five zones.

Zone 1 : from 0 to 50 mm, with only the disc transmitting.

Zone 2 : from 50 to 70 mm, focal point 60 mm, three elements: the disc and two internal rings transmit.

Zone 3 : from 70 to 90 mm, focal point 80 mm.
Zone 4 : from 90 to 140 mm, focal point 110 mm.
Zone 5 : from 140 to 240 mm, focal point 180 mm.
In zones 3, 4, 5 all the seven elements of the probe transmit.

3. Results

The theoretical calculations and experimental measurements of the acoustic pressure distribution were carried out only during transmission. In the calculations a pulse shape closest to one in practice was assumed. This pulse contains five sinusoidal high frequency periods with the envelope $\sin^2\left(\frac{\pi}{2}t\right)$. The theoretical calculations of the acoustic field are based on analysis of transient fields generated by piston surfaces. This analysis consists in the determination of the pulse response of a radiating surface at a given point in space and subsequently in the convolution of this response with the exciting pulses [4].

The acoustic pressure distribution was measured by two different methods. A hydrophone of piezoelectric PVDF foil, with a known directional characteristic was used. The theoretical and experimental results obtained using the two measurement methods are shown in Fig. 3*a*. The half beamwidth can be seen as a function of the distance from the probe, with a decrease of the signal level by 10 dB. In all the cases there are similar changes in the beamwidth shape. For zones 2 and 3 good focusing at the focus and worse at the ends of the zones occur. In zones 4 and 5 slightly worse focusing at focal points, at the expense of more uniform focusing over the whole zone, can be seen. The results of measurement of the ultrasonic beamwidth are very close for two measurement methods.

The results calculated are generally in agreement with the measured ones. The plots also contain the response of a typical system used in an ultrasonograph for examination of the abdominal structures (frequency 2.5 MHz, diameter of transducer 20 mm). The ultrasonic beam radiated by the annular array system is narrower and much more regular over the whole range under study.

The distribution of the measured signal amplitudes over the whole range is shown in Fig. 4*A*. Greater amplitudes occur in zones 3, 4, 5, it should be mentioned, however, that all the elements transmit to these zones. At the ends of zones 2 and 3 there is a distinct effect of the side lobes. The amplitude distribution is rather regular over the whole range under study.

The second part of measurements was made with focusing in zones during transmission and dynamic focusing during reception. The hydrophone was replaced by a small reflector (platinium ball with 0.3 mm diameter). In zone 1

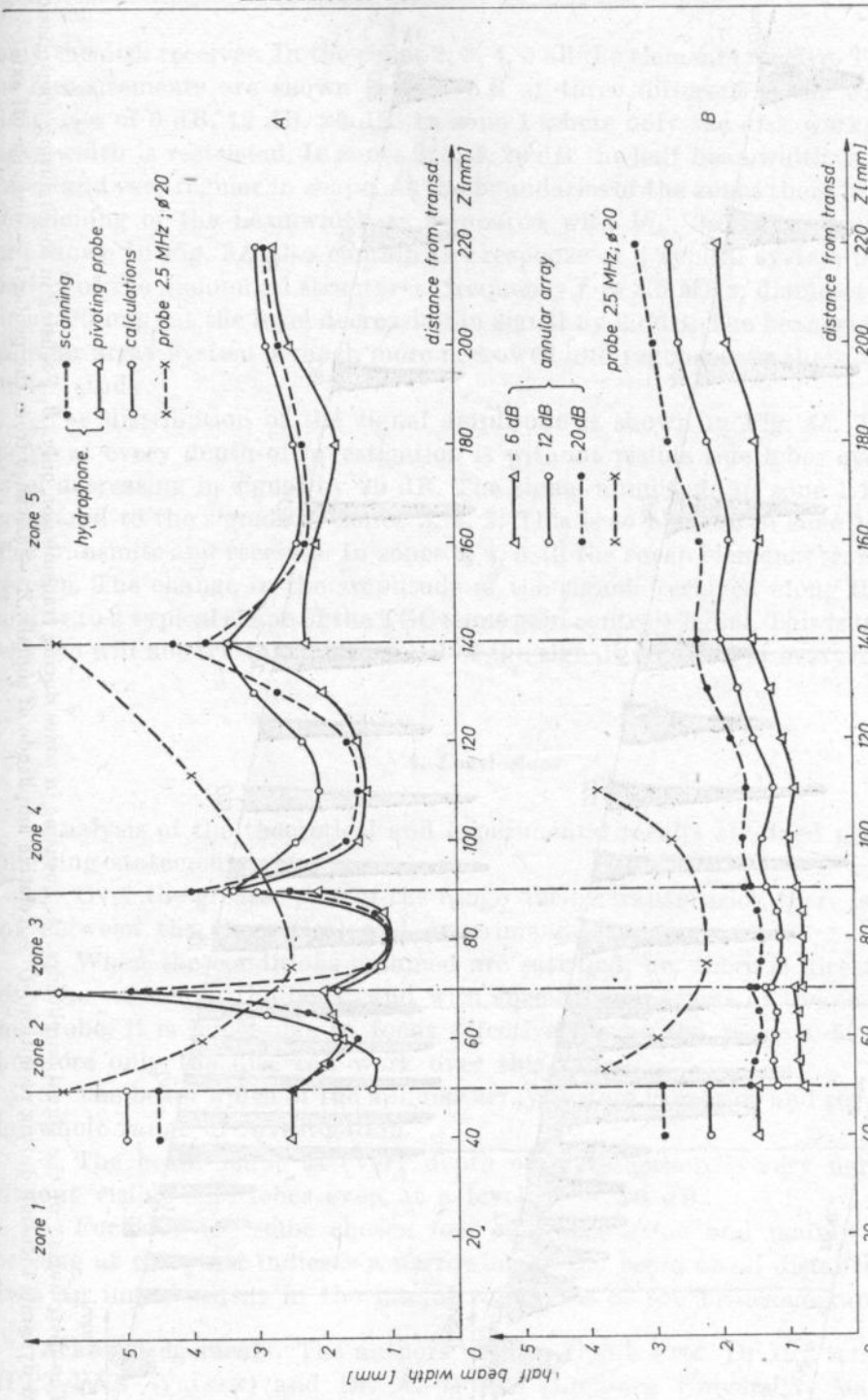

Fig. 3. Half beam width as a function of the distance from the probe. *A*. Focusing in zones during transmission only. Signals drop by 10 dB. *B*. Focusing in zones during transmission and dynamic focusing during reception. Signals drop by 6 dB, 12 dB, 20 dB respectively

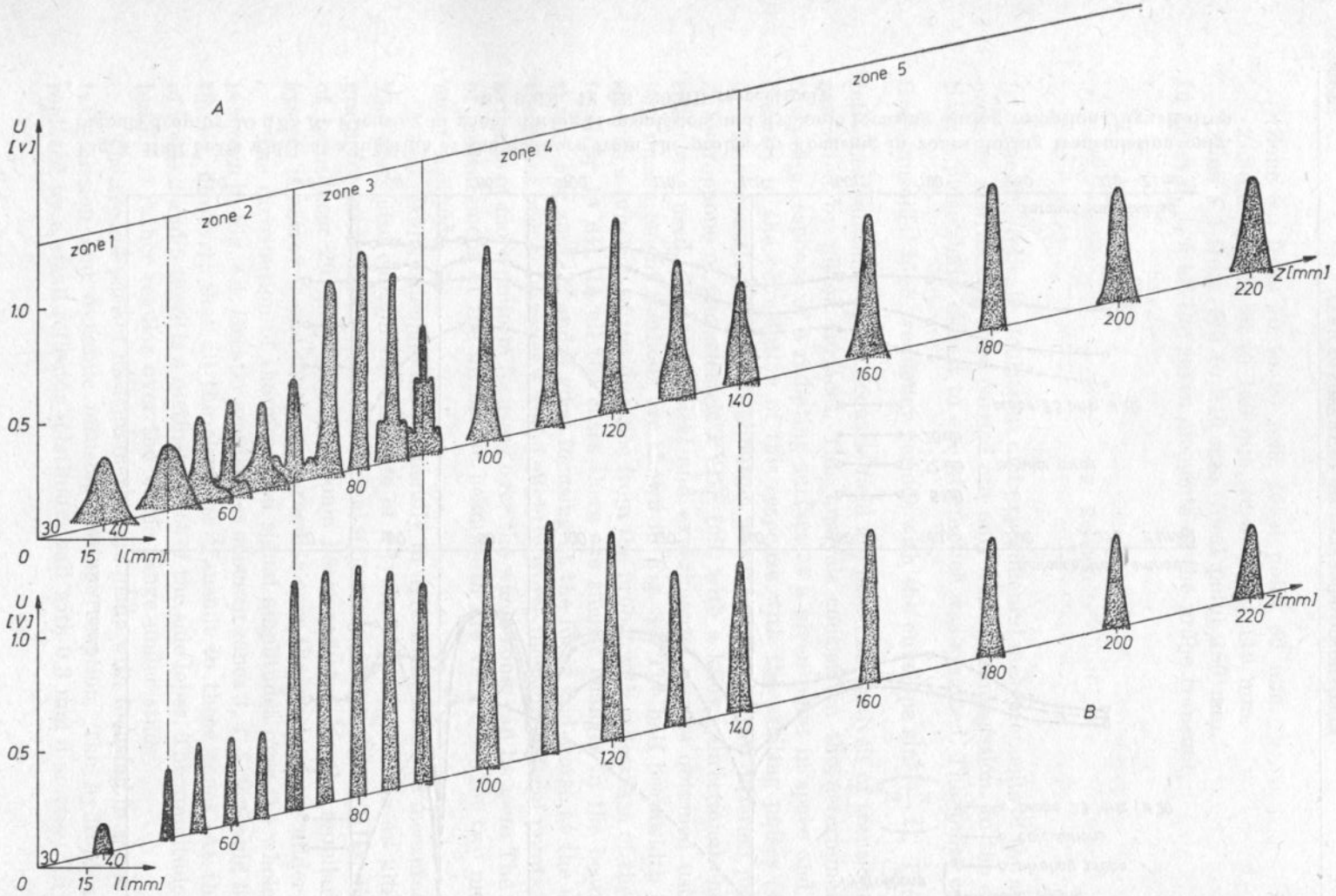

Fig. 4. The distribution of the signal amplitudes. *A*. Focusing in zones during transmission only. *B*. Focusing in zones during transmission and dynamic focusing during reception, U — relative amplitude of signals, Z — distance from the probe, l — distance off axis

only the disk receives. In the zones 2, 3, 4, 5 all the elements receive. The results of measurements are shown in Fig. 3*B* at three different levels with signal decreases of 6 dB, 12 dB, 20 dB. In zone 1 where only the disk works half the beamwidth is restricted. In zones 2, 3, 4, 20 dB the half beamwidth is less than 2 mm and very regular in shape. At the boundaries of the zones there is no visible broadening of the beamwidth as compared with Fig. 3*A*. The results which are shown in Fig. 3*B* also contain the response of a typical system for examination of the abdominal structures (frequency $f = 2.5$ MHz, diameter of transducer 20 mm) at the level decreasing in signal by 20 dB. The beamwidth of the annular array system is much more narrowed and regular over the whole range under study.

The distribution of the signal amplitude is shown in Fig. 4*b*. The beam shape at every depth of investigation is without visible side lobes even at the level decreasing in signal by 20 dB. The signal amplitude in zone 1 is smaller compared to the signals in zones 3, 4, 5. This is so because in zone 1 only the disc transmits and receives. In zones 3, 4, 5 all the seven elements transmit and receive. The change in the amplitude of the signals received along the axis is similar to a typical shape of the TGC (time gain control) signal. This is the reason why we will not try to equalize level of the signals received in every zone.

4. Conclusions

Analysis of the theoretical and experimental results obtained permits the following statements.

1. Over the greater part of the range during transmission there is agreement between the theoretical and experimental results.

2. When the conditions assumed are satisfied, i.e. there is direct contact with the surface of the body, and with specific dimensions of the elements of the probe, it is impossible to focus effectively over the range 0-50 mm and therefore only the disc can work over this range.

3. The beam width of the annular array system is narrow and regular over the whole range of investigation.

4. The beam shape at every depth of investigation is very narrow and without visible side lobes even at a level of — 20 dB.

5. Focusing for some chosen foci at transmission and mainly dynamic focusing at reception indicate a narrowing of the beam at all distances and it gives an improvement in the lateral resolution of the ultrasonograph.

Acknowledgements. The authors wish to thank Prof. Dr L. Filipczyński (IPPT-PAN Warsaw) and Dr. A. Hoeks (Limburg University, Maastricht) for discussion and valuable suggestions in the course of the preparation of this paper.

References

[1] L. FILIPCZYŃSKI, G. ŁYPACEWICZ, J. SAŁKOWSKI, T. WASZCZUK, *Automatic eye vizualization and ultrasonic intensity determination on focused beams by means of electrodynamic and capacitance methods,* Ultrasonics in Medicine Katzner *et al.* (eds.), Excerpta Medica, Amsterdam, Oxford, 1975.

[2] M. HUBELBANK, O. J. TRETIAK, *Focused ultrasonic transducer design,* M.I.T. Res. Lab. Elect. Q.P.R. 1971, 169-177.

[3] G. KOSSOFF *et al., Annular phased arrays in ultrasonic obstetrical examinations,* Advanced Study Institute, Ultrasonic Diagnostics, Milan, June 1974.

[4] T. KUJAWSKA, *Dynamic focusing of an ultrasonic beam by a phased array using the pulse method,* Archives of Acoustics, **8**, 1, (1983).

[5] T. MARUK-KUJAWSKA, *Dynamic focusing of an ultrasonic beam by annular transducers* (in Polish) (doct. diss.), Institute of Fundamental Technological Research, Polish Academy of Sciences, Warsaw 1980.

[6] H. E. MELTON, F. L. THURSTONE, *Annular array design and logarithmic processing for ultrasonic imaging,* Ultrasound in Biology and Medicine, **4**, 1-12 (1978).

[7] T. WASZCZUK, J. C. SOMER, *System for dynamic focusing of an ultrasonic beam using annular array, practical implementation,* Proc. XXVII Open Seminar on Acoustics, Warsaw-Puławy, September 1980.

[8] T. WASZCZUK, J. C. SOMER, T. KUJAWSKA, *Focusing of an ultrasonic beam by means of a piezoelectric annular array,* Archives of Accoustics (in press).

ARCHIVES OF ACOUSTICS
9, 1-2, 163-174 (1984)

CEREBROVASCULAR IMPEDANCE MEASUREMENTS WITH US DOPPLER TECHNIQUE

CARLO ALVISI, MARCO GIULIONI,
MARZIANO CERISOLI, GIULIANO GIULIANI

Institute of Neurological Surgery, University of Bologna, Bologna, Italy

PAOLO MONARI

Department of Statistical Sciences, University of Bologna, Bologna, Italy

CLEMENTE PALLOTTI

Medical Physics, Faculty of Veterinary Medicine, University of Bologna, Bologna, Italy

The Authors present different experimental models performed in the attempt to determine whether the alterations of brain circulation following an increase in the intracranial impedance can be estimated by systolic and diastolic common carotid artery (CCA) velocity Doppler signals recorded at 15-minute intervals until 60 minutes and 10 hours. In model 1 both jugular veins (JV) were ligated and Doppler signals were recorded at 15-minute intervals until 60 minutes. In model 2 ipsilateral external carotid artery (ECA) ligation was added to JV occlusion. In model 3 recording of Doppler signals was performed at 15-minute intervals until 60 minutes and 10 hours in the presence of ipsilateral ECA and bilateral JV occlusion. In model 4 Doppler signals were recorded in the presence of ipsilateral ECA occlusion alone.

Statistically significant results confirming the well-known theoretical relationship between increased encephalic impedance and flow velocity Doppler signals were obtained in model 3. The results demonstrated that a sudden increase in the encephalic impedance can affect both systolic and diastolic flow velocities in afferent vessels.

Later (from 60 minutes to 10 hours), systolic values tend to increase and at 10 hours are always higher than starting values. The diastolic values, however, remain inferior to the starting values, although showing a slight tendency to rise.

The Authors conclude that significative alterations of cerebrovascular impedance can be obtained by clamping both JV. However, these alterations can be recorded on the CCA only if the ipsilateral ECA is occluded, thus eliminating the risk of run-off across it, or if recordings are taken from the internal carotid artery.

1. Introduction

RISBERG and SMITH [12] demonstrated that Doppler carotid velocity determination is highly correlated to hemispheric blood flow measurements by the 133 Xenon inhalation method. A fairly accurate prediction of hemispheric blood flow from Doppler internal carotid and diastolic velocity values is possible in patients without abnormalities in these arterial systems.

For some time now, contributions have been published illustrating the possibility of measuring the variations of cerebrovascular impedance through a valuation in the form of Doppler sound waves which record the blood flow velocity in vascular sections above the cerebral circulation [1, 2, 4-11, 13-16]. There can be different causes for the alterations of impedance in the encephalic flow. Vascular constriction, intravasal obstructions, vasal wall compression with increasing transmural pressure, all contribute to the increase of impedance. This is diminished by arteriovenous malformations, arteriovenous fistula and by anastomosis and pathological shunts in tumoral tissues.

The first-mentioned condition is of great interest to the neurologist and neurosurgeon being more frequently encountered.

2. The purpose of this research

On examination of the available literature, it can be assumed that enough data have been collected to demonstrate the alterations of the blood flow in cerebroafferent vessels compared with cerebrovascular impedance. However, these data refer to two entirely unconnected situations. In fact, they lack mention of phenomena which appear after a sudden alteration of the impedance linked to the Pa02 and PaC02 of the brain and before the modifications of the flow velocity linked with the states of intracranial persistent hypertension reported on by the authors mentioned above.

We planned therefore an experimental model to check the alterations in the blood flow rate in cerebroafferent vessels during massive variations of the cerebrovascular impedance in order to follow their course covering a period of from 15 min. to 10 hours from the start of the increased cerebrovascular impedance.

The impedance increase in the rat is obtained by clamping both JV. The advantages of this model are:

1) an increase in the vasal resistance;

2) an harmonically-diffused increase in the intracranial pressure with no unilateral gradient pressure or different pressure between the various intracranial sectors.

The model thus obtained can be considered similar to the work of CUYPERS *et al.* [3], who blocked the cerebral blood flow by placing an obstacle in the

upper venus cava. They observed that increased venous pressure, which implies increased capillary pressure, causes an enormous swelling of the brain. When the venus cava was blocked the pressure at the Herophili torcular rose from 5.2 to 35.0 mm Hg and the brain tissue pressure rose from 3.8 to 17.6 mm Hg. After a few minutes Herophili torcular pressure began to fall and reached a steady state of 15.5 mm Hg after about 45 min., while the brain tissue pressure, which had risen initially after blocking the venus cava, fell to 4.0 mm Hg. The mean arterial blood pressure abruptly fell 25 ($\pm$20) mm Hg below its initial value, during a long lasting block, however, the mean arterial blood pressure returns to normal in all animals.

In our models, no change in the mean arterial blood pressure was observed. This technique which we created, i.e. clamping JV has been defined as model 1. The Doppler signals were recorded on the common carotid artery (CCA).

In model 2 in addition to the clamping of JV we associated the occlusion of the ipsilateral external carotid artery (ECA) to the CCA on which the recordings were made in order to eliminate the interferences created by the run-off through this vessel because of the technical impossibility of recording a signal at the internal carotid artery (ICA) level in the rat.

Model 4 with the ipsilateral ECA occlusion without JV clamping was planned to check if we are only measuring changes in CCA hemodynamics secondary to the removal of the ECA from the vascular system, rather than a change in the cerebral hemispheric flow due to JV ligation.

3. Materials and methods

The experimental series consisted of 80 white Wistar rats weighing 300 to 400 g, divided in four groups.

Model 1 (20 rats)

The animals were anesthetized with pentobarbital i.p. (30 mg/kg). The left CCA and both JV were exposed through a midline cervical incision. Then, CCA flow velocity signals were recorded by using a 8 MHz directional Doppler CW flowmeter (Angiodop 481, DMS). The distance between the tip of the ultrasonic transducer and the vessel (about 5 mm) was filled by a contact medium for ultrasonic transmission (Aquasonic 100, Parker Laboratories Inc.).

Fast Fourier Transform (FFT) real-time sound spectral analysis (Angioscan, Unigon Industries, Mt Vernon, NY) was also performed. Systolic and diastolic frequency values were obtained by recording sound spectral display in which switching of the cursor up or down allowed the frequency position of the cursor line to be read in Hz at the bottom of the screen.

Immediately after recording Doppler signals, both JV were ligated. Subsequently, CCA Doppler signals recording with spectrum analysis was performed at 15, 30, 45, and 60 min. from the time of initial occlusion.

Model 2 (40 rats)

In this group left ECA ligation was added to bilateral JV occlusion.

Model 3 (10 rats)

In this model the same circulation modifications were provoked as in model 2, but the recording of the systolic and diastolic Doppler signals was made not only at 15, 30, 45, 60 min., but also at 10 hours after the occlusion of the vessels.

Model 4 (10 rats)

In this group only ECA was clamped and the systolic and diastolic values measured every 15 min. up to 60 min.

4. Results

Model 1 (20 rats)

The mean systolic peak values and the mean diastolic peak values show an inconsistent response to clamping both JV. In fact, 50 % of rats show a sig-

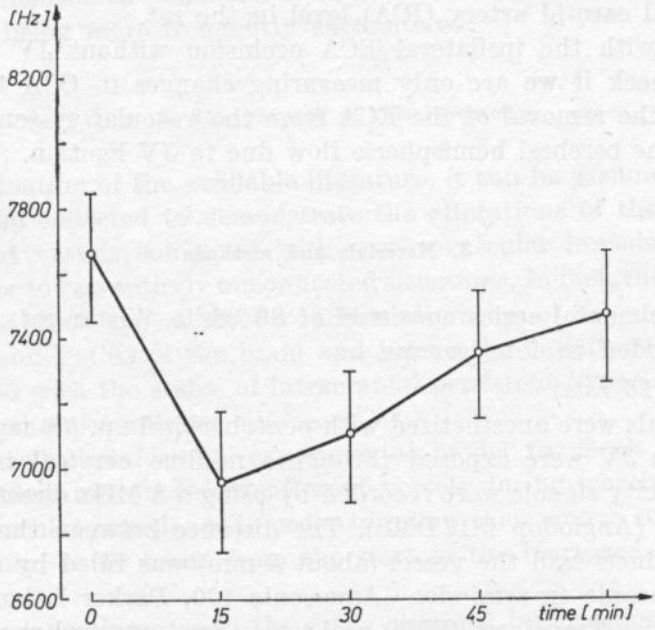

M:	7654.5	6969.5	7104.0	7353.0	7481.0
SD:	1279.7	1396.3	1270.6	1246.1	1262.5
SE:	204.9	223.6	203.5	199.5	204.8
SD/M:	0.1672	0.2003	0.1789	0.1695	0.1688

Fig. 1. Mean systolic peak values of model 2. In all figures: Ordinate-values of frequencies [Hz], abscissae-time of the experiment [minutes], *M* — mean values, *SD* — standard deviation, *SE* — standard error

nificant decrease of the mean systolic peak values 15 min. after JV occlusion; the other 50 % of rats show a significant increase in the mean systolic peak values 15 min. after JV occlusion. At 60 min. peak values were always higher than the starting ones. The diastolic flow pattern parallels the systolic one.

In this model statistical analysis gave significant results (at 0.05 level). Then, we cannot reject the "null hypothesis" and we concluded that there is no significant difference between the series of data.

Model 2 (40 rats)

The mean systolic peak values and the mean diastolic peak values allowed us to appreciate a difference in behaviour following the occlusion of JV and ECA. 74 % of the mean systolic peak values show a significant decrease 15 min.

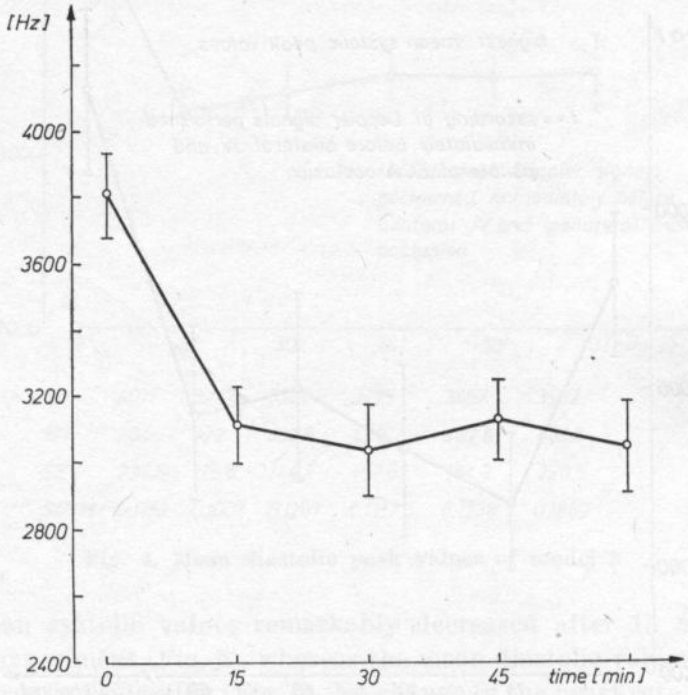

M:	3812	3120	3045	3136	3048.42
SD:	540.26	518.46	558.79	583.04	603.33
SE:	123.95	118.94	128.19	133.76	142.21
SD/M:	0.1417	0.1662	0.1835	0.1859	0.1979

Fig. 2. Mean diastolic peak values of model 2

after JV and ECA clamping. The diastolic mean peak values also decrease at 15 min. in 89 % of cases. At 60 min. the mean systolic peak values were lower than the starting ones in 59 % and the diastolic mean peak values in 89 % (Figs. 1-2).

In this model the sign test was significant ($p < 0.01$) after 15 min. Then, we can reject the "null hypothesis" and may conclude that it is unlikely that the results are purely fortuitous.

The correlation coefficient r used to compare the data of the mean systolic peak values after 15 min. and 60 min. was computed to be 0.60 and differs significantly from zero at 0.001 level. Therefore, the two series of data seem to be positively correlated.

The sign test of the diastolic mean peak values is also significant after 15 min. and 60 min. for $p < 0.001$. The correlation coefficient $r = 0.82$ computed between the data after 15 min. and 60 min. differs significantly from zero at 0.001 level. This situation denotes a systematic stabilisation in the effects.

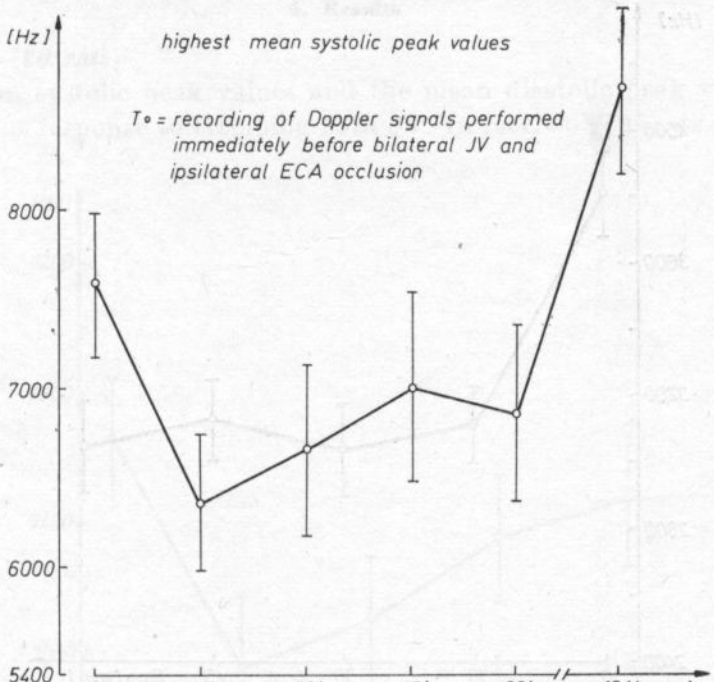

M:	7591	6362	6675	7022	6888	8720
SD:	1192.9	1096.5	1487.6	1650.5	1493.6	1406.2
SE:	397.6	387.6	495.8	550.2	497.9	468.7
SD/M:	0.0523	0.1723	0.0742	0.2350	0.2168	0.1612

Fig. 3. Mean systolic peak values of model 3

Model 3 (10 rats)

In this group the alterations of systolic values observed in the experiment (JV and ECA occlusion = model 2) were similar to those observed in the group of 40 rats treated in the same way. It is interesting to note that at the 10th

hour of ECA and JV occlusion the systolic values were remarkably higher (Fig. 3) compared with the starting values and with those recorded after one hour from the beginning of the experiment. The diastolic values, however, remain inferior to the starting values, although showing a slight tendency to rise (Fig. 4).

Model 4 (10 rats)

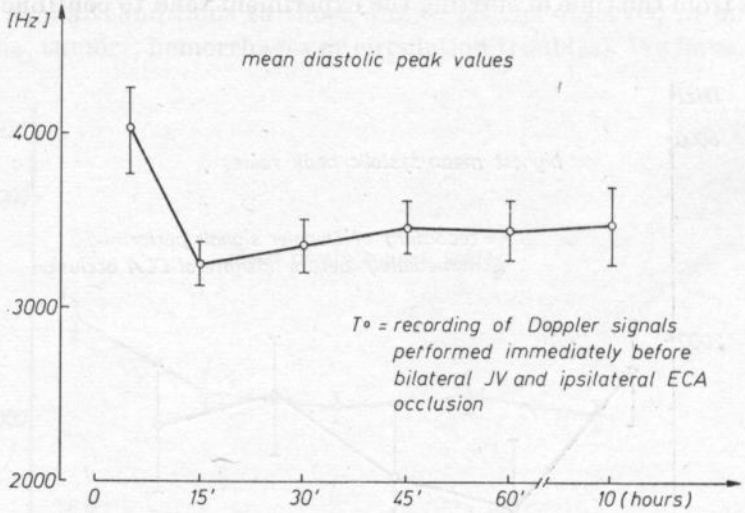

M:	4017	3247	3360	3475	3457	3502
SD:	704	327	432.6	458	462.6	661.8
SE:	234.6	115.6	144.2	152.6	154.2	220.6
SD/M:	0.1752	0.1007	0.1287	0.1317	0.1338	0.1889

Fig. 4. Mean diastolic peak values of model 3

The mean systolic values remarkably decreased after 15 min. from the start of the experiment (Fig. 5), whereas the mean diastolic values after 15 min. did not decrease considerably (Fig. 6). No change in the heart rate was observed. The mean arterial blood pressure did not change. The intracranial pressure was not recorded to avoid trauma to the experimental model. However, brain swelling was constantly observed at the end of the experiments with JV ligation.

5. Discussion

Our experiments have pointed out an alteration of the association rate/cerebrovascular impedance linked to the time in which the examination is made with respect to the beginning of the increased cerebrovascular impedance condition.

A clear alteration is noted 15 min. after the beginning of the experiment, when the occlusion of JV and ipsilateral ECA of the CCA, from which the Doppler signals are taken, suddenly and in great measure abolish most of the draining vessels of the CCA (venous through JV and arterial through the ECA). At this moment both the systolic and diastolic values alter. They decrease considerably. Following this first phenomenon, a progressive increase in the systolic values is registered, which at 60 min. regain their original values and at 10 hours from the time of starting the experiment tend to continue increasing.

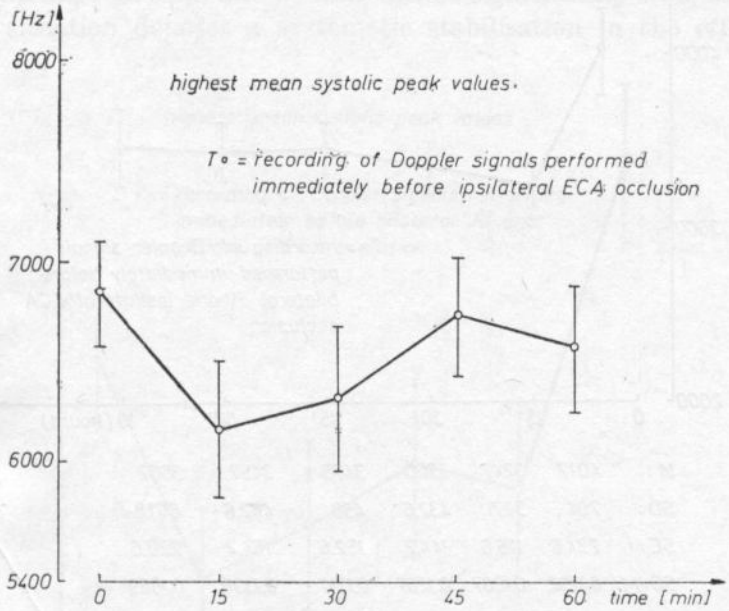

M:	6854	6160	6336	6744	6496
SD:	808.3	1075.9	1134.3	968.8	1038.1
SE:	255.6	340.2	358.7	306.3	328.2
SD/M:	0.1179	0.1746	0.1790	0.1436	0.1598

Fig. 5. Mean systolic peak values of model 4

The diastolic values, instead, behave differently at 60 min. Their values never reach the initial ones even after 10 hours.

It can therefore be confirmed that in cerebroafferent vessels, when the cerebrovascular impedance increases rapidly, there are immediate alterations in both the systolic and diastolic values, but the reciprocal behaviour is very different.

Our findings, therefore, answer the problem facing us when we planned our experiment. From an examination of the flow velocity values, we can

complete the pattern of the behaviour of the blood flow rate in cerebroafferent vessels compared with the cerebrovascular impedance alterations.

From BEASLEY *et al.* [1] we learn that arterial constriction due to an increase of Pa02 causes a decrease in the systolic and diastolic values of the Doppler signals.

From this acute and transitory alteration of the cerebrovascular impedance, as our model illustrates, we pass on to an equally acute but lasting alteration that creates similar conditions to those due to lesions observed in human pathology (edema, tumors, hemorrhages or circulation troubles). We have been able

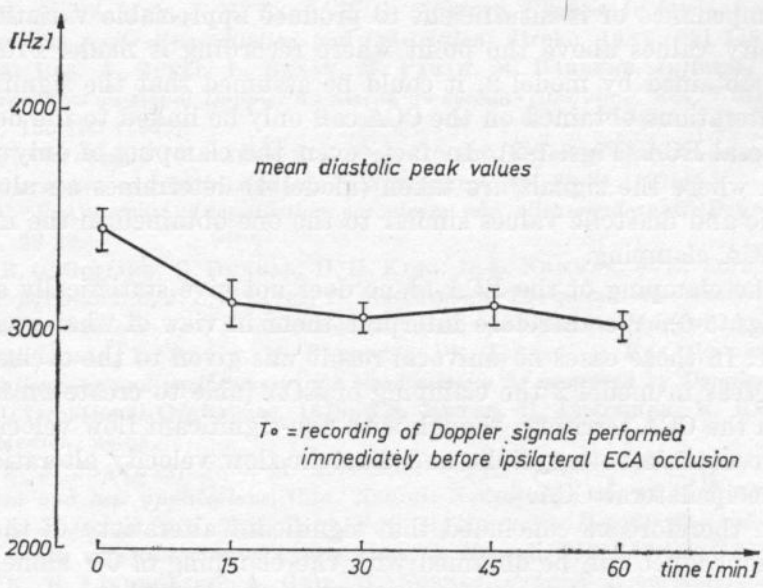

M:	3456	3112	3072	3136	3048
SD:	266.1	316.5	220.5	303.5	214.8
SE:	84.1	100.1	69.7	96	67.9
SD/M:	0.0769	0.1017	0.0717	0.0967	0.0704

Fig. 6. Mean diastolic peak values of model 4

to follow the evolution of the alterations of the blood rate in the cerebroafferent vessels during the period immediately following the start of the increase of cerebrovascular impedance. From this acute period typical alterations of the blood flow are created which precede and rapidly become similar within 10 hours to those observed by JONKMAN *et al.* [8] and STEIGER [14]: an increase in the systolic values and a decrease in the diastolic ones in cases of expansive intracranial lesions which are the cause of stable increased intracranial pressure. The results observed by LINDEGAARD *et al.* [9] (very high systolic values and reverse flow) in cases of the brain tamponade complete the range of the blood

flow velocity alterations of cerebroafferent vessels in time and for different grades of increase in the cerebrovascular impedance. We wish also to discuss the problem of where the Doppler signal reading should be taken from. We believe that the most reliable signals are those taken from the ICA. However, because of lack of space, it is impossible to record signals from the ICA of the rat. They were all therefore taken from the CCA. With regard to this, we should discuss the role the ECA and its clamping play in the development of the phenomena we reported and on the measures we effected.

According to the results obtained in model 1, it could be presumed that the clamping of the JV alone is unable to create an alteration of the cerebrovascular impedance or is insufficient to produce appreciable variations in the flow velocity values above the point where recording is made. From the information obtained by model 2, it could be assumed that the significant flow velocity alterations obtained on the CCA can only be linked to the occlusion of the ipsilateral ECA (Figs. 1-2). In fact, even the clamping of only the ipsilateral ECA where the signals are taken (model 4) determines an alteration in the systolic and diastolic values similar to the one obtained in the model with JV and ECA clamping.

But the clamping of the ECA alone does not give statistically significant results (Figs. 5-6). We therefore interpret them in view of what was observed in model 1. In those cases no univocal result was given to the occlusion of JV alone, whereas in model 2 the clamping of ECA (able to create an impedance increase in the CCA territory, though with non-significant flow velocity values) made more notable both systolic and diastolic flow velocity alterations observed on the ipsilateral CCA.

It can therefore be concluded that significant alterations of the cerebrovascular impedance can be obtained with the clamping of JV alone, but that these alterations can be recorded on the CCA only, if ECA territory is closed, whereby eliminating the risk of run-off across it or if, as pointed out by other authors [1-2, 12, 16], readings are taken from the ICA.

6. Conclusions

From our experiment we have been able to obtain the following information about the reliability of ultrasound Doppler examination in cases of increased cerebrovascular impedance:

1) With the Doppler examination of the cerebroafferent blood flow rate carried out on the ICA or on the CCA with the exclusion of the ipsilateral ECA, significant systolic and diastolic alteration values can be recorded.

2) The diastolic values are highly significant, due to their notably persistent decrease observed from the moment the impedance alteration started and up to 10 hours.

3) The systolic values only decreased notably during the first 15-30 min.

from the impedance increase start. During the interval between 1 hour and 10 hours from the beginning of the experiment the values rose significantly.

4) Remarkable evidence of altered impedance can be obtained within the first hour only if the basic or normal data are known. Only the progressive separating of the systolic values from the diastolic ones during the following hours could let us know without doubt, possibly by employing pulsation indexes, of the existence of an abnormal increase in the impedance.

References

[1] M. G. Beasley, J. N. Blau, R. G. Gosling, *Changes in internal carotid artery flow velocity with cerebral vasodilation and constriction,* Stroke, **10**, 3, 331-335 (1979).

[2] A. Bes, A. Guell, L. Braak, M. Farah, M. Barrere, *Influence de l'age sur quelques paramètres du signal Doppler au niveau du système carotidien,* Rev. EEG. Neurophysiol., **10**, 2, 190-196 (1980).

[3] J. Cuypers, F. Matakas, S. J. Potolicchio, *Effect of central venous pressure on brain tissue pressure and brain volume,* J. Neurosurg., **45**, 89-94 (1976).

[4] C. Franceschi, *Investigation vasculaire par ultrasonographie Doppler,* Masson, Paris 1977, 28-32.

[5] R. G. Gosling, G. Dunbar, D. H. King, D. L. Newman, C. D. Side, J. P. Woodcock, D. E. Fitzgerald, J. S. Keates, D. MacMillan, *The quantitative analysis of occlusive peripheral arterial disease by a nonintrusive ultrasonic technique,* Angiology, **10**, 52-55 (1971).

[6] A. Guell, L. Braak, M. Barrere, Ph. Jauzac, A. Bes, *Correlation between, C.B.T. modifications and variations in the blood velocity as measured by Doppler sonography,* Proc. 9th International Conference, 1978, J.S. Meyer, H. Leachner, R. Reivich (eds.), Excerpta Medica, 93-98.

[7] E. J. Jonkman, P. C. M. Mosmans, *Doppler haematotachography: Problems in interpretation and new applications,* Clin. Neurol. Neurosurg., **80**, 33-45 (1977).

[8] E. J. Jonkman, J. T. J. Tans, P. C. M. Mosmans, *Doppler flow velocity measurements in patients with intracranial hypertension,* J. Neurol., **218**, 157-169 (1978).

[9] K. F. Lindegaard, A. Grip, H. Nornes, *Precerebral haemodynamics in brain tamponade. Part 2; Experimental studies,* Neurochirurgia, **23**, 187-196 (1980).

[10] Th. Planiol, L. Pourcelot, J. M. Pottier, E. Degiovanni, *Etude de la circulation carotidienne par les méthodes ultrasoniques et la thermographie,* Rev. Neurol., **126**, 127-141 (1972).

[11] L. Pourcelot, *Un nouveau debimètre sanguin à effet Doppler,* Ultra-Sonographie Medica, Verlag der Wiener Medizinischen Akademic, Vienna 1971, **1**, 125-130.

[12] J. Risberg, P. Smith, *Prediction of hemispheric blood flow from carotid velocity measurements,* Stroke, **11**, 399-402 (1980).

[13] H. C. Schoonderwaldt, E. Colon, O. R. Hommes, *Changes in carotid flow velocity induced by lowering cerebrospinal fluid pressure in normal pressure hydrocephalus,* Proc. 3rd Europ. Congress on Ultrasonics in Medicine, Bologna, 1978, Minerva Medica, 521-522.

[14] H. J. Steiger, *Carotid Doppler haemodynamics in post-traumatic intracranial hypertension,* Surg. Neurol., **16**, 459-461 (1981).

[15] S. Vogel, G. Pardemann, S. Magnus, *Ultrasound Doppler evaluation of cerebral vessels in newborns and children with disturbances of intracranial pressure,* Proc. 3rd Europ. Congress on Ultrasonics in Medicine, Bologna, 1978, Minerva Medica, 519-520.

[16] S. Yoneda, A. Nishimoto, T. Nukada, Y. Kuriyama, K. Katsurada, H. Abe, *To-and-fro movement and external escape of carotid arterial blood in brain death case. A Doppler ultrasonic study,* Stroke, **5**, 707-713 (1974).

ARCHIVES OF ACOUSTICS
9, 1-2, 175-180 (1984)

RESULTS OF DOPPLER INVESTIGATION OF BLOOD FLOW VELOCITY IN REDUCED INFLOW OR INCREASED RESISTANCE IN THE BRACHIAL ARTERY

A. CHROŚCICKI

Pediatric Institute, Medical Academy, Warsaw, Poland

W. SECOMSKI

Institute of Fundamental Technological Research, Polish Academy of Sciences, Warsaw

Recordings of the blood velocity in the brachial artery were made in healthy persons by means of Doppler ultrasound, ECG and phonocardiography methods. The blood inflow to the brachial artery was reduced at first by a mechanical occluding of the axillary artery, simulating conditions similar to the aortic stenosis, low cardiac output and obstructive cardiomyopathy. In the second stage, peripheral resistance was increased by compression of the forearm, clenching fist or elevation of the upper extremity. In the last stage, respiration influence of arterial and venous flows was evaluated.

Two hundred recordings of the blood velocity in the brachial artery were made in healthy persons during the past fourteen months by means of Doppler ultrasound, ECG and phonocardiography methods. Blood flow measurements were made with a 7.5 MHz *C.W.* Doppler flowmeter applying a specially designed flat probe (20 mm diameter, 5 mm thickness). After receiving an optimal signal from the brachial artery without the vein disturbances, the probe was fixed to the skin with adhesive tape.

The blood inflow to the brachial artery was reduced by mechanical compression produced by the pressure cuff positioned on the arm above the ultrasonic transducer. The cuff was automatically inflated to the required pressure (0-27 kPa or 0-200 mm Hg) in 1-30 s time period and released afterwards. Fig. 1 shows the blood velocity changes in the brachial artery during 8 s occlusion. The flow decreases towards a zero level and returns to normal immediately (less than 1 second) after release.

In the second set of experiments, peripheral resistance was increased by the compression of the forearm, clenching the fist or by the elevation of the arm. Fig. 2 shows influence of the fist clenching on the blood flow in the brachial artery. Amplitude of the systolic flow was practically constant and reversed diastolic component was observed. After release high amplitude of the diastolic flow was recorded during about 10 s or longer. Fig. 3 shows the blood flow during

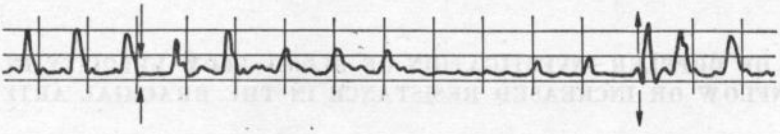

Fig. 1. Inflow reduced by mechanical occlusion

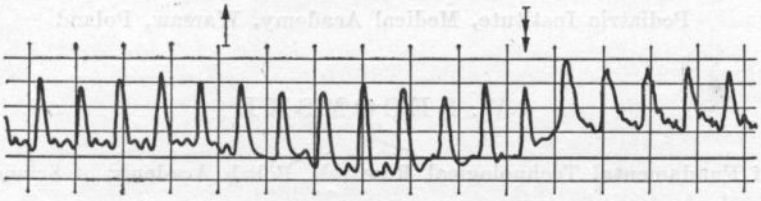

Fig. 2. Influence of the fist clenching on the blood inflow

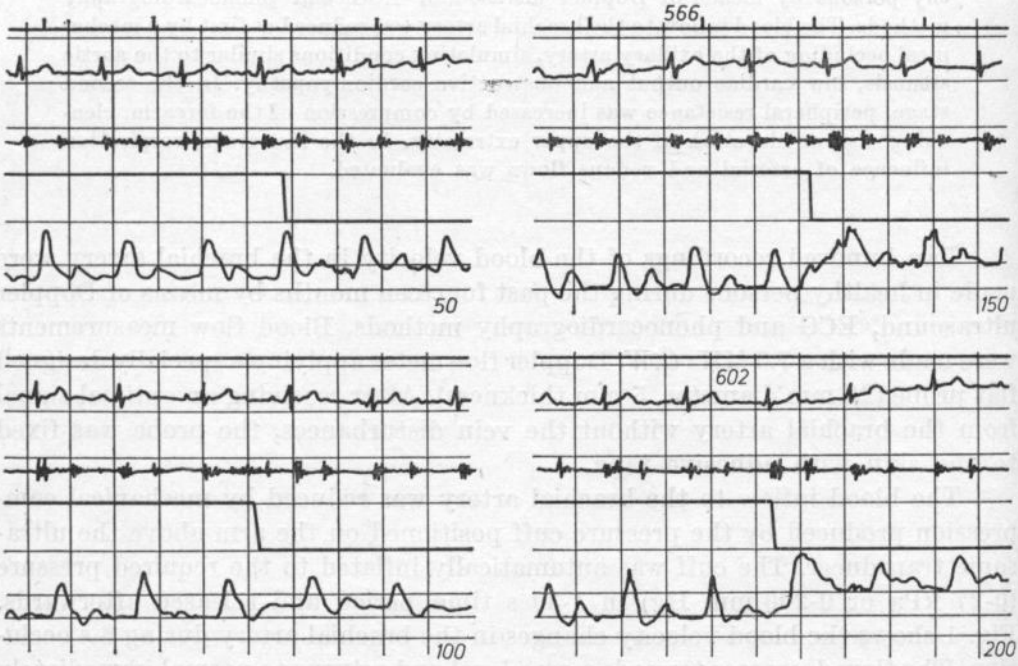

Fig. 3. Increase in the resistance by controlled compression

the controlled compression of the forearm (50, 100, 150, 200 mm Hg) and after release. Notice the increase of the reverse flow in early diastole, changes in the shapes of the flow curve and increased flow after release.

In the last experiment, the influence of the normal respiration on the arterial flow was evaluated. The increase in the diastolic component during aspiration, simulated by changes of the left atrium filling, could be seen. The Valsalva manoeuvre changes the heart rate and the flow shape was dificult to compare with the normal pattern.

1. Results

The reduction of the inflow caused disappearance of the diastolic flow, progressive decrease of the systolic component towards a zero level and a nearly linear increase in the conduction time in a similar way to sphygmographic investigations (Fig. 4*b*, Fig. 5).

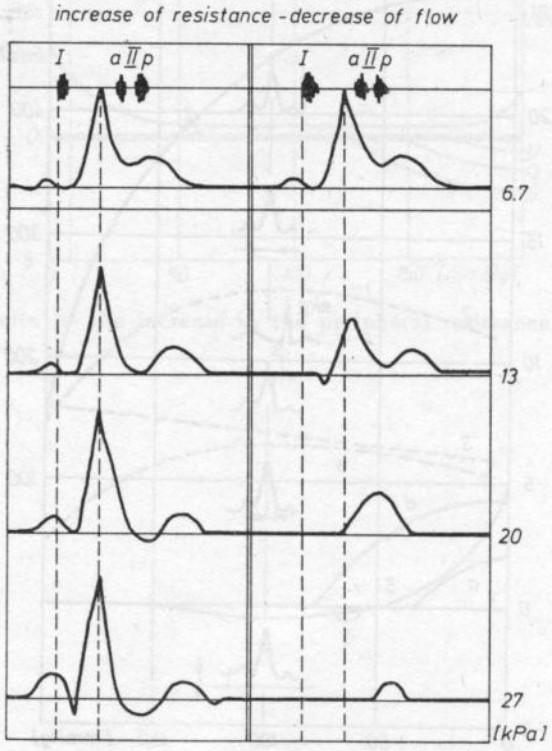

Fig. 4. *a.* (left) Increase in the resistance. *b.* (right) Decrease in the inflow

The increase in the peripheral resistance produced an instantaneous disappearance of the diastolic flow, a reduction of the systolic component duration and short-lived reverse blood flow, immediately after systole (Fig. 4*a*, Fig. 6).

2. Conclusions

The investigations were limited to qualitative measurements rather than quantitative ones. They proved, however, important practical usefulness of the tests performed. Reduced inflow to the brachial artery was effected to simulate conditions similar to the aortic stenosis, low cardiac output and obstructive cardiomyopathy.

This method of investigation should be useful in the functional screening tests of the sick and healthy persons.

Respiration tests showed an influence on the venous flow, but recordings were not repeatable and therefore difficult to study.

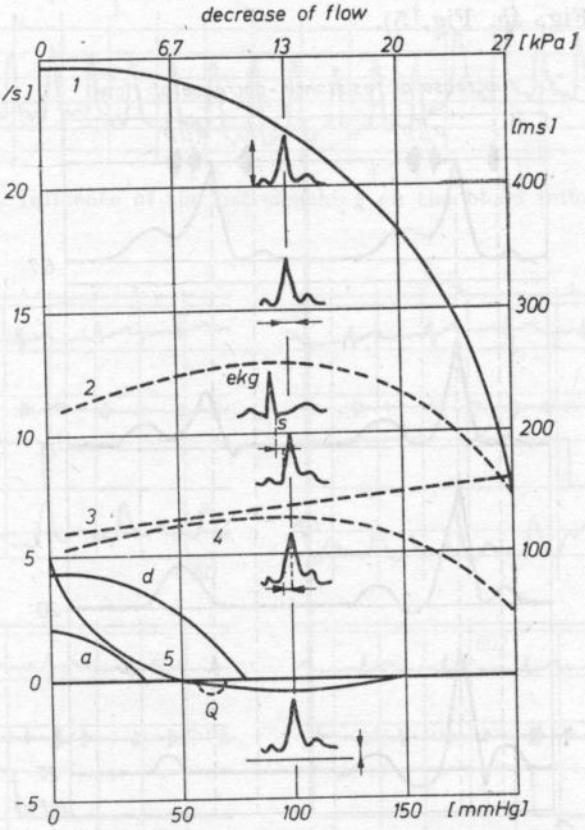

Fig. 5. Results — the reduction of the inflow. *1* — maximum systolic velocity (cm/s), *2* — systolic flow duration (ms), *3* — conduction time (ms) — time interval between the S wave of ECG and the beginning of the systolic flow, *4* — systolic flow acceleration time (ms), *5* — diastolic flow velocity (cm/s), *a*, *d*, *Q*, *S*, *U* — additional waves in the diastolic component (cm/s)

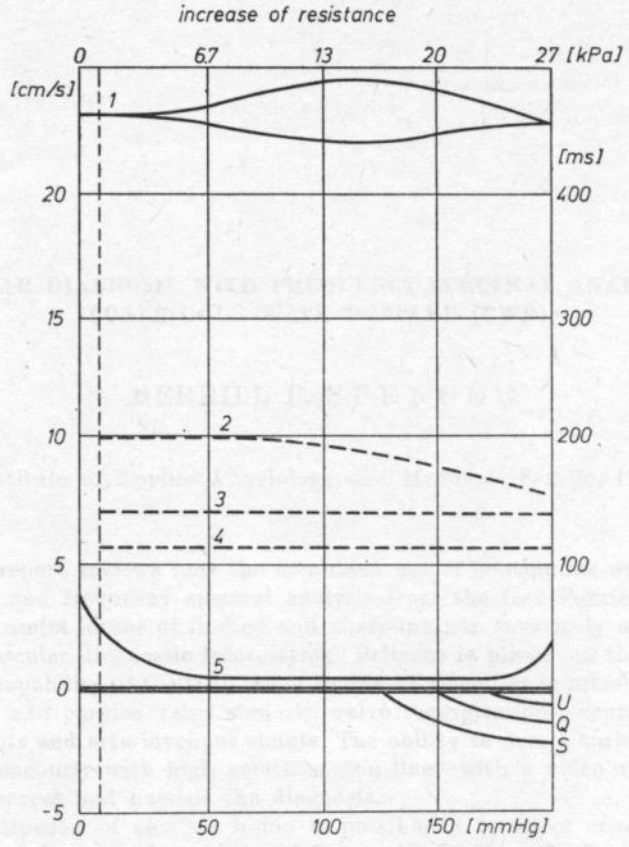

Fig. 6. Results — the increase in the peripheral resistance (see Fig. 5)

ARCHIVES OF ACOUSTICS
9, 1-2, 181-190 (1984)

CARDIOVASCULAR DIAGNOSIS WITH FREQUENCY SPECTRAL ANALYSIS (FSA) AND CONTINUOUS WAVE DOPPLER (CWD)

MERRILL P. SPENCER

Institute of Applied Physiology and Medicine, Seattle, USA

This report reviews how the combined use of continuous wave Doppler ultrasound and frequency spectral analysis from the fast Fourier transform provides a useful means of finding and analysing non invasively a wide range of cardiovascular diagnostic information. Reliance is placed on the frequency resolution capability of CWD to follow increased velocities in arteries produced by arterial and cardiac value stenosis, valve regurgitations, congenital heart septal defects and arteriovenous shunts. The ability to detect turbulence energies simultaneously with high velocities "on line" with a video reproducable format improves and hastens the diagnosis.

Quantitation of stenotic lesion is possible in terms of effective lumen diameter and pressure drop produced by the blood flow. Cardiac output and changes in stroke volume can also be computed.

As Doppler ultrasonic equipment and examination techniques improve the range of Doppler detectable features of the circulatory system is expanding. The frequencies generated by the Doppler effect represent the velocity of blood streams in the heart, arteries and veins as well as motions of the cardiovascular structures. Blood velocity features from which diagnoses of abnormalities can be concluded include flow direction, acceleration, pulsatile waveform, as well as spectrum and spatial distribution of the flow streams. Ultrasonic frequencies from 2 to 10 MHz penetrate the body well and generate frequencies conveniently falling in the audible range allowing the use of the human hearing system as an analytical tool. This arrangement, when used with an understanding of hemodynamics, makes a remarkably cost-effective method for diagnosis of many cardiovascular disorders.

We have exploited the unlimited frequency resolution of CWD where the spatial resolution of pulsed wave Doppler (PWD) was not needed in disease diagnosis and quantitation. PWD is helpful where depth resolution is really

important but works best with 2 dimensional echography and it thus becomes less cost effective. CWD often provides more clear signals, safer power levels and easier location of diagnostic signals.

For documentation and study analogue tracings of selected components from the full spectrum of sounds generated has been widely used on available polygraphs to follow estimations of mean or maximum frequencies. These features, however, can be distorted by high energies produced by disease in the low frequency ranges. Though high pass filtering can eliminate these disturbances much information in the complete spectrum is lost from future analysis. The use of FSA from the fast Fourier transform (FFT) in video format [1] displays a much greater range of Doppler information than an analogue tracing assisting at the time of the patient examination and in future analysis [2]. The directional A and B quadrature signals of the Doppler equipment in the FFT analyses provides the equivalent of 256 band pass filters with a 10 ms updating time. The energies produced in each frequency band are color coded on a thermal scale with white representing the highest energies, red used for the lowest and with oranges and yellows representing the middle ranges. Black and white prints thus provide a gray scale with highest energies being darker. The maximum edge of the spectrum (f_{max}) has the same clinical usefulness desired of the analogue tracings to follow pulsatile contours, while preserving the lower frequency information representing velocity distributions within the vessel.

Normal laminar flow profiles in the internal and external carotid arteries are shown in Figs. 1 and 2. The differences in f_{max} contours are characteristic of the internal and external carotids. Higher diastolic f_{max} contours, when compared with the systolic peak f_{max}, reflects lower peripheral resistance in the brain than in the external carotid.

Fig. 3 illustrates the ability of FSA to simultaneously follow the pulse contours of f_{max} and display severe turbulence phenomena. The high velocity jet emerging from the stenotic arteries, represented by the high frequency (8 KHz) Doppler signals, produces lateral excursions in flow both towards and away from the probe resulting in high energy low frequency signals on either side of the zero reference. The analogue tracings of the zero crossing meter output are biased toward the lower frequencies and cannot follow the mean frequency in this situation. FSA can assist CWD to increase spatial resolution by displaying the superimposed spectra of two arteries lying in the ultrasonic beam (Fig. 4). The use of the CWD imaging technique [3, 4] also assists in specifying which branch at a bifurcatian is stenotic and which is nornal. CWD imaging of the carotid bifurcation is achieved by holding the probe in a mechanical arm fixing the angle of the ultrasound beam at 60° with the body axis. If the same angle is assumed for an artery running parallel to the body axis the frequency spectrum can be calibrated in m/s. For 5 MHz, in the case of Fig. 4, one kHz is equivalent to 0.3 m/s.

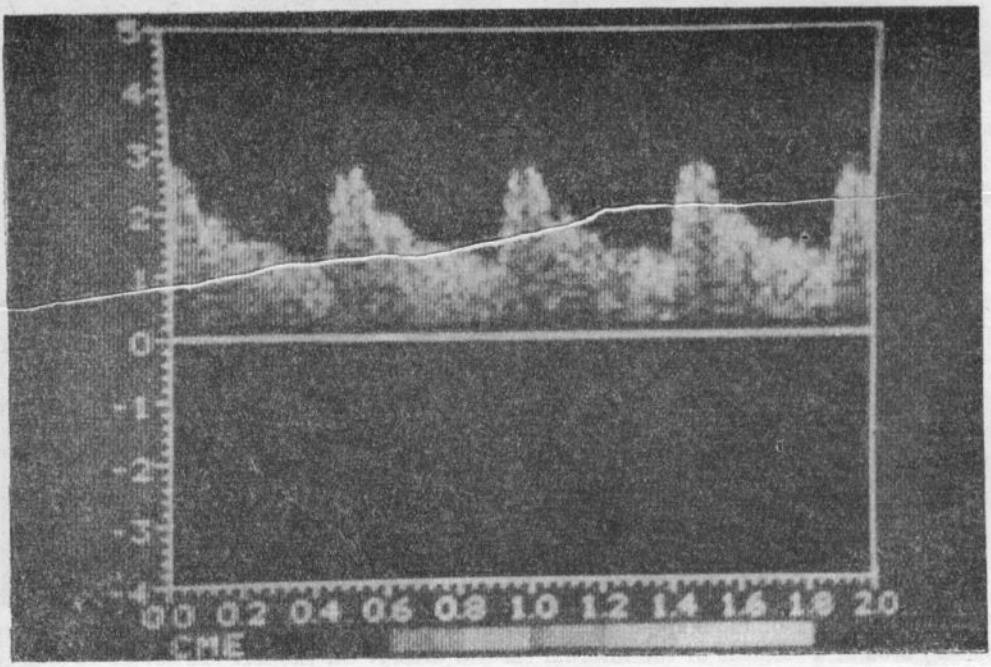

Fig. 1. FSA of Doppler frequencies detected in the normal internal carotid artery. The abcissa presents a 2 second sweep. The ordinate is calibrated in kHz with velocities away from the transducer represented above the zero line. Laminar flow with a blunt profile can be concluded from this display because of the concentration of energies near the upper edge of the spectrum (f_{max}). The high diastole and downsloping contours of f_{max} is characteristic of blood flow in arteries perfusing the brain

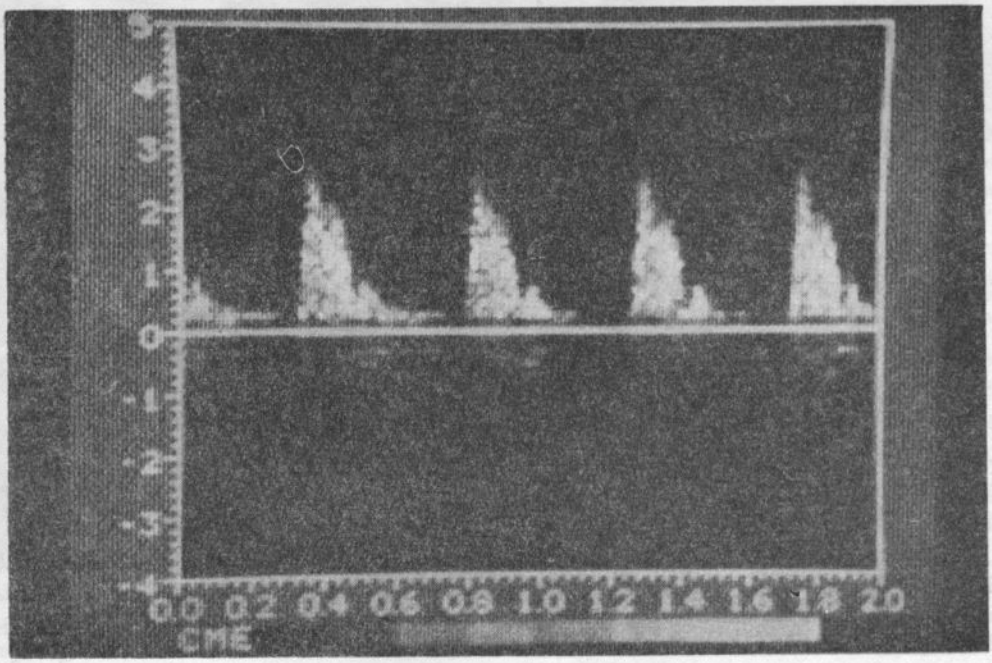

Fig. 2. FSA of Doppler signals in the normal external carotid artery. The probe beam angle is approximately 45° with the vessel as in Fig. 1. The frequency energies are rather evenly distributed across the spectrum indicating a more parabolic flow profile. The waveform is typical of the external carotid with lower diastolic velocities represented

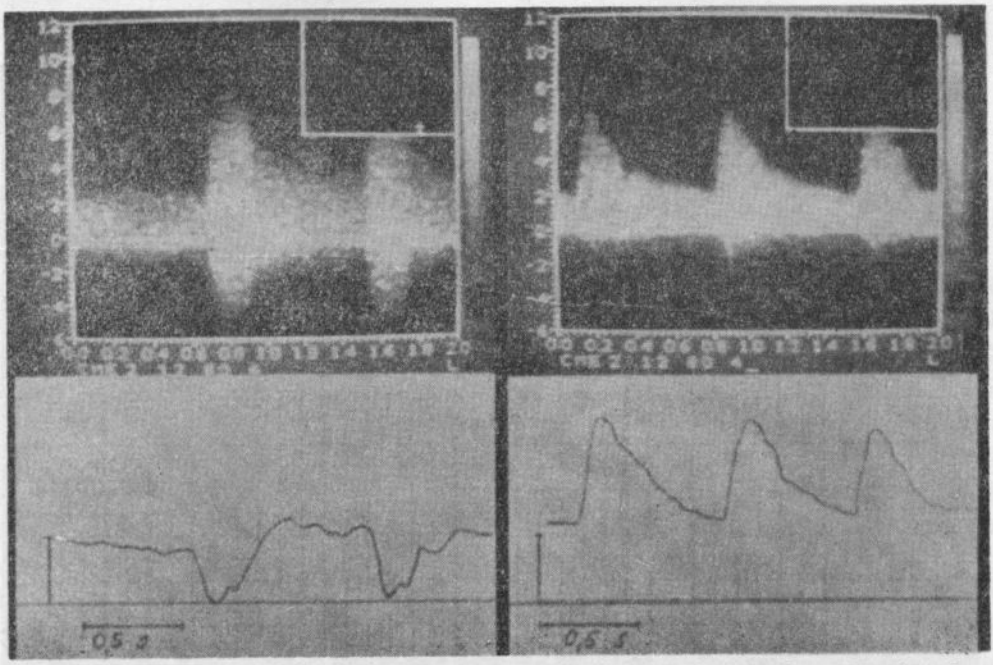

Fig. 3. Comparison of FSA (upper panels) with zero crossing meter analogue tracing (lower panels) around a stenosis of the internal carotid artery. On the left the severe turbulence produces strong dual directional energies in the lowest frequency ranges displayed on both sides of the zero reference causing the zero crossing output to decrease when, in fact, the maximum velocity is increasing. On the right where turbulences are not as strong the meter can follow the increased velocities

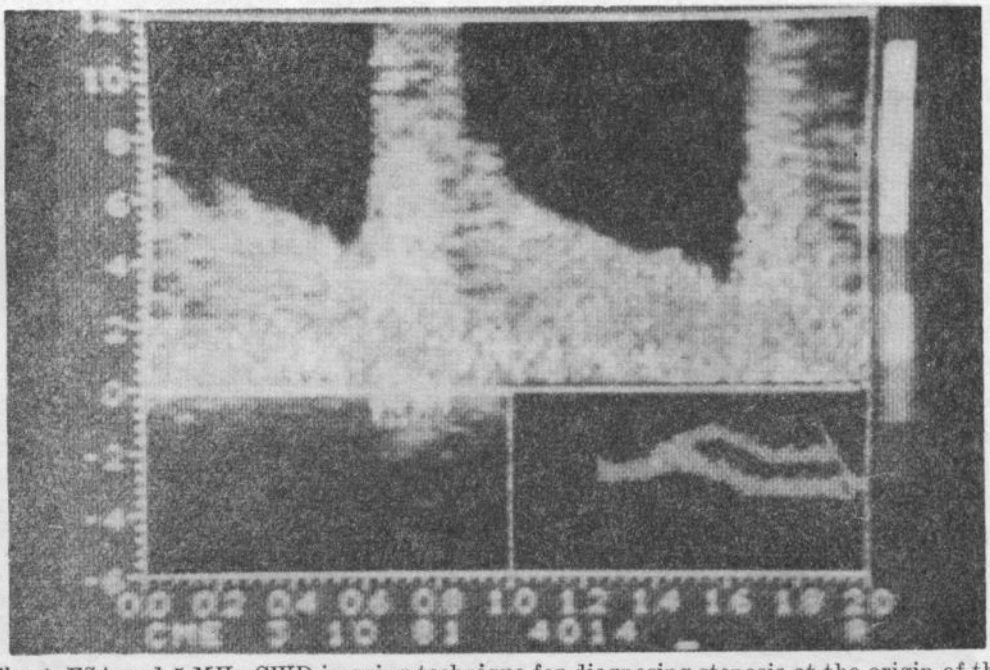

Fig. 4. FSA and 5 MHz CWD imaging technique for diagnosing stenosis at the origin of the internal carotid artery at its origin from the common carotid. A CWD image of the carotid bifurcation is seen in the lower right corner of the figure. The bright spot on the image represents the source of the spectrum displayed. The high frequency contour (> 12 kHz at peak systole), with a typical internal carotid contour, indicates stenosis of this artery while the superimposed external carotid spectrum, with only slightly elevated frequencies represents collateral flow velocities. Turbulence, associated with stenosis, is represented by the high systolic energies on both sides of the zero line

The maximum CWD frequency sound within a stenotic segment of the internal carotid artery can be used to estimate the degree of stenosis in terms of both stenosis diameter [5] (equivalent cross-sectional area) and the pressure drop produced [6] by the stenosis. Fig. 5 illustrates the relationship between peak systolic frequency and minimum diameter found in arteriographic examinations. The ability of CWD with FSA to predict the arteriographic diameter of the carotid is very good in the middle velocity range from 1.5 to 3.5 m/s.

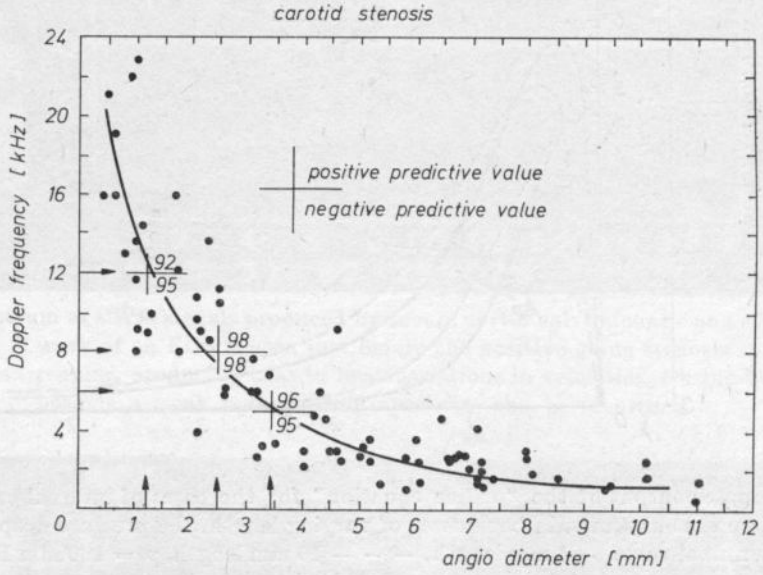

Fig. 5. Relationship found by clinical experience between the CWD peak systolic f_{max} and the angiographically determined diameter of 108 internal carotid arteries. One or both sides were stenotic. The predictive values are for accuracy limits set at ± 0.7 mm and ± 1 kHz (the limits of accuracy for both angiography and Doppler)

Mathematical modelling of the "orifice equation" is helpful in understanding the hemodynamics of stenosis. The total pressure drop (Δp) produced by a stenosis can be calculated by combining the three principle terms of Bernoulli, boundary effects, and Poiseuille [7]. Fig. 6 provides a computer solution output to such an equation for two cases of stenosis length showing how velocities v increase with increasing degrees of stenosis, as in the clinical data of Fig. 5, until the stenosis radius is less than 0.5 mm where velocities are diminishing to zero. Though the relationship between radius and both Δp and v is affected by stenosis length, the relationship between Δp and v is constant. For example, at a velocity of 4 m/s, in both cases, Δp reaches 1/2 of its terminal value. Also for all cases > 0.5 mm, where turbulence is quite apparent:

$$\Delta p\,[\text{mm Hg}] = 4v^2\,[\text{m/s}].$$

This simple relationship between Δp and v has been shown to hold for stenosis of heart valves and probably is correct for carotid artery stenosis. CWD combined with FSA provides a good method of applying these principles to compute an important hemodynamic parameter.

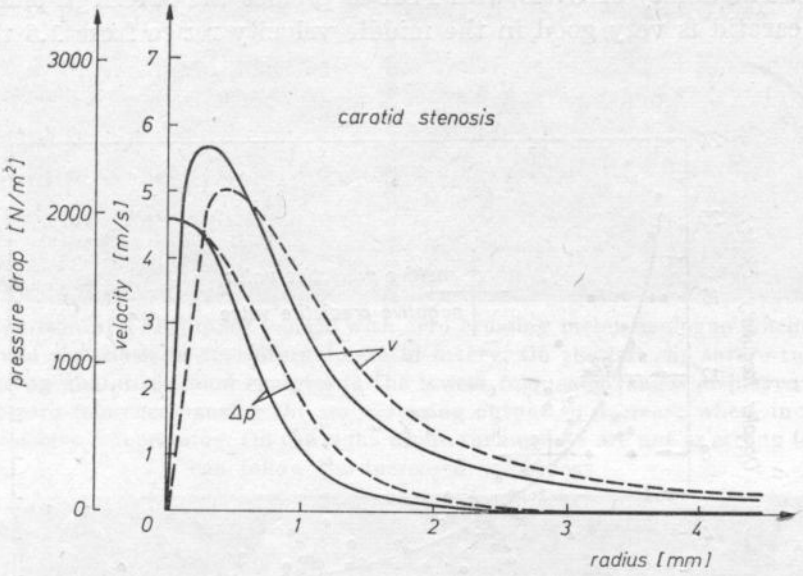

Fig. 6. Computer output of the "orifice equation" for the cases of internal carotid artery stenosis. Note that at 4 m/s, in both cases of varying length, the pressure drop reaches one half of its terminal value. — 1 mm length, — — — 10 mm length, p = 160 mm Hg, R_p = 0.3 mm Hg/ml/min

Cardiac diagnoses, with combined CWD and FSA, include stenosis and regurgitation of the valves, congenital septal defects as well as aortic coarctation and patent ductus arteriosus [8]. The diagnosis is made from the contour and timing of f_{max} which is increased above normal to follow elevated blood velocities through these orifices. Strong cardiac motion signals and severe turbulence energies must be attenuated by means of a high pass filter. A few examples of CWD spectra that occur in aquired valve lessions will illustrate the usefulness of the technique. Fig. 7 demonstrates the high velocity signals of aortic valve stenosis in a patient when directing a 2.5 MHz CW ultrasound beam from the precordium apical region. Since this probe position produced the highest Doppler frequencies we can assume the beam was to be in line with the jet stream allowing the ordinate to be transposed to m/s. The pressure drop accross the stenotic orifice can the be calculated from the equation previously given.

CWD with FSA is especially sensitive to valve regurgitations and probably is more sensitive than standard contrast cineangiography. Slight aortic

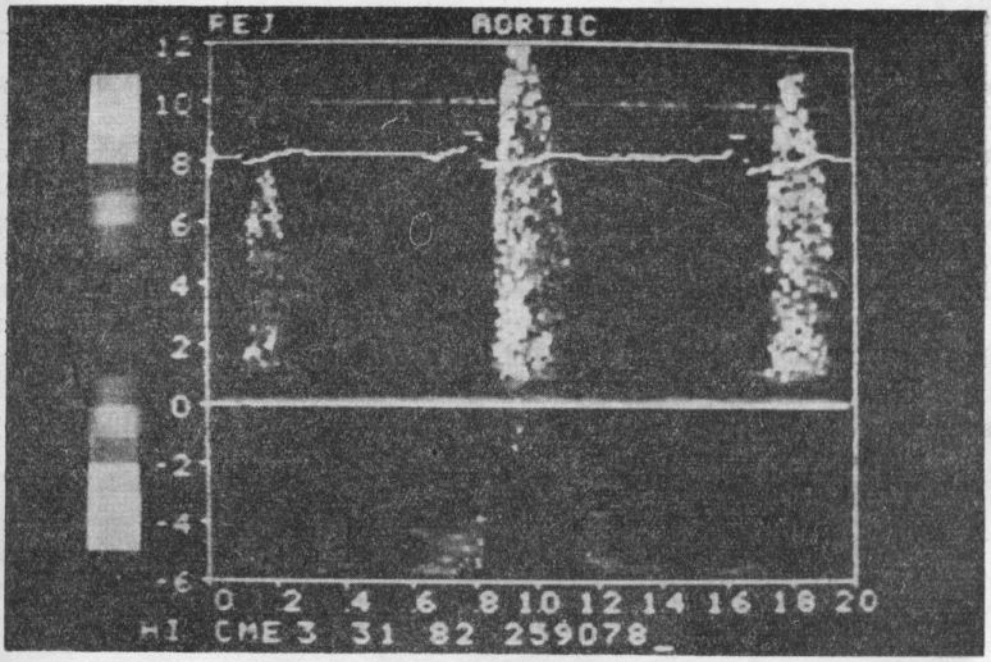

Fig. 7. Spectrum of CWD signals produced by severe aortic valve stenosis and slight regurgitation. The *R* wave of an ECG is seen just before the positive going stenosis spectrum. The heart rate is irregular, producing beat to beat variations in velocities. During both diastolic periods a weak regurgitation spectrum can be identified

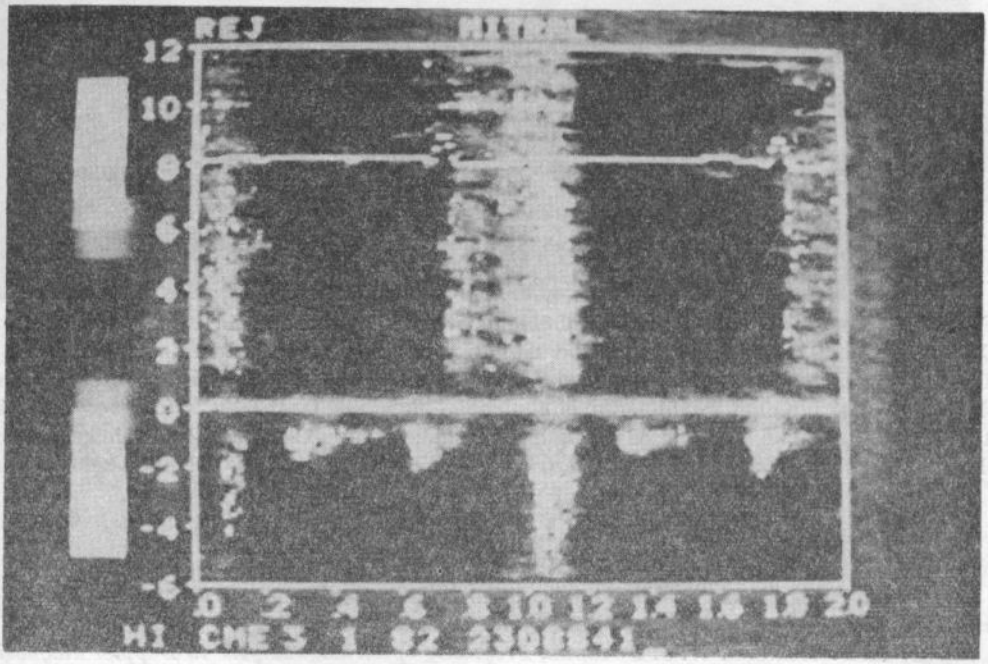

Fig. 8. Mitral valve prolapse regurgitation spectrum of CWD. Note accentuation of jet in late systole with dual directional turbulence represented

regurgitation is represented in Fig. 7 by the spectrum seen below the zero line during diastole. Fig. 8 illustrates the regurgitant signals of mitral valve prolapse where accentuation of the lower ranges of the spectrum occurs in late systole. The leak becomes large enough to produce strong turbulence signals displayed both above to below the zero line. Normal mitral inflow signals are seen during diastole below the zero line indicating no stenosis of the valve is present and also the leak is not severe enough to noticably increase inflow velocities.

Changes in stroke volume of the left ventricle can also be followed from the systolic velocity contours found in the ascending aorta and stroke volume and cardiac output may be calculated when the diameter of the ascending aorta is known from echocardiographic angiographically recorded sources [9] (Fig. 9).

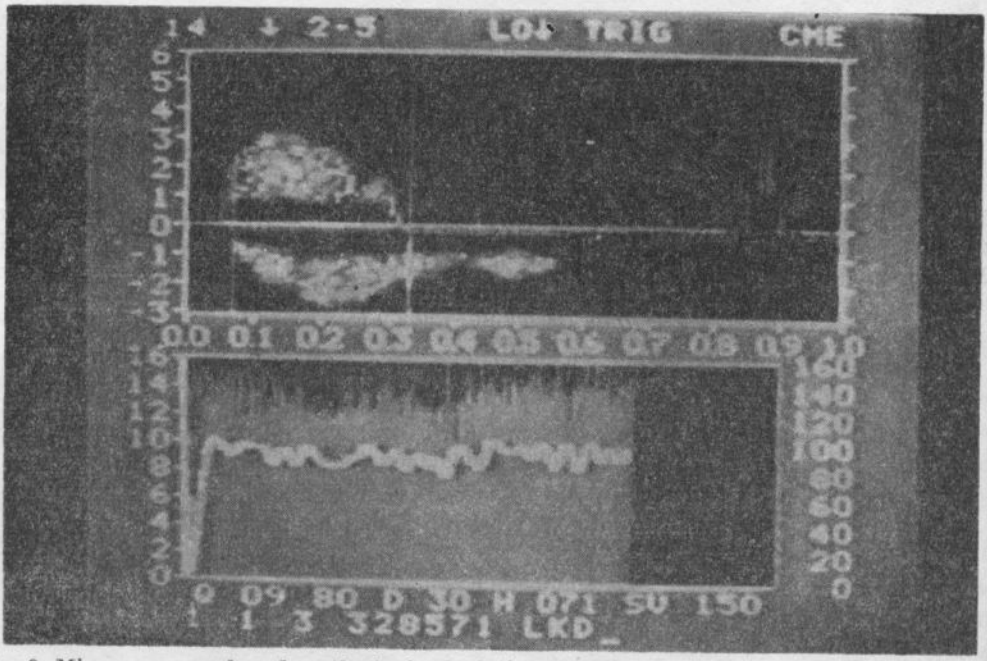

Fig. 9. Microprocessor based method of calculating stroke volume and cardiac output from CWD spectra of velocities found in the ascending aorta of a normal subject. The probe is directed from the suprasternal notch and only the spectrum of velocities directed towards the probe (positive ones in this case) is analysed. The mean frequency is followed near the upper edge, f_{max}. The diameter of the ascending aorta is set in each case. In the lower section the trend of the cardiac output from heart rate and stroke volume is followed beat to beat

References

[1] M. P. Spencer, R. E. Hileman, *Cardiac diagnosis with directional CW Doppler and FFT color video spectral display*, J. Ultra. Med, **1**, 117 (1982).

[2] M. P. Spencer, W. J. Zwiebel, *Frequency spectrum analysis in Doppler diagnosis*, chapter 8, in: *Introduction to vascular ultrasonography*, W. J. Zwiebel (ed.), Grune Stratton, New York 1982.

[3] M. P. SPENCER, J. M. REID, *Cerebrovascular evaluation with Doppler ultrasound,* Martinus Nijhoff, The Hague-Boston-London, 1981.

[4] M. P. SPENCER, J. M. REID, D. L. DAVIS, P. S. PAULSON, *Cervical carotid imaging with a continuous wave Doppler flowmeter,* Stroke, **5**, 145-154 (1974).

[5] M. P. SPENCER, J. M. REID, *Quantitation of carotid stenosis with continuous wave (C-W) Doppler ultrasound,* Stroke, **10**, 326-330 (1979).

[6] J. HOLEN, R. AASLID, K. LANDMARK, S. SIMONSEN, *Determination of pressure gradient in mitral stenosis with a non-invasive ultrasound Doppler technique,* Acta Med. Scand., **199**, 455 (1976).

[7] M. P. SPENCER, T. ARTS, *Hemodynamic principles for cardiac Doppler diagnosis,* chapter 14, in: *Cardiac Doppler diagnosis,* M. P. SPENCER (ed.), Martinus Nijhoff, The Hague, 1983.

[8] L. HATLE, B. ANGELSEN, *Doppler ultrasound in cardiology. Physical principles and clinical applications,* Lea and Febiger, 1982.

[9] L. L. HUNTSMAN, E. GAMS, C. C. JOHNSON, E. FAIRBANKS, *Transcutaneous determination as aortic blood flow velocities in man,* Am. Heart J., **89**, 609 (1975).

ARCHIVES OF ACOUSTICS
9, 1-2, 191-198 (1984)

ESTIMATION OF THE COLLATERAL CIRCULATION INDEX (CCI) IN THE LOWER EXTREMITIES USING THE IMPEDANCE RHEOGRAPHY AND ULTRASONIC METHODS

JERZY WESOŁOWSKI, ANDRZEJ NOWICKI,
BARBARA TOPOLSKA, GRZEGORZ PAWLICKI,
TADEUSZ PAŁKO, LESZEK FILIPCZYŃSKI,
HENRYK RYKOWSKI

Clinic of Vessel Surgery, Medical Center of Postgraduate Education
Department of Ultrasound, Institute of Fundamental Technological Research, Polish Academy of Sciences
Institute of Precision and Biomedical Engineering, Technical University of Warsaw, Warsaw, Poland

In this study values of volumetric blood flow in the thigh, measured using the impedance rheography, were compared with values of volumetric flow in the common femoral artery, measured using the ultrasonic method. We examinated 32 healthy and 46 sick people with occlusion of the pelvic limb arteries. More than 120 measurements were made on these subjects. We ascertained diagnostic usefulness of both methods to simultaneous measurement of blood flow in the peripheral vessels. It seems that association of both of the methods — rheographic and ultrasonic — permits the collateral blood flow to be calculated.

1. Introduction

One of the more significant hemodynamic parameters is the volumetric flow which permits quantitative evaluation of blood supply in the area of tissue investigated. Studies concerning quantitative determination of the volumetric flow have not so far been carried out to a large extent in clinical practice because of lack of an appropriate measuring method. Methods known for a long time and applied in physiological investigations are not adequate for routine measurements. Only the introduction of the ultrasonic and impedance methods makes possible quantitative appreciation of this important parameter. Both methods are non-invasive, harmless, painless for pa-

tients. Besides that, their common feature is the use of the passive properties of organism: in the case of impedance rheography this is change of impedance for highly alternating current in the area of tissue examined, caused by a pulsating wave of blood [1]. In the case of the ultrasonic technique there is the interaction of the ultrasonic wave with moving blood cells [3]. The purpose of this work is a comparison between the volumetric intensity of a thigh blood flow (determined by the rheographic method) and the volumetric intensity of blood flow in the main vessel supplying the pelvic limb — the femoral common artery (determined by the ultrasonic method).

2. Methods

Rheographic investigation consists in measuring and recording changes of electric impedance of tissue and the rate of these changes i.e. the first derivative. The volumetric blood flow (in relation to the segment investigated) can be qualified using this method on the basis of KUBICEK's formula as follows:

$$Q_R = \varrho \frac{L^2}{(Z_0)^2} \frac{dZ}{dt_{\max}} \times T \times HR \quad [\text{ml/min}], \tag{1}$$

where ϱ — resistance of blood, L — distance between the measuring electrodes, Z — impedance, $dz/dt_{\max}$ — amplitude of the first derivative of impedance changes, T — duration of blood flow, HR — heart rate.

In the pulse Doppler ultrasonic technique used in the hemodynamic investigations both echo and Doppler's phenomena are combined. These phenomena appear in the interaction of ultrasonic wave with moving blood cells [3, 4].

Adoption of the ultrasonic pulse technique and the triangulation head permit the measurement of the diameter of a vessel and a distribution of velocities in the cross-section of the vessel. The volumetric flow in the vessel examined was calculated according to the following formula [8]

$$Q_U = 0.67 \times V_{\text{av max}} \times \pi \times \frac{d^2}{4} \times 60 \quad [\text{ml/min}], \tag{2}$$

where d — diameter of the vessel, $V_{\text{av max}}$ — mean flow velocity in the center of the vessel.

Patients were examined in the supine position and then the ECG and rheographic electrodes for limb off take were fixed. Previously the electrodes were moistened or covered with special electrode-paste. For the rheographic investigations the applique and striped receiving electrodes (made of aluminium-foil and equipped with special fixing snaps) were used.

The distance L for the receiving electrodes was on the average 10 cm.

The ultrasonic investigations were carried out using a special ultrasonic triangulation head which was applied on the skin over the common femoral artery. The position of the electrodes and the head is shown in Fig. 1.

Signals from both units were simultaneously recorded on a three-channel recorder: the instantaneous flow velocity in the common femoral artery, ECG and the first derivative — from changes in impedance in the tissue examined.

On the basis of the curves recorded and using the formulae given above (eg. (1), (2)), the parameters Q_R and Q_U were calculated.

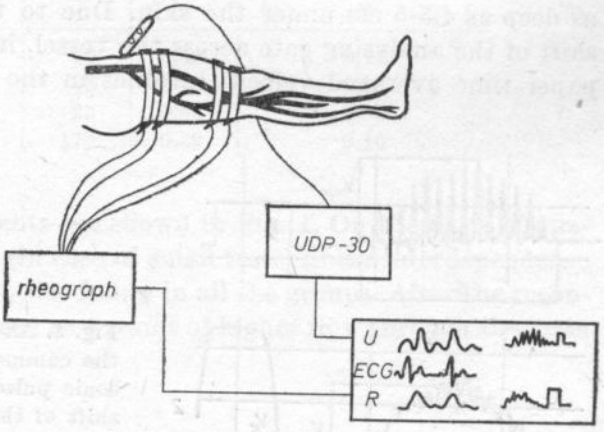

Fig. 1. Means of investigation of blood flow in the thigh using the rheographic and ultrasonic methods. U — velocity of blood flow in the common femoral artery (UDP-30), R — derivative of changes of impedance (rheograph)

3. Materials

In the rheographic investigations a two-channel impedance rheograph RJ — 2k (working in a four-electrode electric system) was used. This rheograph was developed at the Institute of Precision and Biomedical Engineering, Technical University, Warsaw, Poland. The device has a generator of rectangular

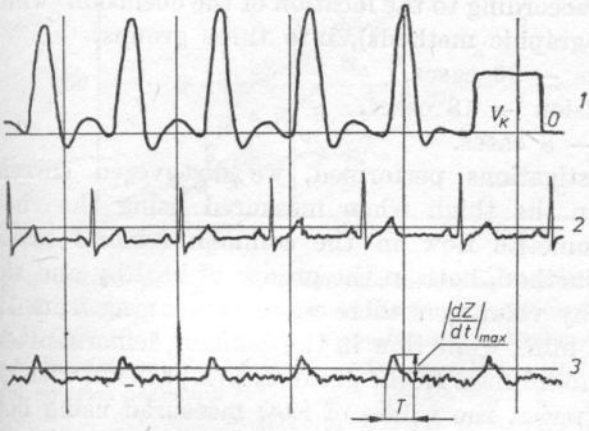

Fig. 2. An example of blood flow recording from the healthy common femoral artery. *1* — instantaneous velocity of the blood flow in the center of the vessel (UDP-30), *2* — ECG, *3* — velocity of changes of impedance in the segment of the thigh, evoked by the pulsating wave of blood (dZ/dt)

wave of 60 kHz and a two-channel detection system, permitting measurements in two ranges of the basic resistance: 30 Ω and 100 Ω. Each channel of the rheograph has an indicator of the basic resistance Z_0 and two outputs: for the variable component of impedance Δ_z and for the first derivative of Δ_z. Sensitivity of the recording system was set on a level of 10 m Ω/cm for Δ_z and 0.1 Ω/s/cm for dz/dt [6, 7].

In the ultrasonic investigations a pulse Doppler ultrasonic flowmeter was used. The flowmeter was built at the Institute of Fundamental Technological Research, Polish Academy of Sciences. This device permits detection of flow as deep as 4.5-5 cm under the skin. Due to the application of an automatic shift of the analysing gate across the vessel, it is possible to record directly on paper time averaged velocity profiles in the vessel under examination.

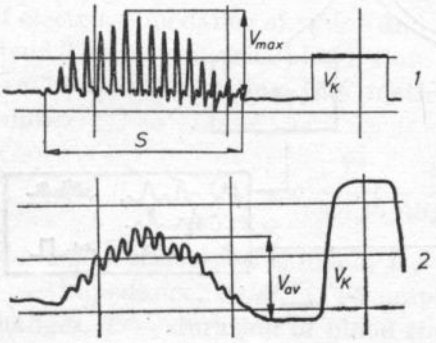

Fig. 3. An example of blood flow recording from the common femoral artery by means of ultrasonic pulse Doppler flow-meter with automatic shift of the analysing gate. *1* — distribution of the instantaneous velocity, *2* — distribution of mean velocity

4. Results

Investigations were carried out on 32 healthy and 46 sick patients. Volumetric intensities of flow, Q_R and Q_U, were measured more than 120 times.

Sick patients were divided, according to the location of the occlusion (which was qualified using the arteriographic methods), into three groups:

the aorto-femoral occlusion — 20 cases,

the femoral-popliteal occlusion — 18 cases,

the multi-level occlusion — 8 cases.

As a result of the investigations performed, we discovered correlation of the volumetric flow in the thigh when measured using the rheographic method with the volumetric flow in the common femoral artery measured using the ultrasonic method, both in the groups of healthy and sick patients. In the group of healthy volunteers there was flow ranging from 120 to 600 ml/min., average 260 ml/min., while flow in the common femoral artery was 110-300 ml/min., average 175 ml/min. In the group of sick patients with the occlusion of the pelvic limb arteries, the values of flow measured using both

methods are lower than in the healthy subjects. There are also differences in the level of the occlusion. The mean values of flow intensity in the thigh, Q_R, and in the common femoral artery, Q_U, in the separate groups of patients, along with the index of collateral circulation CCI (ratio of collateral blood flow to the total thigh flow) are shown in Table 1.

Table 1

Occlusion type	Q_R	Q_u	CCI	Standard deviation σ
aorto-femoral	110	50	0.55	0.12
femoral-popliteal	185	55	0.70	0.08
multi-level	60	25	0.58	0.08
normal	260	175	0.33	0.10

The results of the measurements are shown in Fig. 4. On the basis of analysis of regression and correlation (in case of small tests) linear interdependence between the parameters Q_R and Q_U was found in all the groups. After the reconstruction of the artery CCI decreased as a result of higher flow through the main vessel (Figs. 5, 6, 7).

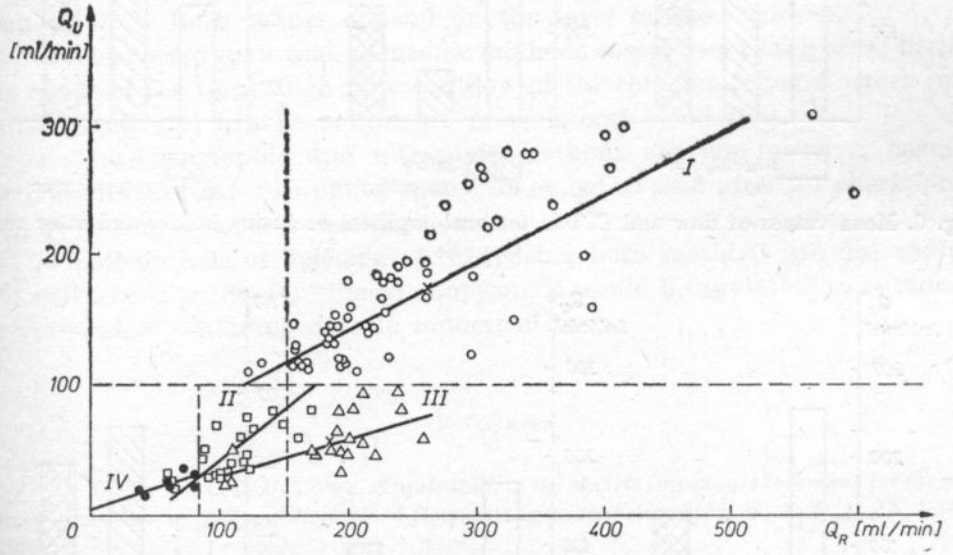

Fig. 4. Interdependence between the measurements of flow in the common femoral artery Q_u (UDP-30) and in the segment of the thigh Q_u (rheograph). ○ – healthy subjects (I) – $Q_u = 0.48\,Q_R + 57$, $r = 0.78$; □ – aorto-femoral occlusion (II) – $Q_u = 0.78\,Q_R - 35$, $r = 0.95$; △ – femoral-popliteal arterial occlusion (III) – $Q_u = 0.79\,Q_R + 1$, $r = 0.62$; ● – multi-level arterial occlusion (IV) – $Q_u = 0.34\,Q_R + 4{,}5$, $r = 0.82$; × – mean values. I (250, 175); II (110, 50); III (180, 55); IV (60, 26)

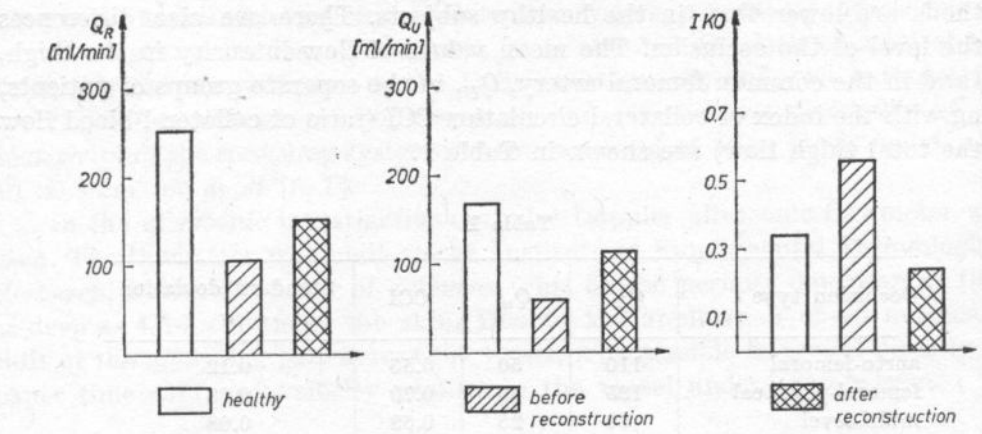

Fig. 5. Mean values of flow and CCI in aorto-femoral occlusion before and after reconstruction

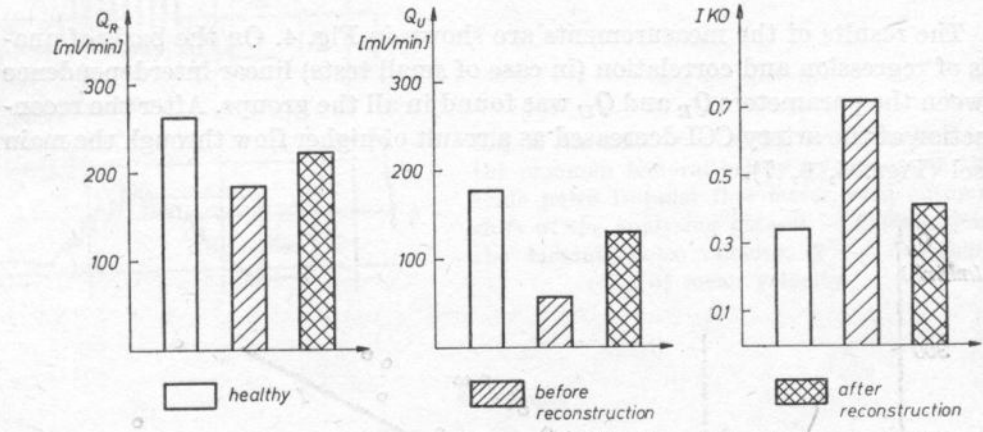

Fig. 6. Mean values of flow and CCI in femoral-popliteal occlusion before and after reconstruction

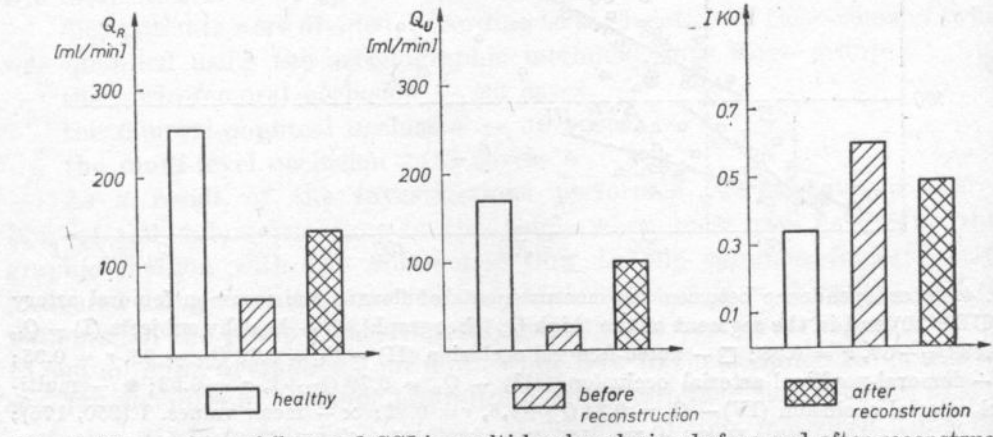

Fig. 7. Mean values of flow and CCI in multi-level occlusion before and after reconstruction

5. Discussion

Taking advantage of the simultaneous measurement of flow in the whole cross-section of the thigh and in the common femoral artery, both values were calculated. In the case of the occlusion of the pelvic limb arteries the value of the entire thigh flow and of flow in the main vessel supplying the pelvic limb with blood permits estimation of collateral circulation. We also noticed that the value of collateral blood flow in proportion to the total thigh flow changes, depending on the level of the occlusion. We call it the "index of collateral circulation". In the group of healthy subjects the mean value of the index of collateral circulation is 0.33. This value increases as flow in the main vessel decreases. The mean values of ICC, depending on the level of the occlusion, are also shown in Table 1.

6. Conclusions

1. The volumetric flow in a segment of the thigh measured using the rheographic method reveals higher values than the volumetric flow in the common femoral artery measured using the ultrasonic method.

2. The values of flow through the thigh and in the common femoral artery are lower in the group of patients suffering from the occlusion of the pelvic limb arteries. Both values depend on the level of the occlusion.

3. The rheographic and ultrasonic methods complement each other because the result of the total thigh flow and flow of the common femoral artery (measured selectively) can be a measure of collateral blood flow.

4. The rheographic and ultrasonic methods are non-invasive, harmless for patients and can be applied many times before and after an operation, as well as during a control examination.

5. Calculations of velocity of flow using both methods are not complex but still laborious. So, for clinical adoption, it would be advisable to automatize the process of obtaining data in numerical form.

References

[1] D. W. Hill, H. J. Lowe, *Application of the electric impedance technique for the monitoring of cardiac output and limb blood flow during anaesthesia,* Med. Biol. Eng., **IX**, 534-545 (1973).

[2] W. G. Kubicek, A. M. L. From *et al., Impedance cardiography as a noninvasive means to monitor cardiac function,* J. Assoc. Adv. Med. Instrum., **4**, 79 (1970).

[3] A. Nowicki, *Ultrasonic pulse Doppler method of measuring of blood flow,* Archives of Acoustics, **2**, 4, 75-93 (1977).

[4] A. Nowicki, *Simplified automatic measurements of blood flow by means of ultrasonic pulse Doppler method,* Archives of Acoustics, **4**, 4 359-366 (1979).

[5] T. PAŁKO, G. PAWLICKI *et al., Devices for impedance investigations by a tetrapolar technique,* Prob. Techn. Med., **3**, 169 (1976).

[6] G. PAWLICKI, *Impedance electropletysmography — the non-invasive diagnostic method in application to the examination of circulatory system,* Proceedings of Institute of Precision and Biomedical Engin., Technical University, Warsaw, November 1976.

[7] J. WESOŁOWSKI, A. NOWICKI, *Application of ultrasonic pulse Doppler blood flowmeter,* Pol. Prz. Chir., **50**, 41 (1978).

ARCHIVES OF ACOUSTICS
9, 1-2, 199-204 (1984)

DOPPLER ECHOCARDIOGRAPHY: VALIDITY OF A QUANTITATIVE ANALYSIS OF VELOCITY CURVES

G. COLONNA, B. DIEBOLD, R. TOUATI,
D. BLANCHARD, P. PERONNEAU,
J. L. GUERMONPREZ, P. MAURICE

Unité I.N.S.E.R.M. 256 et Clinique Cardiologique Hôpital Broussais, 96 rue Didot, 75674 Paris Cedex 14, France

The clinical evaluation of the Doppler diagnosis was performed at the level of inferior vena cava for quantification of tricuspid insufficiency (TI) and in the aortic arch for evaluation of aortic insufficiency (AI). The ratios were calculated between systolic and diastolic components: 1. for AI, between peak systolic and end diastolic components, 2. for TI between peak systolic and peak diastolic components. The results showed that: 1. the compliance of the vessels may prevent the propagation of moderate modifications of velocity curves; 2. associated valvular stenosis may disturb curves even far downstream; 3. systolodiastolic variations of vessel diameter may modify the relationship between angiographic grades and ratios: 0.890 for TI (61 patients) and 0.86 for pure AI (65 patients); for both lesions, the differences between the groups, defined according to the angiographic grade, were significant.

1. Introduction

Doppler velocimeters display spectral distributions or velocity curves which depend on both the accuracy of the signal processing, the signal-to-noise ratio, the occurrence of turbulences and the angle between the ultrasonic beam and the axis of displacement of blood cells [2]. This angle has to be assessed in three dimensions and, mainly at the level of cardiac chambers, the orientation of stream lines with respect to walls is not well defined; thus the angle cannot be measured in many instances. These problems, usually, prevent a quantitative measurement of velocity. The purpose of this paper is to study the theoretical and clinical value of a method for overcoming this limitation.

2. Principle

The principle of this method is to analyse velocity with a high signal-to-noise ratio, in a region where the shape of velocity profile does not vary along the cardiac cycle and where there is no turbulence. Provided those conditions, the different components of a velocity curve along the cardiac cycle are considered as corresponding to stream lines analysed with the same angle with respect to the ultrasonic beam. Therefore, the calculation of a ratio between two components of a curve cancells out the angle factor, since it is the same for numerator and denominator. In order to achieve these conditions, it is necessary to perform the measurements within straight vessels, at some distance from the lesions, instead of within the heart, at the level of the valves.

3. Evaluation of the apparatus

3.1. Apparatus

Commercially available spectrum analysers provide a visual presentation of the distribution of Doppler frequencies; some systems allow calculation of mean velocity which have an accuracy limited in many instances. Moreover, a comparison of the zero-crossing counter output with the data obtained using a spectrum analyser has demonstrated that the zero-crossing counter is accurate in all the cases where the spectral presentation demonstrates the presence of a rather narrow velocity distribution within the sample volume. For this reason, we decided to use the output of a zero-crossing counter and a small sample volume [5]. Some potential sources of limitation were studied: signal-to-noise ratio, low frequencies due to wall motion, high-pass filters, occurrence of aliasing.

3.2. Signal-to-noise ratio

In order to test the influence of the signal-to-noise ratio, the bandwidth of the apparatus was screened using single frequencies mixed with electronically generated noise. The input frequency was compared with the output of the velocimeter for different levels of noise. The results show that the relationship between the two latter parameters is a straight line over a range which increases with the signal-to-noise ratio. For the values encountered in practice, the upper limit of this range corresponds approximatively to one third of the pulse repetition rate [4].

3.3. Wall motion

The artifacts related to wall motion were studied by adding a low frequency with increasing amplitude to a Doppler signal. The results show that low frequency introduces errors in the assessment of the direction of velocity. It emphasizes the importance of high-pass filters, in spite of the limitations that

they introduce in the vicinity of the zero velocity: low frequencies are ignored and measurements are no longer accurate over a range that depends on the cut-off frequency of the filter.

3.4. Aliasing

Aliasing may occur in pathological or, even, in physiological conditions. It can be detected and avoided by increasing the pulse repetition rate and/or the angle between the ultrasonic beam and the axis of the flow.

4. Clinical evaluation

The clinical value of the method was evaluated with the purpose of a quantitative evaluation of aortic and tricuspid insufficiency.

4.1. Aortic insufficiency

4.1.1. Method

The modifications of flow due to aortic incompetence were studied at the level of the aortic arch, at the beginning of its descending part: this position was selected in order to avoid asymetries of velocity profile occurring in the ascending and the horizontal part of the aortic arch [6]. The recording was performed using a transducer positioned in the suprasternal notch and orientating the ultrasonic beam posteriorly and to the left; the descending part of the aorta is recognized by its echo landmark and its flow running away from the transducer during systole. It can be analyzed using a 2*D* echo transducer but, in order to set a high signal-to-noise ratio, it is often necessary to use a single crystal probe.

4.1.2. Velocity curves

If the aortic valve is normal, the velocity has a negative U shaped component during systole, a brief and small reversal component during the beginning of diastole and is equal to zero during the end diastolic phase. In case of significant aortic insufficiency there appears a positive reversal velocity throughout diastole. The ratio was calculated between the peak systolic and the end diastolic amplitude of the velocity curve.

4.1.3. Results

The calculated ratio was compared to a four-stage semi-quantification obtaine using selective supravalvular aortography on a series of 93 patients [3]. The correlation coefficient was 0.81; it increased up to 0.86 when considering only patients without associated aortic stenosis (pressure drop of less than 10 mm Hg at the level of the aortic orifice). All the differences between the groups were highly significant.

4.1.4. Comments

Some sources of limitation appeared clearly, some moderate regurgitation did not produce any end diastolic flow reversal at the level of the descending aorta; it may be due to the high-pass filters and/or to the compliance of the upstream part of the aortic arch.

Usually, for clinical needs, an evaluation of regurgitant flow is considered as more useful than the measurement of velocity; therefore the systolo-diastolic variations of diameter may be misleading; fortunately, the more severe the insufficiency is, the more variations are important.

4.2. Tricuspid insufficiency

4.2.1. Method

Tricuspid insufficiency was studied using velocity curves recorded within the inferior vena cava: the transducer was located in the epigastric area on the patient lying in a supine position, in order to display the inferior vena cava behind the liver; it is recognized according to its echo landmarks and its flow pattern regulated both by the heart and respiration. Recordings were made during the expiratory apnea in order to prevent any Valsalva manoeuver.

4.2.2. Velocity curves

The normal flow pattern was studied on 10 healthy subjects: there is a predominent negative systolic component, the diastolic negative component has a smaller amplitude and it ends at the onset of the atrial contraction that may produce a brief reversal flow. In the case of atrial fibrillation, the amplitude of the systolic component is smaller and the end diastolic flow reversal disappears.

In case of mild regurgitation, the amplitude of the systolic component decreases; if the regurgitation is moderate or severe, a positive systolic flow reversal appears.

The Doppler index of tricuspid regurgitation was calculated between the systolic velocity amplitude (measured at the top of the T wave of the ECG) and the peak diastolic anterograde velocity.

4.2.3. Results

The Doppler index was compared with a 5 grade semiquantification obtained using selective right ventricular angiography [1]. On a series of 62 patients, the correlation between angio and Doppler parameters is highly significant ($r = 0.89$), all the differences between the groups are significant; and using a variance analysis, we found an F value of 47.84.

4.2.4. Comments

At the level of the vena cava, variations of vessel diameter appeared to be small. The limitations due to high-pass filters were not important because a low cut-off frequency was used, according to limited wall motion. Otherwise, in some instances the index could not be calculated owing to atrial arrhythmias such as atrial flutter.

5. Conclusions

In order to obtain accurate relative velocity measurements using Doppler echocardiography, it is necessary:

— to have an appropriate setting of the pulse repetition rate and of the highpass filters,

— to have a good position of the sample volume with respect to velocity profiles,

— to have a high signal-to-noise ratio.

Provided those conditions, it is worthwhile to calculate the ratios between the parameters of the velocity curves, namely at the level of the great vessel. This procedure allows an accurate evaluation of tricuspid or aortic insufficiencies.

References

[1] D. Blanchard, B. Diebold, J. L. Guermonprez, P. Peronneau, J. Forman, P. Maurice, *Non-invasive quantification of tricuspid regurgitation by Doppler echocardiography,* 54th Scientific Sessions of the American Heart Association, 1981, Dallas, Texas, Abstract in Circulation, 64, IV, 256 (1981).

[2] C. B. Burckhardt, *Comparison between spectrum and time interval histogram of ultrasound Doppler signals,* Ultrasound in Med. and Biol., **7**, 79-82 (1981).

[3] B. Diebold, P. Péronneau, D. Blanchard, G. Colonna, J. L. Guermonprez, S. Forman, S. Sellier, P. Maurice, *Non invasive quaatification of aortic regurgitation by Doppler echocardiography,* British Heart J., **49**, 167-173 (1983).

[4] R. S. Meltzer, B. Diebold, N. K. Valk, D. Blanchard, J. L. Guermonprez, C. T. Lancée, P. Péronneau, S. Roelandt, *M-Mode contrast echocardiography can yield similar velocity information to Doppler echocardiography,* British Heart J., **49**, 244-249 (1983).

[5] P. Péronneau, J. Hinglais, M. Pellet, F. Léger, *Vélocimètre sanguin par effet Doppler à émission ultrasonore pulsée,* L'Onde Electrique, **50**, 369-384 (1970).

[6] P. Péronneau, *Analyse de l'écoulement sanguin dans les gros vaisseaux par méthode ultrasonore,* Doctorat d'Etat, Sciences Naturelles, Université de Paris-Sud, 1977.

ARCHIVES OF ACOUSTICS
9, 1-2, 205-214 (1984)

PULSED AND CONTINUOUS WAVE DOPPLER IN HEART LESIONS

LIV HATLE

Regional Hospital, Trondheim, Norway

Valvular obstructions and regurgitations can be diagnosed with either pulsed or CW Doppler. By recording the maximum velocities with CW Doppler the pressure drop across obstructions and across regurgitant valves can be obtained, permitting assessment of the severity of obstructions and providing information on the right heart pressures. Congenital lesions can be diagnosed, obstructions assessed and shunt size indicated.

1. Blood flow velocities

Flow velocity across the various valves in the heart can be recorded with Doppler when a small angle is obtained between ultrasound beam and velocity. With larger angles the velocity will be underestimated (at 25° the underestimation will be 9 per cent). With pulsed Doppler the velocities are recorded in a small area at a certain variable depth. The advantage is that a flow signal can be localized in depth, the drawback that there is a limit to the velocities that can be recorded. With continuous wave (CW) Doppler velocities are recorded all along the beam, a flow signal cannot be localized in depth, but there is no limit to the velocities that can be recorded.

The audio signal from the Doppler contains the frequency shifts from the blood flow that is recorded. The higher the velocities the larger the frequency shift will be and the higher frequency will be characteristic of the audio signal. The audio signal will also be of the higher frequency the smaller the angle to the velocity. The signal can therefore be used to find high velocities and the positions and beam directions with the smallest angle to flow.

Obstructions to flow cause an increase in the flow velocity across an obstruction. This increase in velocity is related to the pressure drop across the obstruction, and the relationship is described by the Bernoulli equation. By inserting the mass density for blood and conversion to mm Hg a simple formula

is obtained where the pressure drop is calculated from 4 times the maximum velocity squared. From the maximum velocity recorded across obstructions, the pressure drop has been obtained in valve stenoses, across prosthetic valves and regurgitant valves [1–11]. In ventricular septal defects it can be used to obtain the pressure difference between the two ventricles [12].

In most cases the velocity prior to an obstruction is so low that it can be ignored in the calculation. But if it increases it should be considered, and the pressure drop is then obtained by subtracting the squared velocity prior to the obstruction from the velocity recorded past the obstruction squared.

When good Doppler signals with mostly high frequencies are obtained, the maximum velocity can be recorded either with a maximum frequency estimator or with spectral analysis. With the estimator the maximum velocity during systole or diastole is seen as a single line, with spectral display the various frequencies present in the Doppler signal at one time are shown. With weak Doppler signals or signals which contain only few high frequencies, these are more easily recorded with spectral analysis. Less than optimal Doppler signals can occur from large depths or when a high velocity jet is only partly recorded or in mild regurgitations. It is then more likely that the maximum velocity present will be recorded using a spectral display and underestimation of the maximum velocity and pressure drop less likely. The use of the audio signal to obtain a small angle to flow is therefore likely to cause less error than an attempt to correct for an assumed angle from the image.

The combination of Doppler with two-dimensional echo usually helps to make the examination quicker, and in some patients abnormal flow signals are more easily found. But the opposite also occurs, that these can be easier to find with a separate Doppler without imaging. This can partly be due to improved concentration and movement of the transducer when there is no image, and partly to better access and higher sensitivity with the smaller separate Doppler transducer.

2. Valvular obstructions

In mitral stenosis the increased flow velocity into the left ventricle in diastole is recorded toward the transducer at the apex, or flow direction may be slightly more medial. The velocity is highest in early diastole, it decreases more slowly than normal, and in sinus rhythm there is a second peak following the atrial contraction. The pressure drop can be calculated for 3-6 points during diastole, the course of the pressure drop can then be drawn and the mean pressure drop obtained. Fig. 1 shows mitral stenosis and mitral regurgitation in two patients, one in sinus rhythm and one in atrial fibrillation. The great variation in the mean pressure drop calculated with varying diastolic length can be seen, and this also illustrates the great variation in the pressure drop in mitral stenosis with changes in the heart rate.

When ultrasound and pressure measurements are carried out simultaneously, there is good correlation between the two methods [1, 2]. When optimum Doppler signals with a concentrated band of the highest frequencies are recorded, the calculated pressure drop can be almost identical to that recorded with pressure. In sinus rhythm the increase in velocity and pressure drop with atrial contraction may be more clearly seen in the velocity recording than in the pressure tracing, unless the left atrial, and not the pulmonary capillary venous pressure, is recorded [13].

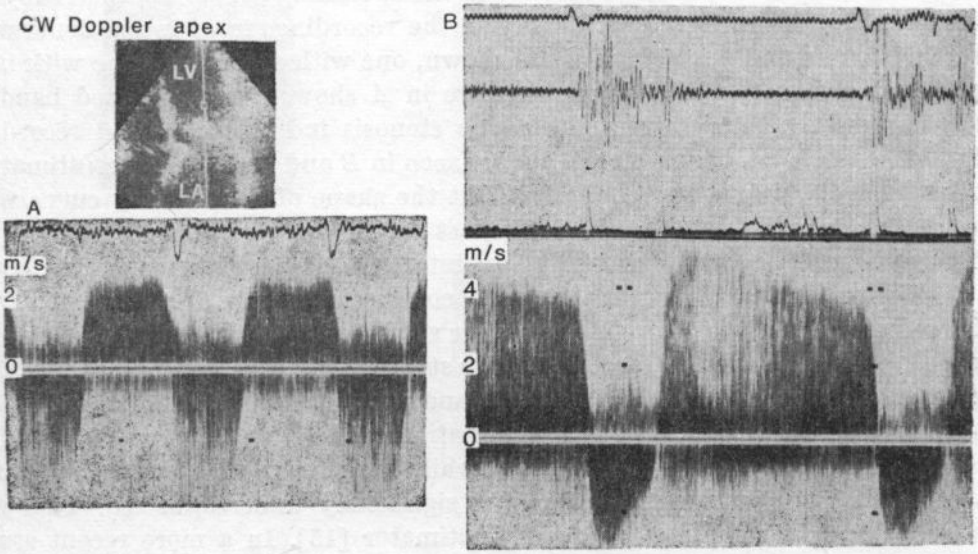

Fig. 1. When recording with CW Doppler from the apex the high velocity through the mitral orifice is recorded toward the transducer in diastole and mitral regurgitation away from the transducer in systole. In sinus rhythm there is a second peak following atrial contraction (*A*). In the patient with atrial fibrillation (*B*) there is still a pressure difference between the left atrium and ventricle even in a long diastole, indicating significant obstruction. The calculated mean pressure drop in *A* is 22 mm Hg, in *B* it varies with diastolic length, early diastolic pressure difference is 25 mm Hg and at end diastole it is 2 and 13 mm Hg for the two beats shown. Regurgitation is seen to start at mitral valve closure and it continues past aortic closure, lasting until the mitral valve opens again

The degree of obstruction at the mitral orifice also influences the course of the pressure difference during diastole. With more severe obstructions equalization of pressures occurs more slowly and this is seen as a slower decrease in velocity. The time it takes for the initial pressure drop to be reduced to half that value is easily measured directly from the velocity curve. Half the initial pressure drop will be where the maximum velocity is reduced to $v/\sqrt{2}$ or $v/1.4$. The pressure half-time increases with an increase in obstruction, it is less influenced by flow than the pressure drop is, and can therefore be used to assess the severity of obstruction, also when there is associated regurgitation [14].

The pressure half-time in normal subjects is less than 60 ms, in mild to moderate mitral stenosis from 100-200, and from 200 up to 5-600 with increasing severity of obstruction. It is especially helpful in patients with low pressure drop due to low cardiac output where a long pressure half-time will help to avoid underestimation of severity. Tricuspid stenosis can be diagnosed and assessed in the same way as mitral stenosis.

In aortic stenosis the best direction to the high velocity jet through the orifice can be from the suprasternal notch, the upper right sternal border or from the apex. The maximum velocity in the ascending aorta in normal subjects usually ranges from 1-1.7 m/s. In Fig. 2 the recordings from two patients with aortic stenosis and regurgitation are shown, one with severe and one with insignificant obstruction. The spectral curve in *A* shows a concentrated band of the highest frequencies from the aortic stenosis indicating a good recording from the aortic jet. This is not so clearly seen in *B* and possible underestimation of the velocity might be questioned. But the shape of the velocity curve with an early peak and low velocities in the last part of systole also indicates insignificant obstruction with practically no late systolic pressure difference.

The peak velocity gives the instantaneous peak pressure drop during systole. By calculating the pressure difference for some points during systole, the mean pressure drop can be obtained. In earlier studies good correlation with recorded pressure drops were found in children and young adults where good Doppler signals are easily obtained [4]. In older patients there was only moderate underestimation with good Doppler signals while with few high frequencies in the signal velocity and pressure drop was significally underestimated. This was a study using a maximum frequency estimator [15]. In a more recent study with the use of spectral display, correlation with recorded pressures was good also in older patients, there was a slight underestimation of the peak pressure drop and a moderate underestimation of the mean pressure drop [16]. The aortic jet could be reached in all, and the severity of obstruction was correctly assessed in all.

The shape of the velocity curve reflects the course of the pressure drop during systole and gives additional information about the severity of obstruction. In a study of more than 100 patients with aortic stenosis the time of the peak velocity in systole was early in all patients with mild obstruction, and when the time of the peak velocity was related to the left ventricular ejection time (LVET) a ratio of more than 0.54 was found in patients where surgery was indicated [15]. This was done using a maximum frequency estimator, with spectral display the peak velocity will be shown earlier in systole, due to less delay in the spectral recording. The severity of obstruction can therefore be assessed also if there are significant changes in flow accross the valve. With increased flow, as with associated regurgitation, there will be a relatively high velocity early in systole followed by a marked decrease, with severe obstruction and reduced flow the velocity may not be so high, but with less decrease dur-

ing systole. The LVET is another useful indicator of the severity of aortic valve disease and it is easily measured from the amplitude of the Doppler signal (Fig. 2). By combining the pressure drop, the time of the peak velocity and the LVET a good assessment of the severity of aortic stenosis can be obtained [15].

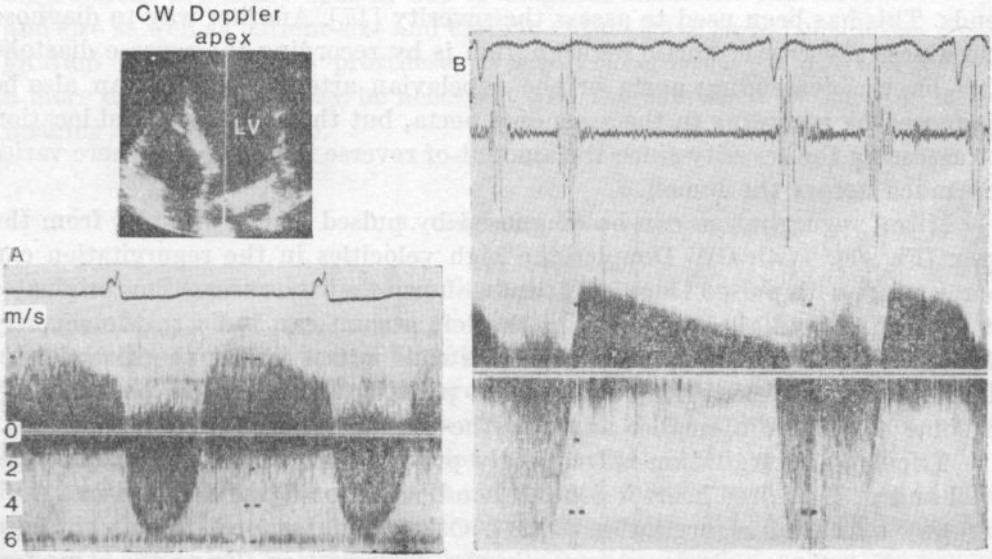

Fig. 2. Aortic stenosis and regurgitation recorded with CW Doppler from the apex, aortic flow is away from and regurgitation is toward the transducer. In *A* the obstruction is severe with a calculated peak pressure drop of 125 mm Hg, and the velocity stays high during most of systole. In *B* obstruction is insignificant, the calculated peak pressure drop is 34 mm Hg, but the velocity decreases rapidly and is low in late systole showing almost equalization of left ventricular and aortic pressures. Note difference in scale from *A* to *B*. Velocity in aortic regurgitation is high due to the pressure difference between the aorta and the left ventricle in diastole, and velocity decreases as aortic pressure falls. The amplitude curve below the phonocardiogram in *B* shows aortic valve opening and closure. Forward and regurgitant flows are continuous. Note the concentrated band of the high frequencies in the aortic stenosis in *A* which indicates that the jet is well recorded

3. Regurgitations

Doppler is a very sensitive method to diagnose regurgitations and this has clearly shown the lower sensitivity of the clinical diagnosis. Mild regurgitations cannot often be diagnosed clinically and even significant regurgitations can occasionally be present in the absence of a systolic or diastolic murmur.

The clinical diagnosis of mitral and tricuspid regurgitation can also be difficult when there is a systolic murmur due to another lesion.

Aortic regurgitation can be diagnosed by recording with CW Doppler toward the aortic valve, as shown in Fig. 2. With pulsed Doppler the high velocities in the regurgitation will not be recorded, there will be aliasing with the Doppler signal shown on both sides of the zero line [6], but the pulsed mode can be used to record how far down in the left ventricle the regurgitation extends. This has been used to assess the severity [17]. Another way to diagnose and assess severity of aortic regurgitation is by recording the reverse diastolic flow on the descending aorta or the subclavian arteries [18]. It can also be diagnosed by recording in the ascending aorta, but this is not a useful location for assessing the severity since the amount of reverse flow velocities here varies too much across the lumen.

Mitral regurgitation can be diagnosed by pulsed or CW Doppler from the apex (Fig. 1). With CW Doppler the high velocities in the regurgitation can be recorded, with pulsed Doppler it can be shown that the reverse flow originates at the orifice and the extension in the left atrium can indicate the severity [19, 20]. In the mitral valve prolapse or flail mitral leaflet the direction of the regurgitant jet may vary more and a parasternal transducer position may in some cases give a smaller angle to the regurgitation.

Tricuspid regurgitation is frequently present both in patients with congenital and with aquired heart lesions. It can be diagnosed and assessed in a similar way as mitral regurgitation [9, 21]. Other useful information is obtained by recording the maximum velocity in the regurgitation. Using the same formulae as in obstructions the pressure difference between the right ventricle and atrium in systole can be calculated and the right ventricular systolic pressure can then be obtained noninvasively [9]. If the right atrial pressure increases the elevation of pressure as judged from the neck veins should be added. Good correlation with pressure recording has been obtained [9, 10], and in the absence of the right ventricular outflow obstruction this gives the systolic pressure in the pulmonary artery.

Pulmonary regurgitation can also be more frequently recorded with Doppler than suspected from clinical findings, it is frequently present in patients with some degree of pulmonary hypertension, but also seen without this [22]. When there is no increase in diastolic pressure in the pulmonary artery velocity in the regurgitation is low, but it becomes higher when the pressure increases. From the maximum velocity in the regurgitation the pressure difference between the pulmonary artery and the right ventricle during diastole can be calculated and this is a sensitive method to detect increases in diastolic pressure in the pulmonary artery. In mild regurgitations the Doppler signal can be weak, and in mild tricuspid and pulmonary regurgitation the maximum velocities are far easier to record using spectral analysis than with a frequency estim ator

4. Prosthetic valves

Prosthetic valves usually cause some obstruction and Doppler can be used to assess this in the same way as for valvular obstructions. For both mitral and aortic valve prostheses both the course of the pressure difference and the mean pressure drop are useful to diagnose increased obstruction. Significant obstructions are easily shown, but to diagnose moderate increases valve type and size as well as patient size and cardiac output have to be considered. Regurgitation in aortic valve prostheses is easily diagnosed, in mitral prostheses a more careful search may be necessary and the combined use of Doppler and imaging can be of help.

5. Congenital lesions

The increased velocities in pulmonary stenosis can be recorded with CW Doppler from a low parasternal position in some cases, a higher one in others and in some from an apical or subcostal position. Calculated pressure drops correlate well with pressures recorded at catheterization [5, 6]. With pulsed Doppler the level of obstruction can be shown; if it is subvalvular the increase in velocity will be recorded below the valve.

In ventricular septal defects the maximum velocity can be used to calculate the pressure difference between the two ventricles. When a high velocity is recorded, there will be a large pressure difference. If a low velocity is recorded this may be due to a low pressure difference, but also to underestimation of the velocity. In ventricular septal defects the high velocities are easier to record with spectral analysis.

The velocity across atrial septal defects is quite low and is best recorded with simultaneous imaging. The size of the shunt may be estimated from the increase in flow velocity across the tricuspid and pulmonary valves, compared to mitral and aortic flow velocities.

The patent ductus arteriosus can be diagnosed either by recording flow into the pulmonary artery from a parasternal position, or reverse diastolic flow in the descending aorta below the level of the duct. When recording with CW Doppler up through the main pulmonary artery high velocities toward the transducer can be recorded throughout systole and diastole when there is no pulmonary hypertension. With pulmonary hypertension the velocity will be low and flow through the duct may be found only during part of the cardiac cycle.

In coarctations of the aorta increased velocity can be recorded with CW Doppler toward the descending aorta. The pressure drop can be obtained and is useful especially in the assessment following surgery.

References

[1] J. HOLEN, R. AASLID, K. LANDMARK, S. SIMONSEN, *Determination of pressure gradient in mitral stenosis with a noninvasive ultrasound Doppler technique,* Acta Med. Scand., **199**, 455-460 (1976).

[2] L. HATLE, A. BRUBAKK, A. TROMSDAL, B. ANGELSEN, *Noninvasive assessment of pressure drop in mitral stenosis,* Br. Heart J. **40**, 131-140 (1978).

[3] L. HATLE, B. A. ANGELSEN, A. TROMSDAL, *Noninvasive assessment of aortic stenosis by Doppler ultrasound,* Br. Heart J., **43**, 284-292 (1980).

[4] L. HATLE, *Noninvasive assessment and differentiation of left ventricular outflow obstruction by Doppler ultrasound,* Circulation, **64**, 381-387 (1981).

[5] C. OLIVEIRA LIMA, D. J. SAHN, L. M. VALDES-CRUZ, S. J. GOLDBERG, J. VARGAS BARRON, H. D. ALLEN, E. GRENADIER, *Noninvasive prediction of transvalvular pressure gradient in patients with pulmonary stenosis by quantitative two-dimensional echo Doppler studies,* Circulation, **67**, 866-8 (1983).

[6] L. HATLE, B. ANGELSEN, *Ultrasound in cardiology,* Lea and Febiger, Philadelphia 1982, 97.

[7] J. HOLEN, S. SIMONSEN, T. FRØYSAKER, *An ultrasound Doppler technique for the noninvasive determination of the prressure gradiednt in the Bjork-Shiley mitral valve,* Circulation, **59**, 436-442 (1979).

[8] L. HATLE, *Combined 2D-echo and Doppler compared to Doppler without imaging,* in: *Cardiac Doppler diagnosis,* M. SPENCER (ed.), Martinus Nijhoff, The Hague 1983.

[9] T. SKJAERPE, L. HATLE, *Diagnosis and assessment of tricuspid regurgitation with Doppler ultrasound,* in: *Echocardiology,* H. RIJSTERBORGH (ed.), Martinus Nijhoff, The Hague 1981, 299-304.

[10] T. SKJAERPE, L. HATLE, in: *Cardiac Doppler diagnosis,* M. SPENCER (ed.), Martinus Nijhoff, The Hague 1983.

[11] L. HATLE, B. ANGELSEN, *Doppler ultrasound in cardiology,* Lea and Febiger, Philadelphia (in press).

[12] L. HATLE, R. ROKSETH, *Noninvasive diagnosis and assessment of ventricular septal defect by Doppler ultrasound,* Acta Med. Scand., **645**, 47-56 (1981).

[13] J. HOLEN, S. SIMONSEN, *Determination of pressure gradient in mitral stenosis with Doppler echocardiography,* Br. Heart J., **41**, 529-535 (1979).

[14] L. HATLE, B. ANGELSEN, A. TROMSDAL, *Noninvasive assessment of atrioventricular pressure half-time by Doppler ultrasound,* Circulation, **60**, 1096-1104 (1979).

[15] L. HATLE, *Aortic valve stenosis,* in: *Cardiovascular applications of Doppler echography,* P. PERONNEAU, B. DIEBOLD (eds.), Inserm, Paris 1983, 313-322.

[16] L. HEGRENAES, *Noninvasive assessment of aortic stenosis with Doppler ultrasound,* Proc. Third Joint Meeting of European Society of Cardiology, 1983.

[17] M. CIOBANU, A. S. ABBASI, M. ALLEN, A. HERMER, R. SPELLBERG, *Pulsed Doppler echocardiography in the diagnosis and estimation of severity of aortic insufficiency,* Am. J. Cardiol., **49**, 339-343 (1982).

[18] D. R. BOUGHNER, *Assessment of aortic insufficiency by transcutaneous Doppler ultrasound,* Circulation, **52**, 874-879 (1975).

[19] A. S. ABBASI, M. W. ALLEN, D. DECRISTOFARO, J. UNGAR, *Detection and estimation of the degree of mitral regurgitation by range-gated pulsed Doppler echocardiography,* Circulation, **61**, 143-147 (1980).

[20] K. MIYATAKE, N. KINOSHITA, S. NAGATA, S. BEPPU, Y. PARK, H. SAKAKIBARA, Y. NIMURA, *Intracardiac flow pattern in mitral regurgitation studied with combined use of the ultrasonic pulsed Doppler technique and cross-sectional echocardiography,* Am. J. Cardiol., **45**, 155-162 (1980).

[21] K. Miyatake, M. Okamoto, N. Kinoshita, M. Ohta, T. Kozuka, H. Sakakibara, Y. Nimura, *Assessment of severity of tricuspid regurgitation with the combined use of ultrasonic pulsed Doppler technique and two-dimensional echocardiography,* in: *Cardiovascular applications of Doppler echography,* P. Peronneau, B. Diebold (eds.), Inserm, Paris 1983, 389-396.

[22] A. Waggoner, M. A. Quinones, J. B. Young, T. A. Brandon, A. A. Shah, M. S. Verani, R. R. Miller, *Pulsed Doppler echocardiographic detection of rightsided valve regurgitations,* Am. J. Cardiol., **47**, 279-286 (1981).

ARCHIVES OF ACOUSTICS
9, 1-2, 215-222 (1984)

CONTRAST DOPPLER ECHOCARDIOGRAPHY

P. NIEDERLE, P. FRÍDL, E. KOUDELKOVÁ,
P. JEBAVÝ, M. HACO

Institute of Clinical and Experimental Medicine, Prague, Czechoslovakia

A new technique in the scope of cardiac ultrasound — "contrast Doppler echocardiography" — is introduced and its first clinical applications are presented. The presence of contrast material within the right heart cavities following the peripheral vein injection is easily recognized by characteristic Doppler signal changes. This knowledge was used to detect a small amount of contrast passing through atrial (ASD) or ventricular septal defect (VSD) towards the left heart cavities despite the dominant left-to-right shunting. The high sensitivity of contrast Doppler in those conditions was presented by correct diagnosis of 10 ASD and 3 VSD. Besides that, the other application of this technique is in selected cases of tricuspid regurgitation.

Therefore, the combination of both pulsed Doppler and contrast echo-investigation seems to be advantageous in the diagnosis of the mentioned diseases. However, further research in this very specialized method is required.

1. Introduction

Both pulsed Doppler and contrast echocardiography are well established methods evaluating the character of blood flow within the heart and the great vessels. Recently, it has been shown that microbubbles are very good for Doppler studies [4], however, the clinical value of this technique still remains to be defined.

Contrast Doppler echocardiography (CDE) has been used in our laboratory since 1982 and here the first clinical experiences with the application of the method in some heart diseases are presented.

2. Material and methods

For the examination by CDE we selected the following groups of patients:

Group 1, atrial septal defect — ASD

10 patients with ASD proved by heart catheterization were studied. A catheter introduced into the right atrium passed through the defect to the left

atrium in all of them. Then, using a standard dye-dilution technique a left-to-right ($L-R$) shunt was demonstrated ranging between 20-80 per cent of total pulmonary blood flow (TPBF).

Group 2, tricuspid regurgitation — TR

The group comprised 11 patients — 9 with rheumatic mitral valve disease and relative tricuspid insufficiency, 1 with Ebstein's anomaly and 1 with advanced coronary heart disease with mitral and tricuspid regurgitation due to dilation of both ventricles. TR was positive on right ventriculograms in 4 patients, in the other 7 subjects clinical and pulsed Doppler findings suggested the presence of TR.

Group 3, ventricular septal defect — VSD

Only 3 patients were included in this group: 2 with congenital VSD proved by catheterization with existing L—R shunt of 69 and 17 per cent of TPBF, respectively, and 1 patient with acquired ASD due to the muscular septum rupture in acute myocardial infarction. The last diagnosis was confirmed at autopsy.

3. Contrast Doppler echocardiography — CDE

A one-dimensional ATL 500 A Pulsed Doppler system was used to detect the passage of contrast material within the heart cavities or the great vessels. Contrast echocardiography was performed according to the recommendations of ROELANDT [7]. As the contrast we used 5—15 ml of aereated saline or 5 per cent dextrose injected via a teflon cannula introduced into the antecubital vein of the left arm. The Doppler measurement and recording started simultaneously with the injection of the contrast medium.

In agreement with the recent report of GOLDBERG *et al.* [4], we observed the characteristic changes of Doppler output due to the passage of microbubbles through the sample volume. An audible flow signal was altered to a very typical high-pitched crackling sound whenever the microbubbles acted as ultrasonic reflectors. The character of this sound is so specific that according to our experience it cannot be mistaken for Doppler reflections from red blood cells or heart structures. Another pattern seen on the graphical Doppler display was a marked rise in the signal strength indicator followed by an obvious dispersion of the time interval histogram (TIH) dots indicating the turbulent flow. However, both of the latter events following the rapid injection are partly due to the actual and temporary flow increase. Therefore, we consider only the presence of all the mentioned Doppler abnormalities necessary for true microbubble detection.

The simultaneously recorded M-mode tracing allowed us to observe the presence of the contrast within the heart cavities, correct localization of Doppler sample volume and timing of Doppler signal changes.

4. Results and discussion

Atrial septal defect — ASD

The alterations of the Doppler signal as described above were distinctly observed in all of the 10 patients investigated. Doppler sampling performed within the left atrial outflow tract, i.e. under the echo of the anterior mitral leaflet, indicated an abnormal passage of isolated microbubbles (Fig. 1). Our

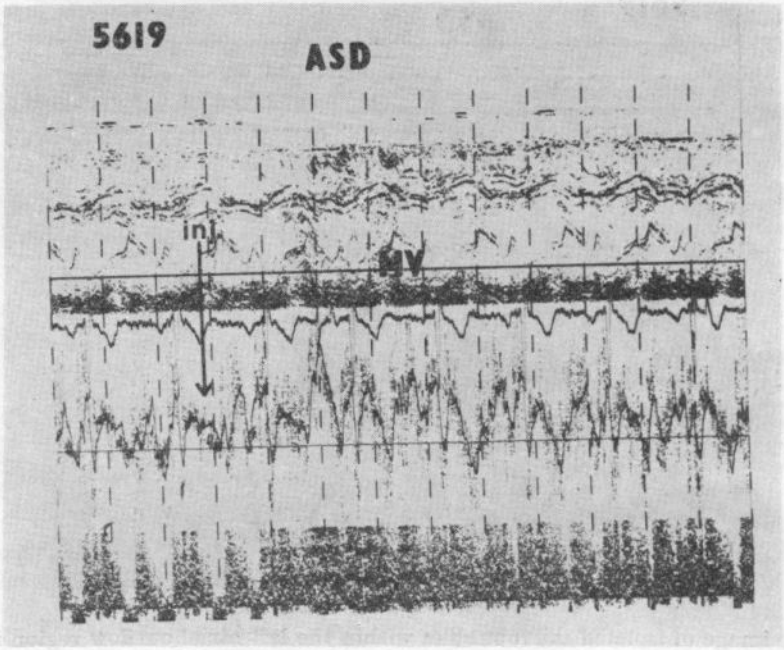

Fig. 1. Atrial septal defect. After the contrast injection the contrast appears within the right ventricle and some isolated microbubbles passing through the mitral orifice cause the turbulence pattern on TIH (the dispersion of the dots along the mean velocity curve) and a marked rise in the signal strength indicator (bottom). The sample volume (a solid line in *M*-mode tracing) is inserted into the mitral orifice (MV)

results support some previous studies dealing with contrast echocardiography in cases with dominant $L-R$ atrial shunts [1-3, 5, 6, 8]. However, single contrast echocardiography detected some isolated microbubbles only in 7 of our 10 patients (Fig. 2). Therefore, we believe that the CDE findings yield more impressive and convincing results than a single one dimensional echocardiography. The enhanced sensitivity of CDE makes it a method of the first choice in direct non-invasive ASD detection. The other advantage of CDE seems to be the possibility of reducing the number of contrast injections to obtain the positive result.

To evaluate the specificity of CDE in ASD, we examined another group of 10 patients with various rheumatic valve diseases but without any evidence of ASD. The only observed abnormality following the contrast injection in 6 of them was a temporary increase in the Doppler flow signal within the left heart cavities, with no audible signal indicating the presence of microbubbles. We are convinced that there exists no possibility of false positive findings for an experienced Doppler investigator excluding the occurrence of spontaneous contrast.

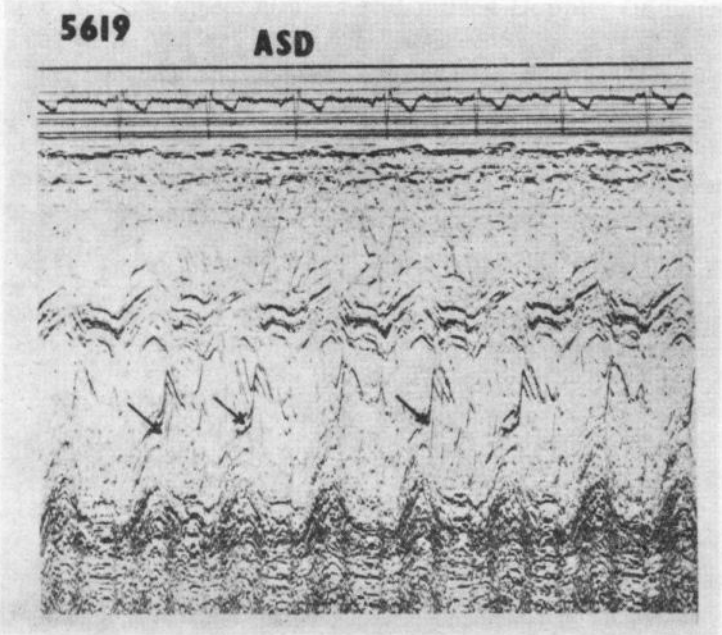

Fig. 2. The image of isolated microbubbles within the left atrial outflow region in *M*-mode recording (arrow indicates the microbubbles)

Besides the patients with ASD, one subject with patent foramen ovale (PFO) and haemodynamically insignificant $L-R$ shunt of 9 per cent of TPBF showed a negative CDE finding. Nevertheless, we must stress that we did not use the Valsalva maneuver to increase the right atrial pressure and thus reverse the direction of the shunt flow. Perhaps, in such cases this provocation is valuable and should be recommended [5].

Tricuspid regurgitation — TR

In our study we used two different positions of the Doppler sample volume to detect regurgitant microbubbles in tricuspid insufficiency.

The first sampling was performed within the right atrial outflow tract, i.e. under the echo of the anterior tricuspid leaflet. This approach yielded truly positive results in all of the 11 successive patients. After the contrast injection

a very strong and typically modified Doppler signal was detected in this region during systole (Fig. 3). In fact, the finding resembles closely the conventional Doppler abnormality in this condition, but it is much more pronounced and convincing.

The other Doppler sampling was done within the inferior vena cava (VCI). Using only *M*-mode echocardiography in the subcostal approach, successful imaging of the VCI was possible in 5 of 11 cases. Every successful positive

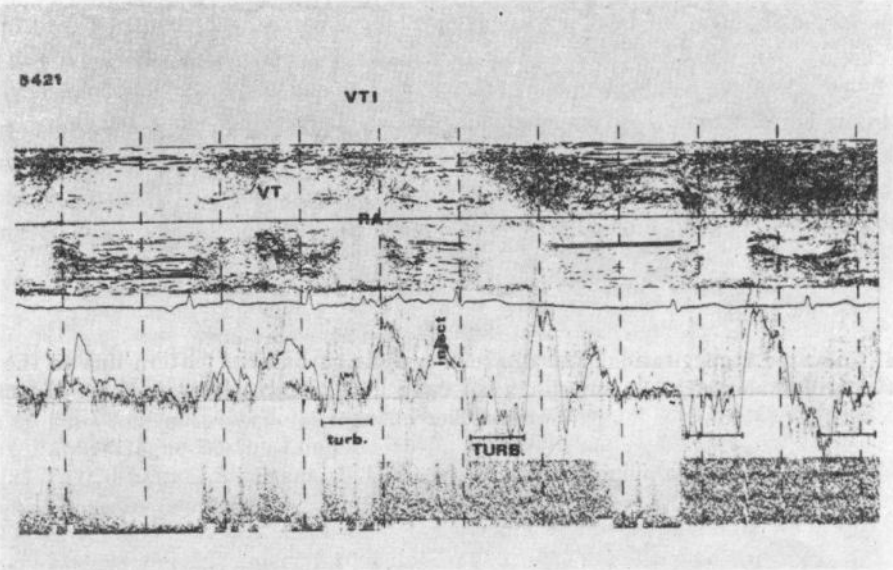

Fig. 3. Tricuspid regurgitation (VTI). The typical Doppler changes due to the regurgitant microbubbles towards the right atrial outflow tract-RA (sample volume under the echo of anterior tricuspid leaflet VT)

finding presented itself as Doppler signal change during several successive systoles (Fig. 4). Although the microbubbles were recorded in *M*-mode recording in all positive investigations, the Doppler signals of the present contrast lasted markedly longer than its visualization. Sometimes the Doppler sampling helped us to recognize the VCI more easily than *M*-mode echocardiography did.

With respect to the high sensitivity of CDE in TR, we would recommend this technique as a selective procedure only in cases with non-convincing Doppler or contrast findings.

Ventricular septal defect — VSD

Our experience with VSD to data is limited to a very small number of examined patients — 2 with congenital VSD and 1 subject with muscular septum rupture due to an acute myocardial infarction. In all the three cases the CDE investigation revealed the abnormal passage of isolated microbubbles from

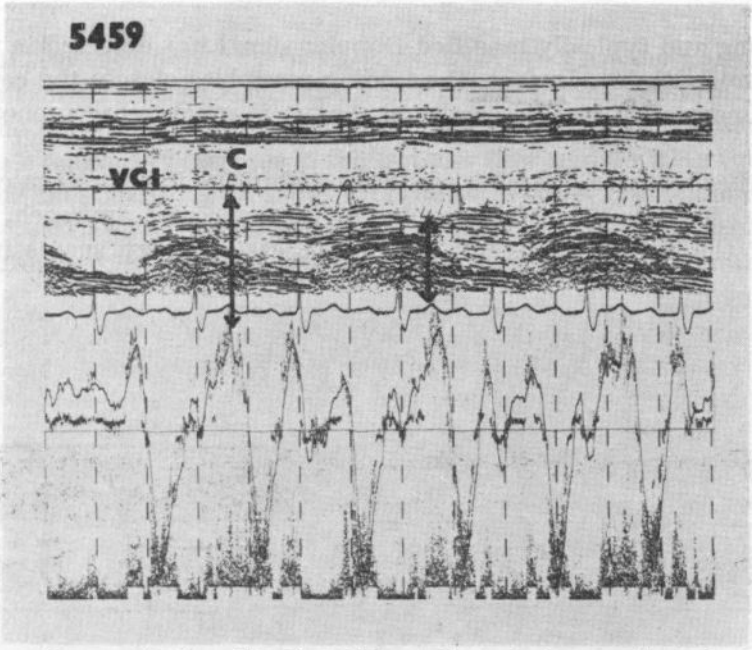

Fig. 4. Tricuspid regurgitation. The diastolic-systolic turbulence pattern due to the regurgitant microbubbles into the inferior vena cava (VCI). The arrows indicate the moment of Doppler changes

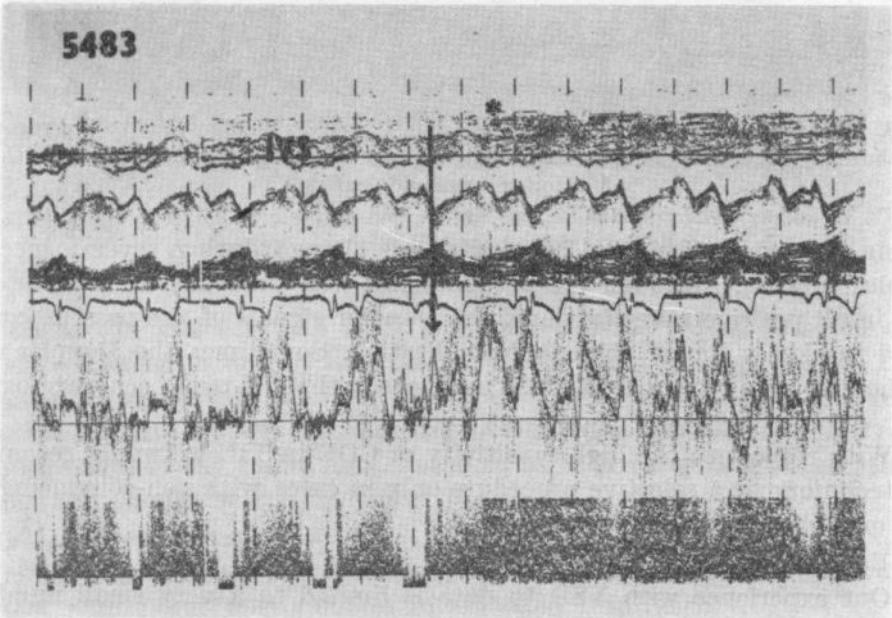

Fig. 5. Ventricular septal defect. The Doppler tracing changes due to the microbubbles entering the left ventricular outflow tract (see arrow). Doppler sampling performed in the left ventricular outflow tract, close to the left septal border. (IVS... septum, asterisk indicates the contrast within the right ventricle)

the right ventricle towards the left ventricular outflow tract that cannot be observed in healthy persons (Fig. 5). Despite a dominant $L-R$ shunt our results indicate the presence of a small interventricular $R-L$ shunt that might probably be facilitated by the turbulence of shunt flow.

The diagnosis of VSD by M-mode echocardiography is extremely difficult, if ever possible, and completion of the examination by pulsed Doppler increases the sensitivity to approximately 50 per cent, according to our experience in adults. Therefore, any other non-invasive approach to detect this condition is valuable. From this point of view, our results would be promising; nevertheless, they would need further verification.

In conclusion we dare say that the CDE combines the advantages of both pulsed Doppler and contrast echocardiography with encouraging results in the detection of atrial and ventricular $L-R$ shunts and tricuspid regurgitation. We believe that this completely new application of cardiac ultrasound will become a selective procedure in every well established echo-laboratory.

References

[1] P. D. V. Bourdillon, R. A. Foale, A. F. Rickards, *Assessment of atrial septal defects by cross-sectional echocardiography,* in: *Echocardiology,* C. T. Lancée (ed.), Martinus Nijhoff Publ., Hague-Boston-London, 1979, 61-65.

[2] T. D. Fraker, S. Myers, J. A. Kisslo, *Detection and exclusion of interatrial shunts by contrast two-dimensional echo,* Circulation, **58**, suppl. II, 187 (1978).

[3] B. W. Gilbert, M. Drobac, H. Rakowski, *Contrast twodimensional echocardiography in inter-atrial shunts,* Amer. J. Cardiol., **45**, 2, 402 (1980).

[4] S. J. Goldberg, L. M. Valdes-Cruz, Y. Carnahan, H. Hoenecke, H. D. Allen, D. J. Sahn, *Comparison of microbubble detection by M-mode echocardiography and two-dimensional echo/Doppler technique,* in: *Echocardiology,* H. Rijsterborgh (ed.), Martinus Nijhoff Publ., Hague-Boston-London, 1981, 263-267.

[5] G. Kronik, *Contrast M-mode echocardiography in patients with interatrial communications,* Ultrasound in Med. Biol., **8**, 5, 501-508 (1982).

[6] P. Niederle, P. Fridl, E. Koudelková, P. Jebavý, M. Haco, *Contrast echocardiography* (in Czech, summary in English), Vnitřní Lék, **29**, 8, 791-801 (1983).

[7] J. Roelandt, *Contrast echocardiography,* Ultrasound in Med. Biol., **8**, 5, 471-492 (1982).

[8] P. W. Serruys, M. van den Brand, P. G. Hugenholtz, J. Roelandt, *Intracardiac right-to-left shunts demonstrated by twodimensional echocardiography after peripheral vein injection,* Brit. Heart J., **42**, 5, 429-437 (1979).

ARCHIVES OF ACOUSTICS
9, 1-2, 223-232 (1984)

METHOD OF CHECKING THE FUNCTION OF IMPLANTED ARTIFICIAL VALVE BY PULSED DOPPLER ECHOCARDIOGRAPHY – IN VITRO STUDY

ANTONÍN GROŠPIC, EVA KOUDELKOVÁ,
PETR NIEDERLE

Institute for Clinical and Experimental Medicine, Prague, Czechoslovakia

FRANTIŠEK KLIMEŠ

Institute of Hydrodynamics, Czechoslovak Academy of Sciences, Prague

The usefulness of pulsed Doppler echocardiography for verifying the function of implanted Björk-Shiley tilting disc valve prosthesis was checked experimentally in vitro. The valve was built into a physical model of central blood circulation. This arrangement permitted simulating examination of the implanted valve by a pulsed Doppler device with the advantage of simplified and well defined hydrodynamic conditions.

Detection of valvular insufficiency is very sensitive and specific in contrast to valvular obstruction. This is due to the masking of the hydrodynamic signs of obstruction by flow disturbances downstream the valve despite its normal function.

The same experience was made following the clinical application of pulsed Doppler echocardiography in our Institute. The examination technique has become a routine part of the periodic postoperative follow-up of patients with implanted artificial valves.

1. Introduction

The diagnostic criteria for a routine evaluation of the function of a natural valve by pulsed Doppler echocardiography (PDE) have already been established [1, 3]. However, they cannot readily be applied to artificial valves because of some of their hydrodynamic peculiarities. Such special properties are also inherent to the Björk-Shiley (B–S) tilting disc valve prosthesis, which is most commonly implanted in our institute.

In order to define the role of PDE in the postoperative follow-up of patients with implanted B–S valves, we used two parallel approaches: the direct clinical experiment and the experiment in vitro on a hydrodynamic model of the heart. The latter approach, which has the advantage of defined circulatory conditions, is the object of this paper.

2. Method and instrumentation

The study was performed under three basic conditions: 1. normal valve function, 2. regurgitation, 3. obstruction.

The circulation model schematically represented in Fig. 1 was filled with a liquid, resembling blood in density, viscosity, electric conductivity and corpuscular character [2]. It is composed of distilled water, glycerine, sodium chloride and stabile copolymeric spherical particles averaging 10 μm in diameter.

Valve obstruction was achieved by reducing the valve disc opening angle, while regurgitation was simulated by mechanical prevention of the disc closure.

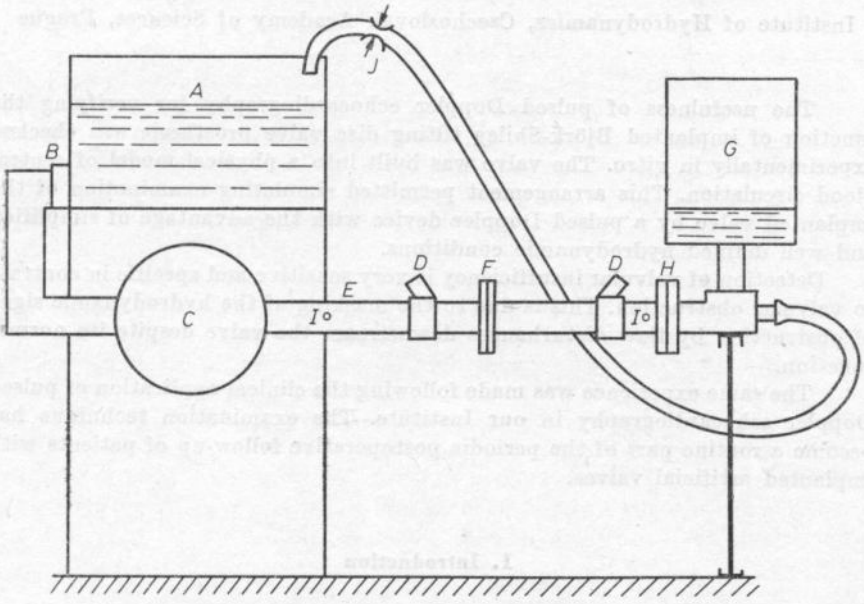

Fig. 1. Scheme of the circulation model. *A* – suspension container, *B* – valve allowing the suspension to flow only from the contained to the pump, *C* – electromagnetically driven piston pump, *D* – ultrasonic probe holders (movable along the tube *E* and rotatable around it), *E* – tube 23 mm *i.d.*, *F* – tested B–S valve, *G* – windkessel substituting the compliance (capacity) of the arterial system, *H* – probe of the electromagnetic flowmeter, *I* – fittings for pressure transducers, *J* – clamp for the control of peripheral resistance

For the PDE examination we used the module 500 *A* (Advanced Technology Lab., USA) together with the standard Echocardiovisor (Organon Teknika, Holland).

3. Results

Normal valve function

Local flow was sensed by placing the ultrasonic sample volume (SV) at various sites close to the B–S valve (up to 25 mm down – as well as upstream with respect to the valve disc).

In general, the flow downstream the valve is disturbed by the disc anb displays a turbulent character. The scheme in Fig. 2 explains the nomenclature used in further text. It also shows two basic (among many others used during the study) rotation angles β of the ultrasonic probe on the downstream side of the valve.

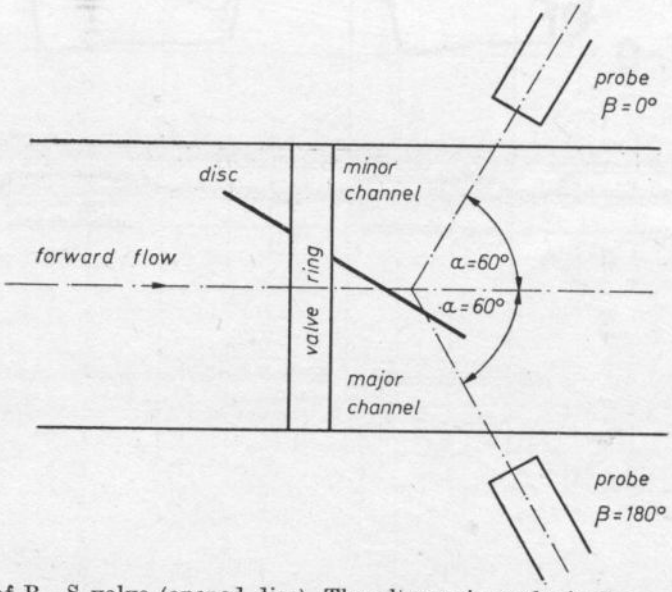

Fig. 2. Scheme of B–S valve (opened disc). The ultrasonic probe is drawn in two specific downstream positions defined by the angles of rotation $\beta = 0°$ and 180°. The ultrasonic beam is always directed under the angle $\alpha = 60°$ against the valve regardless whether the probe is on the up- or downstream side of the valve

Fig. 3 shows the experimental results with SV placed above the disc in the minor channel for $\beta = 0°$ (see the legend for curve identification). During the pump systole the flow was turbulent (abnormally scattered dots along the wave of the spatial average velocity). A negative wave during the first third of diastole mimicks regurgitation, which is, however, not confirmed by the elec-

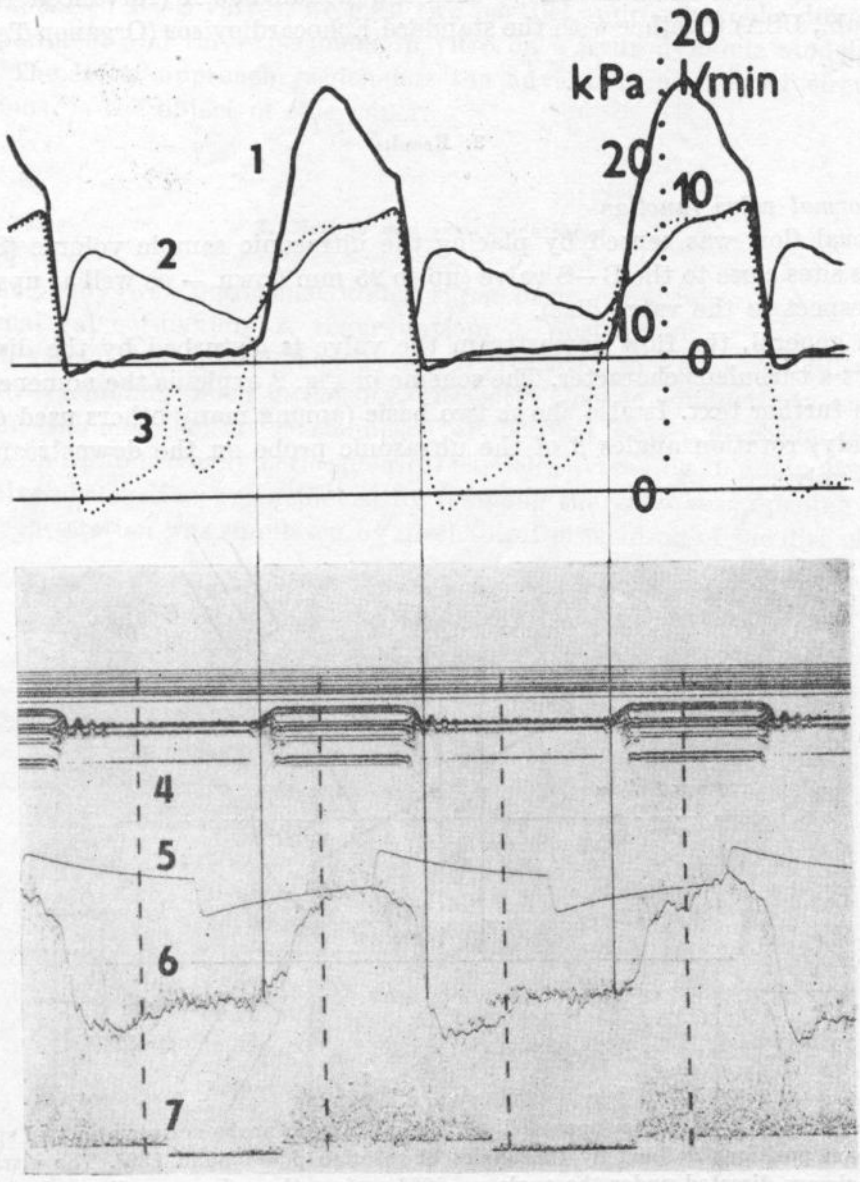

Fig. 3. Normal valve function. SV in the minor channel approximately 3 mm downstream the valve ring and 5 mm from the tube wall (i.e. $\beta = 0°$). 1 — flow sensed electromagnetically, 2 — "systemic" pressure, i.e. downstream the valve, 3 — pressure in the pump ventricle, i.e. upstream the valve, 4 — M-mode record of the valve disc action (with numerous reverberations), 5 — pump control pulses, 6 — local flow velocity sensed by the PDE system (solid line = wave of spatial average velocity within SV, dots: their scattering gives a qualitative knowledge about the width of Doppler signal frequency spectrum — this facilitates identification of the turbulence induced spectral broadening), 7 — instantaneous power of the Doppler signal (used mostly only for optimal setting of the pulsed Doppler device)

tromagnetic flowmeter. This phenomenon may be explained by flow reflection due to disc closure.

A recirculation zone with zero forward net velocity was found close to the disc [5] (Fig. 4).

In contrast to Figs. 3 and 4, Fig. 5 illustrates the situation when the ultrasonic beam was directed almost parallel to the stream in the major channel

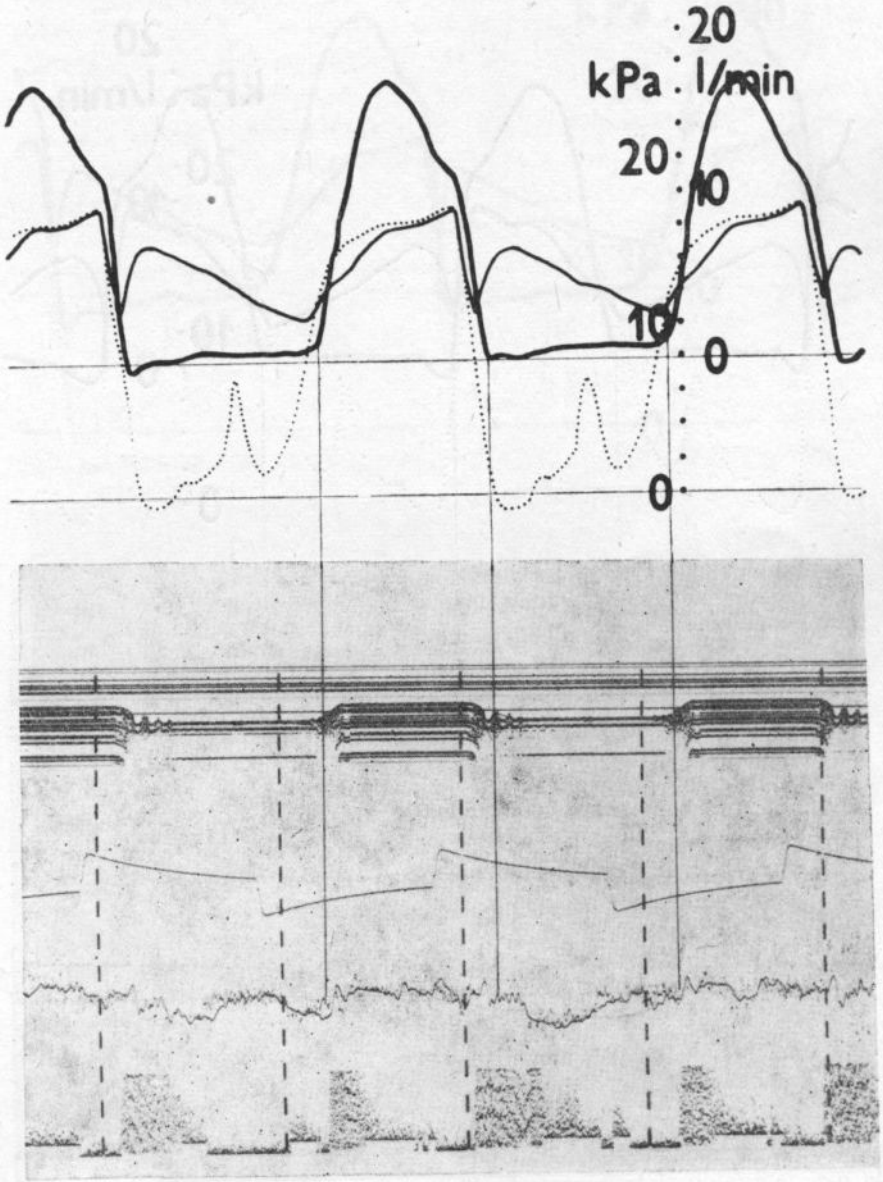

Fig. 4. Normal valve function. SV in the recirculation zone — above and close to the disc ($\beta = 0°$)

($\beta = 180°$). SV was located beneath the disc. The Doppler shift exceeded the Nyquist limit with respect to the repetition frequency of ultrasonic bursts so that higher Doppler frequencies could not be unambiguously detected. Consequently, the average velocity wave changes sharply its polarity.

Further downstream, approximately 100 mm from the valve ring, flow disturbances fade out and the flow profile becomes axisymmetrical and rather flat.

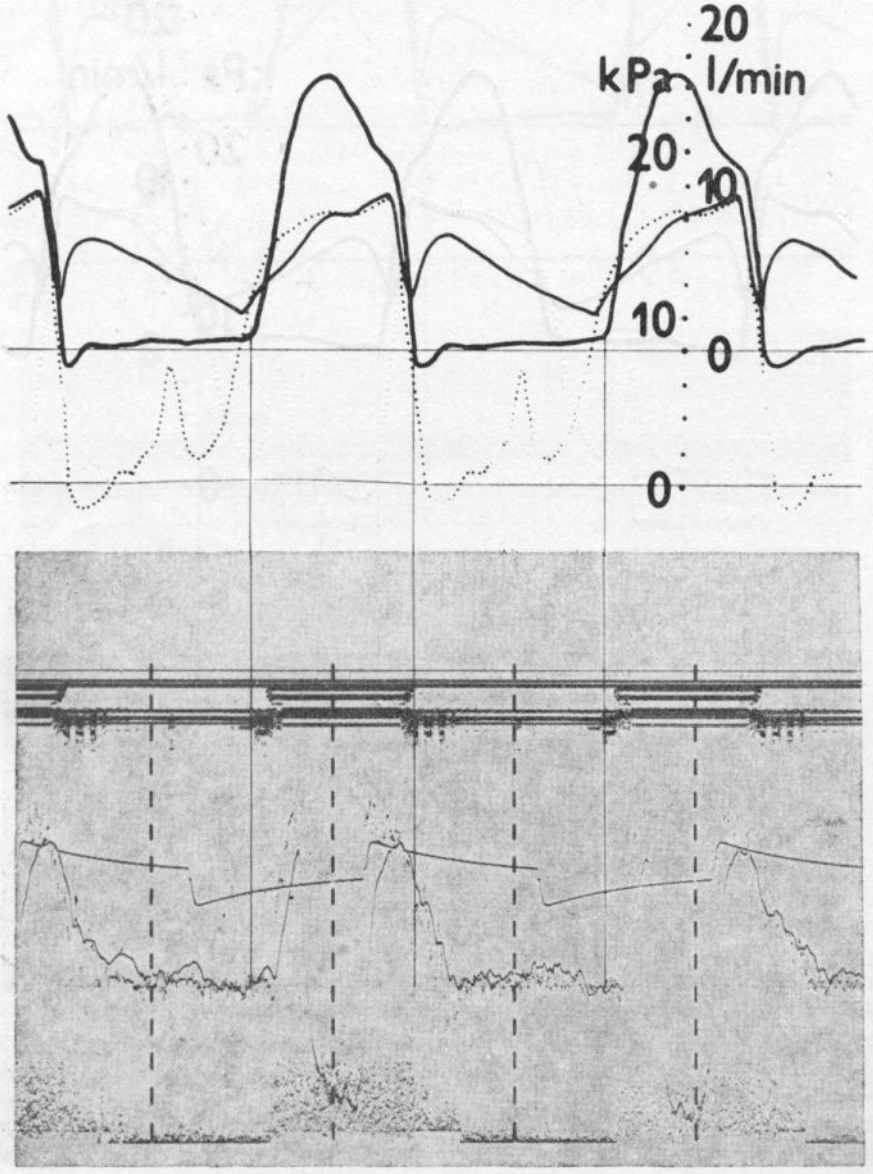

Fig. 5. Normal valve function. SV in the major channel beneath the disc ($\beta = 180°$). Nyquist limit is exceeded

As expected, the flow on the upstream side of the valve is laminar.

Obstruction

The presence of distal flow disturbances seen on examination of natural valves is a reliable sign of valvular stenosis. However, this criterion does not hold for the B—S valve because, as shown above, turbulence in the distal

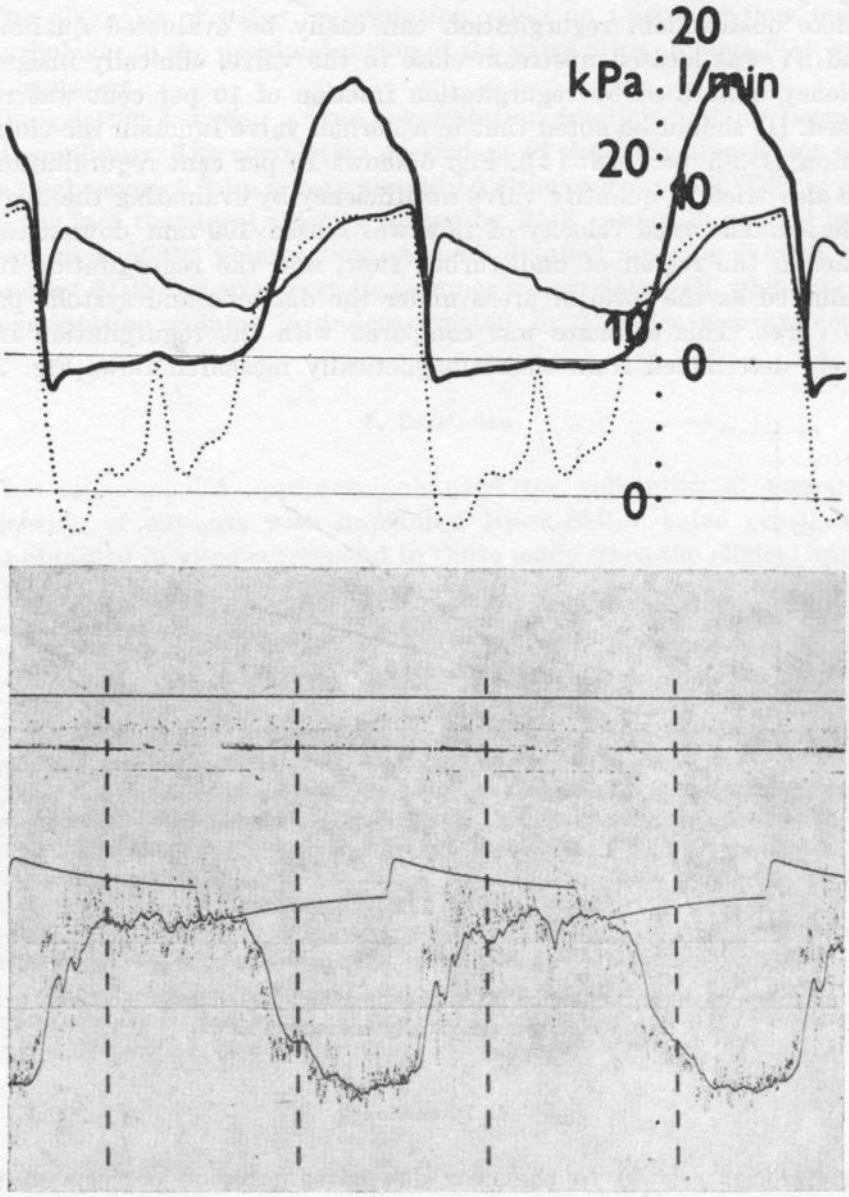

Fig. 6. Regurgitation (10 per cent). SV is placed in the near vicinity of the valve on its upstream side. Regurgitation is objectivized by electromagnetic flowmeter and also shown on velocity record by PDE

vicinity of the valve is normal. Therefore, SV should be placed further downstream where the valve disc no longer affects flow. On the other hand, the thus located SV fails to reflect sensitively and reliably even a meaningfull valve obstruction — for instance, a mean pressure gradient of 5.3 kPa in our experiment.

Regurgitation

Unlike obstruction, regurgitation can easily be evaluated qualitatively. Provided SV was located upstream close to the valve, clinically insignificant insufficiency quantified by regurgitation fraction of 10 per cent was reliably recognized. (It should be noted that in a normal valve function the closing regurgitation is 3-5 per cent [4]). Fig. 6 shows 10 per cent regurgitation.

We also tried to quantify valve insufficiency by evaluating the regurgitation fraction. The axial velocity of flow was sensed 100 mm downstream the valve, i.e. in the region of undisturbed flow, and the regurgitation fraction was evaluated as the ratio of areas under the diastolic and systolic parts of velocity curve. This estimate was compared with the regurgitation fraction objectively determined from electromagnetically measured flow (Fig. 7).

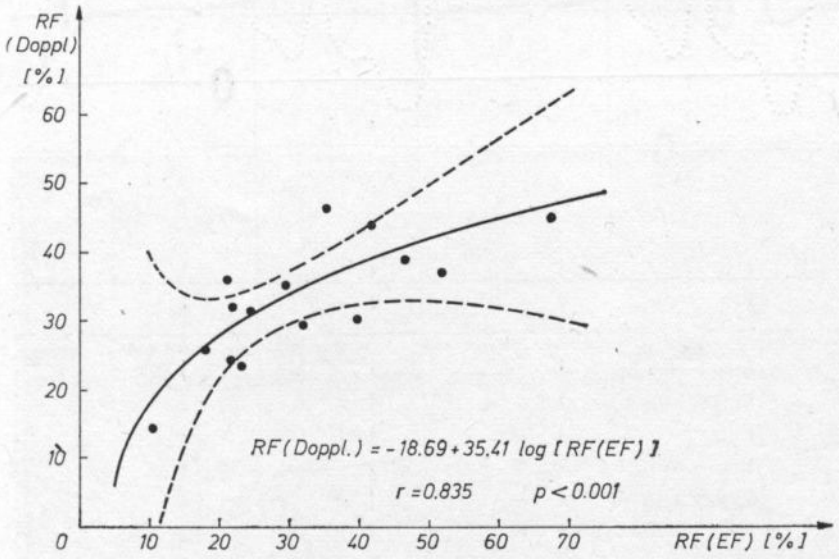

Fig. 7. Comparison of the regurgitation fraction estimated by PDE and objectively evaluated from electromagnetically measured flow

4. Discussion

Our findings related to the near downstream region correspond to the results of YOGANATHAN [5], who performed a complex flow measurement using a laser-Doppler anemometer. The valve disc induces major flow disturbances

which may thus mask obstruction. Moreover, PDE flow patterns strictly depend on SV location and ultrasonic beam direction. In clinical praxis, these topological relations cannot, however, be reliably defined, especially because of the unknown position of the valve disc plane with respect to the chest surface. On the other hand, in a more distal region, where the hydrodynamic situation becomes clear, the sensitivity of PDE to valve obstruction decreases.

The diagnosis of valve regurgitation relies on upstream flow inspection. Any turbulence in the proximal region of the valve is an obvious PDE symptom of regurgitation.

The relation between a true regurgitation fraction and its Doppler estimate is nonlinear. The correlation coefficient of the regression is not too high, as one might expect from a very simplified circulatory model. This is probably due to the fact that local velocity sensed by PDE cannot in general be a good representation of the volume flow. A more detailed analysis showed both the true and by PDE measured systolic volumes to correlate well, while in contrast, the regurgitation volume is underestimated by Doppler measurement.

5. Conclusion

This experimental approach enhanced the reliability of periodic PDE examination of patients with implanted Björk-Shiley valve prostheses. Our results obtained in vitro correspond to those made since the clinical application of PDE.

References

[1] D. W. Baker, S. A. Rubenstein, G. S. Lorch, *Pulsed Doppler echocardiography: principles and applications,* Amer. J. Med., **63**, 69-80 (1977).

[2] A. Grošpic, J. Hladovec, F. Švec, F. Klimeš, *A liquid substituting blood in experiments in vitro with ultrasonic flowmetres* (in Czech), Lékař a technika, **5**, 90-93 (1982).

[3] P. Niederle, A. Grošpic, J. Ressl, I. Beránek, *Pulsed Doppler echocardiography: physical principles, methodology and clinical application* (in Czech), Vnitř. lék., **26**, 9, 896-907 (1980).

[4] H. A. Richter, J. Schoenmackers, *Insuffizienz, Druck — and Arbeitsverlust kuenstlicher Herzklapen in Mitralposition,* Biomedizinische Technik, **24**, 43-46 (1979).

[5] A. P. Yoganathan, W. H. Corcoran, E. C. Harrison, J. R. Carl, *In vitro velocity measurements in the near vicinity of the Björk-Shiley aortic prosthesis using a laser-Doppler anemometer,* Med. Biol. Eng. and Comp., **17**, 453-459 (1979).

ARCHIVES OF ACOUSTICS
9, 1-2, 233-242 (1984)

ESTIMATION OF CARDIAC FLOW IN CHILDREN BY MEANS OF IMAGING GATED PULSE DOPPLER

A. NOWICKI, W. SECOMSKI

Institute of Fundamental Technological Research, Polish Academy of Sciences, Warsaw

M. PLESKOT

Pediatric Institute, Medical Academy, Warsaw, Poland

Imaging pulse cardiac Doppler was used to investigate congenital heart conditions in children. Preliminary investigations were carried out in a group of 15 healthy children and in 23 children with congenital heart diseases. The recordings in normal children and in children with ventricular septal defect (VSD), atrial septal defect (ASD), patent ductus arteriosus (PDA) and with coarctation of aorta (CoA) will be shown.

1. Introduction

Encouraged by the excellent work and results of HATLE and ANGELSEN [1] we modified the previously described 4 MHz Imaging Gated Pulse Doppler (IGPD) [3] to investigate congenital heart conditions in childrens. Important modifications were made to increase the workable Doppler frequency range (maximum velocity). Double repetation frequency rate was introduced; 6.7 kHz for the whole penetration range of about 12 cm corresponds to $V_{max} = 63$ cm/s (0°) and 126 cm/s (60°), 13.4 kHz (6 cm) corresponds to $V_{max} = 126$ cm/s (0°) and 252 cm/s (60°).

A set of variable high-pass Doppler filters was used to prevent the output signals of the artifacts due to the movements of the heart walls and valves. The low cut off frequency was adjustable at 200 Hz, 600 Hz or 1200 Hz. The last one was in fact the most preferable in our investigation.

The upper range of the maximum velocity 2.5 m/s at 6 cm depth was often too low for estimation of the jet velocity in VSD and CoA. In order to minimize the aliasing problems due to the range — velocity ambiguity, in pulse

Doppler systems, a new type of alias tracking technique was implemented on the basis of the HARTLEY approach [2]. The tracking unit extends the workable range of Doppler frequencies from — 1/2 PRF to PRF. In terms of velocity it is equal to 1.2 m/s and 2.5 m/s (0°) for PRF, 6.7 kHz and 13.4 kHz respectively. With some additional limitation the frequency range can be extended even up to 1 1/2 PRF.

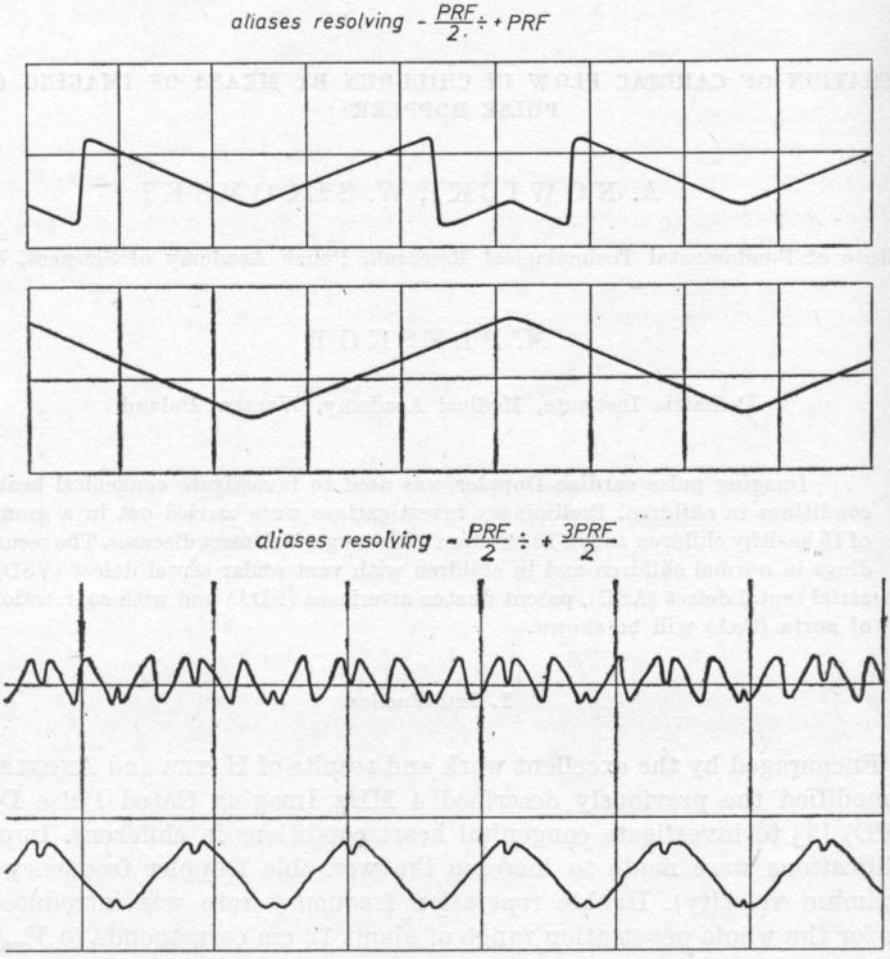

Fig. 1. Alias resolving trucker simulation for PRF (*a*) and 1 1/2 PRF (*b*)

The sample volume was 3×5 mm — transmision duration of 4 μs corresponds to ~ 3 mm in the tissue and the diameter of the ultrasonic beam in the zone of weak focusing does not exceed 5 mm.

The advantage of IGPD with its *A* scan Doppler in examination for congenital heart conditions results from the ability to visualize landmark signals in front or behind the region of interest and thus facilitate the localization of diagnostic signals.

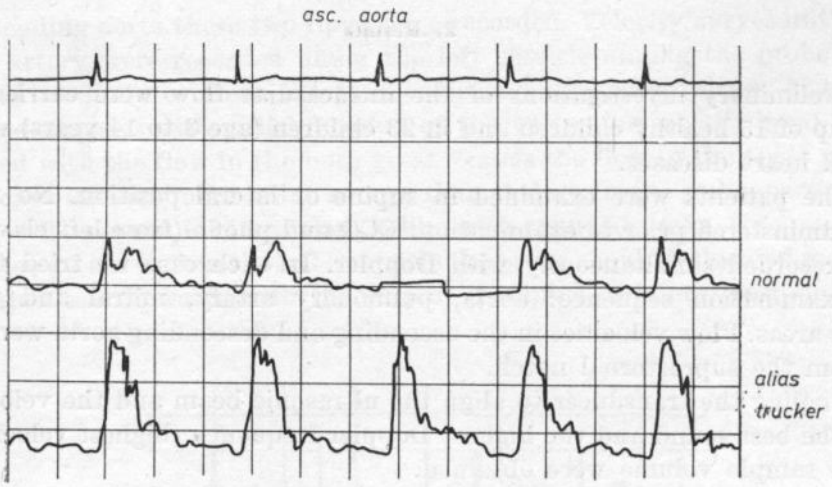

Fig. 2. Resolving of aliasing in the ascending aorta

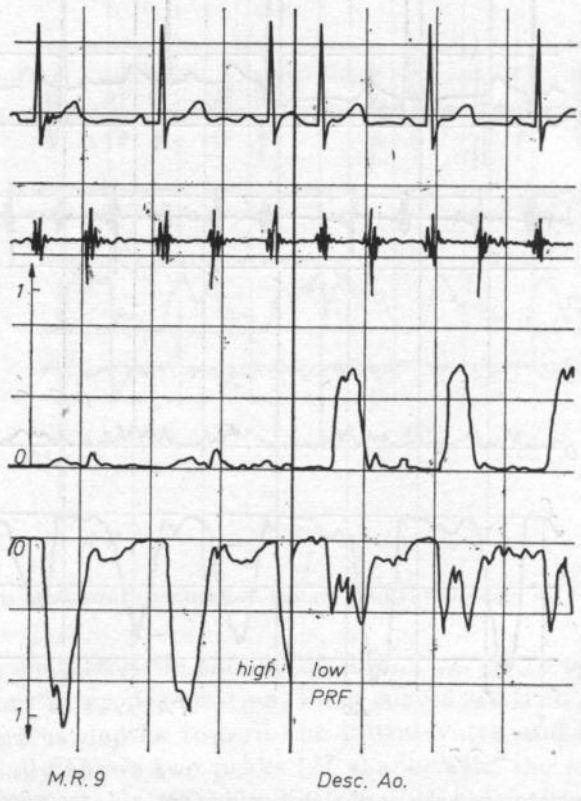

Fig. 3. Velocity recording in the descending aorta with low (6.5 kHz) and high (13 kHz) PRF. Obvious aliasing seen for low PRF

2. Results

Preliminary investigations of the intracardiac flow were carried out in a group of 15 healthy children and in 23 children (age 3 to 14 years) with congenital heart diseases.

The patients were examined in supine or lateral position. No medicine was adminstered prior to examination. ECG and phono (from left clavicle site) were recorded simultaneously with Doppler. In each case we tried to follow the examination sequence: aorta, pulmonary artery, mitral and tricuspid valves areas. Flow velocities in the ascending and descending aorta were recorded from the suprasternal notch.

Angling the transducer to align the ultrasonic beam and the velocity vectors, the best sound and the highest Doppler frequency (highest velocity peak) in the sample volume were obtained.

Aiming the probe forward and little to the right for the flow in the ascending aorta and backward to the left for the reverse (slightly smaller) flow in

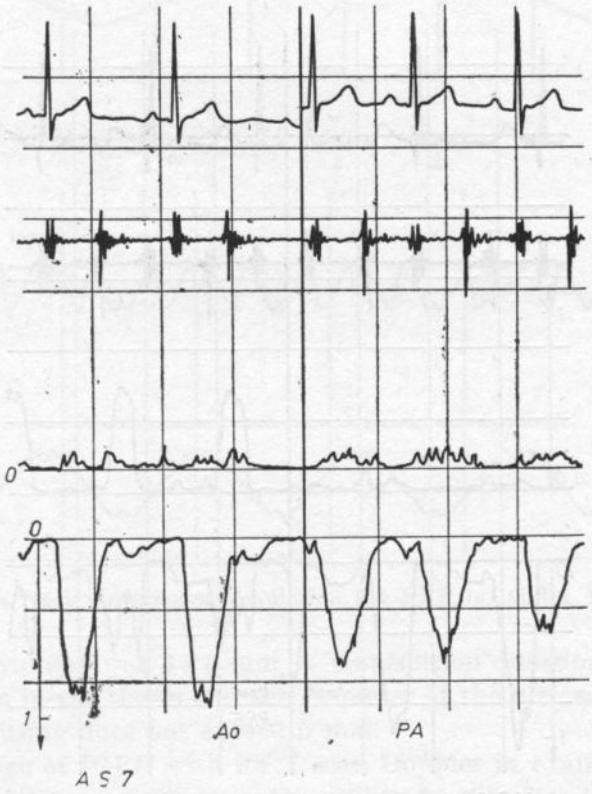

Fig. 4. Flow velocity paterns in the normal descending aorta A_0 recorded from the suprasternal notch and in the pulmonary artery PA recorded from the second intercostal space

the descending aorta these two flows were recorded. Velocity curves in the pulmonary artery were recorded under the left clavicle aiming the probe downward and medially or from the first or second intercostal space. The curve shape and characteristic "click" sound of the valves are usually good guides. Compared with the flow in the both great vessels the flow in the aorta is faster and reaches its maximum value sooner than it does in the pulmonary artery, where the flow curve is often triangle-like with rounded peaks.

To record the flow in the left ventricle the probe should be located medically to the apex and upward, with the patient in supine or lateral position.

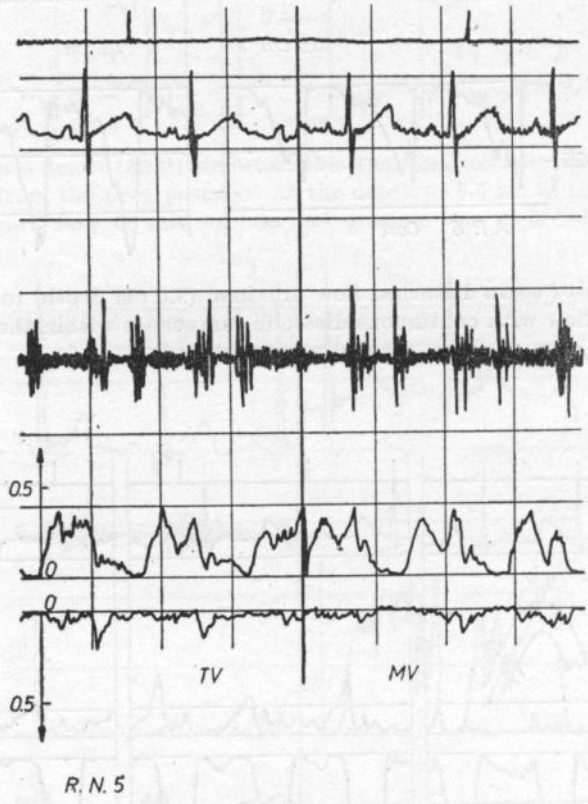

Fig. 5. Flow velocity patterns (normal) at the level of the triçuspid TV and mitral MV valves

Again, the characteristic sounds of the mitral value opening and closure clicks are primary in proper location. Flow curves are then recorded in the left ventricle at various depths toward the mitral valve and in the left atrium. Mitral flow usually shows two peaks (*M* shape) with the second peak slightly smaller — the first one in the early diastolic filling and the second in the atrial contraction.

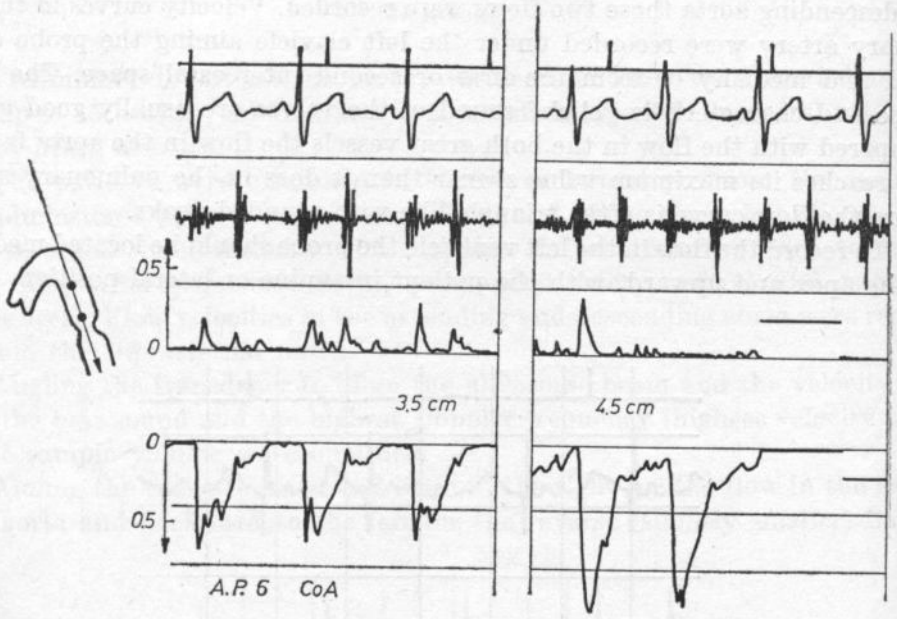

Fig. 6. Coarctation of aorta disturbed flow proximal (3.5 cm depth) to the coarctation and increased systolic flow with continuous diastolic component within the coarctation (4.5 cm depth) were recorded

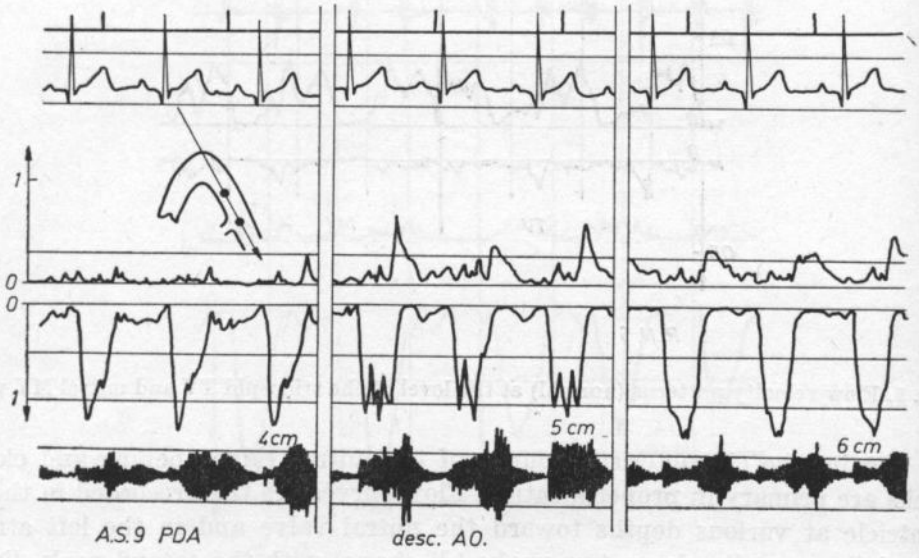

Fig. 7. Velocity patterns in the descending aorta at 4 cm, 5 cm, and 6 cm depth at patent ductus arteriosus (PDA) level (5 cm); disturbed flow was recorded in one channel and reverse flow in diastole in the second channel was recorded

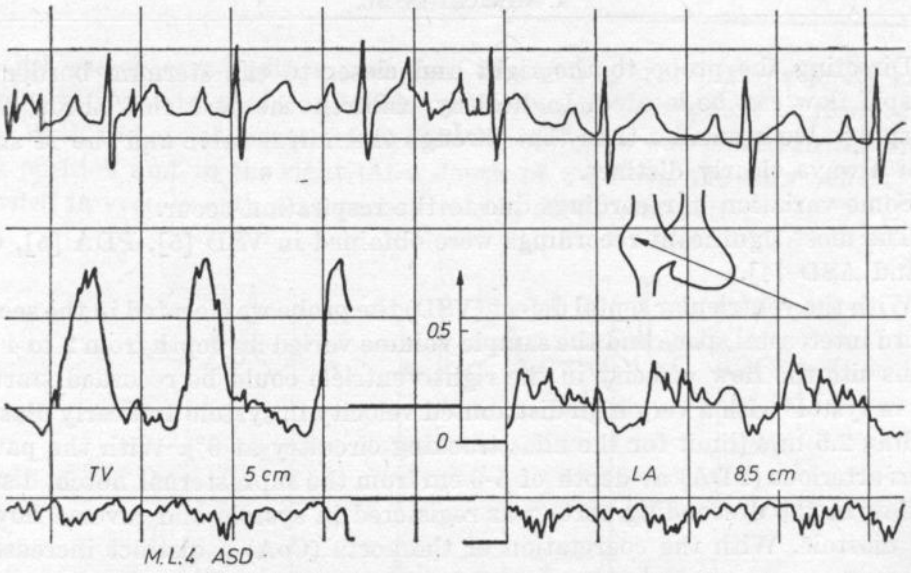

Fig. 8. For atrial septal defect (ASD) almost double abnormal velocity was recorded through the tricuspid valve from the apex position. At the depth of 8.5 cm in the right atrium forward flow in mid systole and diastole was recorded

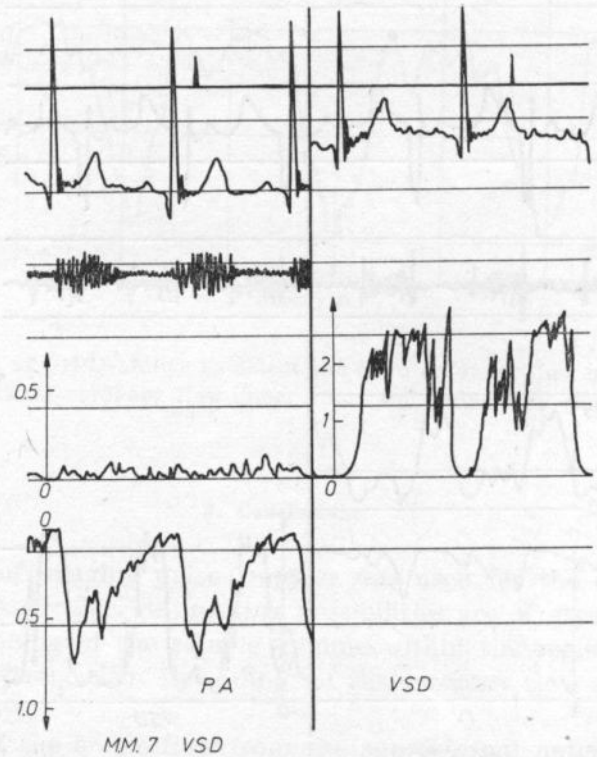

Fig. 9. Velocity recordings for ventricular septal defect (VSD). Increased velocity with irregular and prolonged descending arm in diastole in the pulmonary artery PA is noticed. High velocity (jets) through VSD exceeds velocity range (2.5 m/s) resolved with aliasing trucker

Directing the probe to the right and closer to the sternum border the tricuspid flow can be located. In healthy children the peak flow through the tricuspid valve is smaller than that through the mitral valve and the *M* shape is not always clearly distinct.

Some variation in recordings due to the respiration occur.

The most significant recordings were obtained in VSD [5], PDA [5], CoA [4] and ASD [4].

With the ventricular septal defect (VSD) the probe was located in the second or third intercostal space and the sample volume varied its depth from 2 to 4 cm. At this site the flow velocity in the right ventricle could be recorded starting early in systole with a very high distributed velocity in systole and early diastole exceding 2.5 m/s (limit for the alias tracking circuitry at 0°). With the patent ductus arterious (PDA) at depth of 5-6 cm from the suprasternal notch, disturbed flow in the descending aorta was registered in systole and reverse flow in early diastole. With the coarctation of the aorta (CoA) a distinct increase in

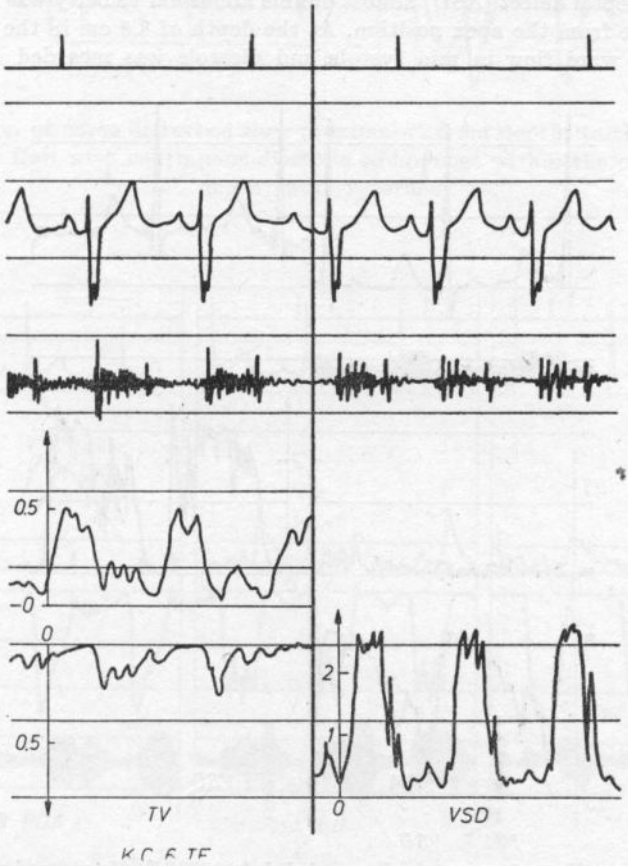

Fig. 10. Child with tetralogy of Fallot. Flow velocity through ticuspid valve is slightly increased. High velocity (over 2.5 m/s) through VSD

velocity was observed with a prolonged descending arm of the velocity curve. In general, next to the coarctation, a continuous component of flow can be seen. With the atrial septal defect (ASD), the probe was placed in the medial apex position and to the right. At a depth of 8.5-9 cm the flow velocity was recorded in systole with a secondary rise in atrial contraction.

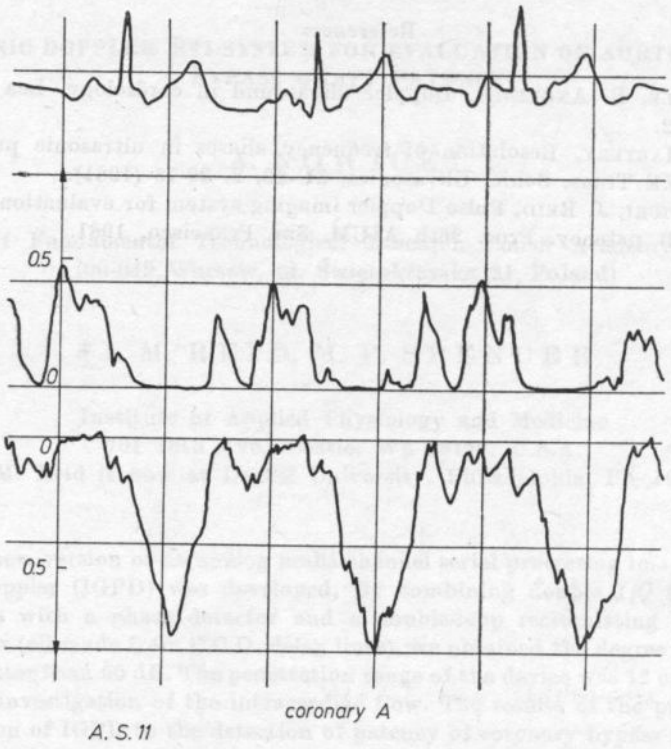

Fig. 11. An example of IGPD ability to detect the main coronary flow in a healthy child. Diastolic (two peaks: coronary flow-upper trace and pulmonary flow-lower trace)

3. Conclusions

A new type of imaging pulse Doppler was used for the examination of cardiac flow. In particular, its imaging possibilities are of great assistance in the proper positioning of the sample volume within the region of the heart chamber under investigation. Recordings of the coronary flow are good examples of this ability.

Recordings of the aortic flow from the suprasternal notch were easy to obtain in all cases (for ascending and descending aorta), giving us the important diagnostic information on the coarctation of aorta and patent ductus arteriosus.

The examination of the flow through the tricuspid and mitral valves require more experience, especially in the left and right atrium.

Location of VSD and its high jet velocities was easily performed after proper positioning of the sample volume, however, we could not estimate the peak velocity due to the maximum Doppler frequency limit of 2.5 m/s.

References

[1] L. Hatle, B. Angelsen, Doppler ultrasound in cardiology, Lea and Febiger, Philadelphia 1982.

[2] C. J. Hartley, Resolution of frequency aliases in ultrasonic pulsed Doppler velocimeters, IEEE Trans. Sonic. Ultrasonics, **SU-28**, 2, 69-75 (1981).

[3] A. Nowicki, J. Reid, Pulse Doppler imaging system for evaluation of aortocoronary bypass graft patency, Proc. 26th AIUM, San Francisco, 1981.

ARCHIVES OF ACOUSTICS
9, 1-2, 243-250 (1984)

ULTRASONIC DOPPLER MTI SYSTEM FOR EVALUATION OF AORTOCORONARY BYPASS GRAFT PATENCY

A. NOWICKI

Institute of Fundamental Technological Research Polish Academy of Sciences
(00-049 Warsaw, ul. Świętokrzyska 21, Poland)

J. M. REID, M. P. SPENCER

Institute of Applied Physiology and Medicine
701 16th Ave., Seatle, Wa 98122, U.S.A.
(J.M. Reid is now at Drexel University, Philadelphia, PA 19104)

A new version of an analog multi-channel serial processing imaging gated pulse Doppler (IGPD) was developed. By combining double I/Q fixed echo cancellers with a phase detector and a double-loop recirculating delay line integrator (all made from C.C.D. delay lines), we obtained the degree of cancellation better than 60 dB. The penetration range of the device was 12 cm permitting the investigation of the intracardiac flow. The results of the preliminary application of IGPD to the detection of patency of coronary bypass grafts will be shown.

1. Introduction

Some existing ultrasonic instrumentation has shown great promise in being effective in examination of the coronary circulation [2, 7]. The left main coronary artery has been reliably detected and stenosis at this site has been diagnosed. The technique has not had a wide use, perhaps because of difficulty in use and restriction to only some vessels.

Our work seeks to improve ease of use and ability to detect the coronary vessels by imaging the flow in the vessels. This mapping requires the rejection of echoes from the strongly reflecting but slower moving structures of the heart tissues, while retaining the weak echoes scattered by the blood. Ideally the output A mode trace amplitude should be proportional to Doppler frequency.

The first successful efforts towards practical digital realisation of such system were made by GRANDCHAMP [3], BRANDESTINI [1], and recently by HOEKS [4]. An analog solution was sought for simplicity and to provide a large dynamic range, since the strong fixed echoes from the heart could surpass the range of available "flash" $A-$to$-D$ converters.

We developed an economical and workable system which combines cancellation and phase detection to achieve a fixed-echo cancellation ratio of greater than 50 dB, thus allowing application of this technique in vivo. The first task was to build an improved pulse Doppler with a greater penetration depth than the original IGPD, developed at our Institutes [5]. The first prototype device developed in 1977 to 1978 had a penetration depth limited to about 4.5 cm, which was much too short for cardiac measurements in adults. Because of the quartz delay lines used in the stationary canceller, that system had to be operated with a frequency of 4.3 MHz. A new approach to the IGPD was developed using a stationary canceller, directonal phase detector and sweep integrator, all based on charge-coupled delay lines which have been manufactured by Reticon. The schematic diagram in Fig. 1 shows the double canceller which uses two of

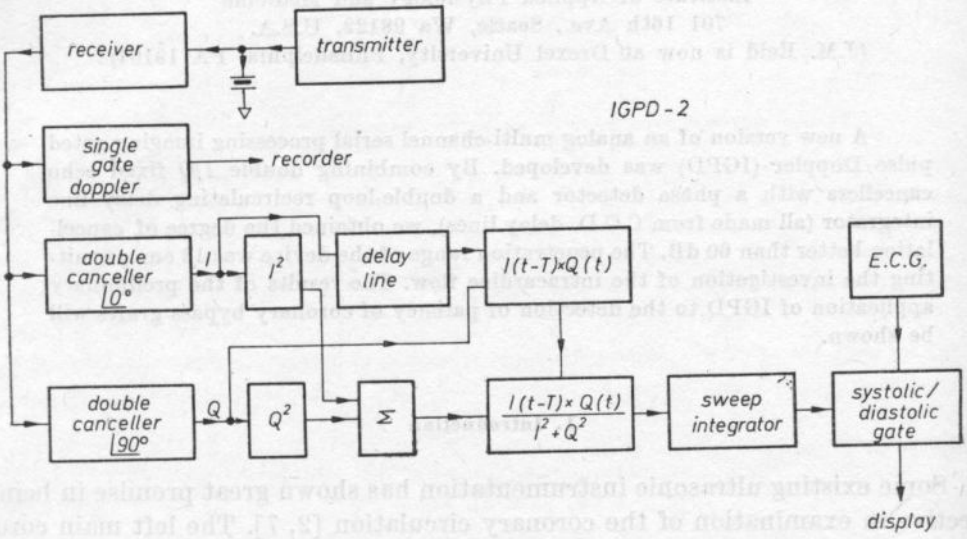

Fig. 1. A schematic diagram of the current IGPD

the CCD shift registers. The output of the double canceller consists of moving echoes only since the fixed echoes are suppressed by more than 60 dB. The only trade-off of this design, compared to the one based on quartz analog delay lines, is that the continuous delay available with quartz delay lines allowing an "infinite" number of gates has been replaced by CCD delay lines allowing 295 receiver gates of 0.5 μs duration overlapping due to 1 MHz bandwidth (along

11.5 cm penetration depth). The canceled I/Q signal after phase detection and sweep integration is applied to the diastolic gate producing the output only in diastolic gate producing the output only in diastole, when most of the coronary LAD flow occurs.

The *D.C.* Fourier transform of the output signal is equal to

$$F(\Delta\omega_d)_{D.C.} = -\frac{1}{2}j\frac{\int_{\infty}[\exp(j\Delta\omega_d T)-1]^2[\exp(-j\Delta\omega_d T)-1]^2\exp(j\Delta\omega_d T)}{\int_{\infty}[\exp(j\Delta\omega_d T)-1]^2[\exp(-j\Delta\omega_d T)-1]^2}\times$$

$$\times\frac{S(\Delta\omega_d)d\Delta\omega_d}{S(\Delta\omega_d)d\Delta\omega_d}, \tag{1}$$

where $S(\Delta\omega_d)$ is the spectral density of the input signal $f(t)$, $\Delta\omega_d$ — Doppler frequencies, T — delay time.

The term $[\exp(\pm j\Delta\omega_d T)-1]^2$ stands for double cancelation function, $\exp(j\Delta\omega_d T)$ is due to the convolution in the phase detector.

For one scatterer or ensemble of particles moving with the same velocity the received signal is $A\sin\omega_d t$. The resulting output signal (real part of (1)) is given by $1/2\sin\omega_d T$.

The interpretation of the first formula is a little more troublesome. Taking the new function,

$$K(\omega) = [\exp(j\omega T)-1]^2[\exp(-j\omega T)-1]^2 S(\omega), \tag{2}$$

we can consider it as the spectral density superimposed on periodic function. Then we obtain a very similar expression to the one for the average frequency

$$F(\omega)_{D.C.} = -\frac{1}{2}j\frac{\int_{\infty}\exp(j\omega T)K(\omega)d\omega}{\int_{\infty}K(\omega)d\omega}. \tag{3}$$

According to the Taylor series, it is equal to the sum of the first, third and higher moments of the Doppler spectrum.

The signal-to-noise ratio of the IGPD was significantly increased by the addition of a sweep integrator. Due to the nature of the flow and variations in scattering intensity in the arteries, the resulting output from the canceller varies from pulse to pulse. For that reason a double-loop recirculating delay line integrator was added [6]. The effective number of integrated profiles corresponds to $(1-k)^{-1}$, where $1-k$ is the positive feedback loop gain. We achieved a $k = 0.97$ in our implementation. This integrator exibits no unwanted oscillation even for such a high value of k. Approximately 30 successive profiles are added, thereby increasing the signal-to-noise ratio by the square root 30. The principle of sweep integration is illustrated in Fig. 2. The lower trace represents a signal from the double canceller at the input to the sweep integrator.

The middle trace represents the train of succeeding pulses at the output of the sweep integrator when the delay time of the analog shift register is set purposely to be smaller than the repetition rate. The upper trace is the final output from the integrator when the delay time is equal to the repetition rate.

The actual performance of this system is illustrated in Fig. 3. The upper trace represents the flow profiles in the common carotid artery during a 500

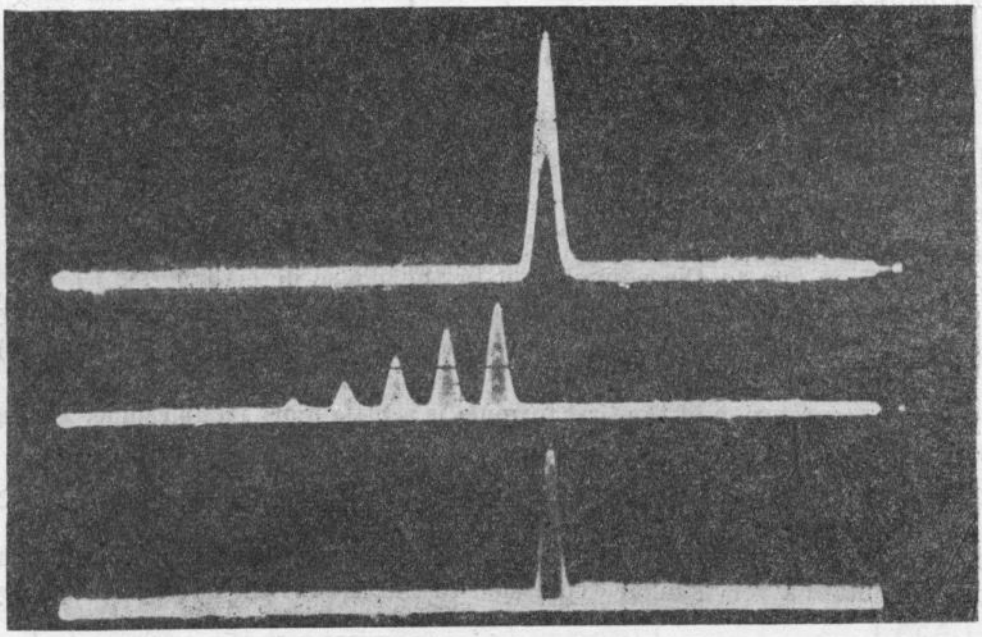

Fig. 2. The principle of sweep integration

millisecond period, this being a superposition over 100 signals from the integrator. The bottom trace represents the *RF* signal at the input to the canceller. In this case the degree of cancellation is better than 60 dB.

Improved penetration depth was achieved through a variety of improvements to the system. The addition of the sweep integrator, the lowering of the ultrasonic frequency to 4 MHz, and the use of low insertion loss, high sensitivity transducers obtained from Precision Acoustic Devices all contributed to this increased penetration depth. Flow signals were obtained from depth of 7-8 cm and large signals from valve motions were observed as deep as 11 cm. These improvements in the dynamic range and penetration depth of the IGPD have allowed us to progress to preliminary clinical evaluation of this system for detection of patency of coronary bypass grafts.

Future directions are the development of a wider range Doppler frequency determination, and the development of a true mapping display system to allow the full advantages of the instrument to be realised.

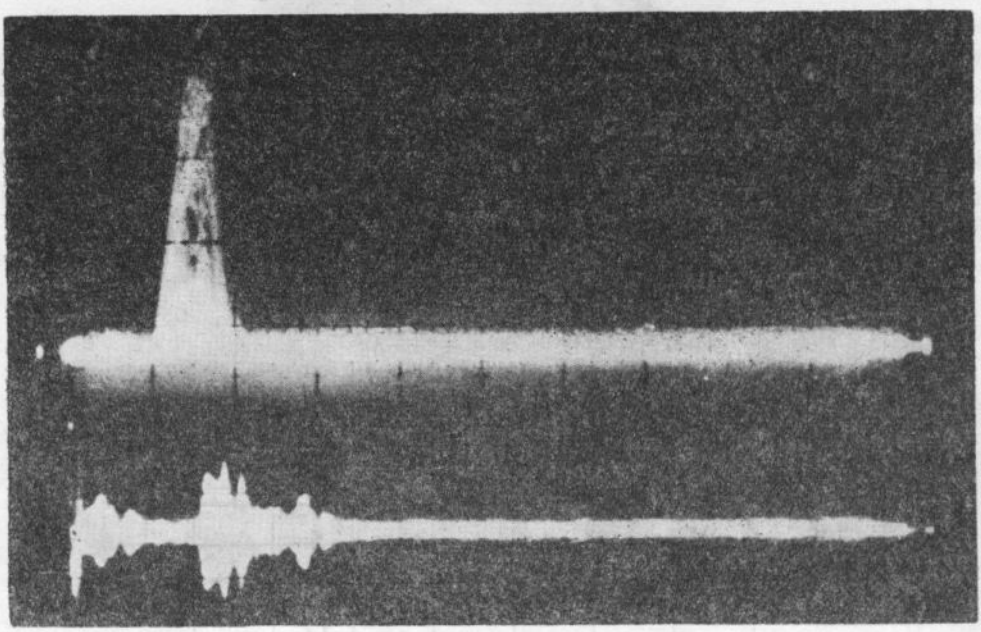

Fig. 3. The performance of the IGPD

2. Clinical results

At present we are completing the first stage of the validation of the application of the IPGD to detection of the patency of coronary bypass grafts. We concentrated mainly on grafts to the left anterior descending coronary artery LAD, because this graft is the most easily attainable via pulse Doppler. Patients were examined in the left lateral position with the probe located in the second or third intercostal space. The signal from the patent graft is expected to be found in the vicinity of the right ventricular outflow tract. The criteria of diastolic flow in close approximation to the right ventricular outflow tract was chosen to determine the patency of LAD bypass grafts. To avoid possible errors the Valsalva maneuver was often performed to eliminate signals coming from the mammary vein which may be located close to the graft. Once the graft had been located by displaying the whole penetrated range covered by the 295 gates from the IGPD, the single gate was located to provide a ZCC output for the signal corresponding to the bypass graft. An example recording of this zero-crossing output is shown in Fig. 4. Both ECG and zero-crossing output are shown in this figure. Diastolic flow is clearly evident. Separation of bypass graft signal from mammary vein signal by Valsalva maneuver is illustrated by Fig. 5. As can be seen, two diastolic signals were present before the Valsalva maneuver was performed.

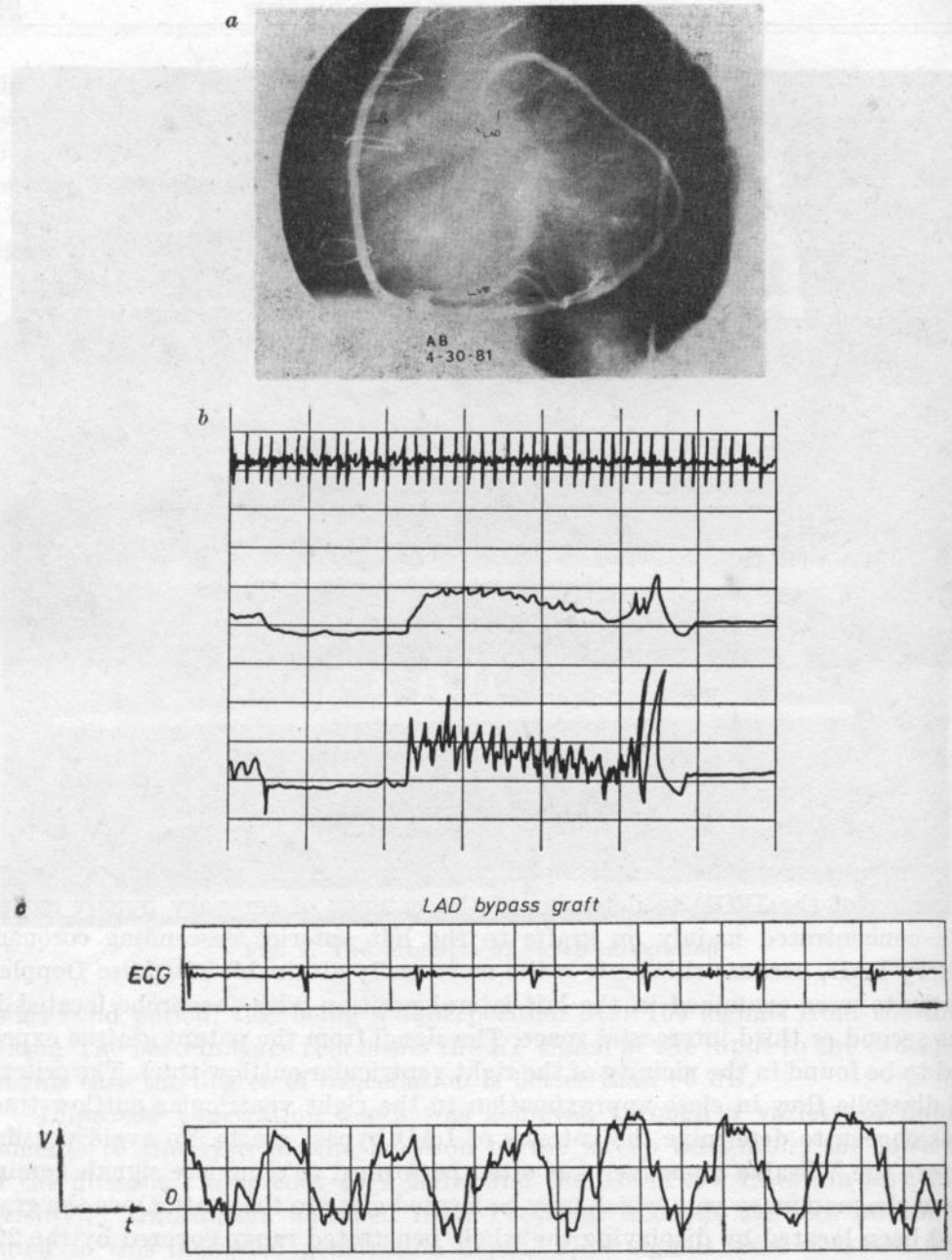

Fig. 4. A sample zero-crossing output of an LAD bypass graft signal measured transcutaneously with the IGPD. (*a*) is a left later oblique angiogram of the bypass graft done post-operatively; (*b*) is the electromagnetic flowmeter tracing of the bypass graft done inter-operatively, the middle trace being the average output for calibration and the lower trace illustrates the pulsatile waveform exhibiting the diastolic waveform when compared with the ECG; (*c*) is the zero-crossing output of the IGPD when the signale-gate is located in depth in the LAD bypass graft

After, or during the Valsalva maneuver, the diastolic flow component from the mammary vein is removed and only a diastolic flow component from the LAD bypass graft is present in the zero-crossing output.

To date this study has included examination of 15 patients with saphenous vein bypass grafts. These 15 patients were studied blind after the state of patency of their LAD bypass graft was determined by angiography. Of the 15 patients studied, 10 had patent LAD bypass grafts, and 5 had occluded LAD bypass grafts. No appropriate diastolic signal was found in the five patients

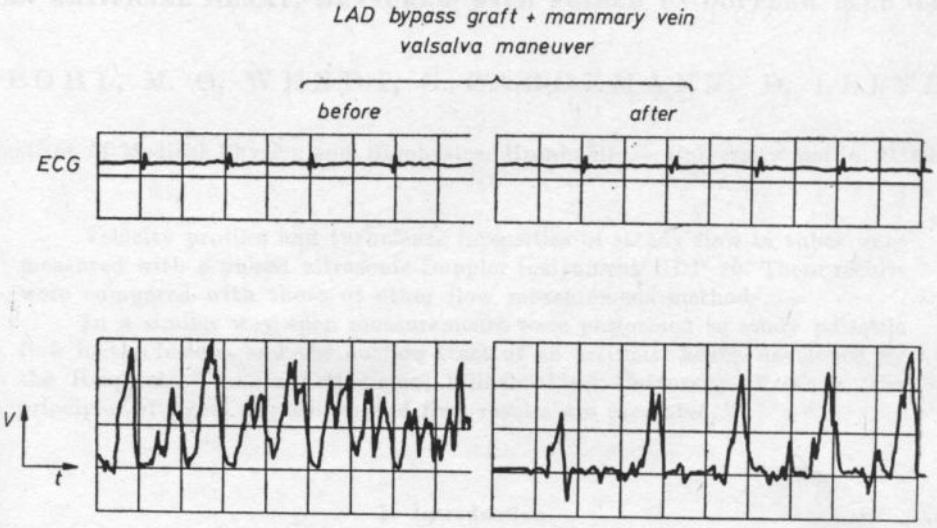

Fig. 5. Superposition of LAD bypass graft and mammary vein signals separated by the Valsalva maneuver

with occluded LAD grafts, which could be interpreted as a flow signal in such a graft. Of the ten patients determined to have a patent graft by angiography, six were found to have patent grafts via examination using the IGPD. Of those four patients with patent grafts that were not detected through our examination, three were patients examined very early in the study. This indicates a significant learning curve may be present with the use of the IGPD in its current signale *A*-mode output state.

References

[1] M. Brandestini, *Topoflow digital full range Doppler velocity meter,* IEEE Trans. on Sonics and Ultrasonics, **SU-25**, 287 (1978).

[2] B. Diebold *et al., Noninvasive assessment of aortocoronary bypass graft patency using pulse Doppler echocardiography,* Am. J. Cardiology, **43**, 10-16 (1979).

[3] P. A. Grandchamp, *A novel pulsed directional Doppler velocimeter. The phase detection principle,* E. Kazner (ed.), Publ. Exc. Medica (1975), Amsterdam, 122-132.

[4] A. P. G. Hoeks *et al., A multi-gate pulse Doppler system with serial data processing,* IEEE Trans. on Sonics and Ultrasonics, **SU-28**, 4, 242-247 (1981).

[5] A. Nowicki, J. Reid, *An infinite gate pulse Doppler,* Ultrasound in Med. and Biol., **7**, 41-50 (1981).

[6] H. Urkowitz, *Analysis and synthesis of delay line periodic filters,* IRE Trans. on Circuit Theory, **CT-4**, 2 (1957).

[7] A. Weyman *et al., Noninvasive visualization of the left main coronary artery by cross-sectional echocardiography,* Circulation, **54**, 2, 169-174 (1976).

ARCHIVES OF ACOUSTICS
9, 1-2, 251-256 (1984)

CHARACTERISTICS OF FLUID DYNAMICS IN TUBES AND THE OUTFLOW TRACT OF AN ARTIFICIAL HEART, MEASURED WITH PULSED US DOPPLER TECHNIQUE

M. POHL, M. O. WENDT, G. PARDEMANN, D. LERCHE

Institut of Medical Physics and Biophysics, Humboldt – University Berlin, GDR

Velocity profiles and turbulence intensities of steady flow in tubes were measured with a pulsed ultrasonic-Doppler instrument UDP 30. These results were compared with those of other flow measurement methods.

In a similar way such measurements were performed to study pulsatile flow in the inflow- and the outflow-tract of an artificial heart, developed by the Hospital of Internal Medicine, Wilhelm-Pieck-University, Rostock. The principles of signal acquisition and first results are presented.

1. Introduction

Interest in flow characteristics of artificial hearts – inside the ventricle and in the inflow and the outflow tract – is stimulated by the development of these implantable organs.

The knowledge of distributions of velocities in flowing blood and of the existence of so-called dead zones and regions with high degree turbulences is important. If the shear stresses exceed upper and lower borderline-values, blood cells and vessel walls may be damaged. Perhaps, these effects may contribute to thrombosis.

In vitro measurements of flow characteristics are made with laser Doppler anemometers, hot film anemometers and pulsed ultrasonic Doppler techniques. Furthermore, the flow behaviour can be watched by photographic or cinematographic methods. Flow patterns were studied in a model of circulation outside of artificial hearts by STEVENSON [1], REUL [2], CHANDRAN [3] and PELISSIER [4]. Their results are transferable to our system only with restric ions, because the flow characteristics are influenced strongly by the geometric forms of the ventricle and valves. Therefore, it is our aim to study the flow patterns inside and outside of the artificial heart.

2. Experimental methods and results

We used for flow velocity measurements the range-gated (ultrasonic) Doppler instrument, UDP 30, produced by Techpan, Warsaw. In order to test the aptitude of the Doppler unit to our purposes, the steady flow in tubes was studied by a simple set up, presented in Fig. 1.

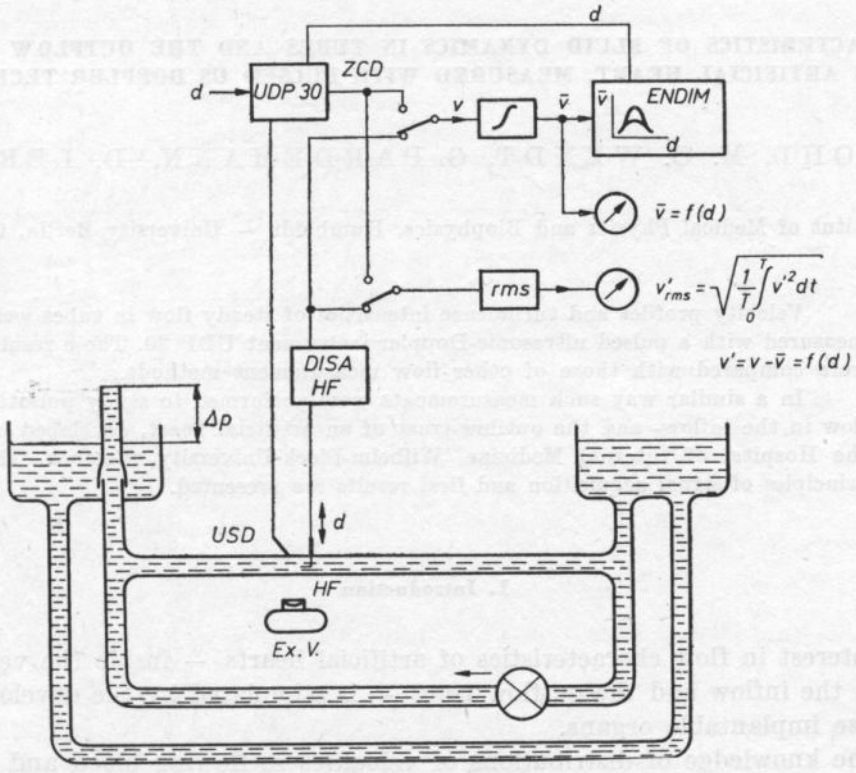

Fig. 1. Set up for steady flow measurements

We used as backscattering particles Callocryl in water, diameter 100 to 150 μm. Doppler measurements in circular tubes were compared with hot film flow measurements using a Disa electronic instrument (with physical parameters: entry length of 2 m; Reynolds numbers of 800 to 6000).

The results, shown in Fig. 2, demonstrate that UDP 30 is suitable for measurements of velocity profiles in such tubes, also in cases with non-laminar flow. The root mean square-values of velocity fluctuations are a useful measure of turbulence intensities, obtained with the UDP 30 and the hot film anemometer. The results of the measurements differ considerably near the wall, probably due to the limited resolution in depth of the UDP 30 instrument (1 to 2 mm).

The limited time resolution of the zero-crossing detector built in the UDP 30 is another reason for the observed differences. Furthermore, it should be stressed that from these measurements it is not possible to calculate the Reynolds shear-stresses. But these values would be very important in the sense of mechanical damage of blood cells (RBC and platelets) and vessel walls.

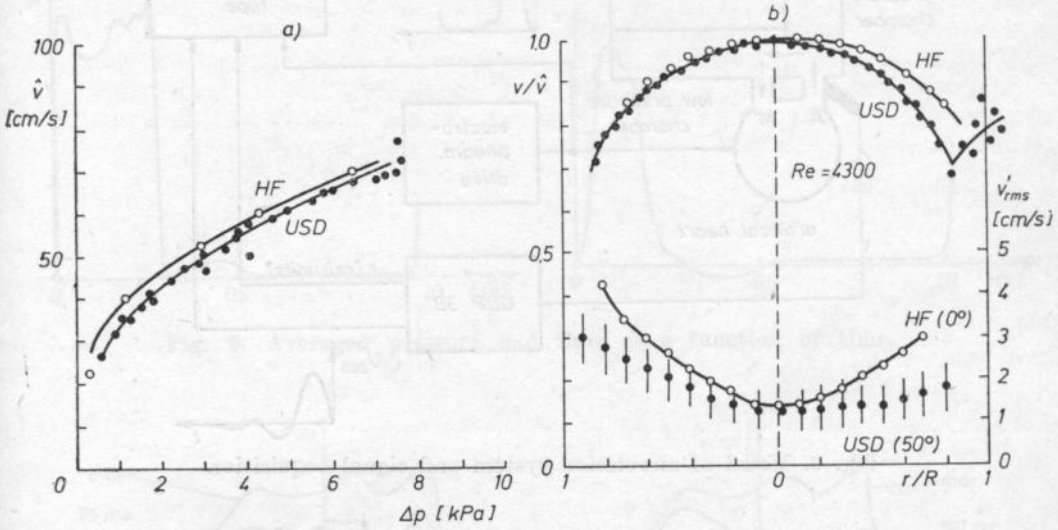

Fig. 2. Comparison between UDP 30 and hot film flow measurements: *a.* flow velocity maximum as a function of pressure, *b.* velocity profile and turbulence intensity for $Re = 4300$

In order to measure the inflow and outflow characteristics of the artificial heart, the ventricle is connected with a model of the circulation system, consisting of two pressure chambers, as depicted in Fig. 3. The high pressure chamber with a variable windkessel is connected with a low pressure chamber by an adjustable gap, simulating peripheral resistance. A pneumatic device drives the membrane of the ventricle. The beat frequency and systolic flow time can be adjusted. There are also shown the data processing, off-line registration on Thermionic magnetic tape and averaging in a DEC LINC 8 computer. An exact triggering signal was derived from the steepest ascent of the pressure curve.

Aortic flow curves are shown in Fig. 4, measured at a distance of 9 cm from the valve of Björk-Shiley type (*R*-flow near the wall, *Z*-central flow). These curves are not averaged. Here are clearly demonstrated the strong velocity fluctuations after the systolic flow period due to turbulent flow conditions.

The flow conditions in the inflow tract are similar, also measured at a distance of 9 cm from the mitral valve.

Fig. 5 presents pressure and flow as a function of time, measured in a selected volume element of the aorta. The curves are averaged over 32 cycles.

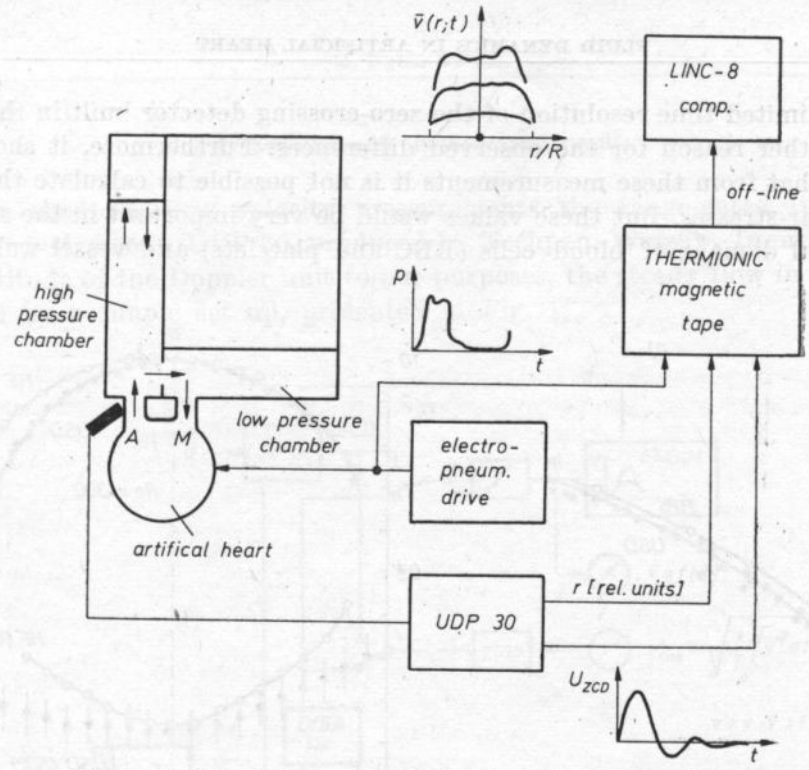

Fig. 3. Model of circulation system and signal acquisition

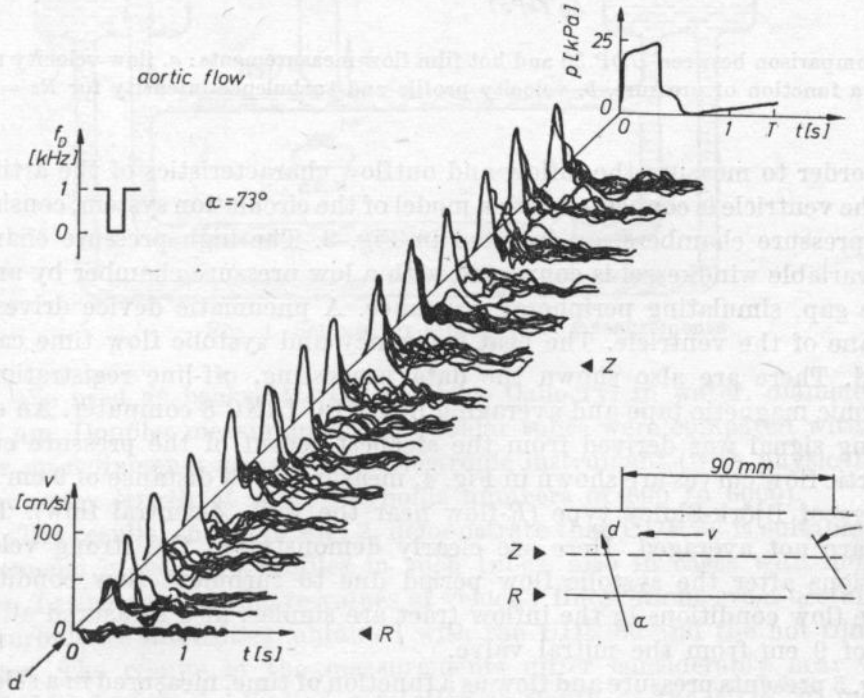

Fig. 4. Aortic flow curves (non-averaged) at different depth of tube

Velocity profiles are constructed from such curves for different times in the cardiac cycle (Fig. 6). From these, it is obvious that the velocity maximum depends on the time and radial position in the aorta. It should be noted that the flow behaviour in the aorta, especially the backflow after the systolic time, corresponds to theoretical predictions, given by WOMERSLEY [5].

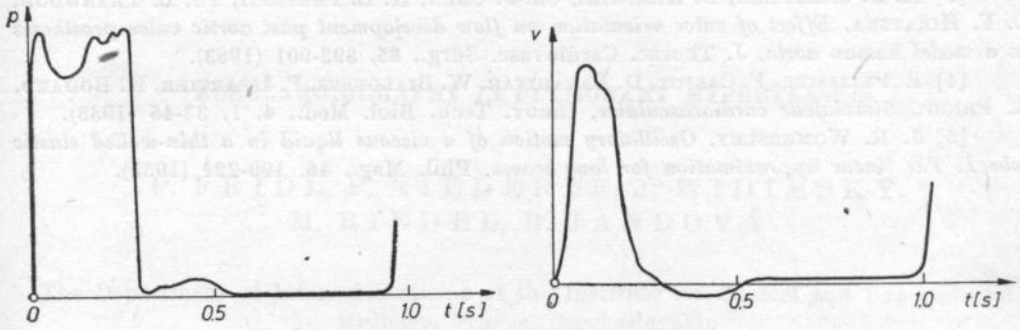

Fig. 5. Averaged pressure and flow as a function of time

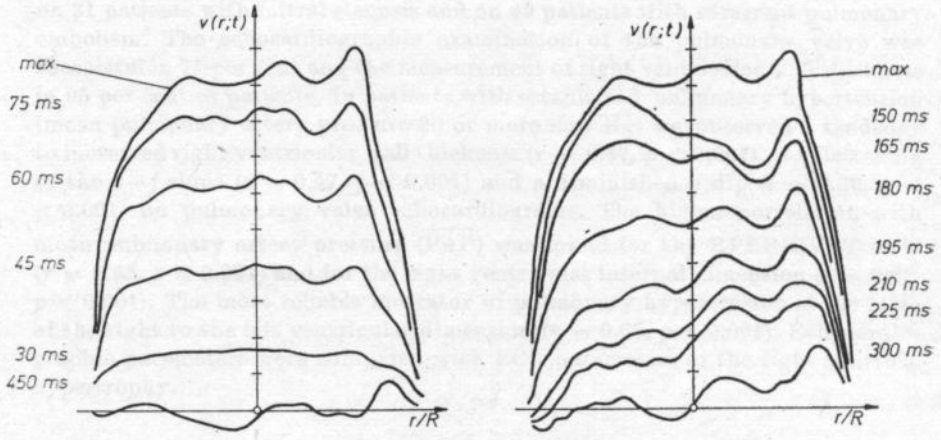

Fig. 6. Velocity profiles for different times in the cardiac cycle

3. Conclusions

The pulsed US Doppler technique is useful for measurement of velocity distributions in steady and pulsatile flow, results for turbulence intensities and shear stresses from zero-crossing signals are possible only to a limited extent.

Further measurements with combined *B*-mode/pulsed Doppler technique and FFT-spectral analysis in real time are in preparation.

References

[1] D. M. Stevenson, A. P. Yoganathan, R. H. Franch, *The Björk-Shiley heart valve prostheses,* Scand. J. Thor. Cardiovasc. Surg., **16**, 1-7 (1982).

[2] H. Reul, *In-vitro evaluation of artificial heart valves,* Adv. Cardiovasc. Phys., **5**, IV, 16-30 (1983).

[3] K. B. Chandran, B. Khalighi, Ch.-J. Chen, H. L. Falsetti, Th. L. Yearwood, L. F. Hiratzka, *Effect of valve orientation on flow development past aortic valve prostheses in a model human aorta,* J. Thorac. Cardiovasc. Surg., **85**, 893-901 (1983).

[4] R. Pelissier, F. Cassot, D. Farahifar, W. Bialonski, P. Issartier, H. Bodard, A. Friggi, *Simulateur cardiovasculaire,* Innov. Tech. Biol. Med., **4**, 1, 33-45 (1983).

[5] J. R. Womersley, *Oscillatory motion of a viscous liquid in a thin-walled elastic tube I. The linear approximation for long waves,* Phil. Mag., **46**, 199-221 (1955).

ARCHIVES OF ACOUSTICS
9, 1-2, 257-266 (1984)

ECHOCARDIOGRAPHY IN PULMONARY HYPERTENSION

P. FRÍDL, P. NIEDERLE, J. WIDIMSKÝ,
M. RIEDEL, R. JANDOVÁ

The Department of Internal Medicine of the Institute for Clinical and Experimental Medicine, Prague, Czechoslovakia

Echocardiographic and haemodynamic examinations were performed on 31 patients with mitral stenosis and on 49 patients with recurrent pulmonary embolism. The echocardiographic examination of the pulmonary valve was successful in 71 per cent and the measurement of right ventricular wall thickness in 95 per cent of patients. In patients with established pulmonary hypertension (mean pulmonary artery pressure 20 or more mm Hg) we observed a tendency to increased right ventricular wall thickness ($r = 0.47$, $p < 0.001$), the flattening of the $e-f$ slope ($r = 0.47$, $p < 0.001$) and a diminished a dip ($r = 0.36$, $p < 0.001$) on pulmonary valve echocardiograms. The higher correlation with mean pulmonary artery pressure ($\overline{PAP}$) was found for the RPEP/RVET ratio ($r = 0.55$, $p < 0.001$) and for the right ventricular internal dimension ($r = 0.65$, $p < 0.001$). The most reliable indicator of pulmonary hypertension is the ratio of the right to the left ventricular dimension ($r = 0.68$, $p < 0.001$). Echocardiographic parameters were compared with ECG parameters of the right ventricle hypertrophy.

1. Introduction

The degree of pulmonary hypertension (PH) is one of the most important prognostic factors in chronic pulmonary diseases. Moderate PH (mean pulmonary artery pressure 20-30 mm Hg) cannot be reliably detected by clinical methods — it can be only confirmed by direct pulmonary artery pressure measurements. Echocardiography is a modern non-invasive method, which makes possible the detection of the pulmonary valve (PV) and the measurement of the right ventricle (RV). The aim of our study is the critical reassessment of the diagnostic value of echocardiography in the detection of PH.

2. Methods

We studied two groups of patients: one group with reccurent pulmonary embolism (PE), who underwent heart catheterization and pulmonary angiography and another group with mitral stenosis (MS), also confirmed by haemodynamic examination. Echocardiographic examination was carried out by the one-dimensional *M*-mode technique with the Echo-cardio-Visor 03 (Organon Teknika, Holland). A 2.25 MHz transducer placed in the standard left parasternal position was used. We paid special attention to the echocardiogram of PV and RV. The interval between the invasive and non-invasive examinations ranged from 2 to 4 days.

The PV was examined in 49 patients with PE and in 31 patients with MS (average age 45.5 years). In the echocardiogram of the PV we evaluated diastolic $e-f$ slope, systolic opening $b-c$ slope and the maximum amplitude of the a dip. Using simultaneously recorded ECG we determined the right ventricular preejection period (RPEP) – as the interval between Q-wave and the onset of the valve opening, and the right ventricular ejection time (RVET) – as the interval between the valve opening and its closure. We used the RPEP/RVET ratio in our study.

RV examination was performed in 36 patients with PE and in 31 subjects with MS (average age 44.2 years). The right ventricular internal dimension (RVID) and right ventricular wall thickness (RVWT) were estimated at the peak of the R-wave of ECG. In cases when the endocardium could not be reliably identified, we suggest the RVD estimation 5 mm behind the anterior chest wall, as recommended by MATSUKUBO *et al.* [13]. The examined echoparameters of the PV and the RV were compared with the mean pulmonary artery pressure ($\overline{PAP}$).

We decided to prove the possibility of the combination of echocardiographic and electrocardiographic examinations in the detection of PH. We considered the echocardiographic examination to be positive when the right ventricular diameter was above 30 mm and/or the ratio of the right to the left ventricular diameter was higher than 0.5. In the case when the right ventricular wall was above 5 mm we considered the echofinding as positive only when at least one abnormal pulmonary valve parameter was present (i.e. the $e-f$ slope above 15 mm/s, the a dip 2 mm or less, and the RPEP/RVET ratio 0.5 or more). The electrocardiographic criteria of PH established by WIDIMSKÝ [25] were evaluated in our study. For positive diagnosis of PH in combination of both methods, either the positive echocardiography or the positive ECG was considered sufficient.

3. Results and discussion

The PV echogram of good quality was obtained for 57 patients, i.e. in 71 per cent. Echocardiographic detection of the PV is very difficult due to the anatomic position of the PV with respect to the anterior chest wall and its ten-

dency to be overlapped by pulmonary tissue during at least a part of the respiratory cycle [23]. Successful imaging of the PV is reported to range between 19.6 and 80 per cent [1, 2, 9, 11, 14, 15, 19] and this percentage seems to be higher in PH, when the PV echo becomes stronger and more easily detectable [6, 19]. The success rate is rather low in patients with chronic obstructive lung disease.

We observed only loose correlation between $\overline{PAP}$ and the pulmonary valve $e-f$ slope flattening (Fig. 1) with correlation coefficient 0.47 ,and no correlation was found between the mean pulmonary artery pressure and the pulmonary $b-c$ slope.

We found an inverse but also loose linear correlation between $\overline{PAP}$ and the depth of the a dip (correlation coefficient was 0.36 — Fig. 2). All of these parameters may vary with respiration and, therefore, regular breathing should be maintained during echocardiographic examination [6, 23]. The depth of the a dip is caused by the contraction of the right atrium and it depends significantly on the pressure gradient between the pulmonary artery and the right ventricle in the end diastole [14]. In patients with severe PH ($\overline{PAP}$ over 40 mm Hg) it is completely absent, but in the presence of RV failure the a dip occurs again, or its depth increases [1, 2, 7, 10, 12, 14, 24]. It may also be influenced by the contraction of the enlarged left atrium in patients with MS [16]. We think therefore that the $e-f$ slope and the a dip yield only complementary information in patients with existing PH.

The highest correlation coefficient in PV examination was found between the RPEP/RVET ratio and $\overline{PAP}$: $r = 0.55$ (Fig. 3). This ratio is the most frequently used parameter for detection of the present PH, because it does not vary with respiration and age [8]. As the difficulties with the accurate determination of the end of the RVET are well known (we were successful in 46 subjects), it was recommended to record the echocardiogram and the phonocardiogram together [17, 20].

The evaluation of the RVID and especially the determination of the RVWT are also associated with a number of technical problems (the precise identification of the endocardium and the epicardium of RV). The successful rate of good quality of the RVWT echogram depends on the site of visualisation, the position of the patients, the position, angulation and type of transducer [22]. In our study the successful estimation of this parameter was possible in 95 per cent of patients.

The RVWT exhibited a loose correlation with $\overline{PAP}$: $r = 0.47$ (Fig. 4), the specificity of this seems to be limited as well, probably due to technical problems with precise measurement.

A various degree of RV dilatation was demonstrated in patients with PH [5, 11, 15, 18, 21]. DEVEREUX *et al.* [4] demonstrated a significant relation between the RVID and the RV mass at autopsy. We found a significant correlation between this parameter and $\overline{PAP}$: $r = 0.65$ (Fig. 5). The increase of this

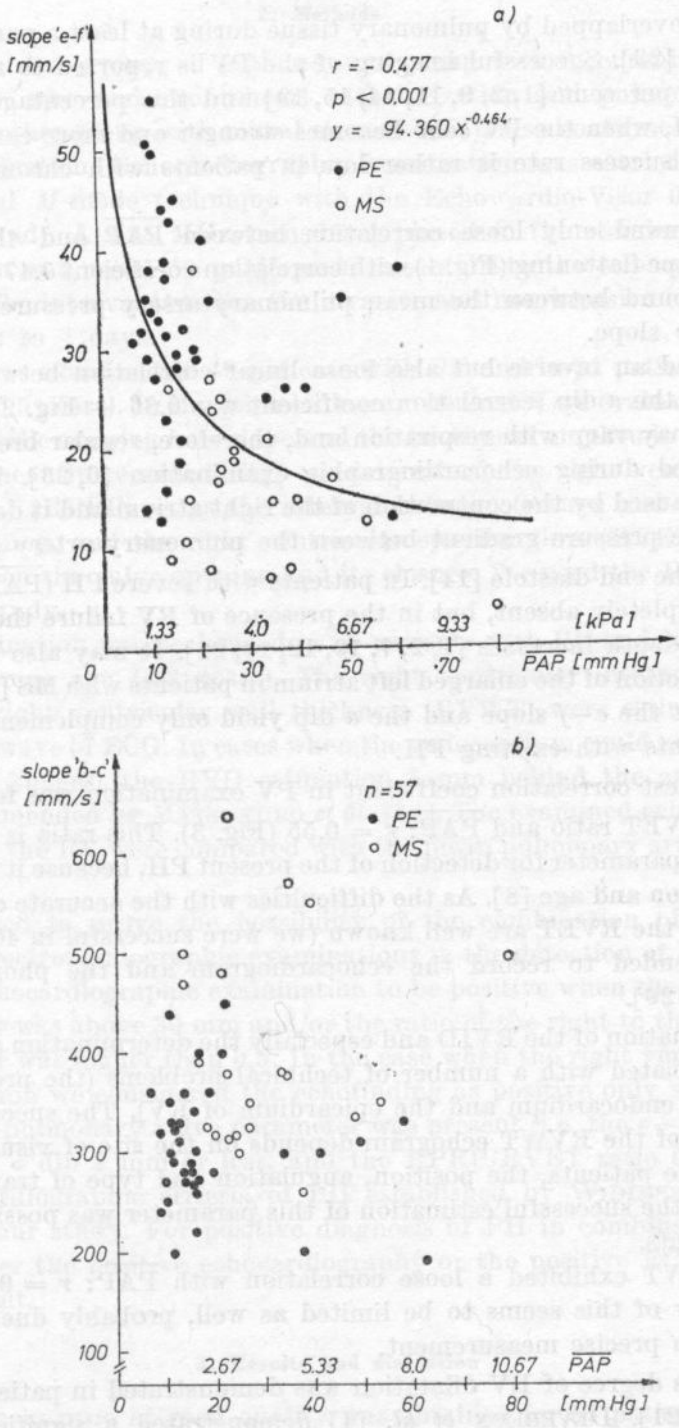

Fig. 1. The correlation between $e-f$ slope, $b-c$ slope and $\overline{PAP}$

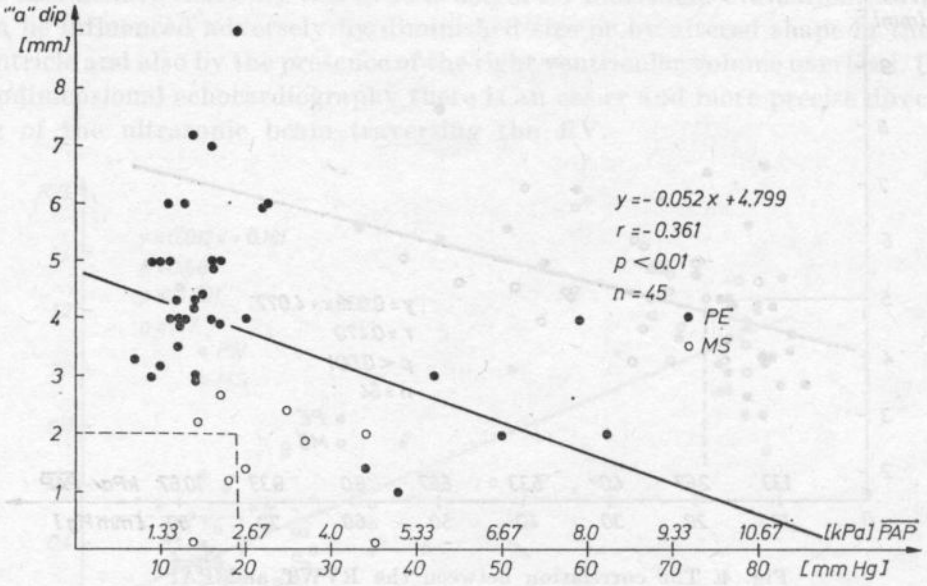

Fig. 2. The correlation between the *a* dip of the pulmonary valve and $\overline{PAP}$

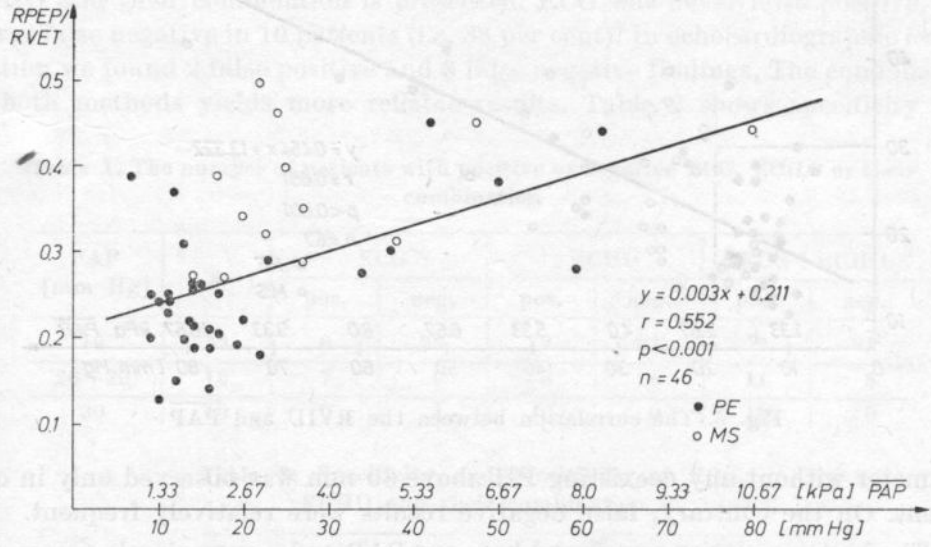

Fig. 3. The correlation between the RPEP/RVET ratio and $\overline{PAP}$

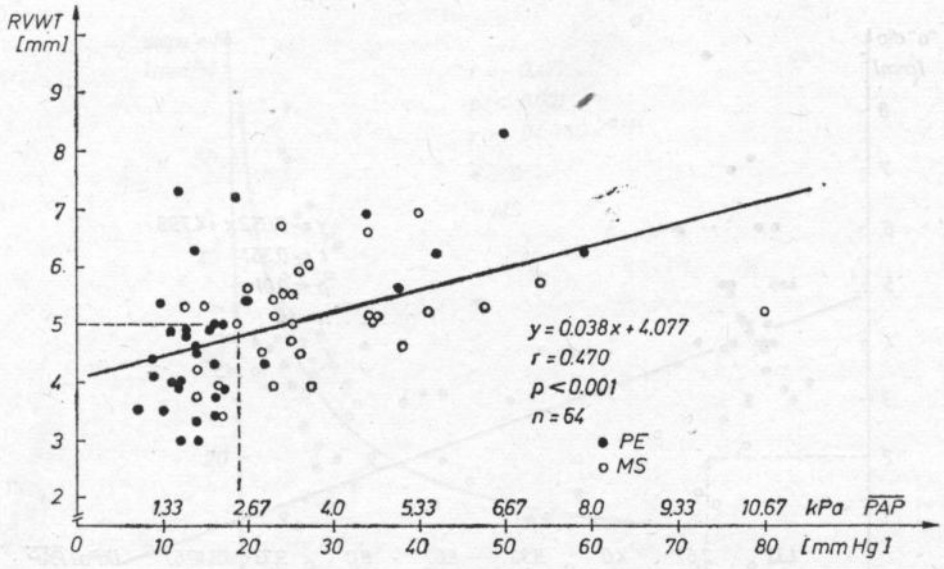

Fig. 4. The correlation between the RVWT and $\overline{PAP}$

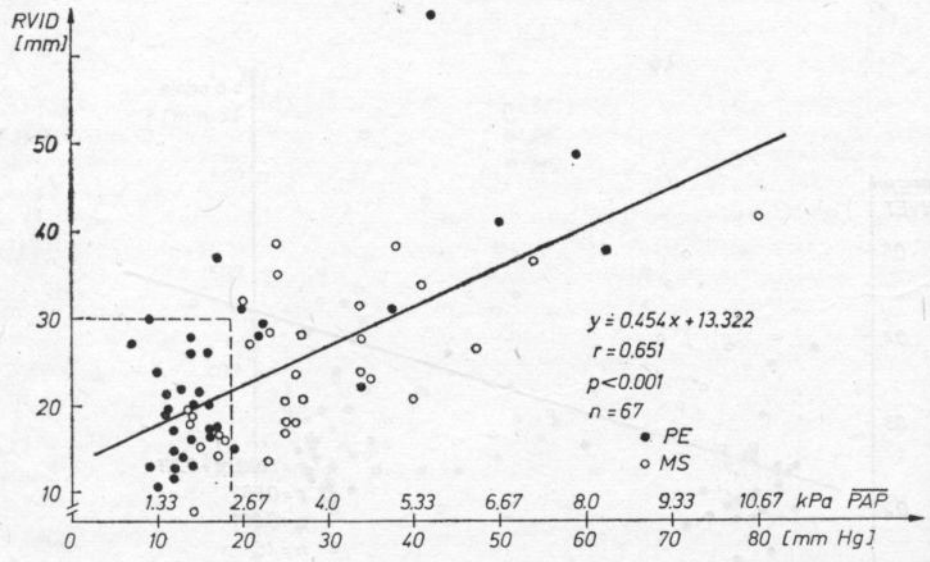

Fig. 5. The correlation between the RVID and $\overline{PAP}$

parameter without any coexisting PH above 30 mm was observed only in one patient. On the contrary, false negative results were relatively frequent.

The best correlation was found between $\overline{PAP}$ and a very simple parameter that was the ratio of the right to the left ventricular diameter (R/L), Fig. 6. We consider the increase of this ratio above 0.5 a reliable indicator of severe PH.

We also believe that only this ratio is useful for individual evaluation. Its value can be influenced adversely by diminished size or by altered shape of the left ventricle and also by the presence of the right ventricular volume overload. Using twodimensional echocardiography there is an easier and more precise directioning of the ultrasonic beam traversing the RV.

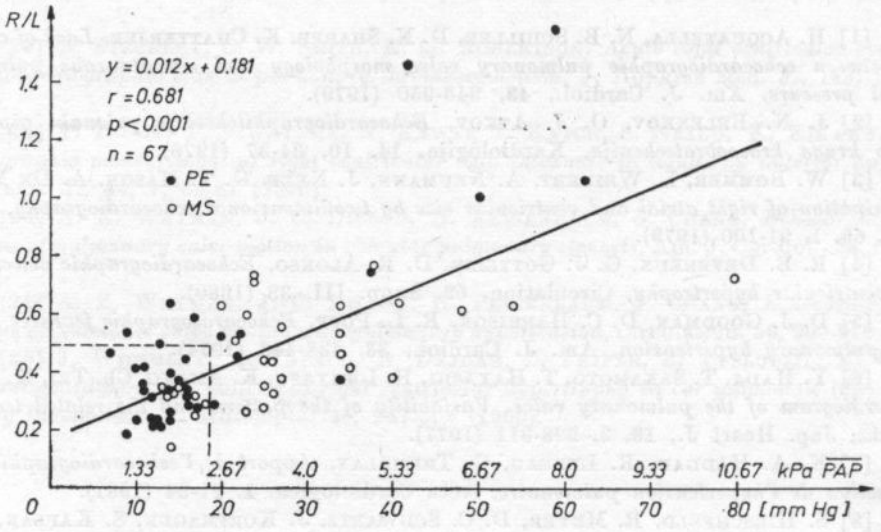

Fig. 6. The correlation between the R/L ratio and $\overline{PAP}$

In Table 1 the number of patients with positivity or negativity of ECG, ECHO and their combination is presented. ECG was never false positive, but it was false negative in 10 patients (i.e. 38 per cent). In echocardiographic examination we found 2 false positive and 8 false negative findings. The combination of both methods yields more reliable results. Table 2 shows specificity and

Table 1. The number of patients with positive or negative ECG, ECHO or their combination

$\overline{PAP}$ [mm Hg]	n	ECG		ECHO		ECG+ECHO	
		pos.	neg.	pos.	neg.	pos.	neg.
19	33	0	33	2	31	2	31
20–29	16	7	9	8	8	11	5
30	10	9	1	10	0	10	0

Table 2. Specificity and sensitivity of ECG, ECHO and their combination

Specification	ECG	ECHO	ECG+ECHO
sens. [%]	61.5	69.2	80.8
spec. [%]	100.0	93.9	93.9

sensitivity of both methods. As the ECG was never false positive, the specificity in combination remained high and the sensitivity raised. The results indicate that both methods should be used together.

References

[1] H. Acquatella, N. B. Schiller, D. N. Sharpe, K. Chatterjee, *Lack of correlation between echocardiographic pulmonary valve morphology and simultaneous pulmonary arterial pressure,* Am. J. Cardiol., **43**, 946-950 (1979).

[2] J. N. Belenkov, O. J. Atkov, *Echocardiographitcheskije priznaki gipertonii malovo kruga krovoobratschenija,* Kardiologija, **14**, 10, 34-37 (1976).

[3] W. Bommer, L. Weinert, A. Neumann, J. Neef, D. T. Mason, A. De Maria, *Determination of right atrial and ventricular size by twodimensional echocardiography,* Circulation, **60**, 1, 91-100 (1979).

[4] R. B. Devereux, G. J. Gottlieb, D. R. Alonso, *Echocardiographic detection of right ventricular hypertrophy,* Circulation, **62**, Supp. III, 33 (1980).

[5] D. J. Goodman, D. C. Harrison, R. L. Popp, *Echocardiographic features of primary pulmonary hypertension,* Am. J. Cardiol., **33**, 438-443 (1974).

[6] Y. Hada, T. Sakamoto, T. Hayashi, H. Ichiyasu, K. Amano, Ch. Tei, K. Kato, *Echocardiogram of the pulmonary valve. Variability of the pattern and the related technical problems,* Jap. Heart J., **18**, 3, 298-311 (1977).

[7] K. A. Haddad, R. Lebeau, G. Tremblay, *Apport de l'echocardiographie dans la detection de l'hypertension pulmonaire,* Acta Cardiologica, **1**, 21-34 (1981).

[8] S. Hirschfeld, R. Meyer, D. C. Schwartz, J. Korfhagen, S. Kaplan, *Measurement of right and left ventricular systolic time intervals by echocardiography,* Circulation, **51**, 304-309 (1975).

[9] S. Hirschfeld, R. Meyer, D. C. Schwartz, J. Korfhagen, S. Kaplan, *The echocardiographic assessment of pulmonary artery pressure and pulmonary vascular resistance,* Circulation, **52**, 642-650 (1975).

[10] R. Kaku, A. Neumann, W. Bommer, L. Weinert, D. T. Mason, A. N. De Maria, *Sensitivity and specificity of the pulmonic valve echogram in the detection of pulmonary hypertension,* Am. J. Cardiol., **41**, 2, 436 (1978).

[11] W. Kasper, T. Meinertz, F. Kersting, H. Löllgen, P. Limbourgh, H. Just, *Echocardiography in assessing acute pulmonary hypertension due to pulmonary embolism,* Am. J. Cardiol., **45**, 567-572 (1980).

[12] W. Lew, J. S. Karliner, *Assessment of pulmonary valve echogram in normal subjects and in patients with pulmonary arterial hypertension,* Br. Heart J., **42**, 147-161 (1979).

[13] H. Matsukubo, T. Matsuura, N. Endo, J. Asayma, T. Watanabe, K. Furukawa, H. Kunishige, H. Katsume, H. Ijichi, *Echocardiographic measurement of right ventricular wall thickness,* Circulation, **56**, 2, 278-284 (1977).

[14] N. C. Nanda, R. Gramiak, T. I. Robinson, P. M. Shah, *Echocardiographic evaluation of pulmonary hypertension,* Circulation, **50**, 575-581 (1974).

[15] P. Niederle, P. Frídl, J. Widimský, M. Riedel, *Echocardiographic diagnosis of pulmonary hypertension,* XVIth International Congress of Internal Medicine, Prague 1982, 388.

[16] D. J. Pocoski, P. M. Shah, *Physiologic correlates of echocardiographic pulmonary valve motion in diastole,* Circulation, **58**, 6 1064-1071 (1978).

[17] T. Riggs, S. Hirschfeld, G. Borkat, J. Knoke, J. Liebman, *Assessment of the pulmonary vascular bed by echocardiographic right ventricular systolic time intervals,* Circulation, **57**, 5 939-947 (1978).

[18] G. Rizzato, A. Rezzano, G. Sala, R. Merlini, L. Ladelli, G. Tansini, G. Montanari, L. Bertoli, *Detection of right heart impairment in sarcoidosis. Haemodynamic and echocardiographic study* (in press).

[19] T. Sakamoto, M. Matsuhisa, T. Hayaschi, H. Ichiyasu, *Echocardiogram of the pulmonary valve,* Jap. Heart J., **15**, 4, 360-373 (1974).

[20] T. Sakamoto, M. Matsuhisa, T. Hayashi, H. Ichiyasu, *Echocardiogram and phonocardiogram related to the movement of the pulmonary valve,* Jap. Heart J., **16**, 2, 107-117 (1975).

[21] R. Steckley, C. W. Smith, R. M. Robertson, *Acute right ventricular overload: an echocardiographic clue to pulmonary thromboembolism,* J. Hopkins Med. J., 143, 122-125 (1978).

[22] T. Tsuda, T. Sawayama, N. Kawai, T. Katch, S. Nezuo, K. Kikawa, *Echocardiographic measurement of right ventricular wall thickness in adults by anterior approach,* Br. Heart J., **44**, 1, 55-61 (1980).

[23] A. E. Weyman, J. C. Dillon, H. Feigenbaum, S. Chang, *Echocardiographic patterns of pulmonary valve motion in valvular pulmonary stenosis,* Am. J. Cardiol., **34**, 644-651 (1974).

[24] A. E. Weyman, J. C. Dillon, H. Feigenbaum, S. Chang, *Echocardiographic patterns of pulmonic valve motion with pulmonary hypertension,* Circulation, **50**, 905-910 (1974).

[25] J. Widimský, A. Valach, R. Dejdar, Z. Fejfar, Z. Vysloužil, M. Lukeš, *The electrocardiographic pattern of right ventricular hypertrophy in cor pulmonale (due to pulmonary tuberculosis,)* Cardiologia, **36**, 287-308 (1960).

ARCHIVES OF ACOUSTICS
9, 1-2, 267-274 (1984)

ECHOCARDIOGRAPHY IN THE FOLLOW-UP OF PATIENTS WITH PROSTHETIC HEART VALVES

E. KOUDELKOVÁ, A. GROŠPIC,
P. NIEDERLE

Institute for Clinical and Experimental Medicine, Prague, Czechoslovakia

In 26 patients with aortic and in 25 with mitral valve disease changes in the size, hypertrophy and function of the left ventricle (LV) within 2 years of aortic or mitral valve replacement were evaluated and compared with the preoperative echocardiographic findings.

LV size decreased significantly within the first month after aortic valve replacement as well as after operation for pure or predominant mitral insufficiency. LV hypertrophy regressed in both groups of aortic valve disease. However, in patients with maximum LV dilatation and hypertrophy valve replacement failed to effect complete normalization of LV size and mass. Postoperative evaluation of LV function showed a distinct improvement in patients operated for aortic stenosis. In the groups of patients with mitral stenosis and pure aortic or mitral insufficiencies no significant change of LV function after surgery was demonstrated.

Preoperative echocardiographic measurements of the LV end systolic dimension and the end systolic wall stress proved to be very useful noninvasive predictors of long-term postoperative changes of the LV function after surgical correction of the aortic or mitral valve disease.

1. Introduction

The noninvasive evaluation of postoperative changes of the left ventricular size, hypertrophy and function in patients after heart valve replacement provides useful data about the reversibility of morphological and functional abnormalities of the left ventricle after surgical correction of the valvular disease. In this study, the patients after successful aortic and mitral valve replacement were followed-up up to 2 years after operation and preoperative echocardiographic findings of the patients with reversible left ventricular dilatation, hypertrophy and dysfunction were compared with those of patients with ir-

reversible left ventricular impairment. We tried to answer the question if any of the preoperative echocardiographic parameters can be valuable in predicting the long-term postoperative course and in detecting the patients at high risk of irreversible dysfunction of the left ventricle.

2. Methods

Using *M*-mode echocardiography, we examined 26 patients with aortic and 25 patients with mitral valve disease within a month before and after implantation of the Björk-Shiley prosthetic valve. Fifteen patients underwent valve replacement for predominant aortic stenosis, 11 patients for aortic insufficiency. In the mitral valve disease group, 15 patients had pure or predominant mitral stenosis with calcification or advanced fibrosis of the mitral valve, 10 patients had pure mitral insufficiency. Echocardiography was performed with an Echocardio-Visor 03 system (Organon Teknika — Holland), using a standard technique of left ventricular measurements. Echocardiographic parameters of the left ventricle that were evaluated in half-year intervals up to 2 years after operation, are summarized in Table I. From the measurements of the end-diastolic diameter and wall thickness, the left ventricular mass was calculated according to the formula recommended by Teichholz. The index R/Th represents the end-diastolic (or end-systolic) radius to the wall thickness ratio and provides important information about the character of hypertrophy. The wall thickness was calculated as the average of the posterior wall and the septal thicknesses.

Table 1. Echocardiography — LV measurement

Size	Hypertrophy	Function
D_d	T_{PW}	FS
D_s	T_{IVS}	EF
	LVM	V_{CF}
	R/Th	ESS

D_d — end-diastolic left ventricular dimension, D_s — end-systolic dimension, T_{PW} — left ventricula posterior wall thickness at end-diastole, T_{IVS} — interventricular septal thickness at end-diastole, LVM — left ventricular mass, R/Th — end-systolic radius to wall thickness ratio, FS — fractional shortening, EF — ejection fraction, V_{CF} — mean velocity of circumferential fiber shortening, ESS — end-systolic left ventricular wall stress.

The end-systolic stress, the recently developed noninvasive index of the left ventricular peak circumferential wall stress, was derived in the groups of patients with pure aortic or mitral insufficiency from the product of peak systolic arterial blood pressure, measured by a cuff manometer, and echocardiographic end-systolic radius to the wall thickness ratio, using the formula recommended by Quinones [4].

3. Results

Examination after aortic valve replacement demonstrated normalization of the left ventricular size in most patients within the first month after surgery (Fig. 1). However, in patients with maximum dilatation of the left ventricle before operation, despite a significant decrease in the end-diastolic dimension in the first month after replacement, the left ventricular size failed to normalize completely in the following postoperative period.

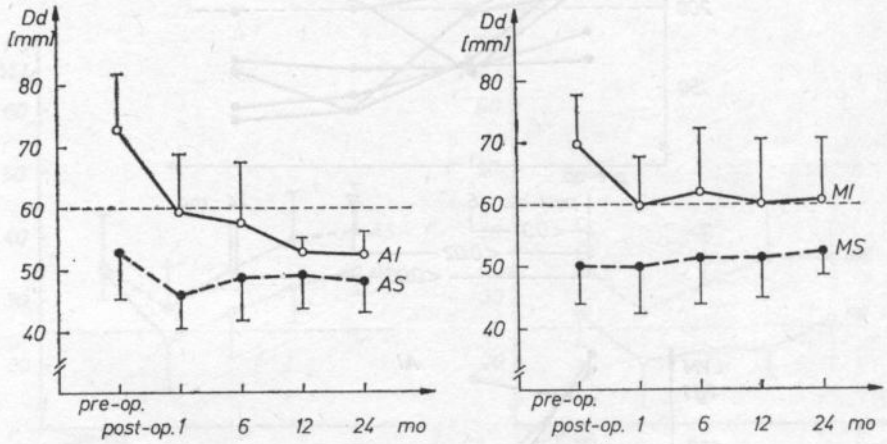

Fig. 1. Postoperative changes of the left ventricular end diastolic dimension (D_d) after aortic and mitral valve replacement. AI — aortic insufficiency, AS — aortic stenosis, MI — mitral insufficiency, MS — mitral stenosis

The left ventricular hypertrophy regressed significantly after aortic valve replacement, both for predominant aortic stenosis and predominant or pure aortic insufficiency (Fig. 2). However, echocardiographic as well as electrocardiographic signs of left ventricular hypertrophy normalized only in patients with a lesser degree of left ventricular hypertrophy before operation.

In a group of patients operated for aortic stenosis, the postoperative follow-up showed a distinct improvement of the echocardiographic parameters of the left ventricular function (Fig. 3). On the other hand, in the group of patients with aortic insufficiency no significant change in left ventricular functional parameters was demonstrated both 1 and 2 years after operation in comparison with the preoperative values.

In mitral stenoses, the size of the left ventricle did not change after operation. In the group of patients with predominant mitral insufficiency, mitral valve replacement was followed by a significant diminution of left ventricular dimensions (Fig. 1). This notwithstanding, the left ventricle remained enlarged in more than a half of those patients. Moreover, no significant improvement

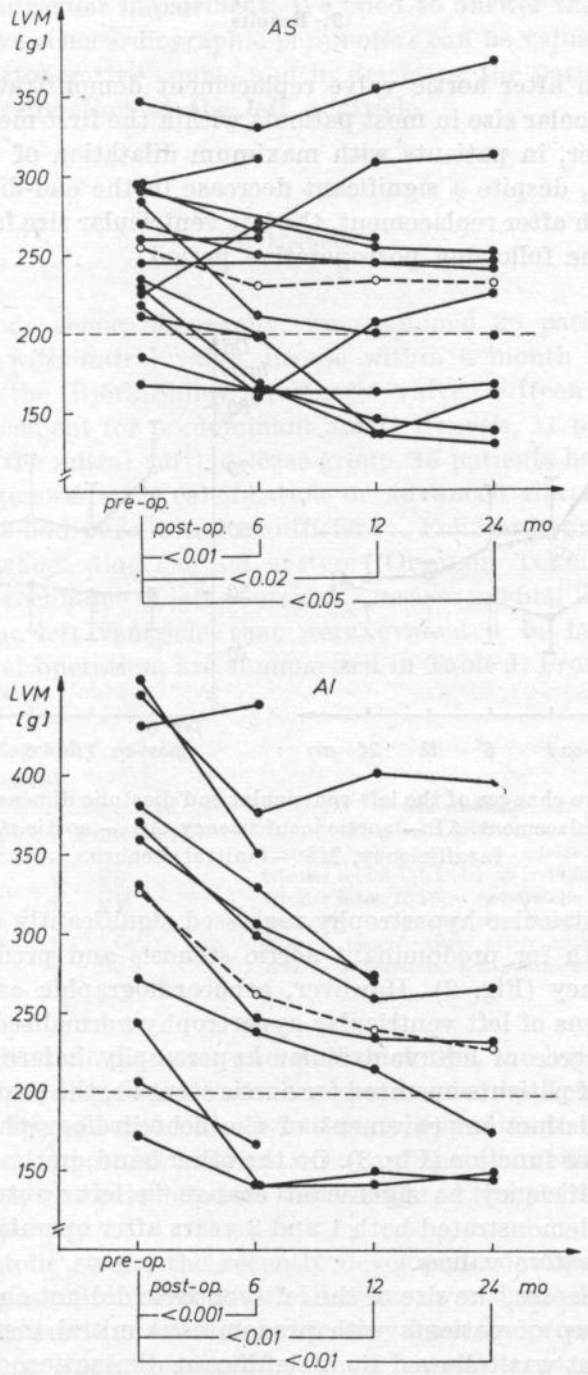

Fig. 2. Postoperative changes of the left ventricular mass after valve replacement for predominant aortic stenosis (AS) and aortic insufficiency (AI)

of the left ventricular function was found after operation for predominant mitral insufficiency in the patients with the evidence of left ventricular dysfunction before operation (Fig. 3).

Comparison of the preoperative echocardiographic parameters of the left ventricle in patients with reversible left ventricular dilatation and dysfunction with those with irreversible left ventricular impairment showed that the combination of a marked end-systolic dilatation of the left ventricle with inappropriate hypertrophy, which resulted in an increase in the wall stress, was the most sensitive and specific index determining patients at high risk for persistent

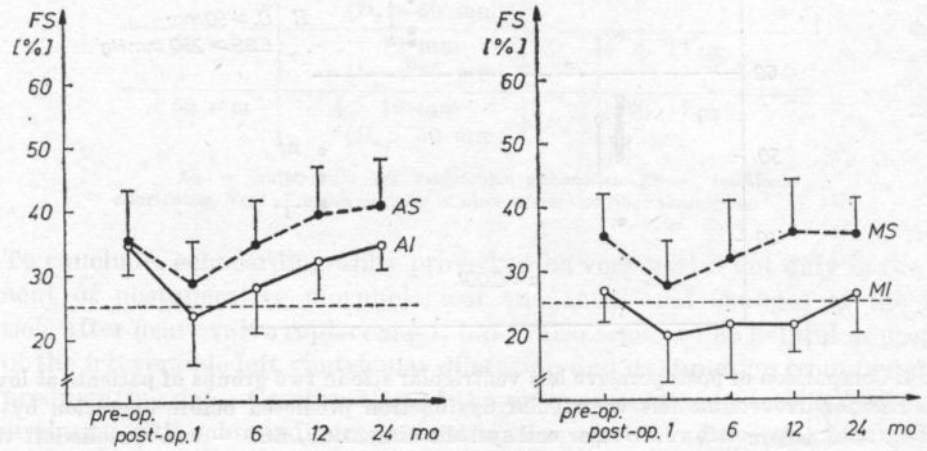

Fig. 3. Postoperative changes of echocardiographic parameters of the left ventricular systolic function after aortic and mitral valve replacement (FS — fractional shortening)

left ventricular dilatation and dysfunction. All patients with preoperative end-systolic dimension greater than 50 mm and simultaneously increased end-systolic left ventricular wall stress above the value of 250 mm Hg, had a marked and progressive left ventricular dysfunction after surgery, when evaluating postoperative echocardiographic parameters of the systolic ejection function of the left ventricle (fractional shortening and ejection fraction), as well as parameters of left ventricular contractility (especially the mean rate of circumferential fiber shortening). Five of the 8 patients in this high risk group failed to improve after surgery and had symptoms of chronic cardiac decompensation (III-IV class of the NYHA), 2 patients died due to congestive heart failure. Figs. 4 and 5 show a significant postoperative difference in the left ventricular size and parameters of function in two groups of patients with good and bad prognosis that can be separated using the above mentioned preoperative echocardiographic indexes.

Only a marked end-systolic dilatation of the left ventricle before operation, even with a simultaneous decrease in the left ventricular wall stress can be

reversible and the left ventricular function can improve after operation even in these cases. We found that the long-term improvement of the left ventricular function after operation depends on the early change of the end-systolic dimension of the left ventricle within the first month after surgery. This change when evaluated simultaneously with preoperative parameters of the left ventricular function, seems to be useful in prediction of the long-term postoperative course and in identifying the patients, in whom we can expect an improvement of the

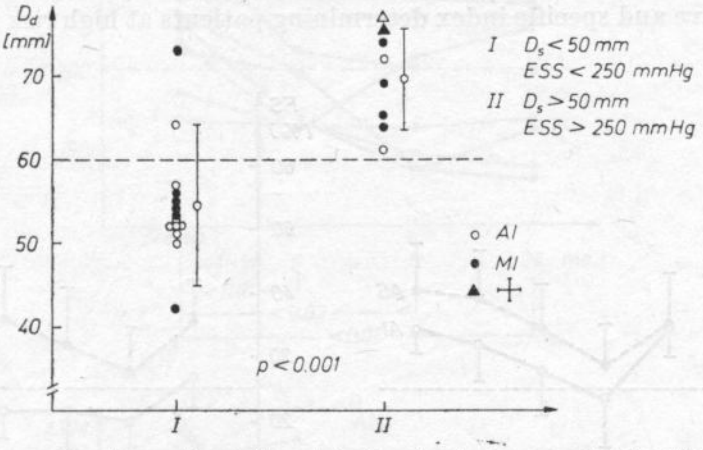

Fig. 4. Comparison of postoperative left ventricular size in two groups of patients at low and high risk for irreversible left ventricular dysfunction predicted before operation by echocardiography (D_s — left ventricular end systolic dimension, ESS — end-systolic left ventricular wall stress)

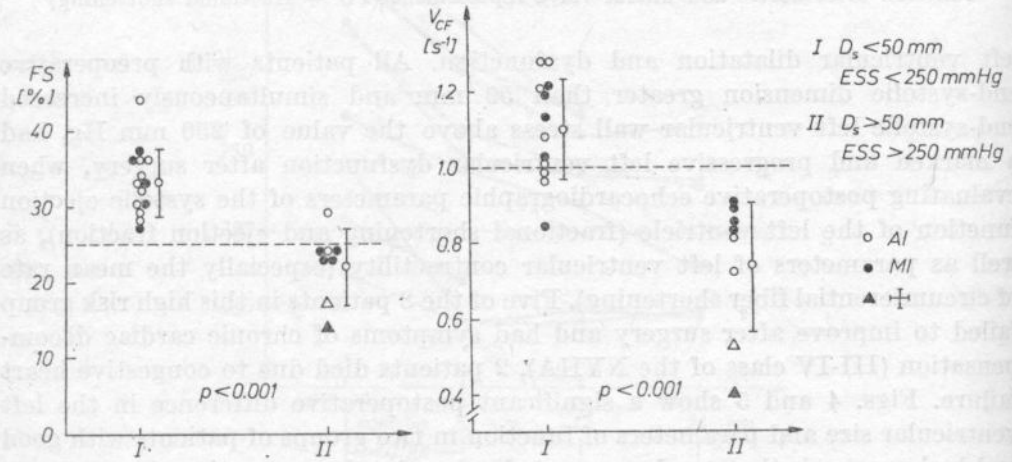

Fig. 5. Comparison of postoperative values of echocardiographic functional parameters in two groups of patients at low and high risk for irreversible left ventricular dysfunction predicted before operation by echocardiography. FS — fractional shortening, V_{CF} — mean velocity of circumferencial fiber shortening of left ventricle, D_s — end-systolic left ventricular dimension, ESS — end-systolic left ventricular wall stress

left ventricular function from those with persistent or progressive impairment of the left ventricular function (Table 2).

Table 2. Prediction of postoperative changes of LV function

Pre-op. D_s	ΔD_s 1 month after op.	ΔLV function 1–2 years after op.
> 50 mm	$\downarrow >$ 10 mm ($D_s <$ 50 mm)	$\uparrow$FS, $\uparrow V_{CF}$
> 50 mm	$\downarrow <$ 10 mm ($D_s >$ 50 mm)	$\downarrow$FS, $\downarrow V_{CF}$
< 50 mm	$\downarrow <$ 10 mm ($D_s <$ 50 mm)	$\downarrow$FS, $\downarrow V_{CF}$
<50 mm	$\downarrow >$ 10 mm ($D_s >$ 50 mm)	$\downarrow$FS, $\downarrow V_{CF}$

D_s – end-systolic left ventricular dimension, FS – fractional shortening, V_{CF} – mean velocity of circumferential fiber shortening

To conclude, echocardiography proved to be very useful not only in the assessment of postoperative morphological and functional changes of the left ventricle after heart valve replacement, but it also seems to be helpful in prediction of the irreversible left ventricular dilatation and dysfunction from noninvasive preoperative data. Combination of the preoperative end-systolic dimension measurement with echocardiographic estimation of the end-systolic left ventricular wall stress was superior to the end-diastolic dimension measurement or calculation of echocardiographic indexes of the left ventricular systolic function in identifying patients at high risk for persistent or progressive left ventricular impairment. If both end-systolic left ventricular dimension and end-systolic wall stress were increased above the cut off values, more accurate prediction could be made. If only end-systolic dilatation of the left ventricle was present before operation, it was helpful to assess the early change in the parameter simultaneously with preoperative values of dilatation and the function of the left ventricle that correlated well with long-term postoperative changes in the left ventricular function and was valuable in prediction of normalization versus persistence of the preoperative left ventricular dysfunction. Our preliminary results were promising, but the groups of patients operated for pure aortic and mitral insufficiencies are still small. Therefore further studies will be necessary to verify the results on a greater number of patients.

References

[1] B. A. Carabello, N. P. Stanton, L. B. McQuire, *Assessment of preoperative left ventricular function in patients with mitral regurgitation. Value of the end systolic wall stress-end-systolic volume ratio,* Circulation, **64**, 6, 1212-1217 (1981).

[2] W. H. Gaasch *et al., Chronic aortic regurgitation. Prognostic value of left ventricular end-systolic dimension and end-diastolic radius thickness ratio,* J. Am. Coll. Cardiol, **1**, 3, 775-782 (1983).

[3] A. G. Kumpuris *et al., Importance of preoperative hypertrophy, wall stress and end-systolic dimension as echocardiographic predictors of normalization of left ventricular dilatation after valve replacement in chronic aortic insufficiency,* Amer. J. Cardiol, **49**, 5, 1091-1100 (1982).

[4] M. A. Quinones *et al., Noninvasive quantification of left ventricular wall stress. Validation of method and application to assessment of chronic pressure overload,* Amer. J. Cardiol, **45**, 4, 782-790 (1980).

[5] G. Schuler *et al., Temporal response of left ventricular performance to mitral valve surgery,* Circulation, **59**, 6, 1218-1230 (1979).

ARCHIVES OF ACOUSTICS
9, 1-2, 275-284 (1984)

STROKE VOLUME ESTIMATION BY RHEO-ECHOCARDIOGRAPHY DURING ATRIAL FIBRILLATION CONVERTED TO SINUS RHYTHM

TADEUSZ PAŁKO, LEONARD KOMPIEL,
KRYSTYNA ILMURZYŃSKA

Postgraduate Medical Centre, Goszczyńskiego 1, 02-616 Warsaw, Poland

The impedance rheographic and echocardiographic methods were used to investigate changes in the stroke volume (SV) and the cardiac output (CO) in the course of atrial fibrillation and after electroversion. 12 patients were examined. CO increased on average by 11 per cent and 9 per cent after electroversion using respectively rheographic and echocardiographic methods.

1. Introduction

Atrial fibrillation is characterized by arrhytmia, e.g. big fluctuation in time of the cardiac cycle (over 20 per cent) and by the lack of atrial contraction. Atrial fibrillation causes cardiac performance worsening which is manifested in decreasing stroke volume, cardiac output, atrial pressure and time of blood circulation and in increasing central venous pressure, right atrial pressure and arterio-venous difference in the oxygen saturation of blood [1].

Many authors report that lack of sinus rhythm causes a decrease in the cardiac output from 7 do 25 per cent [2, 10]. First of all, it is the result of a loss of effective pumping action of the atrial, but also loss of the rhythm as well as speed up of the cardiac function. A decrease in CO may intensify symptoms, for example, the appearance of latent circulation insufficiency (heart failure) or chest pain of stenocardial effect. Restoration of sinus rhythm improves hemodynamics of the heart.

Thus, it is reasonable to assume that the consequences of sinus rhythm loss depend on the degree of hemodynamic disorders.

The purpose of the study was to investigate changes in stroke volume (SV) and cardiac output (CO) in the course of atrial fibrillation and after electrical cardioversion.

2. Materials and methods

Twelve patients with atrial fibrillation were investigated. The group consisted of 9 males and 4 females, aged from 28 to 52, 47 years on average. Atrial fibrillation persisted from 3 days to 6 months, 44 days on average.

The group investigated (Table I) consisted of:

1. 1 patient with heart failure in course of mitral insufficiency (case 11);
2. 4 patients after commissurotomy (cases 1, 3, 5, 10);
3. 2 patients with double valve replacement (cases 9 and 12);
4. 3 patients with coronary disease and arterial hypertension (cases 7, 8, 9);
5. 2 patients with paroxyzmal atrial flutter (cases 2 and 4).

Before the sinus rhythm was restored, all medicines with possible influence on heart contractility were discontinued (especially digitalis). Two hours prior to cardioversion chinodine (0.4 g) was administered orally to all patients.

Both echographic and rheographic measurements were conducted before and immediately after electrical treatment. Energy applied to the patients was in range of 50 to 300 Ws, depending on the weight as well as condition of patient.

Echographic measurements were made by the *TM* technique, using a UKG-10 device, produced by TECHPAN.

The left ventricular stroke volume (SV) was calculated using the Teichholz formula where:

The end diastolic volume

$$V_d = (DD)^3 \frac{7}{2.4+DD};$$

The end systolic volume

$$V_s = (SD)^3 \frac{7}{2.4+SD},$$

where *DD* and *SD* respectively: the diastolic and systolic diameter of the left ventricle (Fig. 1).

The stroke volume

$$SV = V_d - V_s.$$

Rheocardiographic study was performed by the tetrapolar current impedance method developed by T. PAŁKO [6, 7], which is generally based on the Kubicek method.

In that method (Fig. 2), two band electrodes feeding the current are located around the neck and the waist. Through the electrodes there flows the alternating current with a frequency of 60 kHz at the constant amplitude of 1 mA.

Table 1. Clinical data

Patients		Atrial fibrillation					Electroversion				
No	Initials Sex-Age	SV [cc]		CO [l/min]		HR [b/min]	SV [cc]		CO [l/min]		HR [b/min]
		Rheo	Echo	Rheo	Echo		Rheo	Echo	Rheo	Echo	
1	*NR – M* 50	45	50	5.0	5.6	112	56	63	5.6	6.3	100
2	*DJ – M* 49	33	28	5.9	5.1	180	76	80	6.1	6.4	80
3	*GH – F* 48	54	43	5.6	4.5	102	75	73	6.0	5.9	80
4	*ZJ – M* 48	62	63	5.2	5.3	84	80	78	5.6	5.5	70
5	*GG – F* 30	50	54	6	6.5	120	92	80	6.4	5.6	70
6	*MF – M* 58	62	61	4.8	4.7	77	83	80	5.6	5.5	68
7	*PS – F* 61	62	59	6.6	6.3	106	72	73	6.8	7.0	95
8	*FT – M* 51	58	69	4.7	5.6	81	84	96	5.6	6.5	67
9	*JJ – M* 28	42	46	4.8	5.3	115	72	72	4.8	4.9	67
10	*KM – F* 60	24	47	3.6	7.0	150	48	73	4.8	7.3	100
11	*LZ – M* 36	55	67	6	7.4	110	72	70	7.2	7	100
12	*RW – M* 37	50	60	5.2	6.2	104	62	70	5.9	7	100
Average SV and CO		49.75	53.92	5.28	5.79	111.75	72.67	75.67	5.87	6.25	83.08
Standard deviation		11.51	11.22	0.76	0.86	27.86	11.83	7.82	0.68	0.73	14.12

The changes in the impedance ΔZ and first derivative dZ/dt are detected by 2 disc electrodes (instead of band electrodes in the Kubicek method) located above and below the sternum.

The investigation used the impedance rheograph designed by one of us (*T.P.*).

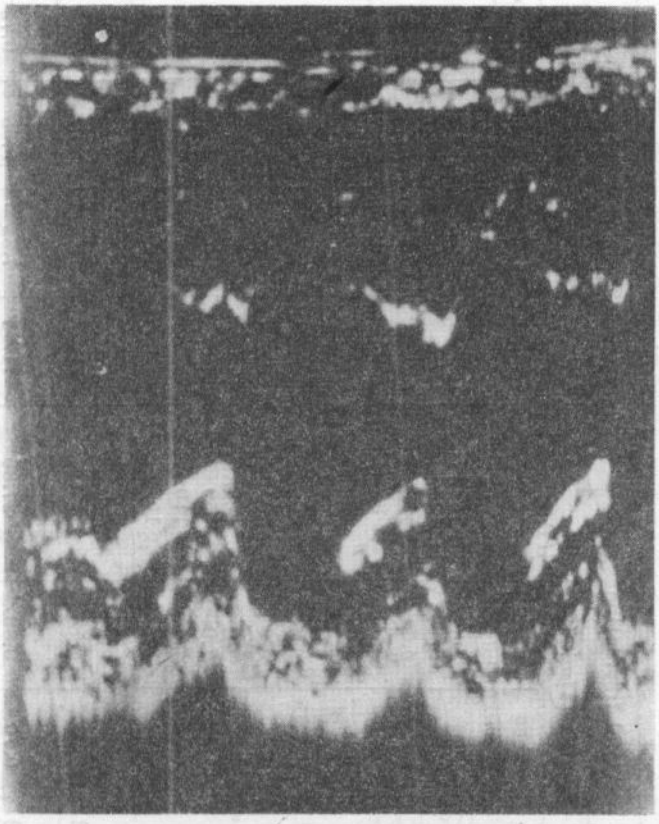

Fig. 1. Measuring method of systole and diastole diameter of the left ventricle by the echocardiographic — *TM* technique

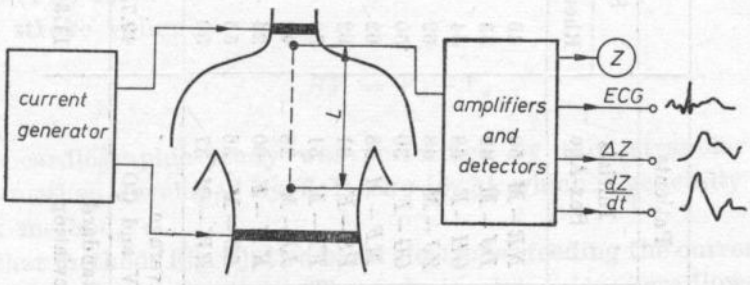

Fig. 2. Principle of the tetrapolar current method for determination of stroke volume

The stroke volume (SV) was calculated using the Kubicek formula:

$$SV = \varrho \frac{L^2}{Z^2} \left| \frac{dZ}{dt} \right| T,$$

where ϱ — resistivity of blood dependent mainly on hematocrite, L — distance between inner electrodes, Z — basis impedance, $|dZ/dt|$ — amplitude of first derivative of impedance change (Fig. 3), T — left ventricle ejection time (Fig. 3).

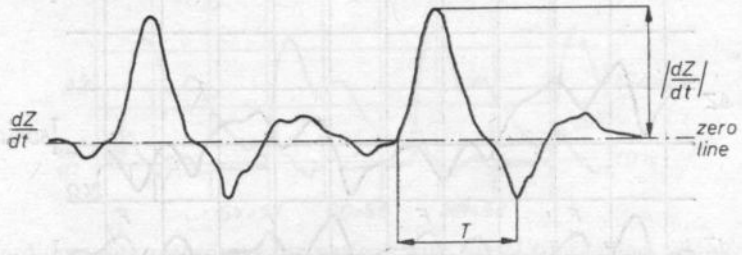

Fig. 3. Principle of dZ/dt amplitude and T - ejection time assessment from rheocardiographic dZ/dt signal

The reliability of this method for computing SV was verified [8] by comparison with the invasive computerized termodilution method. For healthy subjects the results obtained by the two methods differ less than 15 per cent. The impedance method proved to be very useful for change trend observation.

3. Results

Examples of rheocardiographic recordings and the calculated stroke volume (SV) and the cardiac output (CO) for 2 patients with atrial fibrillation (FA) (Figs. 4 and 5) and a patient with atrial flutter (VA) (Fig. 6) are shown in Figs. 4-6.

The results indicate that SV during atrial fibrillation in rest changes very distinctly. It depends not only on the ventricular filling time. We suggest that the influence of the atrial activation conducted to the ventricular activation changing electromechanical effect should be considered. In this situation the CO, measured during over 1 min. is almost constant in spite of the very large beat-to-beat SV changes. Immediately after synchronized electrical atrial defibrillation SV and CO appeared virtually stable. The CO value after cardioversion is usually distinctly higher than that during atrial fibrillation.

The results of SV and CO obtained by the methods from the examination of patients with atrial fibrillation (FA) are shown in Table I and a diagram (Fig. 7).

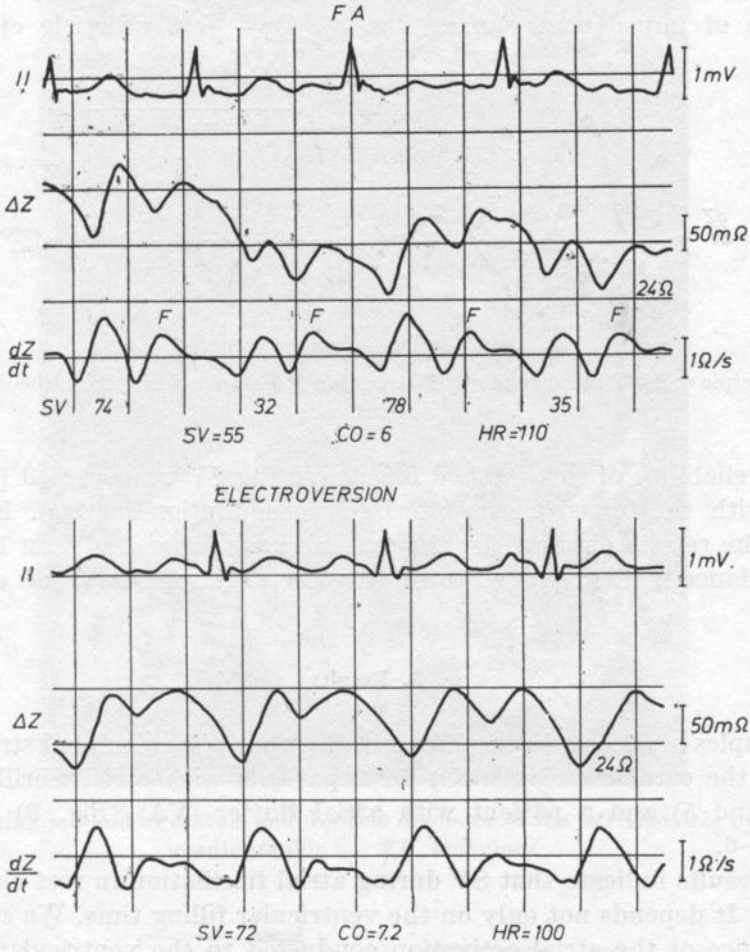

Fig. 4. Rheocardiographic recordings for patient with atrial fibrillation with fast ventricle rate and after electroversion. Signs of mitral insufficiency evident (big *F* wave)

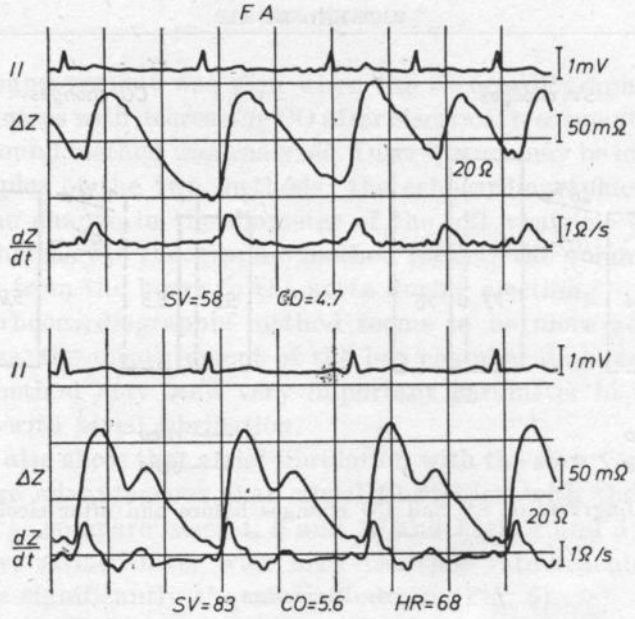

Fig. 5. Rheocardiographic recordings for patient with atrial fibrillation with slow ventricle rate and after electroversion

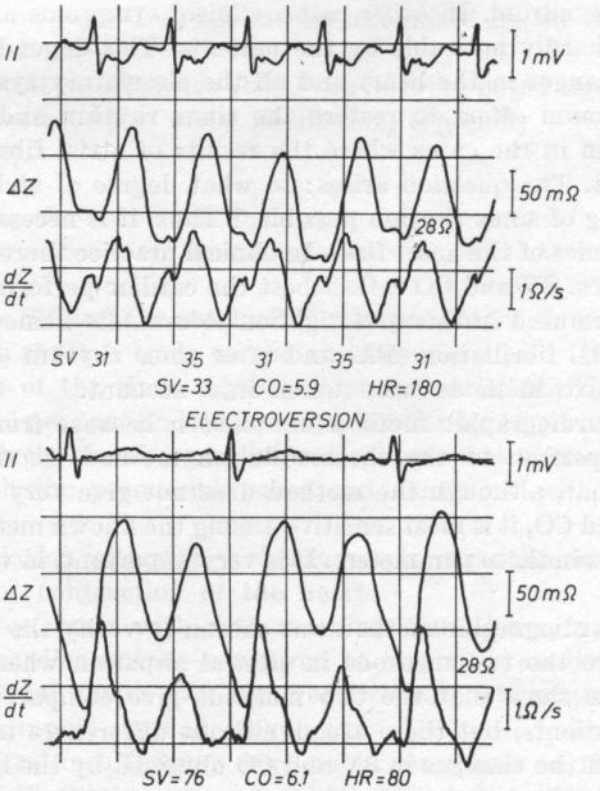

Fig. 6. Rheocardiographic recordings for patient with atrial flutter — VA and directly after electroversion

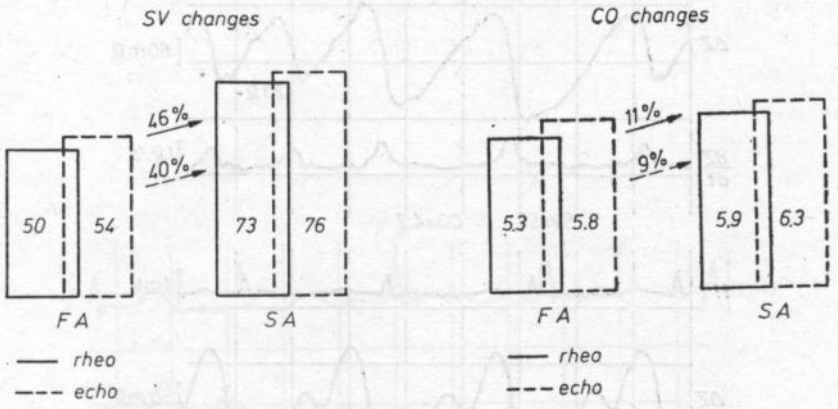

Fig. 7. Diagrams of SV and CO changes before and after electroversion

4. Discussion

Atrial fibrillation causes different degrees of hemodynamic disorders. In some cases they are very heavy and lead to edema or acute brain ischemia and the MAS syndrom. In other cases, clinical symptoms are so insignificant that they are hardly noticable by the patients. This depends on the origin of the disease, changes in the heart and all the circulatory system.

The maximum effort to restore the sinus rhythm and its consolidation should be taken in the cases where the results of atrial fibrillation are heavy and permanent. The question arises: to what degree of atrial hypertrophy is the maintaining of sinus rhythm possible ? Thus, it is necessary to investigate the hemodynamics of the heart first. In clinical practice there are several hemodynamic indexes. SV and CO reflect best the cardiac performance. Thus, these parameters were used in this investigation to evaluate hemodynamic disorders in cases of atrial fibrillation (FA) and after sinus rhythm (SR) was restored. Only noninvasive methods were taken into account.

The rheocardiographic method was chosen because from previous verification in comparison to the thermodilution method (as mentioned above), it is evident that, although the method does not give very accurate absolute values of SV and CO, it is most sensitive among the known methods to determine relative changes in these parameters. It is very important, in view of the purpose of this study.

The echocardiographic method was chosen to verify the Teichholz formula and to compare the two methods in clinical situation where FA occurs.

The results show that the two methods give comparable results in our group of 12 patients, but there are significant differences in particular cases.

Analyses of the changes in SV and CO obtained by the impedance method prove that this reflects better the clinical condition of the patient. In all cases

hemodynamic improvement was seen when the rheocardiographic method was used, whereas 3 cases with decreasing CO after electrical treatment were observed when the ultrasound method was analysed. Discrepancy may be explained by the different principles of the two methods: the echocardiographic method takes into account the change in the diameter of the left ventricle only in systole and diastole, whereas the rheographic method reflects the volume of the blood that is expelled from the heart to the aorta during ejection.

Thus, the rheocardiographic method seems to be more adequate.

Nevertheless, the measurement of the left chamber diameter in the echocardiographic method may be a very important parameter in the evaluation of the patients with atrial fibrillation.

The results also show that atrial fibrillation with the slow ventricle contraction rate is more advantageous than atrial fibrillation with the fast ventricle action (Table I — compare cases 4, 6 and 10 and Figs. 4 and 5).

Surprisingly, atrial flutter with high ventricle rate reaching 180 b/min. does not change significantly the cardiac output (Fig. 6).

Analysis of the findings leads us into 2 additional resolutions, essentially not connected with the purpose of this work, namely:

1. During atrial fibrilation and atrial flutter with high ventricle rate, alternating phenomena may occur and it can be recognized by the rheocardiographic method (Figs. 4 and 6).

2. Signs of mitral insufficiency (big *F* wave) were noted sometimes on the heocardiographic waveform of atrial fibrillation, especially with fast ventricle contraction (Fig. 4).

5. Conclusions

Analysis of the SV and CO obtained for the patients with atrial fibrillation converted to sinus rhythm leads to the conclusions:

1. Restoration of the sinus rhythm from the atrial fibrillation increases stroke volume by 46 per cent and 40 per cent, but CO by 11 per cent and 9 per cent using respectively the rheographic and echographic methods; the results are consistent with the permissible error and consistent with the literature [1, 10].

2. Atrial fibrillation with slow ventricle rate is advantageous to fibrillation with more frequent contraction of the heart.

3. Atrial flutter, even with rate reaching 180 b/min., practically does not diminish the cardiac output compared to one after cardioversion.

4. In case of atrial flutter with high ventricle rate, alternating pulse-recognized by the rheographic method may occur.

5. Signs of mitral insufficiency were noted sometimes on the rheographic waveform of atrial fibrillation case, especially with fast ventricle contraction.

6. Final conclusion

Sinus rhythm should be restored in the consideration of the hemodynamic improvement, especially for patients with a long history of heart failure, as well as fatal thrombogenesis. It has to be taken into account that restoration of sinus rhythm may cause embolism, as a result of moving thrombus produced earlier during long-term atrial fibrillation.

References

[1] C. H. Best, N. B. Taylor, *The physiological basis of medical practice*, The Williams and Wilkins Company, Baltimore 1966.

[2] M. I. Ferrer, R. M. Harvey, *Some hemodynamic aspects of cardiac arrhythmias in man*, Am. Heart J., **68**, 153 (1964).

[3] N. J. Fortuin *et al.*, *Determination of left ventricular volume by ultrasound*, Circulation, **44**, 575 (1971).

[4] K. Ilmurzyńska, *Diagnostyka ultrasonograficzna*, PZWL, Warszawa 1980.

[5] J. Kwoczyński, E. Gürtler-Krawczyńska, T. Pałko, *Verapamil effect on stroke volume in supraventricular arrhythmias*, Materia Medica Polonia, **11**, 235-241 (1979).

[6] T. Pałko, G. Pawlicki, *The use of passive electrical properties of the tissues in medical diagnosis. Electrical impedance measurements*, Biocybernetics (in press).

[7] T. Pałko, G. Pawlicki, J. Hewelke-Pałko, J. Bieniek, B. Żukowski, *Equipment for impedance examination with the use of tetrapolar technique*, Probl. Techn. Med., **3**, 169-176 (1976).

[8] T. Pałko, W. Rużyłło, Z. Purzycki, J. Hewelke-Pałko, P. Kamiński, M. Szymańska, *Comparison of cardiac output changes during of atrial stimulation and effort*, 33 Scientific Conference of Pol. Card. Soc., 1977, 44-45.

[9] L. E. Teichholz, T. Kreulen, M. W. Herman, *Problems in echocardiographic volume determinations echocardiographic — angiographic correlations in presence or absence of asynergy*, Am. J. Cardial., **37**, 7 (1976).

[10] E. Żera, W. Rydlewska-Sadowska, *Electric cardioversion in treatment of atrial fibrillation*, Pol. Med. J., **8**, 8-13 (1969).

ARCHIVES OF ACOUSTICS
9, 1-2, 285-295 (1984)

CLINICAL APPLICATIONS OF FETAL ECHOCARDIOGRAPHY

HIDEYO SHIMADA, MICHIKO TAKAHASHI,
SHIZUO KATAGIRI

Department of Medicine, Kitasato Institute Hospital, Tokyo, Japan

HIDEO KOBAYASHI

Department of Gynecology

KAZURU SAITO

Central Laboratory

Recent advances of echocardiography have made it possible to study cardiac anatomy and circulatory physiology of fetus.

We studied the foetal cardiac structures and physiology by cross-sectional and *M*-mode echocardiography in 200 fetuses at 32-40 weeks of gestation. Fetuses were reexamined within 2-5 days after birth to provide comparative data for assessment of circulatory changes at birth.

In these echocardiographic studies, we examined three cases with congenital cardiac malformations (DORV, TGA, and VSD). We diagnosed DORV before birth, when two great arteries rising from one single ventricle were observed. But TGA and VSD were only diagnosed after birth. Therefore, we concluded that this technique is useful to diagnose malformations of the cardiac chambers or correlations between the cardiac chambers and the two great arteries.

We also examined mitral valve diastolic descent rate (MVDDR), mitral valve excursion (MVE), tricuspid valve diastolic descent rate (TVDDR), tricuspid valve excursion (TVE) and aortic dimension (AOD).

In conclusion, fetal echocardiography may be applicable to diagnose cardiac malformations and also to evaluate cardiac functions before birth.

1. Introduction

Ultrasound technique has made it possible to analyse the physiological states of the various organs of the human body. In the field of cardiology, many new approaches have been tried, and nowadays the ultrasound technique is believed to be an indispensable method for the diagnosis of heart and the great vessels.

Especially, the recent advances in the cross-sectional echocardiography and Doppler method enabled us to record the states of the fetal heart and to analyse the fetal cardiac anatomy and physiology.

The present study explains the technique to record fetal echocardiogram and its clinical applications based on our experiences over the past 3 years.

2. Method

Three-hundred and twenty-five fetuses of healthy mothers, varying 30 to 40 weeks of gestation were selected for this study.

Cross-sectional and *M*-mode echocardiography were used for recording in all cases. In our first attempt, we failed to obtain good tracings in 1/3 of the cases, but we tried again within the same week on the failed cases. Finally, from 85 per cent of all the cases, we could get enough information to evaluate the foetal heart.

Ten cases from which clear four chamber view tracings could be obtained, went to Doppler study.

Fetuses were re-examined within 4 to 7 days after birth, to provide comparative data for the assessment of circulatory changes at birth.

A Toshiba SSH 11 real-time, phased-array ultrasonic sector scanner with a hand-controlled 2.4 MHz transducer, was used to perform cross-sectional and *M*-mode echocardiography.

Pulsed Doppler examinations were performed with a Doppler flowmeter combined with the echocardiograph systems.

The most important thing to get a good fetal echocardiograms is the transducer positions.

When the fetus is in the right occipito-anterior position or left occipito-anterior position, echocardiograms can be obtained from maternal right or left flank, respectively (position *A* in Fig. 1).

From this position, the ultrasonic beam passes through the fetal heart via the fetal spine and fetal lung. Therefore, the sector images of te fetal heart along its mirror imaged long axis view can be obtained (Fig. 2). It is especially easy to estimate the orientation of the fetus and fetal heart in this position.

A long axis view tracing, a short axis view tracing and a four chamber view tracing can be obtained, when the transducer is placed on the maternal

naval region, as shown in position *B* in Fig. 1. But it is rather difficult to determine the transducer position to get stable tracings.

We proceeded with Doppler examinations as soon as a clear four chamber view tracing had been obtained. The sampling site of the left side of the heart was the left ventricular outflow tract just below the mitral valve, and the right side of the heart, it was the right ventricular outflow tract just below the tricuspid valve.

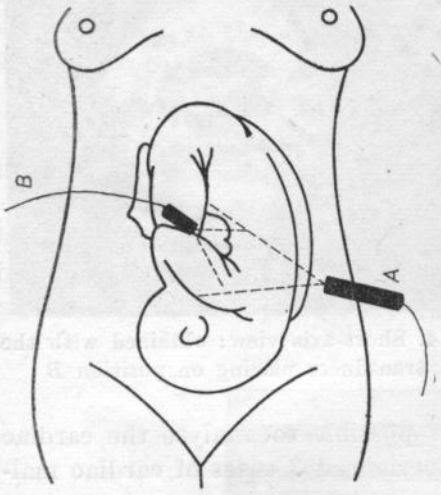

Fig. 1. Two standard transducer positions: *A* – transducer is placed in maternal flank; *B* – transducer is placed in maternal navel region.

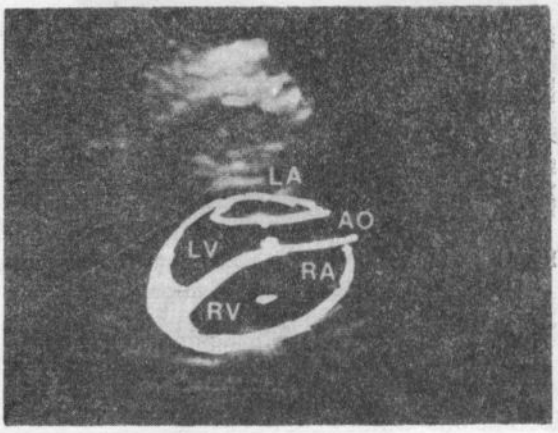

Fig. 2. Long-axis view: obtained with the transducer placing on position *A*.

The flow velocity was calculated by using the formula as follows.

$$v = \frac{f_2 C}{2 f_0 \cos\theta},$$

where v – maximum velocity, f_2 – frequency shift, f_0 – transducer frequency, θ – angle between ultrasound beam and velocity.

3. Results

1. Normal cross-sectional echocardiogram of the fetus

Fig. 2 shows a long axis view tracing obtained from the material flank (position *A* in Fig. 1). Instead of the usual long axis view pattern obtained from the chest wall, a mirror imaged pattern was detected through the echocardiogram.

Fig. 3 shows a long axis view tracing obtained from the material naval region (position *B* in Fig. 1). The pattern is quite similar to that of the one obtained from the chest wall.

Fig. 4 is a short axis view tracing and Fig. 5 is a four chamber view tracing. These echocardiogram patterns are quite similar to those obtained from the chest wall.

Fig. 3. Long-axis view: obtained with the transducer placing on position *B*

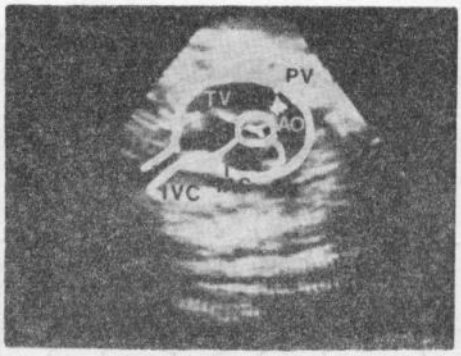

Fig. 4. Short-axis view: obtained with the transducer placing on position *B*

By utilizing these echocardiograms, it is possible to analyse the cardiac anatomy to a certain extent. We already experienced 3 cases of cardiac malformations among 325 cases.

2. Abnormal cross-sectional echocardiogram of fetus

As mentioned above, we experienced 3 cases of cardiac malformations. These are DORV, VSD and TGA. We diagnosed DORV before birth, but we could not make diagnosis of VSD and TGA before birth.

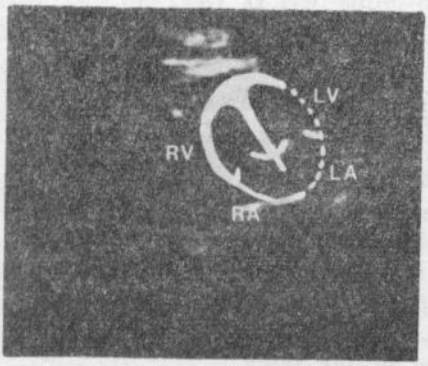

Fig. 5. Four-chamber view: obtained with the transucer placing on position *B*

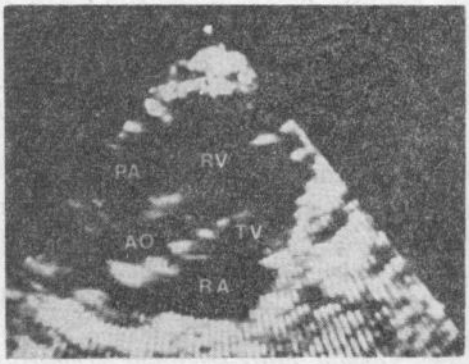

Fig. 6. Double outlet right ventricle. The view obtained with transducer placing on position *B*. Two great arteries which arise from the single ventricle are displayed to the left of the image

Fig. 6 is the cross-sectional echocardiogram of the fetus with DORV. It shows a quite abnormal findings, i.e. two great arteries arise from the single ventricle which has coase trabeculations.

This finding suggests a case of either DORV or single ventricle.

The fetus was born at 40 weeks as a girl weighing 3040 grams, but cyanosis was not observed at birth. At one month of age, the girl began to experience cyanosis by crying. At this point catheterization and angiography were performed and DORV was diagnosed. Cyanosis and dyspnea developed gradually and she died at the age of 2 months. Autopsy revealed DORV, polysplenia and dextrocardia.

3. Normal M-mode echocardiogram of the fetus

M-mode echocardiograms are also recordable from various places in fetal heart.

Fig. 7 is a mitral valve echocardiogram pattern obtained from the image in Fig. 2. The mitral valve pattern shows a mirror image from the pattern obtained from the chest wall, i.e. as shown in the figure, the anterior leaflet of the mitral valve moves posteriorly during the diastolic phase.

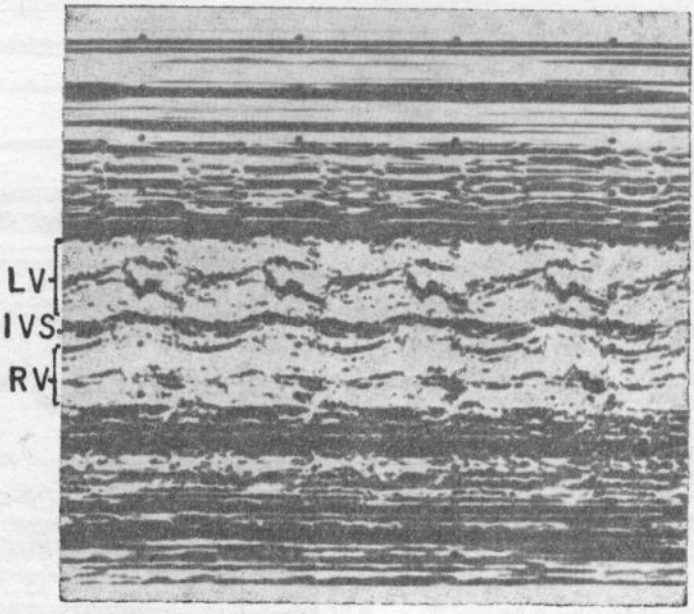

Fig. 7. A mitral valve echocardiogram pattern obtained from the image in Fig. 2

Fig. 8 is an aortic valve pattern obtained from the same image. The top of the panel is the left atrium and the bottom is the right ventricle, and the middle part is the aorta. The aortic valve moves posteriorly during the systolic phase.

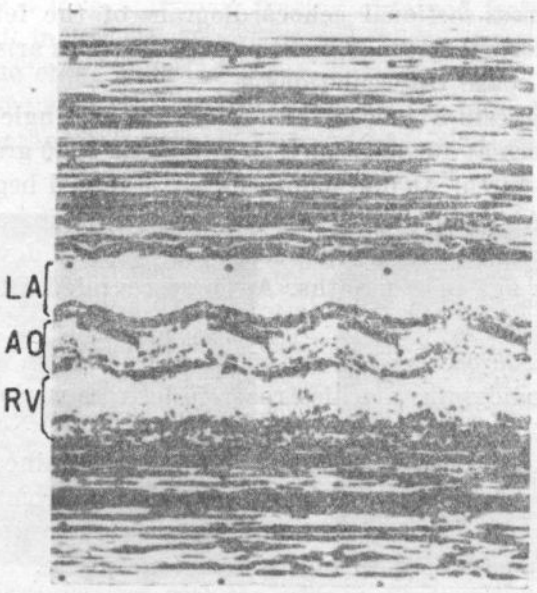

Fig. 8. An aortic valve pattern obtained from the image in Fig. 2

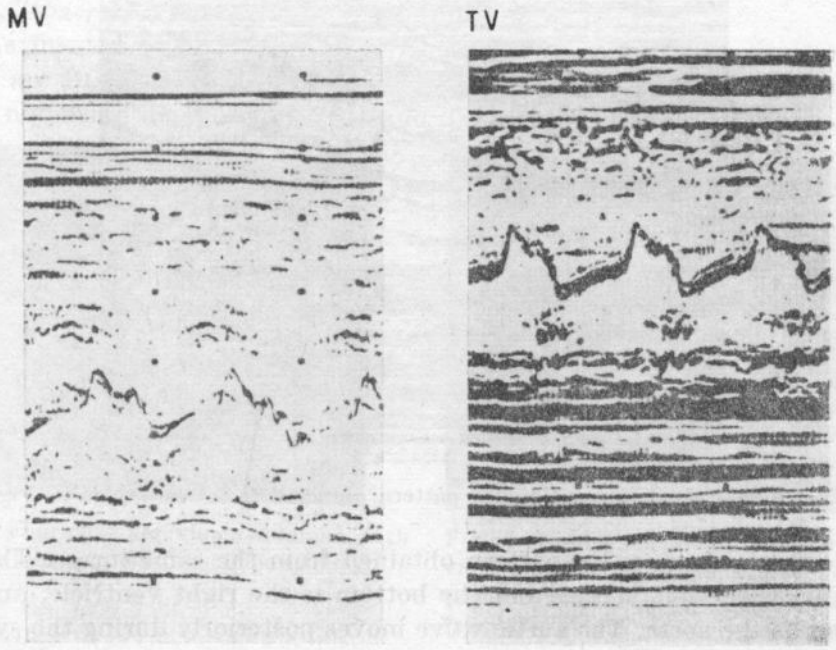

Fig. 9. Echocardiogram patterns of mitral valve and tricuspid valve

Fig. 9 shows echocardiogram patterns of the mitral valve and the tricuspid valve. These are quite similar to the pattern obtained from the chest wall.

Fig. 10 shows the echocardiogram pattern of the aortic and pulmonary valves. The aortic valve pattern here is quite similar to that of the usual pattern, but the pulmonary valve pattern is lacking an *a* dip, probably due to pulmonary hypertension.

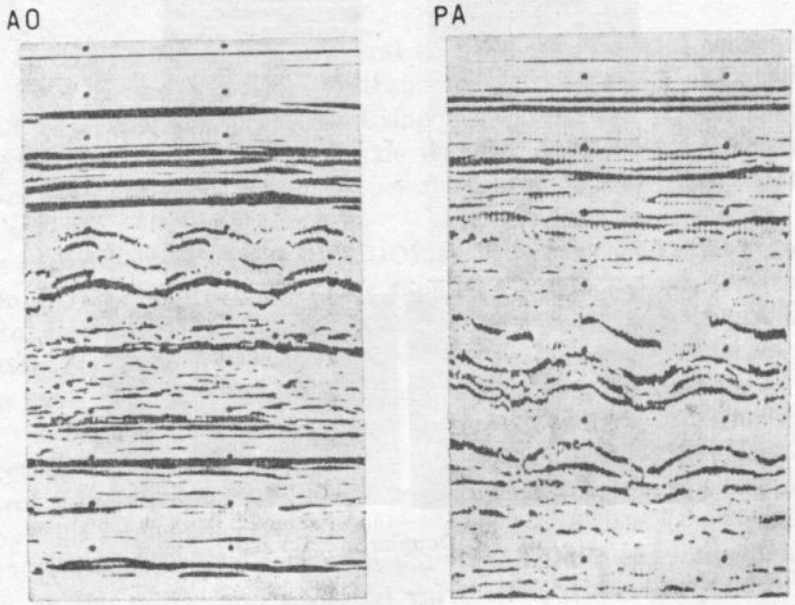

Fig. 10. An echocardiogram pattern of the aortic and pulmonary valves

4. Normal values of the M-mode echocardiogram of the fetus

The normal values of the fetal *M*-mode echocardiograms were calculated from the above mentioned figures.

The normal data of the fetuses are described in Table 1.

Table 1

Specification	Before birth [mm]	After birth [mm]
MVDDR	43.1±12.4	54.3±7.7
MVE	7.3±0.9	9.5±1.1
TVDDR	49.7±12.8	57.9±9.1
TVE	8.1±1.1	11.1±1.1
AOD	8.8±0.9	11.5±1.0

5. Flow velocity patterns of fetal heart

Doppler spectrum of the mitral and tricuspid valves is shown in Fig. 11. The tricuspid valve flow shows much higher spectrum than that of the mitral

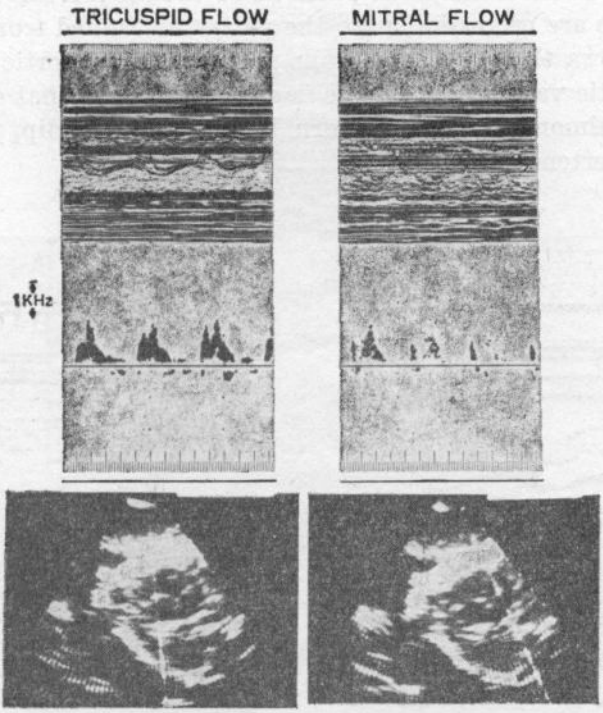

Fig. 11. Doppler spectrum

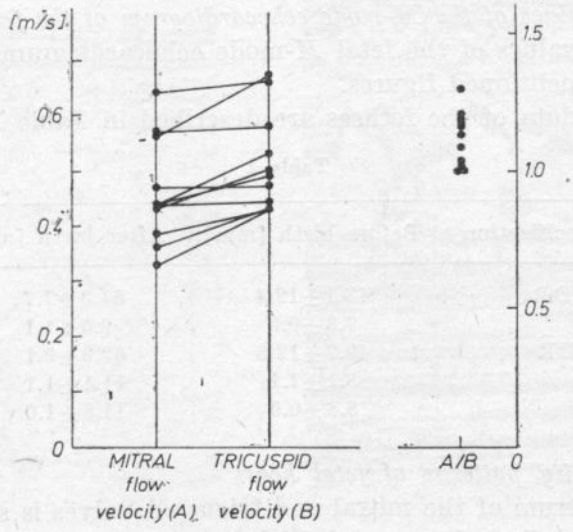

Fig. 12. Comparison between mitral flow velocity and tricuspid flow velocity in fetus

valve flow. On the bases of these patterns, the flow velocity of the mitral and tricuspid valves was calculated. Fig. 12 shows the result. The flow velocity ratio between the mitral and tricuspid valves is 1.0 to 1.3 (mean value is 1.12).

4. Discussion

Only a few studies have been reported in the field of the fetal echocardiography [2].

We have already reported several times about the fetal echocardiography and we have deviced "standard" transducer positions [3], i.e. the maternal flank and maternal naval positions. Using these "standard" transducer positions, a long axis view tracing, a short axis view tracing and a four chamber view tracing can be obtained, and it is possible to analyse cardiac anatomies to a certain extent.

We experimented on cases of DORV, VSD and TGA, but we could only diagnose DORV before birth. This fact may suggest that this technique is useful to diagnose the extreme cardiac malformations of chambers and the correlation between the cardiac chambers and the great arteries.

We have also tried to analyse the physiology of fetuses.

At the fetal stage, since lungs do not work, pulmonary circulation cannot be detected. Therefore, the blood stream through the foramen ovale supplies the mitral valve flow, and the blood stream through the ductus arteriosus is supplied by the tricuspid valve flow.

Since the mitral valve and tricuspid valve DDR and excursion are strongly affected by the mitral and tricuspid valve flow, respectively, it is possible to estimate the circulatory changes at birth, when the mitral valve and tricuspid valve DDR and excursion of the fetus are compared with those of a new born baby.

As shown in Table 1, the increased ratio of the mitral valve DDR and excursion is almost equal to that of tricuspid DDR and excursion. These facts may suggest that the blood flow through the foramen ovale and through the ductus arteriosus is nearly equal.

In order to confirm the hypotesis, Doppler method was performed.

The blood flow ejected from the left ventricle can be detected by measuring the aortic flow. Similarly, the blood flow ejected from the right ventricle can be detected by measuring the pulmonary flow. But it is very difficult to determine the sampling site of the aorta and pulmonary arteries by the Doppler flow meter, on the fetal echocardiogram.

We used the left ventriclar outflow tract just below the mitral valve and the right ventricular outflow tract just below the tricuspid valve as a sampling site for the Doppler flow meter. As mentioned above, mitral valve flow is nearly equal to the blood flow through the foramen ovale, and the tricuspid flow is nearly equal to that of the ductus arteriosus.

As shown in Fig. 12, the flow velocity ratio between the mitral and tricuspid valves was 1.12 (mean). Therefore, when the left ventricle ejects 1, the right ventricle ejects 1.12.

There has been no report about the fetal cardiac circulations in the human heart. The only report by RUDOLPH and HEYMANN [1], based on animal experiments, describes that the left ventricle ejects only 1/3 of the total cardiac output. But our data suggest that about 1/2 of the total cardiac output is ejected from the left ventricle before birth.

5. Conclusions

The technique to record the fetal echocardiograms and its results have been explained. The fetal echocardiography may be applicable to diagnose cardiac malformations and also to evaluate cardiac functions before birth.

References

[1] A. M. RUDOLPH, M. A. HEYMANN, *The fetal circulation,* Ann. Rev. Med., **19**, 2, 195-205 (1968).

[2] D. J. SAHN, L. W. LANGE, H. D. ALLEN, S. T. GOLDBERG, C. ANDERSON, H. GILES, K. HABER, *Quantitative real-time cross-sctional echocardiography in the developing normal human fetus and new born,* Circulation, **62**, 3 588-597 (1980).

[3] M. TAKAHASHI, H. SHIMADA, N. HIRAMA, S. KATAGIRI, K. KIMURA, Y. MORIKAWA, M. OSANO, *Detection of the cardiac anomalies before birth by cross-sectional echocardiography,* Journal of Cardiography, **11**, 2, 661-669 (1981).

ARCHIVES OF ACOUSTICS
9, 1-2, 295-298 (1984)

DIAGNOSTIC ULTRASOUND IN SURGERY CLINICS

V. V. ZARETSKY

USSR, Moscow, National Research Center of Surgery, USSR

The author presents a short survey of ultrasonic applications in diagnosis of various heart diseases, peripheral blood vessel disorders and abdominal pathologies before the operation and intraoperatively and in the treatment of various kinds of disorders. In the author's opinion ultrasound renders nowadays a great help to the surgeon and will become even more useful in the coming years.

The second half of the 20th century and especially the last 20 years have witnessed the coming of the ultrasound era in medicine. With each passing year ultrasound has been used more widely as a diagnostic tool and as a physical agent for treatment of various pathologic conditions.

The present paper deals with ultrasound usage experience which has been acquired within 10 years in the USSR, in National Research Center of Surgery (USSR Academy of Medical Science, Moscow). We have used ultrasound in diagnosis of various heart diseases, peripheral blood vessel disorders and abdominal organ pathology (Table 1). All the cases presented were treated surgically.

Table 1. The use of diagnostic ultrasound

Organs examined	Number of patients	Number of examinations
Heart	5211	14852
Peripheral vessels	2298	6894
Abdominal organs	4166	4704
Total number	11675	26450

Table 2. Echocardiography

Echocardiography techniques	Number of examinations
Onedimensional echocardiography	7956
Twodimensional echocardiography	5014
Doppler echocardiography	1720
Contrast echocardiography	162
Total number	14852

The fact that most of our cases were diagnosed before the surgery made it possible to establish critically the diagnostic value of ultrasound.

Echocardiography is used diagnostically when dealing with heart troubles. Table 2 shows four basic techniques of echocardiography applied in our Center.

The techniques listed in Table 2 were used according to the diagnostic information needed. One dimensional echocardiography is a well established mode for the detection of the prolapsed mitral valve, atrial tumours (myxoma), complete atrioventricular canal, tetralogy of Fallot and hypertrophic subaortic stenosis which had been diagnosed earlier only in autopsy.

Twodimensial echocardiography is in many cases a supplement to the one-dimensional ultrasound technique. It enables one to get a better spatial location of various components inside the heart and makes it possible to determine the type and degree of mitral and aortic orifice stenosis, the degree of insufficiency of these two valves and their mobility. Bacterial endocarditis vegetations are usually very well seen on the twodimensional echocardiograms of the mitral and aortic valves.

Doppler echocardiography is rather a good technique for detecting intracardiac turbulent blood flows — the phenomenon which is always present in such heart pathology as various septal defects, valve incompetance and aortic and pulmonic valve stenosis. Doppler ultrasound makes the diagnosis of these heart abnormalities more precise and more reliable.

The contrast echocardiography makes it possible to visualise the intracardiac blood flows, to detect and measure various intracardiac shunts and blood flow direction and to diagnose the heart valve insufficiency. It helps to verify the dubious structures inside the heart chambers.

Table 3. Doppler echoangiography

Doppler techniques	Number of examinations
Ultrasound pulse detection	5619
Blood vessels scanning and echoflowmetry	1275
Total number	6894

Table 4. Ultrasound scanning of abdominal cavity organs

Techniques of scanning	Number of examinations
Manual scanning	4086
Computerised automatic scanning	618
Total number	4704

The systemic approach to these echocardiographic techniques is a valuable source of information for heart surgeons. They usually find it useful while determining the nature of heart pathology and how risky the operation could be. This significantly lessens the number of invasive diagnostic techniques performed.

Peripheral blood vessels are investigated with the use of various Doppler ultrasound pulse detectors and Doppler flowmeters (Table 3).

Ultrasound pulse detectors are applied when determining the blood flow in regions where simple pulpation does not bring satisfactory results. Those regions are the popliteal space, the region around the malleolus and the patients with hypotony and edema. The Doppler instruments give the sound and graphical information, helping to determine the direction of blood flow and its linear velocity.

Doppler twodimensional flowmeters have the ability not only to produce sound signal and blood flow characteristic curve, but make it possible to give detailed information about the blood vessel walls, their internal surface in longitudinal and cross-sectional views. Besides the linear and volume blood flow can be determined too.

The latest generation of Doppler flowmeters with colour image of the probed vessels possesses the possibility to differentiate between the arterial and venous blood flow.

Thus, nowadays the ultrasound has become a tool for "listening" to the blood flow; it permits determination of its direction and velocity, and what is very important, it gives an opportunity to visualize the blood vessel lumen and to detect various hindrances to the blood flow. The Doppler ultrasound techniques help to diagnose the pathological changes in the brachio-cephalic vessels of the aortic arch and the vessels of the upper and lower extremities. This kind of information is very important when Raynaud, Takaysu and Leriche syndromes are suspected. Its importance is also obvious when dealing with patients suffering from arterior-venous shunts and aneurysms of arteries.

In our Center the ultrasound is also extensively used for detecting pathological changes in such organs of abdominal cavity as liver, gall-bladder, pancreas and kidneys. Usually the contact manual ultrasound scanning and computerized ultrasound tomography are used for that purpose (Table 4).

With the help of these ultrasound scanning techniques we detect stones in the lumen of the gall-bladder and in the bile ducts. Besides we diagnose various abnormal volume tissue formations in the parenchymal organs of the abdominal cavity — the liver, pancreas, kidneys and some other organs. The information we get has become more precise and enabled us to reduce the number of unnecessary diagnostic operations.

Computerized ultrasound tomography gives the possibility not only of seeing the abdominal cavity organ anatomy but also of characterising the microstructure and the level of local blood circulation.

We use ultrasound not only for diagnosis before the operation but intraoperatively as well. The tiny gall stones in the bile ducts, large vessels and peripheral blood flow in kidneys, liver and other abdominal organs are also determined during the operations.

We widely use ultrasound for the treatment of various kinds of disorders.

In the Center it is common to apply the ultrasound in the following procedures:

1. cutting the ribs, sternum and various soft tissues
2. trachea, bronchi and oesophagus endoscopic surgical manipulations
3. endarterectomy
4. hemostasis during the operations
5. surgeon's hands cleaning
6. surgical tools sterilisation
7. cleansing of purulent wounds and cavities
8. phonophoresis of medicines and drugs (antibiotics, hormons etc.).

The present short survey helps to draw the conclusion that ultrasound renders a great help to the surgeons nowadays. And this kind of help will become more useful as with each passing year the ultrasound technique is modernised and so is the clinical experience.